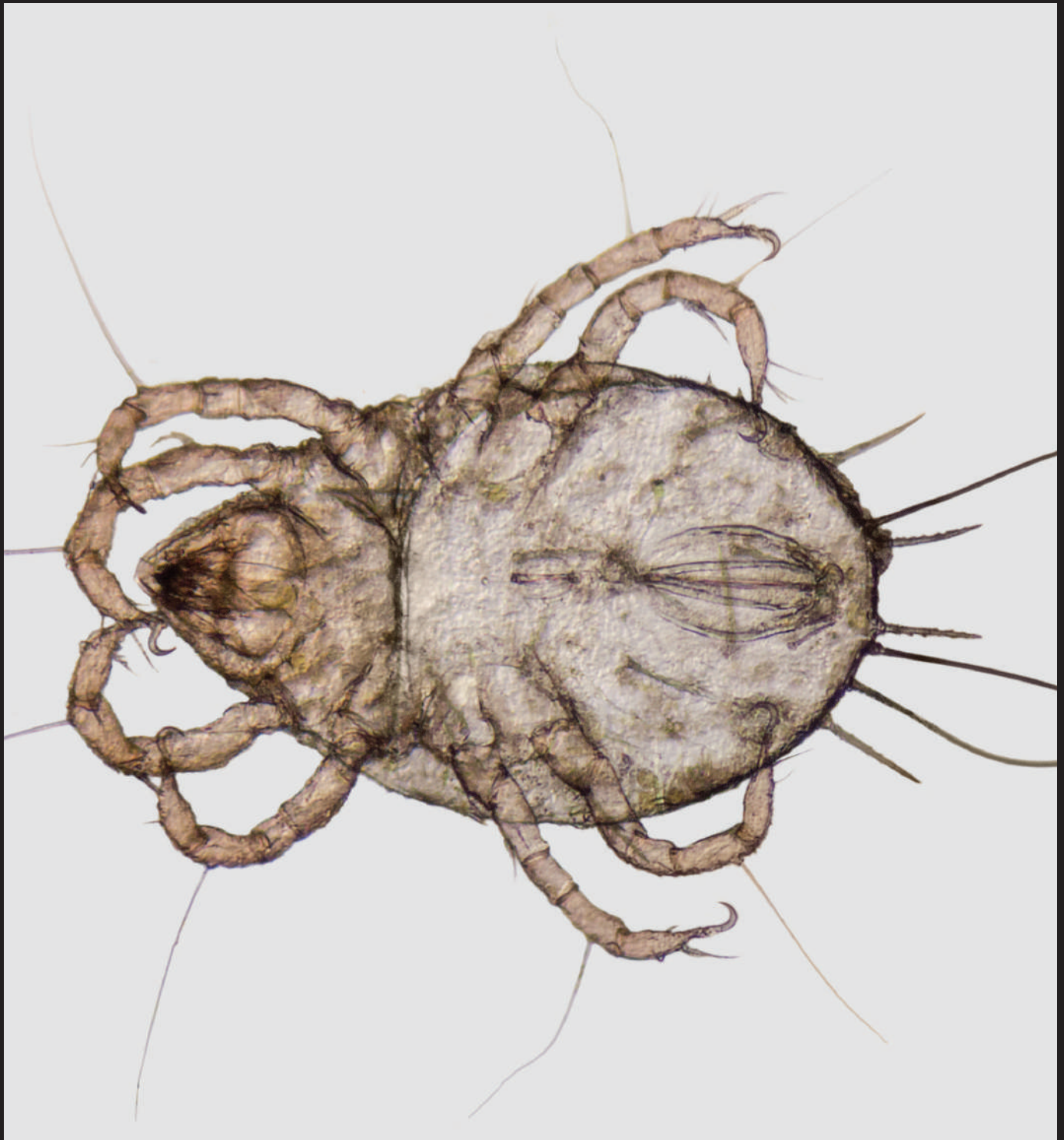


Laboratory Medicine

January 2024 Vol 55 No 1 Pgs 1-108

labmedicine.com



BOARD OF EDITORS

Editor in Chief

Roger L. Bertholf, PhD
Houston Methodist Hospital
Weill Cornell Medicine

Reviews

ASSOCIATE EDITOR

Madhu Menon, MD
ARUP Laboratories

ASSISTANT EDITOR

Rahul Matnani, MD, PhD
Rutgers Robert Wood Johnson Medical School

Biostatistics

ASSOCIATE EDITOR

Michal Ordak, PhD
Medical University of Warsaw

Clinical Chemistry

ASSOCIATE EDITOR

Uttam Garg, PhD
University of Missouri Kansas City School of Medicine

ASSISTANT EDITORS

David Alter, MD
Emory University School of Medicine

Hong Kee Lee, PhD
Endeavor Health

Veronica Luzzi, PhD
Providence Regional Core Laboratory

Alejandro R. Molinelli, PhD
St Jude Children's Research Hospital

Cytology

ASSOCIATE EDITOR

Antonio Cajigas, MD
Montefiore Medical Center

Hematology

ASSOCIATE EDITOR

Shiyong Li, MD, PhD
Emory University School of Medicine

ASSISTANT EDITORS

Elizabeth Courville, MD
University of Virginia School of Medicine

Alexandra E. Kovach, MD
Children's Hospital Los Angeles

Lisa Senzel, MD, PhD
Stony Brook Medicine

Histology

ASSOCIATE EDITOR

Carol A. Gomes, MS
Stony Brook University Hospital

STAFF

EXECUTIVE EDITOR FOR JOURNALS

Kelly Swails, MT(ASCP)

DIRECTOR OF SCIENTIFIC
PUBLICATIONS

Joshua Weikersheimer, PhD

SENIOR EDITOR, JOURNALS

Philip Rogers

Immunohematology

ASSOCIATE EDITOR

Richard Gammon, MD
OneBlood

ASSISTANT EDITORS

Phillip J. DeChristopher, MD, PhD
Loyola University Health System

Gregory Denomme, PhD
Grifols Laboratory Solutions

Amy E. Schmidt, MD, PhD
CSL Plasma

Immunology

ASSOCIATE EDITOR

Ruifeng Yang, MD, PhD
Nova Scotia Health

Laboratory Management and Administration

ASSOCIATE EDITOR

Lauren Pearson, DO, MPH
University of Utah Health

ASSISTANT EDITORS

Kayode Balogun, MD
Montefiore Medical Center

Vrajesh Pandya, MD
ARUP Laboratories

Microbiology

ASSOCIATE EDITOR

Yvette S. McCarter, PhD
University of Florida College of Medicine

ASSISTANT EDITORS

Alexander J. Fenwick, MD
University of Kentucky College of Medicine

Allison R. McMullen, PhD
Augusta University—Medical College of Georgia

Elitza S. Theel, PhD
Mayo Clinic

Molecular Pathology

ASSOCIATE EDITOR

Jude M. Abadie, PhD
Texas Tech University Health Science Center

ASSISTANT EDITORS

Holli M. Drendel, PhD
Atrium Health Molecular Pathology Laboratory

Rongjun Guo, MD, PhD
ProMedica Health System

Shuko Harada, MD
University of Alabama at Birmingham

Hongda Liu, MD, PhD
The First Affiliated Hospital of Nanjing Medical University

Pathologists' Assistant

ASSOCIATE EDITOR

Anne Walsh-Feeks, MS, PA(ASCP)
Stony Brook Medicine

Laboratory Medicine (ISSN 0007-5027), is published 6 times per year (bimonthly). Periodicals Postage paid at Chicago, IL and additional mailing offices. POSTMASTER: Send address changes to *Laboratory Medicine*, Journals Customer Service Department, Oxford University Press, 2001 Evans Road, Cary, NC 27513-2009.

SUBSCRIPTION INFORMATION: Annually for North America, \$182 (electronic) or \$241 (electronic and print); single issues for individuals are \$32 and for institutions \$71. Annually for Rest of World, £118/€167 (electronic) or £154/€220 (electronic and print); single issues for individuals are £21/€30 and for institutions £44/€63. All inquiries about subscriptions should be sent to Journals Customer Service Department, Oxford Journals, Great Clarendon Street, Oxford OX2 6DP, UK, Tel: +44 (0) 1865-35-3907, e-mail: jnl.cust.serv@oup.com. In the Americas, please contact Journals Customer Service Department, Oxford Journals, 4000 CentreGreen Way, Suite 310, Cary, NC 27513, USA. Tel: 800-852-7323 (toll-free in USA/Canada) or 919-677-0977, e-mail: jnlorders@oup.com.

MEMBERSHIP INFORMATION: The ASCP membership fees for pathologists are as follows: fellow membership is \$399; fellow membership plus 1-year unlimited online CE is \$529; 2-year fellow membership is \$749; and 2-year fellow membership plus 2-year unlimited online CE is \$1009. The ASCP membership fees for laboratory professionals are as follows: young professional membership is \$59; annual membership is \$119; annual membership plus 1-year unlimited online CE is \$158; 3-year membership is \$389. All inquiries about membership should be sent to American Society for Clinical Pathology, 33 West Monroe Street, Suite 1600, Chicago, IL 60603, Tel: 312-541-4999, e-mail: ascp@ascp.org.

CLAIMS: Publisher must be notified of claims within four months of dispatch/ order date (whichever is later). Subscriptions in the EEC may be subject to European VAT. Claims should be made to *Laboratory Medicine*, Journals Customer Service Department, Oxford University Press, 4000 CentreGreen Way, Suite 310, Cary, NC 27513, USA, Tel: 800-852-7323 (toll-free in USA/Canada) or 919-677-0977, e-mail: jnlorders@oup.com.

Laboratory Medicine is published bimonthly by Oxford University Press (OUP), on behalf of the ASCP, a not-for-profit corporation organized exclusively for educational, scientific, and charitable purposes. Devoted to the continuing education of laboratory professionals, *Laboratory Medicine* features articles on the scientific, technical, managerial, and educational aspects of the clinical laboratory. Publication of an article, column, or other item does not constitute an endorsement by the ASCP of the thoughts expressed or the techniques, organizations, or products described therein. *Laboratory Medicine* is indexed in the following: MEDLINE/PubMed, Science Citation Index, Current Contents—Clinical Medicine, and the Cumulative Index to Nursing and Allied Health Literature.

Laboratory Medicine is a registered trademark. Authorization to photocopy items for internal and personal use, or the internal and personal use of specific clients, is granted by ASCP Press for libraries and other users registered with the Copyright Clearance Center (CCC) Transactional Reporting Service, provided that the base fee of USD 15.00 per copy is paid directly to the CCC, 222 Rosewood Drive, Danvers, MA 01923, 978.750.8400. In the United States prior to photocopying items for educational classroom use, please also contact the CCC at the address above.

Printed in the USA

© 2024 American Society for Clinical Pathology (ASCP)

Advertising Sales Office Classified and Display Advertising

CORPORATE ADVERTISING

Jane Liss
732-890-9812
jliss@americanmedicalcomm.com

RECRUITMENT ADVERTISING

Lauren Morgan
267-980-6087
lmorgan@americanmedicalcomm.com

ASCP

Laboratory Medicine

33 West Monroe Street, Suite 1600
Chicago, IL 60603

T: 312-541-4999

F: 312-541-4750

OVERVIEW

- 1 **The Diagnostic Value of Circulating miR-29 Family for Digestive System Malignancies: A Meta-Analysis**
Shuhui Zou, Fei Chen, Liqin Zhang, Cong Liu, Huamin Chen

SCIENCE

- 8 **Interleukin 10, but not tumor necrosis factor-alpha, gene variations are associated with factor VII inhibitor development**
Nahid Ramezanzpour, Korosh Khanaki, Akbar Dorgalaleh, Mahmood Shams, Ali Elmi, Farhad Zaker
- 13 **Molecular diagnostic results of a nephropathy gene panel in patients with suspected hereditary kidney disease**
Ali Topak
- 20 **Bronchoalveolar lavage cytology in children with chronic unexplained cough and severely neurologically impaired children**
Ivan Pavić, Draženka Ezgeta Karačić, Iva Hojsak
- 27 **Quantitative Detection of House Dust Mites–Specific IgE by Light-Initiated Chemiluminescence Assay**
Xiaohui Yang, Lisheng Zheng, Yuanmin Sun, Xin Tan, Bei Zhang, Xue Li, Huiqiang Li
- 34 **Optimization of laboratory diagnosis of heparin-induced thrombocytopenia using HemosIL-AcuStar-HIT-IgG assay**
Catherine M. Tucker, Ruben Rhoades, Ruchika Sharma, Jerald Z. Gong
- 40 **Diagnostic value of dual-fluorescence staining in bacterial vaginosis**
Cui Li, Zhongliang Duan, Jing Zhang, Jing Gao, Chunmei Ying
- 45 **Vitamin D Status in Palindromic Rheumatism: A Propensity Score Matching Analysis**
Alireza Khabbazi, Maryam Mahmoudi, Kamal Esalatmanesh, Masoomeh Asgari-Sabet, Azam Safary
- 50 **Elevated methemoglobin levels in patients treated with high-dose hydroxocobalamin**
Martinus Dyrud, Jianli Niu, Lisa Kohler
- 56 **Quantitative Value of Bacteria Associated with Leukocytes in Differential Diagnosis of Lower Respiratory Tract Infection in Children, in Comparison to Sputum Culture and Procalcitonin**
Guoqiang Zhang, Yihui Yao, Ying Gao, Xiaolu Yu, Jiabin Fang

- 62 **Whole-exome sequencing reveals a likely pathogenic LMNA variant causing hypertrophic cardiomyopathy**
Mohammad Mahdavi, Neda Mohsen-Pour, Majid Maleki, Serwa Ghasemi, Avisā Tabib, Golnaz Houshmand, Niloofer Naderi, Tannaz Masoumi, Hamidreza Pouraliakbar, Samira Kalayinia
- 71 **Metagenomic next-generation sequencing for the identification of infections caused by Gram-negative pathogens and the prediction of antimicrobial resistance**
Yang-Hua Xiao, Zhao-Xia Luo, Hong-Wen Wu, De-Rong Xu, Rui Zhao
- 80 **Identification and analysis of a clinically isolated strain of *Halomonas* based on whole-genome sequencing and comparative genomics**
Pinjia Wang, Chengbin Xie
- 88 **Can lipid mediators and free fatty acids guide acute coronary syndrome diagnosis and treatment?**
Gulbahar Uzun, Aslıhan Unal, Ibrahim Basarici, Murathan Kucuk, Levent Donmez, Cahit Nacitarhan, Sebahat Özdem
- 96 **The value of metagenomic next-generation sequencing for the diagnosis of pulmonary tuberculosis using bronchoalveolar lavage fluid**
Jiali Gao, Lu Zhao, Gongqi Chen, Chunli Huang, Weiqiang Kong, Yuchen Feng, Guohua Zhen

CASE STUDY

- 103 **Digynic monoandric triploidy in the setting of recurrent pregnancy loss: a case report and literature review**
Caitlin Raymond, Song Han, Gengming Huang, Cecilia Clement, Harshwardhan Thaker, Jianli Dong
- 106 **Defect in Automated Antigen Excess Detection Discovered after Reviewing Serum Free Light Chain Results in Context with Clinical Findings**
Kriselle Maris Lao, Ashbita Pokharel, Mai Mohamed Mohamed Ibrahim Elziény, Elizabeth Sykes, Steven M. Truscott



ON THE COVER: House dust mites (HDMs) are a variety of species of nonparasitic mites that belong to the family Pyroglyphidae. HDM droppings contain several allergens, including the digestive enzyme peptidase, and tropomyosin, which is also responsible for shellfish allergy. Sensitized individuals may experience allergic symptoms that can vary from mild to severe, and HDM allergy is a common cause of asthma. Allergic triggers can be identified by several methods, including skin prick tests, challenge tests, and laboratory methods to detect antibodies involved in type 1 hypersensitivity. In this issue of *Laboratory Medicine*, Yang and coworkers describe a light-initiated chemiluminescence immunoassay to detect HDM-specific IgE antibodies.

The Diagnostic Value of Circulating miR-29 Family for Digestive System Malignancies: A Meta-Analysis

Shuhui Zou,^{1,a} Fei Chen,^{2,a} Liqin Zhang,¹ Cong Liu,¹ and Huamin Chen³ 

¹Department of Clinical Laboratory, Ganzhou People's Hospital and ²Department of Nuclear Medicine, Ganzhou Tumour Hospital, Ganzhou, China, ³Department of Gastrointestinal–Cancer Surgery, Second Affiliated Hospital of Hainan Medical College, Haikou, China. Corresponding author: Huamin Chen; min13876051215@163.com. ^aContributed equally.

Key words: digestive system malignant tumors, diagnostic performance, miR-29, colorectal cancer, diagnostic odds ratio, summary receiver operating characteristic

Abbreviations: CEA, carcinoembryonic antigen; CA15-3, cancer antigen 15-3; PRISMA, Preferred Reporting Items for Systematic Reviews and Meta-Analyses; TP, true-positive; FP, false-positive; FN, false-negative; TN, true-negative; QUADAS-2, Quality Assessment of Diagnostic Accuracy Studies–2; QC, quality control; PLR, positive likelihood ratio; NLR, negative likelihood ratio; DOR, diagnostic odds ratio; SROC, summary receiver operating characteristic; ESCC, esophageal squamous cell carcinoma; CCA, cholangiocarcinoma; CA19-9, carcinogenic antigen 19-9

Laboratory Medicine 2024;55:1-7; <https://doi.org/10.1093/labmed/lmad030>

ABSTRACT

Objective: To evaluate the diagnostic value of circulating microRNA-29 (miR-29) in digestive system malignant neoplasms by meta-analysis.

Methods: We searched the PubMed, Embase, Cochrane Library, and Web of Science to collect studies, published through September 2022, on the diagnostic value of miR-29 in digestive system tumors.

Results: We included 7 studies in this meta-analysis, including colorectal cancer, esophageal squamous cell carcinomas, and cholangiocarcinoma. The pooled sensitivity, specificity, positive likelihood ratio, negative likelihood ratio, and diagnostic odds ratio were 0.64 (95% CI, 0.53–0.74), 0.83 (0.60–0.94), 3.75 (1.42–9.91), 0.44 (0.31–0.61), and 8.63 (2.54–29.26), respectively. The area under the summary receiver operating characteristic curve was 0.75. The sensitivity of miR-29 derived from serum was higher than that of miR-29 derived from plasma for malignant digestive system tumors (0.71 vs 0.54; $P = .04$).

Conclusion: This meta-analysis suggests that the circulating miR-29 family has good diagnostic performance for digestive system malignant tumors, with moderate sensitivity and good specificity.

The common types of digestive system malignant tumors mainly include esophageal cancer, gastric cancer, pancreatic cancer, hepatocellular carcinoma (HCC), gallbladder cancer, and colorectal cancer (CRC). In particular, digestive system malignant tumors have a high incidence and mortality rate worldwide. According to the epidemiological survey data published in China in 2015,¹ malignant tumors of the digestive system are among the most common causes of death from malignant tumors in China, accounting for about half (gastric cancer, HCC, and esophageal cancer are the most common causes). Data from the American Cancer Epidemiology Survey showed that, in 2018, there were 319,160 new patients with digestive system malignant neoplasms. Moreover, 160,820 patients died of digestive system malignant neoplasms, accounting for about one-fourth of all cancer deaths.² Cancers of the digestive system, such as CRC, pancreatic cancer, and HCC, are the most lethal cancers after lung cancer.² Hence, malignant tumors of the digestive system seriously threaten human survival and health. Therefore, it is essential that these tumors be diagnosed early.

Histopathological examination is the criterion standard for the diagnosis of malignant tumors. However, its invasiveness and high cost restrict it to being widely used only in cancer diagnosis. At present, a variety of biomarkers, such as carcinoembryonic antigen (CEA), cancer antigen 15-3 (CA15-3), and AFP, have been used in the clinical diagnosis of digestive system malignant tumors, but the sensitivity and specificity of those tests are low.^{3,4} Therefore, it is still necessary to identify novel biomarkers with high diagnostic accuracy and which confer little or no trauma.

It is well known^{5–7} that miRNAs can broadly disrupt targeted mRNAs and functional target mRNAs in different cancers through multiple pathways. The miR-29 family contains 3 mature members (miR-29a, miR-29b, and miR-29c). An increasing number of study results have shown that the expression of the miR-29 family is decreased in various types of cancer (having the ability to inhibit tumorigenesis and metastasis), such as breast cancer, bladder cancer, and pancreatic cancer.

Although several studies^{8–14} have evaluated the diagnostic value of the miR-29 family as biomarkers for digestive system malignant neoplasms, the conclusions are quite different. Thus, it is difficult to accurately estimate the diagnostic value of miR-29 in any single study. Therefore, this study searched online databases to collect relevant literature on circulating miR-29 in the diagnosis of digestive system malignant neoplasms; with this information, we conducted a meta-analysis of the pooled sensitivity, specificity, area under the curve (AUC), etc. We used these data to accurately evaluate the diagnostic value of the circulating miR-29 family in digestive system malignant tumors. This meta-analysis was performed following the Preferred Reporting Items for Systematic Reviews and Meta-Analyses (PRISMA).¹⁵

Retrieval Strategy

We searched PubMed, Embase, the Web of Science, and the Cochrane Library to collect studies on the diagnosis of digestive system malignant neoplasms by the circulating miR-29 family. The retrieval time was from the establishment of each database through September 2022. The search keywords were miRNA-29, miR-29, microRNA-29, miRNA-29a, miR-29a, microRNA-29a, miR-NA-29b, miR-29b, microRNA-29b, miRNA-29c, miR-29c, microRNA-29c, cancer, tumor, carcinoma, neoplasm, and diagnosis. The records were searched by 2 investigators (S.Z. and F.C.) and then cross-checked. If disagreements arose, they were resolved through discussion, or a third researcher (L.Z.) decided. The search language was limited to English.

Inclusion and Exclusion Criteria

Inclusion criteria included diagnostic tests on the accuracy of the miR-29 family in the diagnosis of digestive system malignant neoplasms; true-positive (TP), false-positive (FP), false-negative (FN), and true-negative (TN) results of the miR-29 family only in the diagnosis of digestive system malignant tumors as calculated from the literature or based on data in the literature; blood specimens (serum or plasma); the diagnosis of cases as confirmed by the pathological criterion standard; and patients with tumors who have not undergone surgical procedures or chemoradiotherapy.

Exclusion criteria included reviews, letters, conference abstracts, animal experiments, and cell experiments; duplicate specimens; articles not published in English; and data provided in the literature that were insufficient to extract TP, FP, FN, and TN information.

Data Extraction

Data extraction was carried out by 2 researchers (L.Z. and C.L.), each working alone, and the third researcher (S.Z.) assisted in processing if there were differences in data inclusion. The extracted data included first author, year of publication, sex ratio, age of the members of the cancer group, country of residency, miRNA type, tumor type, specimen source, detection method, TNM stage of tumor, TP, FP, FN, and TN.

Document Quality Control

The Quality Assessment of Diagnostic Accuracy Studies–2 (QUADAS-2) tool was used for quality control (QC) of the included literature.¹⁶ The QUADAS-2 is a commonly used tool for quality evaluation of the diagnostic experimental literature, which is composed of 5 parts, namely, case selection, test to be evaluated, criterion standard, case process, and progress. The landmark issues in each section are evaluated for the risk of bias at 3, including “high,” “low,” and “unclear.”

Statistical Analysis

The combined sensitivity, specificity, positive likelihood ratio (PLR), negative likelihood ratio (NLR), and diagnostic odds ratio (DOR) were calculated by Stata 15 statistical software (StataCorp). Whether the summary receiver operating characteristic (SROC) curve was a typical “shoulder arm” shape was calculated; also, the Spearman correlation coefficient was used to determine whether there was a threshold effect in this meta-analysis. If $P > .05$ and the SROC curve did not show a typical “shoulder arm” shape, there was no threshold effect, and then the effect sizes could be combined.

I^2 statistics were used to estimate the heterogeneity among studies. A bivariate mixed-effects model was used for statistical analysis. The SROC curve

was drawn, with the AUC calculated. In addition, a Fagan nomogram plot was plotted. If $I^2 > 50\%$, or $P < .05$, significant interstudy heterogeneity was considered, and then meta-regression and subgroup analyses were used to explore the sources of heterogeneity. The analysis items of heterogeneity sources included country, tumor type, miRNA type, and specimen source. A Deeks funnel plot was used to detect publication bias. Finally, sensitivity analysis was carried out to verify the robustness of the conclusions.

Results

Literature Search Results

After the strict screening, a total of 7 studies were included in this meta-analysis^{8–14} (FIGURE 1). The identified study reports on digestive system malignant neoplasms included an article on esophageal squamous cell carcinoma (ESCC),¹³ another on cholangiocarcinoma (CCA),⁸ and 5 articles on CRC.^{9–12,14} Of those 7 articles, 3 also mentioned miR-29a,^{9,11,12} another 3 mentioned miR-29b,^{8,10,14} and 1 article mentioned miR-29c.¹³ The basic characteristics of the included studies are shown in TABLE 1. The quality assessment of the included literature is provided in FIGURE 2.

Heterogeneity Detection and Accuracy Evaluation of miR-29 Diagnosis

The results of heterogeneity analysis showed that sensitivity ($I^2 = 88.45\%$; $P < .01$), specificity ($I^2 = 95.57\%$; $P < .01$), PLR ($I^2 = 95.62\%$; $P < .01$), NLR ($I^2 = 93.07\%$; $P < .01$), and DOR ($I^2 = 100\%$; $P < .01$) showed significant heterogeneity. The Spearman correlation coefficient was -0.0857 ($P = .87$), and the SROC curve (FIGURE 3) did not show a typical “shoulder arm” shape, suggesting that the threshold effect was not significant.

The results of the bivariate mixed-effects model showed that the pooled sensitivity, specificity (FIGURE 4), PLR, NLR, and DOR were

FIGURE 1. Record retrieval process.

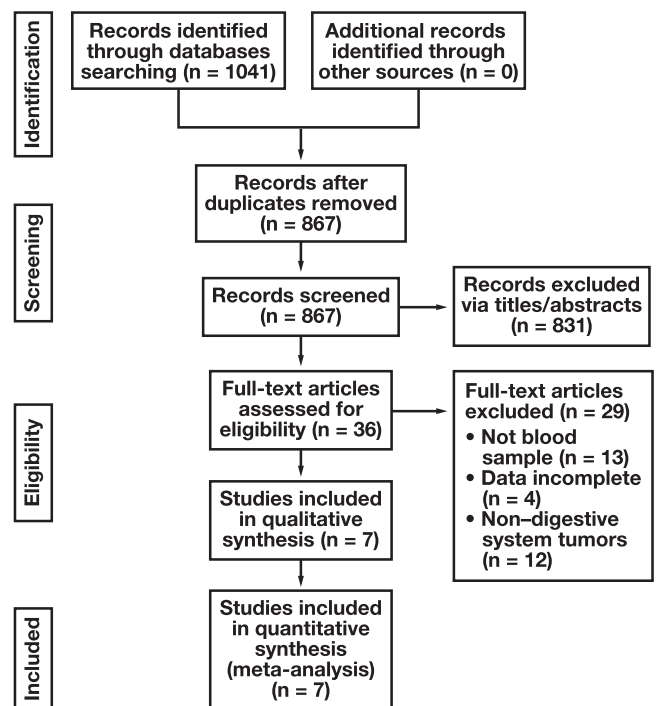


TABLE 1. Basic Characteristics of the Included Studies

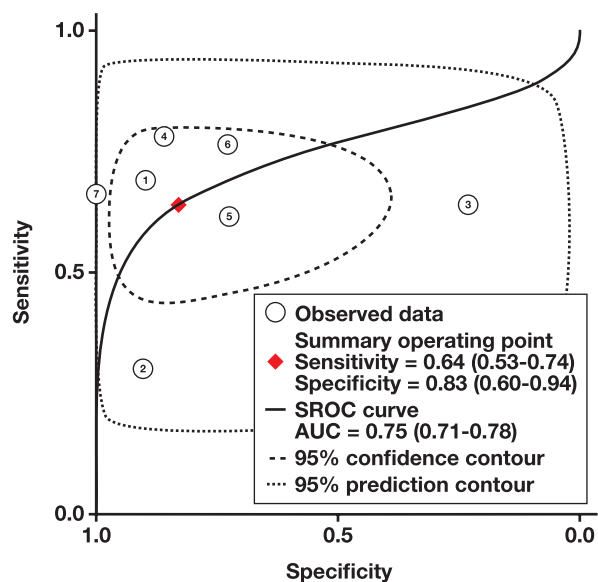
Study	Year	Country	Cancer Type	Sex Ratio (M/F)		TNM Staging	Age of Cancer Group Members (y)	PCR Method	miRNA Type	Specimen Source	TP	FP	FN	TN
				Cancer Group	Control Group									
Huang et al ¹¹	2010	China	CRC	51/49	31/28	I-IV	Mean (SD): 61 (11)	SYBR Green	miR-29a	Plasma	69	6	31	53
Luo et al ¹²	2013	China	CRC	45/35	60/84	I-IV	Mean (SD): 68.0 (10.7)	TaqMan	miR-29a	Plasma	24	14	56	130
Xu et al ¹³	2015	China	ESCC	27/23	30/20	I-IV	Not reported	TaqMan	miR-29c	Serum	39	7	11	43
Yamada et al ⁹	2015	Japan	CRC	93/43	23/29	Not reported	Median (range): 68 (37-86)	TaqMan	miR-29a	Serum	87	40	49	12
Basati et al ¹⁰	2016	Iran	CRC	30/25	31/24	I-IV	Mean (SD): 58.52 (10.02)	SYBR Green	miR-29b	Serum	42	15	13	40
Li et al ¹⁴	2016	China	CRC	135/65	283/117	I-IV	Mean (SD): 66.3 (11.8)	TaqMan	miR-29b	Plasma	123	110	77	290
Loosen et al ⁸	2019	Germany	CCA	54/40	31/9	I-IV	Median (range): 67 (37-84)	SYBR Green	miR-29b	Serum	62	0	32	40

CCA, cholangiocarcinoma; CRC, colorectal cancer; ESCC, esophageal squamous cell carcinoma; FN, false negative; FP, false positive; miRNA, micro RNA; TN, true positive; TP, true positive

FIGURE 2. Literature quality assessment according to QUADAS-2 (Quality Assessment of Diagnostic Accuracy Studies 2). + indicates high risk; -, low risk; ?, unclear.

	Risk of bias			Applicability concerns			
	Patient selection	Index test	Reference standard	Flow and timing	Patient selection	Index test	Reference standard
Huang et al ¹¹	?	+	+	+	+	+	+
Luo et al ¹²	+	+	+	+	+	+	+
Xu et al ¹³	+	+	+	+	+	+	+
Yamada et al ⁹	+	+	+	+	+	+	+
Basati et al ¹⁰	+	+	+	+	+	+	+
Li et al ¹⁴	+	+	+	+	+	+	+
Loosen et al ⁸	+	+	+	+	+	+	+

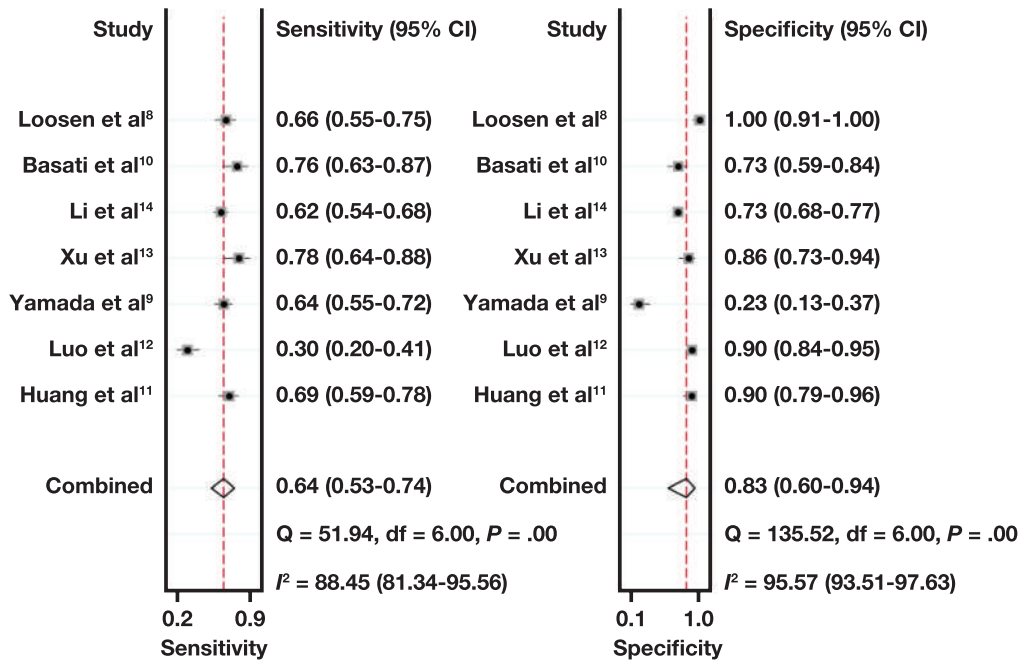
FIGURE 3. Summary ROC (SROC) curve of miR-29 for diagnosing digestive system malignant tumors.



0.64 (95% CI, 0.53-0.74), 0.83 (0.60-0.94), 3.75 (1.42-9.91), 0.44 (0.31-0.61), and 8.63 (2.54-29.26), respectively (TABLE 2). The AUC was 0.75 (0.71-0.78). Also, the Fagan plot (FIGURE 5) showed that when the current probability was 20%, the posttest probability of PLR was 48% and the posttest probability of NLR was 10%. Therefore, the circulating miR-29 family has good diagnostic value for digestive system malignant tumors.

Meta-Regression and Subgroup Analyses

Meta-regression and subgroup analyses were performed on 4 variables, including country of residency, tumor type, specimen source, and miRNA type. The results of the subgroup analysis (FIGURE 6) showed

FIGURE 4. Sensitivity and specificity of miR-29 for diagnosing digestive system malignant tumors.**TABLE 2.** Summary Diagnostic Value of miR-29 Family in Digestive System Malignant Neoplasms

Diagnostic Performance	<i>r</i>	<i>P</i> for <i>r</i>	Sensitivity (95% CI)	Specificity (95% CI)	PLR (95% CI)	NLR (95% CI)	DOR (95% CI)	AUC (95% CI)
miR-29	-0.0857	.8717	0.64 (0.53–0.74)	0.83 (0.60–0.94)	3.75 (1.42–9.91)	0.44 (0.31–0.61)	8.63 (2.54–29.26)	0.75 (0.71–0.78)

AUC, area under the curve; DOR, diagnostic odds ratio; NLR, negative likelihood ratio; PLR, positive likelihood ratio.

that the sensitivity of specimens derived from serum was significantly higher than that of specimens derived from plasma (0.71 vs 0.54; $P = .04$), and the specificity of ESCC and CCA was more than that of CRC (0.96 vs 0.74; $P = .02$). However, no variables were statistically significant in the meta-regression analysis. Therefore, specimen source and tumor type were likely to be the main sources of heterogeneity.

Publication Bias Test and Sensitivity Analysis

The Deeks funnel plot showed $P = .36$ (FIGURE 7), indicating no publication bias in this meta-analysis. Next, the graphical model was conducted for sensitivity analysis. The results showed that the residual basis of the model had a high fit (FIGURE 8A) and conformed to the bivariate normality assumption (FIGURE 8B). Further, influence analysis (FIGURE 8C) and outlier detection (FIGURE 8D) revealed that 1 study¹² might affect the robustness of the conclusion. The meta-analysis results after omitting this article showed that the pooled sensitivity, specificity, PLR, NLR, DOR, and AUC were 0.67 (95% CI, 0.62–0.72), 0.82 (0.53–0.94), 3.6 (1.2–11.1), 0.40 (0.30–0.56), 9 (2–37), and 0.69 (0.65–0.73), respectively. The AUC dropped from 0.75 to 0.69 after excluding this article,¹² showing a slight decline. Therefore, the findings obtained in this meta-analysis are slightly unstable.

Discussion

This study used meta-analysis to explore the diagnostic value of the circulating miR-29 family in digestive system malignant neoplasms. The results showed that the combined sensitivity and specificity of the miR-29 family in the diagnosis of digestive system malignant tumors were

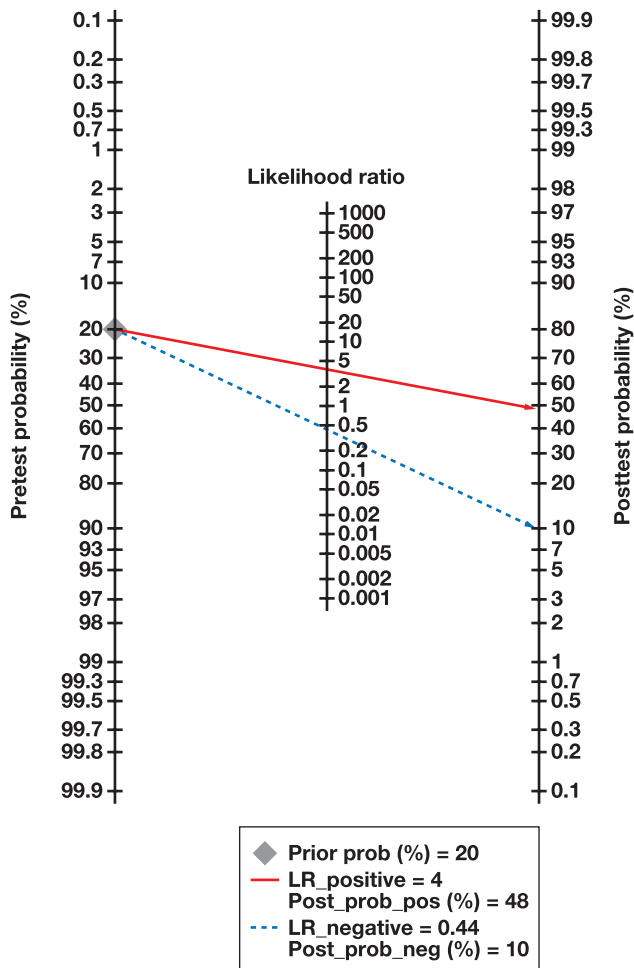
0.64 and 0.83, respectively, indicating that miR-29 had moderate sensitivity and good specificity in the diagnosis of digestive system malignant neoplasms.

The combined PLR of 3.75 indicated that the probability of a positive diagnosis via the diagnostic test was 3.75 times that of a false diagnosis. The combined NLR was 0.44, indicating that the probability of a false-negative result was 0.44 times that of a correct negative result, which reflected the high diagnostic value of this test. DOR is the association between the results of diagnostic experiments and diseases by combining sensitivity and specificity, and the larger value of DOR indicates the better recognition ability of diagnostic experiments.¹⁷ In the findings of this study, the DOR value was 8.63, which suggests that miR-29 could be used as a biomarker for the diagnosis of digestive system malignant neoplasms.

The Fagan plot showed that if the pretest probability of the miR-29 family in the diagnosis of digestive system malignant tumors was set at 20%, when the PLR was 3.75, the posttest probability was increased to 48%. When the NLR was 0.44, the posttest probability decreased to 10%.

AUC is an index used to evaluate the overall performance of diagnostic experiments. $AUC \geq 0.97$ indicates excellent diagnostic accuracy; $0.93 \leq AUC < 0.96$, very good diagnostic accuracy; $0.75 \leq AUC < 0.92$, good diagnostic accuracy; and $AUC < 0.75$, insufficient diagnostic accuracy.¹⁸ In this meta-analysis, the AUC was 0.75, indicating that the miR-29 family has good diagnostic accuracy for digestive system malignant tumors. The funnel plot showed that there was no significant publication bias in this meta-analysis. Sensitivity analysis showed that the results of 1 study¹² might have a great impact on the results. After the deletion of

FIGURE 5. Fagan nomogram plot of miR-29 for diagnosing digestive system malignant tumors. LR, likelihood ratio; neg, negative; prob, probability; pos, positive.



this study, the AUC decreased slightly, indicating that the conclusions obtained in this study are slightly unstable.

The Spearman correlation coefficient was -0.0857 , with $P = .87$, and the SROC curve did not show a typical “shoulder arm” shape, so the heterogeneity of the pooled effect size in this meta-analysis was not caused by the threshold effect. Therefore, meta-regression and subgroup analyses were used to explore the sources of heterogeneity. After grouping according to the 4 variables of country, tumor type, specimen source, and miRNA type, the differences were statistically significant only in the classification of specimen source and tumor type.

The specimens from serum were significantly more sensitive than those from plasma, and the specificity of ESCC and CCA were higher than that of CRC. When these 4 variables were entered into the meta-regression analysis, no variables were statistically significant. Therefore, specimen source and tumor type might be the main sources of heterogeneity in this meta-analysis. In order to obtain high sensitivity, serum can be preferred to detect the miR-29 family in the diagnosis of digestive system malignant neoplasms, which may be a better choice.

The miR-29 family showed not only diagnostic value but also prognostic value for digestive system malignant neoplasms. Inoue et al¹⁹ reported that miR-29b expression was an independent prognostic factor for disease-free survival and lymph node metastasis in CRC. Peng et al²⁰ also showed that the miR-29 family might become promising biomarkers for recurrence,

FIGURE 6. Meta-regression and subgroup analyses. * $P < .05$.

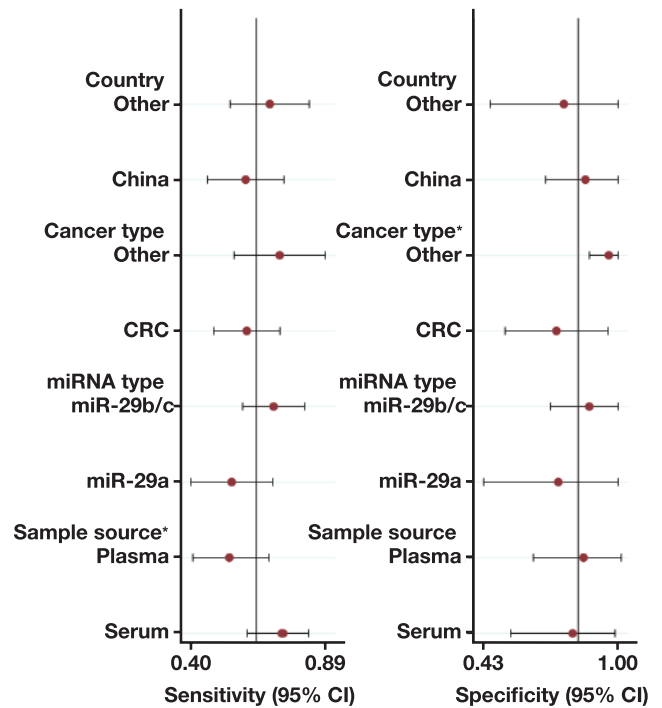
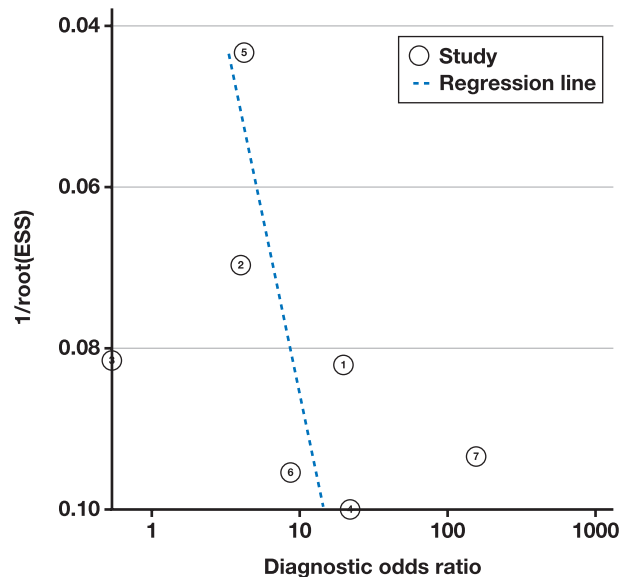


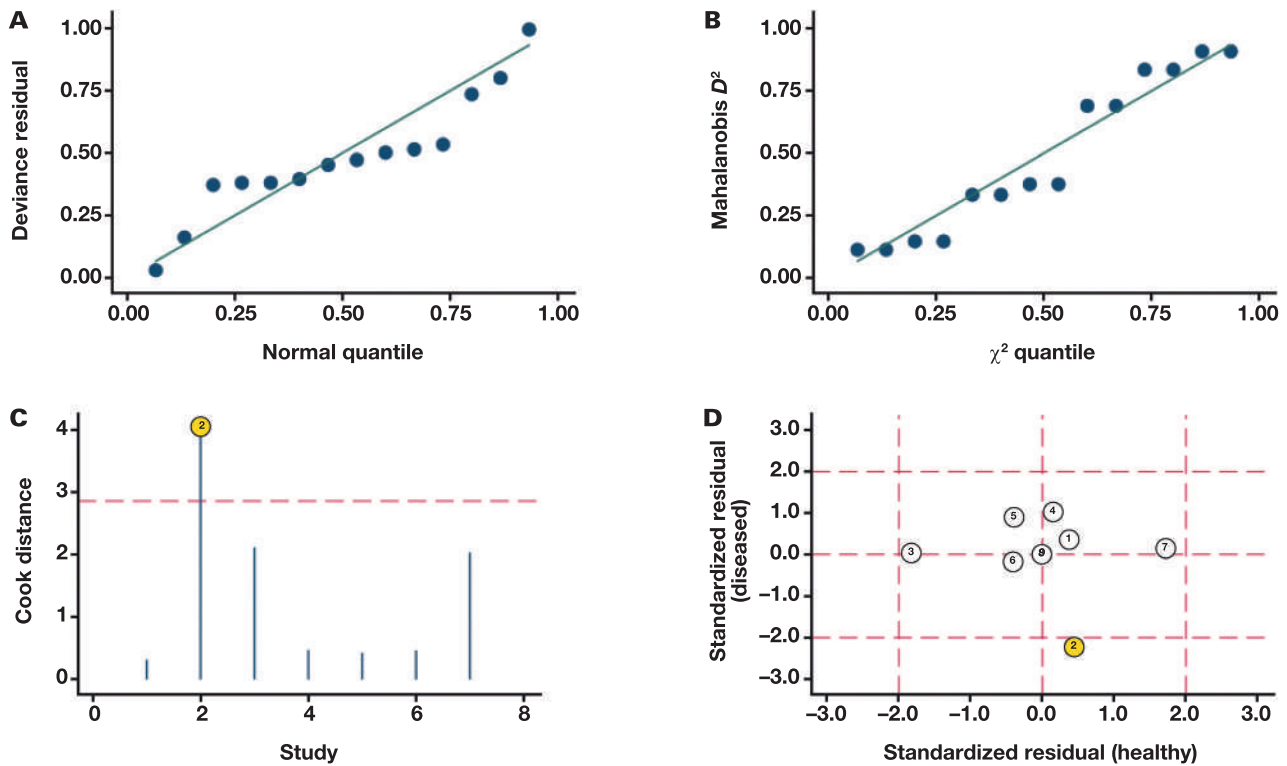
FIGURE 7. Deeks funnel plot asymmetry test to test publication bias ($P = .36$).



metastasis, and survival outcome in CRC. Xiong et al²¹ reported that miR-29 was involved in the regulation of apoptosis in HCC, which suggested the potential application of miR-29 in prognostic prediction.

This is the first meta-analysis in the literature to explore the diagnostic value of the miR-29 family in digestive system malignant tumors, having essential clinical significance. Kang et al²² reported that the AUCs of CEA and carcinogenic antigen 19-9 (CA19-9) in the diagnosis of CRC were 0.726 and 0.603, respectively, which were both lower than the AUC of 0.75 in the diagnosis of digestive system malignant neoplasms by the miR-29 family

FIGURE 8. Sensitivity analysis to verify the robustness of the conclusions. **A,** Goodness of fit. **B,** Bivariate normality. **C,** Influence analysis. **D,** Outlier detection.



in our meta-analysis. Huang et al¹¹ presented that the combined diagnosis of CRC with miR-29a and miR-92a showed an AUC of 0.883.

Inevitably, this meta-analysis has several limitations. First, there was large heterogeneity among studies when calculating the pooled effect size. Only 4 factors were included in the meta-regression and subgroup analyses. Limited information hindered our ability to identify more potential sources of heterogeneity. Second, the studies used different diagnostic cutoff values and tumor stages, which might be the sources of heterogeneity. Moreover, some articles did not report the cutoff values and tumor stage, so these variables could not be used as research factors in the meta-regression and subgroup analyses. Third, sensitivity analysis indicated that the conclusions of this study were slightly unstable. Fourth, the studies included in this meta-analysis did not include all types of digestive system malignant neoplasms.

The number of studies in some subgroups was small, which had certain limitations in evaluating the diagnostic value of the miR-29 family for different digestive system malignant neoplasms. In this study, we examined 5 articles on CRC, and only 2 articles we examined were on other digestive system malignant neoplasm, including ESCC and CCA. From the sources of heterogeneity analysis, we also discovered great differences in the diagnostic value of the miR-29 family for different malignant tumors of the digestive system. Therefore, future studies should focus on the diagnostic value of the miR-29 family for ESCC, CCA, pancreatic cancer, HCC, and other digestive system malignant neoplasms, to determine the differences in the diagnostic value of miR-29 for different types of digestive system malignant neoplasms.

In conclusion, this meta-analysis indicates that the miR-29 family has good diagnostic value for digestive system malignant tumors, with moderate sensitivity and good specificity. Moreover, specimens derived from serum are more sensitive than those derived from plasma in the diagnosis of

digestive system malignant neoplasms using the circulating miR-29 family. Due to the large heterogeneity and the limited number of studies, prospective studies with large specimen sizes are needed to verify the diagnostic value of the miR-29 family in digestive system malignant neoplasms in the future.

Conflict of Interest Disclosure

The authors have nothing to disclose.

REFERENCES

- Chen W, Zheng R, Baade PD, et al. Cancer statistics in China, 2015. *CA Cancer J Clin.* 2016;66(2):115–132. doi:10.3322/caac.21338
- Siegel RL, Miller KD, Jemal A. Cancer statistics, 2018. *CA Cancer J Clin.* 2018;68(1):7–30. doi:10.3322/caac.21442
- He C-Z, Zhang K-H, Li Q, Liu X-H, Hong Y, Lv N-H. Combined use of AFP, CEA, CA125 and CA19-9 improves the sensitivity for the diagnosis of gastric cancer. *BMC Gastroenterol.* 2013;13(1):87. doi:10.1186/1471-230X-13-87
- Lu D-C, Zhang Q-F, Li L, et al. Methylated Septin9 has moderate diagnostic value in colorectal cancer detection in Chinese population: a multicenter study. *BMC Gastroenterol.* 2022;22(1):232. doi:10.1186/s12876-022-02313-x
- Wu Z, Huang X, Huang X, Zou Q, Guo Y. The inhibitory role of Mir-29 in growth of breast cancer cells. *J Exp Clin Cancer Res.* 2013;32(1):98. doi:10.1186/1756-9966-32-98
- Lv M, Zhong Z, Huang M, et al. lncRNA H19 regulates epithelial-mesenchymal transition and metastasis of bladder cancer by miR-29b-3p as competing endogenous RNA. *Biochim Biophys Acta - Mol Cell Res.* 2017;1864(10):1887–1899. doi:10.1016/j.bbmr.2017.08.001

7. Kwon JJ, Willy JA, Quirin KA, et al. Novel role of miR-29a in pancreatic cancer autophagy and its therapeutic potential. *Oncotarget*. 2016;7(44):71635–71650. doi:10.18632/oncotarget.11928
8. Loosen SH, Lurje G, Wiltberger G, et al. Serum levels of miR-29, miR-122, miR-155 and miR-192 are elevated in patients with cholangiocarcinoma. *PLoS One*. 2019;14(1):e0210944. doi:10.1371/journal.pone.0210944
9. Yamada A, Horimatsu T, Okugawa Y, et al. Serum miR-21, miR-29a, and miR-125b are promising biomarkers for the early detection of colorectal neoplasia. *Clin Cancer Res*. 2015;21(18):4234–4242. doi:10.1158/1078-0432.CCR-14-2793
11. Huang Z, Dan H, Ni S, et al. Plasma microRNAs are promising novel biomarkers for early detection of colorectal cancer. *Int J Cancer*. 2010;127(1):118–126. doi:10.1002/ijc.25007
12. Luo X, Stock C, Burwinkel B, Brenner H. Identification and evaluation of plasma microRNAs for early detection of colorectal cancer. *PLoS One*. 2013;8(5):e62880. doi:10.1371/journal.pone.0062880
13. Xu H, Yao YF, Meng FY, et al. Predictive value of serum miR-10b, miR-29c, and miR-205 as promising biomarkers in esophageal squamous cell carcinoma screening. *Medicine*. 2015;94(44):e1558. doi:10.1097/MD.0000000000001558
14. Li L, Guo Y, Chen Y, et al. The diagnostic efficacy and biological effects of microRNA-29b for colon cancer. *Technol Cancer Res Treat*. 2015;15(6):772–779. doi:10.1177/1533034615604797
15. Moher D, Liberati A, Tetzlaff J, Altman DG; for the PRISMA Group. Preferred reporting items for systematic reviews and meta-analyses: the PRISMA statement. *BMJ*. 2009;339. doi: 10.1136/bmj.b2535
16. Whiting PF, Rutjes AWS, Westwood ME, et al; QUADAS-2 Group. QUADAS-2: a revised tool for the quality assessment of diagnostic accuracy studies. *Ann Intern Med*. 2011;155(8):529–536. doi:10.7326/0003-4819-155-8-201110180-00009
17. Glas AS, Lijmer JG, Prins MH, Bossuyt PMM. The diagnostic odds ratio: a single indicator of test performance. *J Clin Epidemiol*. 2003;56(11):1129–1135. doi:10.1016/S0895-4356(03)00177-X
18. Walter S. Properties of the summary receiver operating characteristic (SROC) curve for diagnostic test data. *Stat Med*. 2010;21(9):1237–1256. doi:10.1002/sim.1099
19. Inoue A, Yamamoto H, Uemura M, et al. MicroRNA-29b is a novel prognostic marker in colorectal cancer. *Ann Surg Oncol*. 2015;22(suppl 3):S1410–S1418.
20. Peng Q, Feng Z, Shen Y, et al. Integrated analyses of microRNA-29 family and the related combination biomarkers demonstrate their widespread influence on risk, recurrence, metastasis and survival outcome in colorectal cancer. *Cancer Cell Int*. 2019;19:181. doi:10.1186/s12935-019-0907-x
21. Xiong Y, Fang J-H, Yun J-P, et al. Effects of microRNA-29 on apoptosis, tumorigenicity, and prognosis of hepatocellular carcinoma. *Hepatology*. 2010;51(3):836–845. doi:10.1002/hep.23380
22. Kang Y, Zhu X, Lin Z, et al. Compare the diagnostic and prognostic value of MLR, NLR and PLR in CRC patients. *Clin Lab*. 2021;67(9). doi:10.7754/Clin.Lab.2021.201130

Interleukin 10, but not tumor necrosis factor-alpha, gene variations are associated with factor VII inhibitor development

Nahid Ramezanzpour, MS,¹ Korosh Khanaki, PhD,^{2,3} Akbar Dorgalaleh, PhD,⁴ Mahmood Shams, PhD,⁵ Ali Elmi, PhD,² Farhad Zaker, MS¹

¹Department of Hematology and Blood Transfusion, School of Allied Medicine, Iran University of Medical Sciences, Tehran, Iran, ²Department of Laboratory Sciences, School of Paramedicine, Guilan University of Medical Sciences, Rasht, Iran, ³Department of Clinical Biochemistry, School of Medicine, Guilan University of Medical Sciences, Rasht, Iran, ⁴Hamin Tis Research Institute, Tehran, Iran, ⁵Cellular and Molecular Biology Research Center, Health Research Institute, Babol University of Medical Sciences, Babol, Iran. Corresponding author: Farhad Zaker; zaker.f@iums.ac.ir.

Key words: inhibitor development; factor VII deficiency; gene variant; cytokine; IL-10; TNF α .

Abbreviations: IL, interleukin; TNF, tumor necrosis factor; FVII, coagulation factor VII; RT, replacement therapy; Ig, immunoglobulin;

Laboratory Medicine 2024;55:8-12; <https://doi.org/10.1093/labmed/lmad026>

ABSTRACT

Objective: Development of alloantibodies against coagulation factor VII (FVII) is the main therapeutic challenge in severe congenital FVII deficiency. About 7% of patients with severe congenital FVII deficiency develop an inhibitor against FVII. In this research, the relationship between interleukin (IL)-10 and tumor necrosis factor-alpha (TNF)- α gene variants and inhibitor development was evaluated for a group of Iranian patients with severe congenital factor VII deficiency.

Methods: Patients with FVII deficiency were divided into 2 groups: 6 cases and 15 controls. Genotyping was performed using the amplification-refractory mutation system polymerase chain reaction.

Results: We found that IL-10 rs1800896 A>G gene variant is associated with the risk of FVII inhibitor development (OR = 0.077, 95% CI = 0.016–0.380, $P = .001$), whereas the TNF α -rs1800629G>A variant has no relation with inhibitor development in severe FVII deficiency.

Conclusion: The results show that the IL-10 rs1800896 A>G variant increases the risk of developing an inhibitor in patients with severe congenital FVII deficiency.

Introduction

Congenital factor (F) VII deficiency is a rare coagulation factor deficiency with an estimated prevalence of 1 per 500,000 individuals.¹ As with other autosomal disorders, congenital FVII deficiency is a common disease in societies with a high prevalence of consanguineous marriages.² Patients with severe congenital FVII deficiency (FVIIC <10%) indicate a wide spectrum of clinical symptoms, such as gastrointestinal bleeding, hematoma, hemarthrosis, menorrhagia, and intracranial hemorrhage.^{3–5}

The main treatment option for patients who are suffering from inherited FVII deficiency is replacement therapy (RT). However, the formation of alloantibodies to exogenous FVII is the major treatment challenge that can reduce the efficacy of RT.^{6,7} Inhibitor development is a very rare phenomenon but it is associated with a high prevalence of life-threatening bleeding.² Three available reports showed that anti-FVII alloantibodies are polyclonal and heterogeneous (different immunoglobulin [Ig] IgG subclasses involved), with 2 of these reports showing predominance of the IgG1 subclass,^{8,9} whereas the third suggested the predominance of the IgG4 subclass.¹⁰

The two important cytokines, interleukin (IL-10) and tumor necrosis factor-alpha (TNF α) play vital roles in the immunological balance of the human body.¹¹ The TNF α cytokine is an important mediator that has potent proinflammatory activity and shows immunomodulatory activities. Gene variants in the *TNF α* gene have been linked with autoimmune disorders. The TNF α _308A allele or other *TNF α* gene variants may increase the possibility of inhibitor development.¹² Moreover, TNF α contributes to the development of edema and vasodilatation, leukocyte adhesion to the epithelium through the expression of adhesion molecules, regulation of blood coagulation, oxidative stress at sites of inflammation, and indirect induction of fever.¹³ Furthermore, IL-10 is known as an important anti-inflammatory cytokine that enhances in vitro synthesis of all type of immunoglobulins by peripheral blood mononuclear cells in patients with systemic lupus erythematosus.^{14,15} Moreover, the IL-10 gene promoter region has various haplotypes that are related to a high- or low-level production of this cytokine. Interleukin-10 is essential to control host immune response to infections, prevent host injury, and preserve healthy tissue homeostasis. Increased immunopathology in response to infection and a higher risk of developing various autoimmune disorders are both linked to IL-10 dysregulation.¹⁶

TABLE 1. Primers and PCR conditions

Primers	Sequence	Number of cycles	Annealing temperature (°C)	First denaturation time/temperature	Last denaturation time/temperature	First elongation time/temperature	Last elongation time/temperature
Forward G allele (IL-10)	5'-TACTAAGGCTTCTTTGGGAG-3'	35	65	10 min/95°C	30 s/95°C	1 min/72°C	5 min/72°C
Common reverse (IL-10)	5'-CAGCCCTCCATTTACTTTC-3'	35	65	10 min/95°C	30 s/95°C	1 min/72°C	5 min/72°C
Forward A allele (IL-10)	5'-ACTACTAAGGCTTCTTTGGGAA-3'	35	65	10 min/95°C	30 s/95°C	1 min/72°C	5 min/72°C
Forward G allele (TNF α)	5'-ATAGGTTTTGAGGGGCATCG-3'	35	59.5	10 min/95°C	30 s/95°C	1 min/72°C	5 min/72°C
Common reverse (TNF α)	5'-AAGAATCATTCAACCAGCGG-3'	35	59.5	10 min/95°C	30 s/95°C	1 min/72°C	5 min/72°C
Forward A allele (TNF α)	5'ATAGGTTTTGAGGGGCATCA-3'	35	59.5	10 min/95°C	30 s/95°C	1 min/72°C	5 min/72°C

PCR, polymerase chain reaction; TNF α , tumor necrosis factor- α .

TABLE 2. Patients' demographic information

FVII inhibitor titer (Bethesda unit/mL)	FVII: C	Sex	Patient
170	<1	Male	1
12	<1	Male	2
2	<1	Male	3
3	<1	Male	4
6	<1	Female	5
5	<1	Female	6

Genetic and nongenetic factors can influence patient immune system response to exogenous coagulation factors, and the secretion of 2 aforementioned cytokines might be affected by these genetic factors.^{11,12} Normal gene variation, specifically in the promoter region of IL-10 and TNF α , can decrease or increase the secretion of these cytokines.⁵ Interleukin-10 and TNF α cytokines are the 2 most important factors associated with inhibitor development in coagulation factor deficiencies such as factor VIII.¹² Hence, this study tries to shed light on the relationship of those cytokines with inhibitor development in FVII deficiency. To the best of our knowledge, this is the first research that investigates such a relationship.

Iran has high rates of congenital FVII deficiency with life threatening bleeding. Molecular studies of the development of FVII inhibitor are needed to detect carriers and thereby prevent fatal consequences.¹⁷ This study evaluates the effect of IL-10 and TNF α gene variants on inhibitor development in patients with severe inherited FVII deficiency.

Materials and Methods

Subjects

This study included 21 patients with severe congenital FVII deficiency who were classified into 2 subgroups: the case group (n = 6, patients with inhibitor) and the control group (n = 15, patients without inhibitor). In our study, using patients' medical records, we collected data including ethnicity, FVII coagulation activity, inhibitor history, inhibitor titer in the Bethesda unit (BU), and familial history.

This study was licensed by the Ethical Committee of Iran University of Medical Sciences with the code of IR.IUMS.REC.1400.193.

Methods

In this study, we used subject blood samples in tubes containing K3-EDTA for DNA extraction and genotyping of the samples. The standard coagulation methods were performed on blood samples that contain 3.8% trisodium citrate, and then prothrombin time was used to measure the procoagulant activity of FVII. The FVII inhibitor titer was obtained using the modified Bethesda assay that was based on the well-known Nijmegen technique. We divided subjects into 2 groups based on their inhibitor titer; the first group was patients who had an inhibitor titer >5 BU/mL and the second group was patients with inhibitor titer <5 BU/mL.

DNA Extraction and Polymerase Chain Reactions

Genomic DNA was extracted from 3.8% trisodium citrate-preserved blood using Yekta Tajhiz Azma genomic DNA mini kit (FavorGen Biotech). Agarose gel electrophoresis and a spectrophotometer were used to measure quality and quantity, respectively, of the extracted DNA. Patients were genotyped for the IL-10 rs1800896 A>G and TNF-rs1800629 G>A variations using the amplification-refractory mutation system. To confirm the results, some samples were selected for Sanger sequencing (3130XL, Applied Biosystems-ABI) and the raw data were analyzed using Chromas software. Primers and polymerase chain reaction (PCR) conditions are listed in **TABLE 1**.

Statistical Analysis

The χ^2 analysis was used to investigate the frequency of alleles, quantitative variables, and the percentages in patients with severe congenital FVII deficiency with or without inhibitor. Results were presented as mean \pm SD for categorical variables. Logistic regression analysis was conducted to determine and adjust the association between genotypes and the risk of inhibitor formation. All *P* values were 2-sided; a *P* < .05 was considered to show statistical significance. All statistical analysis was performed using SPSS 23 software. Moreover, we examined the Hardy-Weinberg equilibrium between the case and control groups and in the entire study population. The significance level of .05 for 1 degree of freedom, that is, 3.84, was used as the cutoff value. Hardy-Weinberg equilibrium is found in populations with $\chi^2 < 3.84$.

TABLE 3. Association between IL-10 rs1800896 gene variants and the risk of inhibitor development in patients with severe congenital factor VII deficiency

	Case, n (%)	Control, n (%)	OR (95% CI)	P value	χ^2
IL-10 rs1800896 A>G					
AA	1 (16.7)	11 (73.3)	13.750 (1.207–156.649)	.015	5.619
AG	2 (33.3)	4 (26.7)	0.727 (0.094–5.633)	.762	0.093
GG	3 (50)	0 (0)	Cannot be calculated		
Allele					
A	4 (33.3)	26 (86.7)	13.000 (2.634–64.161)	.001	11.947
G	8 (66.7)	4 (13.3)	0.077 (0.016–0.380)	.001	11.947

TABLE 4. Association between TNF α rs1800629 gene variant and the risk of inhibitor development in patients with severe congenital factor VII deficiency

	Case, n (%)	Control, n (%)	OR (95% CI)	P value	χ^2
TNF α rs1800629 G>A					
GG	4 (66.7)	11 (73.3)	1.375 (0.178–10.650)	.762	0.093
AG	2 (33.3)	4 (26.7)	0.727 (0.094–5.633)	.762	0.093
AA	0 (0)	0 (0)	Cannot be calculated		
Allele					
G	10 (83.3)	26 (86.7)	1.300 (0.205–8.247)	.783	0.078
A	2 (16.7)	4 (33.3)	0.769 (0.121–4.880)	.783	0.078

TNF α , tumor necrosis factor-alpha.

TABLE 5. Calculation of Hardy-Weinberg equilibrium in the entire study population, including case and control groups

	Genotype	Case (n = 6)			Control (n = 15)			Total (n = 22)		
		Expected	Observed	χ^2	Expected	Observed	χ^2	Expected	Observed	χ^2
TNF α rs1800629 G>A	GG	4.17	4	0.24	11.27	11	0.355	16.41	16	0.548
	AG	1.67	2		3.47	4		5.18	6	
	AA	0.17	0		0.27	0		0.41	0	
IL-10 rs1800896 A>G	AA	0.67	1	0.375	11.27	11	0.355	12.50	12	0.72
	AG	2.67	2		3.47	4		5	6	
	GG	2.67	3		0.27	0		0.5	3	

TNF α , tumor necrosis factor-alpha.

Results

The study population included 6 patients with inhibitor and a mean age of 18.33 \pm 8.66 years (maximum: 31 years, minimum: 7 years) and 15 patients without inhibitor with a mean age of 20.46 \pm 9.62 years (maximum: 41 years, minimum: 10 years). The study population included 10 females and 11 males. For the case group, the mean inhibitor level was 33 \pm 4.8 IU (ranging from 2 IU to 170 IU). There were 3 patients (1, 2, and 5) who had high titer inhibitor (inhibitor titer > 5 BU/mL). Patient demographic information is shown in **TABLE 2**. Statistical analysis revealed that the rs1800896 A>G variant in IL-10 increases the proportions of individuals that form an inhibitor. The frequency of the G allele (mutant allele) in the case group was 66.7% (OR = 0.077, 95% CI = 0.016–0.380, P = .001) (**TABLE 3**). The obtained results showed that the TNF α variant rs1800629 G>A was not associated with the risk of inhibitor development in patients with severe congenital FVII deficiency (**TABLE 4**).

Hardy-Weinberg Equilibrium

The Hardy-Weinberg equilibrium results show that the study population for TNF rs1800629 G>A (χ^2 = 0.54) and IL-10 rs1800896 A>G (χ^2 = 0.72) is in equilibrium (**TABLE 5**).

Discussion

The development of an inhibitor of a clotting factor increases morbidity and mortality rates, places an emotional and social burden on patients and their families, increases the cost of treatment, and creates problems for treatment planning. For patients who are suffering from acquired coagulation factor deficiencies with inhibitor, the best treatment options are intravenous immunoglobulin, immunosuppression treatment options, and cyclophosphamide, whereas for patients with congenital coagulation factor deficiencies with inhibitor the best treatment options for RT are plasma-derived FVII, fresh frozen plasma, prothrombin

complex concentrate, and recombinant factor VIIa.^{6,18–20} The mainstay treatment option for patients with severe factor VII deficiency is RT, but developing of inhibitory alloantibodies against the FVII is a significant challenge for RT in these patients. Patients with FVII deficiency and FVII inhibitor have a high rate of severe, potentially fatal bleeding, such as intracranial hemorrhage, which occurs in 60% of patients with FVII inhibitor. However, less than 10% of patients without inhibitor experience severe bleeding.²

According to a systematic literature review, the incidence of FVII inhibitors in patients with inherited FVII deficiency is approximately 7%.² Inhibitor development appears to exacerbate bleeding symptoms in FVII deficiency. Moreover, according to the study of Eshghi et al,²¹ inhibitor formation complicates the treatment and management of bleeding, as is the case with other factor deficiencies, with a higher incidence of treatment failure and subsequent death. The major goals of treatment are to eliminate the inhibitor and control bleeding; the management of bleeding in patients with inhibitor is a complex process.⁶ According to the literature,² virtually all patients with FVII inhibitor had severe FVII deficiency. Exogenous injected factor is more likely to be recognized by a patient's immune system as an antigen that triggers an immunologic response and antibody production. Because of these patients' higher bleeding rate, they are also more likely to receive more RT. Studies on the nature of FVII inhibitors all agreed that it is a polyclonal immune response in which IgG1 or IgG4 subclasses predominate.^{2,8–10}

Unlike classical hemophilia, there has been no study on the association between gene variants and inhibitor development in patients with hereditary FVII deficiency and, to the best of our knowledge, our research is the first to investigate this association. In this study, we found that patients with severe congenital FVII deficiency have a significantly higher risk of developing inhibitor associated with the IL-10 rs1800896 A>G gene variation. However, given the small sample size of our study, further studies on a large number of patients are needed to support this finding. Variations in immunoregulatory genes have been found to have a strong association with the risk of inhibitor development in other factor deficiencies such as factor VIII.^{12,22–24} Some of these genes, including *IL-10* and *TNF*, have an increased risk of inhibitor formation. However, it should be mentioned that the process of inhibitor formation involves multiple variables and can be influenced by a variety of events. Identification of these risk variables may help to improve the care of individuals with severe congenital factor VII deficiency.^{6,7} Although relatively rare, congenital FVII deficiency can lead to the formation of inhibitors that can cause life-threatening bleeding. This presents a major treatment challenge that can have catastrophic consequences. Understanding the many elements of inhibitor formation, such as the relationship between some variations and inhibitor production, may help researchers to treat this potentially fatal condition and prevent inhibitor formation.

Conclusions

The effect of IL-10 and TNF α gene variants on inhibitor development in a group of patients with severe inherited FVII deficiency has been evaluated in this study. The results showed that the IL-10 rs1800896 A>G gene variant can considerably enhance the chance of inhibitor development in Iranian patients with severe congenital FVII deficiency. However, further research in a larger study population is necessary to support this finding.

Acknowledgments

The authors highly appreciate the help of Vice Chancellor for Research and Technology of Iran University of Medical Science to support this study by their source of funding.

Conflict of Interest Disclosure

The authors have nothing to disclose.

REFERENCES

1. See WS, Chang KO, Cheuk DK, et al. Inhibitor development after liver transplantation in congenital factor VII deficiency. *Haemophilia*. 2016;22(5):e417–e422. doi:10.1111/hae.13047.
2. Ramezanpour N, Zaker F, Biswas A, Dorgalaleh A. Inhibitor in congenital factor VII deficiency; a rare but serious therapeutic challenge—a systematic literature review. *J Clin Med*. 2021;10(2):211. doi:10.3390/jcm10020211.
3. Shams M, Dorgalaleh A, Safarian N, et al. Inhibitor development in patients with congenital factor VII deficiency, a study on 50 Iranian patients. *Blood Coagul Fibrinolysis*. 2019;30(1):24–28. doi:10.1097/MBC.0000000000000791.
4. Qu C, Liu W, Chen L, Zhang L, Xue F, Yang R. Factor VII deficiency in China: phenotype, genotype and current status of management. *Br J Haematol*. 2023;200(3):344–352. doi:10.1111/bjh.18514.
5. Ravanbod S, Faranoush M, Changi-Ashtiani M, Rokni-Zadeh H, Shahani T. Extensive genetic screening of Iranian FVII deficient individuals unraveled several novel mutations and postulated founder effects in some cases. *Res Pract Thromb Haemost*. 2023;7(1):100003. doi:10.1016/j.rpth.2022.100003.
6. Dorgalaleh A, Tabibian S, Hosseini MS, Shams M. Pharmacological management of rare coagulation factor deficiencies besides hemophilia. *Expert Rev Hematol*. 2020;13(8):811–834. doi:10.1080/17474086.2020.1796622.
7. Chuansumrit A, Parapakpenjune S, Natesirinikul R, et al. Phenotypic and genotypic analysis of patients with congenital factor VII deficiency in a multicenter study in Thailand. *Pediatr Hematol Oncol J*. 2022;7(4):130–135.
8. Borhany M, Delbes C, Giansily-Blaizot M, et al. A new report of FVII-inhibitor in a patient suffering from severe congenital FVII deficiency. *Haemophilia*. 2015;21(4):e336–e338. doi:10.1111/hae.12708.
9. Branchini A, Baroni M, Pfeiffer C, et al. Coagulation factor VII variants resistant to inhibitory antibodies. *Thromb Haemost*. 2014;112(5):972–980. doi:10.1160/TH14-03-0198.
10. Tokgoz H, Caliskan U, Lavigne-Lissalde G, Giansily-Blaizot M. Successful prophylactic use of recombinant activated factor VII (rFVIIa) in a patient with congenital FVII deficiency and inhibitors to FVII. *Haemophilia*. 2012;18(1):e25–e27. doi:10.1111/j.1365-2516.2011.02666.x.
11. Soori S, Dadashzadeh G, Dorgalaleh A, et al. Relationship between single-nucleotide polymorphisms of tumor necrosis factor alpha, interleukin-10, factor II and factor V with risk of inhibitor development in patients with severe hemophilia A. *Cardiovasc Hematol Disord Drug Targets*. 2019;19(3):228–232. doi:10.2174/1871529X19666190206152315.
12. Astermark J, Oldenburg J, Carlson J, et al. Polymorphisms in the TNFA gene and the risk of inhibitor development in patients with hemophilia A. *Blood*. 2006;108(12):3739–3745. doi:10.1182/blood-2006-05-024711.
13. Iyer SS, Cheng G. Role of interleukin 10 transcriptional regulation in inflammation and autoimmune disease. *Crit Rev Immunol*. 2012;32(1):23–63. doi:10.1615/critrevimmunol.v32.i1.30.
14. Astermark J, Oldenburg J, Pavlova A, Berntorp E, Lefvert AK; MIBS Study Group. Polymorphisms in the IL10 but not in the IL1beta and IL4 genes are associated with inhibitor development in patients

- with hemophilia A. *Blood*. 2006;107(8):3167–3172. doi:10.1182/blood-2005-09-3918.
15. Houssiau FA, Lefebvre C, Vanden Berghe M, Lambert M, Devogelaer JP, Renauld JC. Serum interleukin 10 titers in systemic lupus erythematosus reflect disease activity. *Lupus*. 1995;4(5):393–395. doi:10.1177/096120339500400510.
 16. Zelová H, Hošek J. TNF- α signalling and inflammation: interactions between old acquaintances. *Inflamm Res*. 2013;62(7):641–651. doi:10.1007/s00011-013-0633-0.
 17. Dorgalaleh A, Alavi SER, Tabibian S, et al. Diagnosis, clinical manifestations and management of rare bleeding disorders in Iran. *Hematology*. 2017;22(4):224–230. doi:10.1080/10245332.2016.1263007.
 18. Collins P, Baudo F, Knoebl P, et al; EACH2 registry collaborators. Immunosuppression for acquired hemophilia A: results from the European Acquired Haemophilia Registry (EACH2). *Blood*. 2012;120(1):47–55. doi:10.1182/blood-2012-02-409185.
 19. Malhotra U, Aboulafia DM. Cyclophosphamide treatment for acquired factor viii inhibitor in a patient with AIDS-associated progressive multifocal leukoencephalopathy. *J Int Assoc Provid AIDS Care*. 2016;15(2):109–113. doi:10.1177/2325957415586259.
 20. Yamamoto K, Takamatsu J, Saito H. Intravenous immunoglobulin therapy for acquired coagulation inhibitors: a critical review. *Int J Hematol*. 2007;85(4):287–293. doi:10.1532/IJH97.06222.
 21. Eshghi P, Tara SZ, Baghaipour MR, et al. Inhibitors against rFVIIa in patients with severe congenital FVII deficiency: a case series. *Haemophilia*. 2019;25(5):e345–e349. doi:10.1111/hae.13839.
 22. Lozier JN, Rosenberg PS, Goedert JJ, Menashe I. A case-control study reveals immunoregulatory gene haplotypes that influence inhibitor risk in severe haemophilia A. *Haemophilia*. 2011;17(4):641–649. doi:10.1111/j.1365-2516.2010.02473.x.
 23. Oldenburg J, Pavlova A. Genetic risk factors for inhibitors to factors VIII and IX. *Haemophilia*. 2006;12(s6):15–22. doi:10.1111/j.1365-2516.2006.01361.x.
 24. Witmer C, Young G. Factor VIII inhibitors in hemophilia A: rationale and latest evidence. *Ther Adv Hematol*. 2013;4(1):59–72. doi:10.1177/2040620712464509.

Molecular diagnostic results of a nephropathy gene panel in patients with suspected hereditary kidney disease

Ali Topak[®]

Department of Medical Genetics, Bursa Yüksek İhtisas Training and Research Hospital, Bursa, Turkey. Corresponding author: Ali Topak; at204986@hotmail.com

Key words: nephropathy; NGS; hereditary; kidney disease; novel; polycystic

Abbreviations: ESRD, end-stage renal disease; ACE, angiotensin-converting enzyme; NGS, next-generation sequencing; CRF, chronic renal failure; FSGS, focal segmental glomerulosclerosis; DI, diabetes insipidus; SNVs, single nucleotide variants; indels, insertions/deletions; HGMD, Human Gene Mutation Database; ACMG, American College of Medical Genetics and Genomics; gnomAD, Genome Aggregation Database; VUS, variant of uncertain significance

Laboratory Medicine 2024;55:13-19; <https://doi.org/10.1093/labmed/lmad027>

ABSTRACT

Objective: Clinical diagnosis of hereditary kidney disease can be difficult because of its rarity and severe phenotypic variability. Identifying mutated causative genes can provide diagnostic and prognostic information. In this study, we report the clinical application and outcome of a next-generation sequencing–based, targeted multi-gene panel test for the genetic diagnosis of patients with hereditary kidney disease.

Methods: A total of 145 patients evaluated for hereditary kidney disease who underwent a nephropathy panel with 44 different genes were retrospectively reviewed and included in the study.

Results: Genetic diagnosis of other hereditary kidney diseases, particularly autosomal dominant polycystic kidney disease, was made in 48% of patients. The nephropathy panel changed the preliminary diagnosis in 6% of patients. The variants in 18 (12%) patients had not been previously reported in the literature.

Conclusion: This study demonstrates the utility of the nephropathy panel in identifying patients diagnosed with hereditary kidney disease who are referred for genetic testing. A contribution was made to the variant spectrum of genes associated with hereditary kidney disease.

Introduction

Hereditary kidney disease is the leading cause of chronic kidney disease and accounts for at least 10% of end-stage renal disease (ESRD) cases in Europe. The most common hereditary kidney diseases are cystic and glomerular nephropathies.¹ The clinical and genetic heterogeneity of hereditary kidney diseases poses a major diagnostic challenge. Accurate knowledge of the genetic cause of a disease is becoming increasingly important for treatment, management, prognosis, and genetic counseling. For example, Alport syndrome can be treated with angiotensin-converting enzyme (ACE) inhibition to reduce proteinuria and delay deterioration of renal function. In hereditary podocytopathy causing proteinuria, rapid renal transplantation is recommended because ACE inhibition and immunosuppression are less likely to reduce proteinuria.^{2,3}

One of the benefits of genetic diagnosis is that it can determine the cause of the disease and shorten the diagnostic pathway, regardless of the disease stage, unlike invasive renal biopsies that cannot provide a diagnosis for very early or late stages of the disease.⁴ Due to recent advances in genetic diagnostics, the known number of genes causing various diseases is increasing. This trend can also be seen in the field of nephrology; genes have been discovered that cause various diseases such as renal tubular disorders and hereditary nephrotic syndrome. In recent years, many next-generation sequencing (NGS) diagnostic panels containing these genes have been developed.⁵

This study presents information on genes and variants identified by the nephropathy gene panel in a cohort of 145 index cases with clinically suspected hereditary kidney disease.

Materials and Methods

Patient Cohort

A total of 145 patients with a diagnosis of hereditary kidney disease who presented to the Medical Genetics Department of Bursa Yüksek İhtisas Training and Research Hospital between 2015 and 2019 were retrospectively evaluated. The patients included those diagnosed with polycystic kidney disease, renal tubular acidosis, nephropathy, chronic renal failure (CRF), Bartter syndrome, Gitelman syndrome, Alport syndrome, focal segmental glomerulosclerosis (FSGS), nephrocalcinosis, and nephrogenic diabetes insipidus (DI). Informed consent for genetic testing was obtained from all patients or their legal guardians. The

local ethics committee granted approval for the study (2011-Clinical Research Ethics Committee [CREC]-25 2019/08-01).

Method

An NGS platform (NextSeq 500, Illumina) was used for this study. The nephropathy panel (Nephropathies Solution, Sophia) was studied in patients, and all steps were performed according to the original manufacturer's protocol. The custom panel, Nephropathies Solution, is a capture-based target enrichment kit. Paired-end sequencing was

performed on an Illumina NextSeq 500 system with a read length of 150 × 2. Base calling and image analysis were conducted using Illumina's Real-Time Analysis software. All bioinformatics analysis was performed on the Sophia DDMTM platform, which includes algorithms for alignment, calling single nucleotide variants (SNVs), and small insertions/deletions (indels) (Pepper), calling copy number variations (Muskat), and functional annotation (Moka). Raw reads were aligned to the human reference genome (GRCh37/hg19). The nephropathy pipeline applies default filters related to low coverage, where the cutoff is 50×,

TABLE 1. Nephropathy panel gene list

AGXT	AQP2	ATP6V0A4	ATP6V1B1	AVPR2	BSND	CASR	CEP290
CLCN5	CLCNKB	COL4A3	COL4A4	COL4A5	CRB2	CTNS	CUBN
CYP24A1	DSTYK	EMP2	EYA1	FN1	FOXC1	GRHPR	HNF1B
KANK2	KCNJ1	LAMB2	NPHS2	NR3C2	OCRL	PAX2	PHEX
PKD1	PKD2	PKHD1	SIX1	SLC12A1	SLC12A3	SLC34A1	SLC4A1
SLC4A4	TTC21B	UMOD	WT1				

TABLE 2. Overview of the study cohort

	PKD	NS	AS	GS	BS	FSGS	RTA	Other	Total
No. of index cases	63/145 (40%)	17/145 (11.7%)	11/145 (7.5%)	11/145 (7.5%)	9/145 (6%)	7/145 (4.8%)	7/145 (4.8%)	20/145 (13.8%)	145
Male sex	23/63 (36%)	7/17 (41%)	7/11 (63.6%)	8/11 (72.7%)	4/9 (44.4%)	1/7 (14.2%)	3/7 (42.8%)	12/20 (60%)	65/145 (44.8%)
Positive family history	24/63 (38%)	1/17 (5.8%)	0/11 (0%)	2/11 (18.1%)	0/9 (0%)	2/7 (28.5%)	0/7 (0%)	1/20 (5%)	30/145 (20%)
Reported consanguinity	0/63 (0%)	2/17 (11.7%)	0/11 (0%)	5/11 (45.4%)	4/9 (44.4%)	1/7 (14.2%)	0/7 (0%)	1/20 (5%)	13/145 (8.9%)
Pediatric/cohort	42/63 (67%)	10/17 (58.8%)	3/11 (27.2%)	6/11 (54.5%)	9/9 (100%)	1/7 (14.2%)	6/7 (85.7%)	15/20 (75%)	92/145 (63.4%)
Diagnostic yield	37/63 (58.7%)	3/17 (17.6%)	5/11 (45.4%)	8/11 (72.7%)	6/9 (66.6%)	2/7 (28.5%)	0/7 (0%)	9/20 (45%)	70/145 (48.2%)
VIPD	2/63 (3%)	1/17 (5.8%)	0/11 (0%)	2/11 (18.1%)	2/9 (22.2%)	2/7 (28.5%)	0/7 (0%)	0/20 (0%)	9/145 (6.2%)

AS, Alport syndrome; BS, Bartter syndrome; FSGS, focal segmental glomerulosclerosis; GS, Gitelman syndrome; NS, nephrotic syndrome; PKD, polycystic kidney disease; RTA, renal tubular acidosis; VIPD, variant incompatible with the preliminary diagnosis.

TABLE 3. Nephropathy variants of uncertain significance list

Patient ID	Sex	Age, y	Clinical diagnosis	Gene	Transcript	Nucleotide change	Amino acid change	Zygosity	Mutation type	HGMD	Consanguinity	Family history	ACMG classification
P4	F	15	ESRF	FN1	NM_002026	c.1802C>A	p.Pro601His	Het	Missense	Novel			US
P6	M	13	PKD	PKHD1	NM_138694	c.8492G>A/ c.9725G>T	p.Arg2831Lys/p. Gly3242Val	Compound Het	Missense/ Missense	CM051168/ CM051182			US/US
P10	F	17	PKD	PKD1	NM_001009944	c.4639C>T	p.Arg1547Cys	Het	Missense	—		Yes	US
P12	F	42	FSGS	COL4A3	NM_000091	c.1021C>T	p.Arg341Cys	Het	Missense	—			US
P17	F	17	NS	UMOD	NM_001008389	c.1564A>G	p.Ile522Val	Het	Missense	Novel			US
P22	M	20	PKD	PKD1	NM_001009944	c.9349C>T	p.Arg3117Cys	Het	Missense	—			US
P27	F	3	BS	PKD1	NM_001009944	c.3667G>A	p.Val1223Met	Het	Missense	Novel			US
P51	F	51	PKD	PKD1	NM_001009944	c.4090C>T	p.Arg1364Cys	Het	Missense	—			US
P66	F	23	NS	FN1	NM_002026	c.6269T>A	p.Ile2090Asn	Het	Missense	Novel			US
P71	F	10	PKD	PKD1	NM_001009944	c.8819C>T	p.Pro2940Leu	Het	Missense	CM195189			US
P73	M	35	ESRF	TTC21B	NM_024753	c.1639C>G	p.Gln547Glu	Hom	Missense	Novel			US
P92	M	8	NS	CRB2	NM_173689	c.667G>C	p.Glu223Gln	Hom	Missense	Novel	Yes		US
P94	M	15	PKD	PKD1	NM_001009944	c.10679G>T	p.Gly3560Val	Het	Missense	Novel			US
P105	M	38	NS	SLC5A2	NM_003041	c.394C>T	p.Arg132Cys	Hom	Missense	CM1821251	Yes		US
P120	F	15	BS	SLC12A1	NM_000338	c.595C>T/ c.604T>A	p.Arg199Cys/p. Trp202Arg	Hom	Missense/ Missense	—	Yes		US/US
P121	M	7	NC	CLCN5	NM_001127898	c.152G>A	p.Arg51Gln	Hemi	Missense	—			US

ACMG, American College of Medical Genetics and Genomics; BS, Bartter syndrome; ESRF, end-stage renal failure; FSGS, focal segmental glomerulosclerosis; HEMI, hemizygous; HET, heterozygous; HGMD, Human Gene Mutation Database; HOM, homozygous; NC, nephrocalcinosis; NS, nephrotic syndrome; PKD, polycystic kidney disease.

TABLE 4. General variant list

Patient ID	Sex	Age, y	Clinical diagnosis	Gene	Transcript	Nucleotide change	Amino acid change	Zygoty	Mutation type	HGMD	Consanguinity	Family history	ACMG classification
P2	M	4	PKD	<i>PKD1</i>	NM_001009944	c.11457C>A	p.Tyr3819Ter	Het	Nonsense	CM961117		Yes	P
P7	M	10	NDI	<i>AQP2</i>	NM_000486	c.7_34del/ c.626T>C	p.Glu3LeufsTer51/p. Leu209Pro	Compound Het	Frameshift/ Missense	Novel			P/LP
P8	F	3	NDI	<i>AQP2</i>	NM_000486	c.38T>C	p.Val13Ala	Het	Missense	Novel			LP
P60	F	25	PKD	<i>CLCN5</i>	NM_001127898	c.2102T>C	p.Leu701Pro	Hemi	Missense	Novel			LP
P21	F	4	PKD	<i>PKD1</i>	NM_001009944	c.10183C>T	p.Gln3395Ter	Het	Nonsense	CM010390		Yes	P
P20	F	5	PKD	<i>HNF1B</i>	NM_000458	c.750C>A	p.Tyr250Ter	Het	Nonsense	Novel			P
P26	M	16	PKD	<i>PKD2</i>	NM_000297.4	c.1837C>T	p.Gln613Ter	Het	Nonsense	CM127160		Yes	P
P28	M	34	PKD	<i>HNF1B</i>	NM_000458	c.544 + 1G>T	P?	Het	Splicing	CS031000		Yes	P
P30	F	1	DDS	<i>WT1</i>	NM_001198551	c.721T>C	p.Cys458Arg	Het	Missense	CM982049			LP
P31	F	16	PKD	<i>PKD1</i>	NM_001009944	c.8162-2A>G	P?	Het	Splicing	—			P
P25	M	8	BS	<i>OCRL</i>	NM_000276	c.899C>A	p.Ala300Asp	Hemi	Missense	Novel			LP
P36	F	16	NS	<i>WT1</i>	NM_000378	c.1372 + 14G>A	P?	Het	Splicing	CS920780			P
P37	F	11	PKD	<i>PKD1</i>	NM_001009944	c.10960C>G	p.Leu3654Val	Het	Missense	CM195199			LP
P67	F	15	ESRF	<i>PAX2</i>	NM_000278	c.227G>A	p.Gly76Asp	Het	Missense	Novel			LP
P39	M	16	GS	<i>CLCNKB</i>	NM_000085	c.371C>T	p.Pro124Leu	Hom	Missense	CM970320			LP
P33	F	18	PKD	<i>PKD1</i>	NM_001009944	c.3161 + 5G>T	P?	Het	Splicing	Novel		Yes	LP
P41	F	13	PKD	<i>PKD2</i>	NM_000297.4	c.1837C>T	p.Gln613Ter	Het	Nonsense	CM127160		Yes	P
P42	M	9	PKD	<i>PKD1</i>	NM_001009944	c.9404C>T	p.Thr3135Met	Het	Missense	CM1413140		Yes	LP
P43	M	10	BS	<i>KCNJ1</i>	NM_000220	c.788T>G	p.Ile263Ser	Hom	Missense	—	Yes		LP
P44	F	9	PKD	<i>PKD1</i>	NM_001009944	c.5014_5015delAG	p.Arg1672GlyfsTer98	Het	Frameshift	CD993412		Yes	P
P38	F	41	PKD	<i>PKD1</i>	NM_001009944	c.9225C>A	p.Tyr3075Ter	Het	Nonsense	Novel		Yes	P
P47	F	39	GS	<i>SLC12A3</i>	NM_000339	c.1180G>T	p.Gly394Cys	Hom	Splicing	CS040559	Yes		P
P49	M	9	AS	<i>COL4A4</i>	NM_000092	c.1321_1369 + 3del	p?	Hom	Indel	CG1619909			P
P50	F	9	BS	<i>CLCNKB</i>	NM_000085	c.371C>T	p.Pro124Leu	Hom	Missense	CM970320	Yes		LP
P52	F	17	PKD	<i>PKD1</i>	NM_001009944	c.10821 + 1G>A	P?	Het	Splicing	CS1612645		Yes	P
P40	F	6	PKD	<i>PKD1</i>	NM_001009944	c.10379C>A	p.Ser3460Ter	Het	Nonsense	Novel			P
P45	M	33	PKD	<i>PKD1</i>	NM_001009944	c.4042_4066del	p.Asn1348ProfsTer10	Het	Frameshift	Novel			P
P58	M	9	PKD	<i>PKD1</i>	NM_001009944	c.11996T>A	p.Leu3999Ter	Het	Frameshift	Novel		Yes	P
P59	M	19	GS	<i>SLC12A3</i>	NM_000339	c.2089_2095 delACCAAGT	p.Thr697GlyfsTer2	Hom	Frameshift	CD021441	Yes	Yes	P
P69	F	8	PKD	<i>PKD1</i>	NM_001009944	c.3162-2A>G	P?	Het	Splicing	CS0776651		Yes	P
P63	F	18	NS	<i>COL4A4</i>	NM_000092	c.1334G>C	p.Gly445Ala	Het	Missense	—			LP
P103	F	58	PKD	<i>PKD1</i>	NM_001009944	c.6811dupA	p.Thr2271AsnfsTer149	Het	Frameshift	Novel			P
P109	M	12	PKD	<i>PKD1</i>	NM_001009944	c.12442-2A>G	P?	Het	Splicing	Novel			P
P68	M	33	ESRF	<i>PAX2</i>	NM_000278	c.418C>T	p.Arg140Trp	Het	Missense	—			LP
P108	M	1	PKD	<i>PKHD1</i>	NM_138694	c.4870C>T/c.6003del	p.Arg1624Trp/p. Asp2002ThrfsTer31	Compound Het	Missense/ Frameshift	CM020959/ Novel			LP/LP
P70	F	1	PKD	<i>PKD1</i>	NM_001009944	c.1396G>A	p.Val466Met	Het	Missense	CM1612578			LP
P74	M	46	PKD	<i>PKD2</i>	NM_000297	c.1837C>T	p.Gln613Ter	Het	Nonsense	CM127160		Yes	P
P76	F	14	PKD	<i>PKD2</i>	NM_000297	c.2356_2357del	p.Arg786GlyfsTer25	Het	Frameshift	CD075509		Yes	P
P78	M	9	GS	<i>SLC12A3</i>	NM_000339	c.1928C>T/ c.237_238dup	p.Pro643Leu/p. Arg80ProfsTer35	Compound Het	Missense/ Frameshift	CM014405/ C1962343			LP/P
P80	M	43	PKD	<i>PKHD1</i>	NM_138694	c.2279G>A	p.Arg760His	Het	Missense	CM020957			P
P81	M	3	PKD	<i>HNF1B</i>	NM_000458	c.529C>T	p.Arg177Ter	Het	Nonsense	—			LP
P83	F	14	PKD	<i>PKD1</i>	NM_001009944	c.7300C>T	p.Arg2434Trp	Het	Missense	CM108789		Yes	LP
P56	F	16	NC	<i>SLC12A1</i>	NM_000338	c.811G>A	p.Ala271Thr	Hom	Missense	Novel			LP
P85	F	75	PKD	<i>COL4A4</i>	NM_000092	c.5044C>T	p.Arg1682Trp	Het	Missense	CM120075			LP
P87	M	2	PKD	<i>PKD1</i>	NM_001009944	c.2085dupC	p.Ala696ArgfsTer18	Het	Frameshift	C1010719		Yes	P
P89	M	8	BS	<i>SLC12A3</i>	NM_000339	c.237_238dupCC	p.Arg80ProfsTer35	Hom	Frameshift	C1962343	Yes		P

Downloaded from https://academic.oup.com/labmed/article/55/1/13/7133509 by guest on 17 February 2025

TABLE 4. (cont)

Patient ID	Sex	Age, y	Clinical diagnosis	Gene	Transcript	Nucleotide change	Amino acid change	Zygosity	Mutation type	HGMD	Consanguinity	Family history	ACMG classification
P90	M	7	GS	<i>SLC12A3</i>	NM_000339	c.2089_2095 delACCAAGT	p.Thr697GlyfsTer2	Hom	Frameshift	CD021441	Yes		P
P91	M	11	AS	<i>COL4A5</i>	NM_000495	c.1864C>T	p.Pro622Ser	Hemi	Missense	—			LP
P93	M	2	GS	<i>SLC12A3</i>	NM_000339	c.2089_2095 delACCAAGT	p.Thr697GlyfsTer2	Hom	Frameshift	CD021441	Yes	Yes	P
P101	F	19	FSGS	<i>COL4A5</i>	NM_000495	c.4325G>A	p.Gly1442Asp	Het	Missense	CM990411			LP
P102	F	16	BS	<i>KCNJ1</i>	NM_000220	c.297G>C/c.299A>T/c.752T>C	p.Trp99Cys/p.Tyr100Phe/p.Phe251Ser	Compound Het	Missense	CM970807/CM088244/-			LP/US/LP
P65	F	14	BS	<i>SLC12A1</i>	NM_000338	c.725G>T	p.Gly242Val	Hom	Missense	Novel			LP
P53	M	53	GS	<i>SLC12A3</i>	NM_000339	c.3005G>A	p.Trp1002Ter	Hom	Nonsense	Novel	Yes		P
P84	M	7	ESRF	<i>TTC21B</i>	NM_024753	c.3684 + 2T>C	P?	Het	Splicing	Novel			P
P106	M	29	ESRF	<i>UMOD</i>	NM_001008389	c.263G>A	p.Gly88Asp	Hom	Missense	CM155943	Yes	Yes	LP
P110	F	24	AS	<i>COL4A5</i>	NM_000495	c.2660G>T	p.Gly887Val	Het	Missense	CM052212			LP
P112	F	26	NS	<i>UMOD</i>	NM_001008389	c.263G>A	p.Gly88Asp	Het	Missense	CM155943			LP
P113	F	7	PKD	<i>PKD1</i>	NM_001009944	c.11257C>T	p.Arg3753Trp	Het	Missense	CM003893		Yes	LP
P115	M	59	AS	<i>COL4A4</i>	NM_000092	c.4718C>T	p.Ala1573Val	Het	Missense	—			LP
P116	M	8	PKD	<i>PKD1</i>	NM_001009944	c.5014_5015delAG	p.Arg1672GlyfsTer98	Het	Frameshift	CD993412			P
P117	F	38	PKD	<i>PKD2</i>	NM_000297	c.2614C>T	p.Arg872Ter	Het	Nonsense	CM994295		Yes	P
P124	F	61	PKD	<i>PKD2</i>	NM_000297	c.916C>T	p.Arg306Ter	Het	Nonsense	CM971196		Yes	P
P125	F	30	FSGS	<i>SLC12A1</i>	NM_000338	c.2805dupA	p.Trp936MetfsTer5	Hom	Frameshift	—	Yes		P
P126	F	12	PKD	<i>PKD2</i>	NM_000297	c.2614C>T	p.Arg872Ter	Het	Nonsense	CM994295			P
P127	F	42	PKD	<i>PKHD1</i>	NM_138694	c.4870C>T/c.5513A>G	p.Arg1624Trp/p.Tyr1838Cys	Compound Het	Missense	CM020959/CM032321			LP/P
P132	F	8	PKD	<i>PKD1</i>	NM_001009944	c.7288C>T	p.Arg2430Ter	Het	Nonsense	CM003336			P
P133	F	72	AS	<i>COL4A5</i>	NM_000495	c.2660G>T	p.Gly887Val	Het	Missense	CM052212			LP
P135	M	12	GS	<i>HNF1B</i>	NM_000458	c.1127C>T	p.Thr376Ile	Het	Missense	CM1912543			LP
P141	M	6	HR	<i>PHEX</i>	NM_000444.6	c.1382C>T	p.Thr461Met	Hemi	Missense	—			LP
P144	M	6	PKD	<i>PKD1</i>	NM_001009944	c.695G>A	p.Cys232Tyr	Het	Missense	CM149576/CM1314578		Yes	P

ACMG, American College of Medical Genetics and Genomics; AS, Alport syndrome; BS, Bartter syndrome; DDS, Denys-Drash syndrome; ESRF, end-stage renal failure; FSGS, focal segmental glomerulosclerosis; GS, Gitelman syndrome; HEMI, hemizygous; HET, heterozygous; HOM, homozygous; HR, hypophosphatemic rickets; LP, likely pathogenic; NC, nephrocalcinosis; NDI, nephrogenic diabetes insipidus; NS, nephrotic syndrome; P, pathogenic; PKD, polycystic kidney disease; RTA, renal tubular acidosis.

whereas the variant fraction cutoff for SNV is 20% and 15% for indels; a cutoff for homopolymer regions with a length of 10 bp was also applied. For variant calling, a minimum coverage of 50× is recommended. The raw data obtained were filtered and analyzed using the appropriate program (Sophia DDM). Considering the demographic characteristics, clinical findings, and family history of the patients, variants that could be significant were determined. These significant variants, which were detected during the analysis of the nephropathy panel and could be associated with any disease, were evaluated using the Human Gene Mutation Database (HGMD).⁶ This allowed determination of whether the change had been reported in the literature and, if so, to which disease it was associated. For alterations not reported in the literature, classification by American College of Medical Genetics and Genomics (ACMG) criteria and frequency in population studies (gnomAD, Genome Aggregation Database) were determined using the Varsome Analysis Program (<https://varsome.com/>).^{7,8} This panel includes many disease-associated genes, including polycystic kidney disease, Bartter syndrome, Gitelman syndrome, Alport syndrome, FSGS, nephrocalcinosis, and nephrogenic DI.

The gene content of the panel is shown in TABLE 1. All coding exons and exon-intron boundaries (±15 bp) of 44 genes were sequenced. Missense, nonsense, frameshift, splice variants, and short indels were detected by software. Variants in deep intronic regions and gene rearrangements (gene fusions or inversions) could not be detected. Large insertions or duplications that are larger than ~1/3 read length might be missed.

Results

The demographic characteristics of the 145 patients with hereditary kidney disease included in the study are given in TABLE 2. Consanguinity was most common in patients with Gitelman and Bartter syndromes.

According to the ACMG classification, only pathogenic and likely pathogenic variants were considered in the evaluation of diagnostic yield. Variants with a low minor allele frequency according to the gnomAD and variants of uncertain significance (VUS) according to ACMG that are thought to be clinically relevant are predicted to be pathogenic variants in *in silico* prediction tools and are also listed in TABLE 3.^{7,8}

TABLE 5. Novel variant list^a

Gene	Transcript	Nucleotide change	Amino acid change	Mutation type
<i>AQP2</i>	NM_000486	c.7_34del/c.626T>C	p.Glu3LeufsTer51/p.Leu209Pro	Frameshift/Missense
<i>AQP2</i>	NM_000486	c.38T>C	p.Val13Ala	Missense
<i>CLCN5</i>	NM_001127898	c.2102T>C	p.Leu701Pro	Missense
<i>HNF1B</i>	NM_000458	c.750C>A	p.Tyr250Ter	Nonsense
<i>OCRL</i>	NM_000276	c.899C>A	p.Ala300Asp	Missense
<i>PAX2</i>	NM_000278	c.227G>A	p.Gly76Asp	Missense
<i>PKD1</i>	NM_001009944	c.3161 + 5G>T	P?	Splicing
<i>PKD1</i>	NM_001009944	c.9225C>A	p.Tyr3075Ter	Nonsense
<i>PKD1</i>	NM_001009944	c.10379C>A	p.Ser3460Ter	Nonsense
<i>PKD1</i>	NM_001009944	c.4042_4066del	p.Asn1348ProfsTer10	Frameshift
<i>PKD1</i>	NM_001009944	c.11996T>A	p.Leu3999Ter	Frameshift
<i>PKD1</i>	NM_001009944	c.6811dupA	p.Thr2271AsnfsTer149	Frameshift
<i>PKD1</i>	NM_001009944	c.12442-2A>G	P?	Splicing
<i>PKHD1</i>	NM_138694	c.6003del	p.Asp2002ThrfsTer31	Frameshift
<i>SLC12A1</i>	NM_000338	c.811G>A	p.Ala271Thr	Missense
<i>SLC12A1</i>	NM_000338	c.725G>T	p.Gly242Val	Missense
<i>SLC12A3</i>	NM_000339	c.3005G>A	p.Trp1002Ter	Nonsense
<i>TTC21B</i>	NM_024753	c.3684 + 2T>C	P?	Splicing

^aThe variants in the table have not been previously reported in the literature and Human Gene Mutation Database Professional.

Causal variants (pathogenic and possibly pathogenic) were detected in 70 of the 145 patients who underwent the nephropathy gene panel. Detailed information on the variants is presented in **TABLE 4**. Nineteen of these variants had not been previously described in the literature. A causal variant was detected in 37 (58.7%) of 63 patients referred with a clinical diagnosis of polycystic kidney disease. Causal variants were detected in 6 of 9 patients (66.6%) with a clinical diagnosis of Bartter syndrome, 8 of 11 patients (72.7%) with a clinical diagnosis of Gitelman syndrome, 5 of 11 patients (45.4%) with a clinical diagnosis of Alport syndrome, 2 of 3 patients (66.6%) with a clinical diagnosis of nephrogenic DI, 4 of 8 (50%) patients with a clinical diagnosis of CRF, 3 of 17 patients (17%) with a clinical diagnosis of nephrotic syndrome, 1 of 4 patients (25%) with a clinical diagnosis of nephrocalcinosis, and 1 of 7 patients (14.2%) with a clinical diagnosis of FSGS. No clinically causal variant was identified in patients referred with a clinical diagnosis of renal tubular acidosis. Causal variants were found in the *TTC21B* gene in 2 patients with CRF and dysmorphic findings, in the *PHEX* gene in 1 patient with hypophosphatemic rickets, and in the *WT1* gene in 1 patient with Denys-Drash syndrome.

Pathogenic variants leading to different phenotypes incompatible with the preliminary clinical diagnosis were detected in the *CLCN5* and *COL4A4* genes in 2 patients with polycystic kidney disease and in the *SLC12A3* and *OCRL* genes in 2 patients with a preliminary diagnosis of Bartter syndrome, *COL4A4* gene in 1 patient with a preliminary diagnosis of nephrotic syndrome, *HNF1B* and *CLCNKB* genes in 2 patients with a preliminary diagnosis of Gitelman syndrome, and *SLC12A1* and *COL4A5* genes in 2 patients with a preliminary diagnosis of FSGS. These patient rates were reported in **TABLE 2** as “variant incompatible with the preliminary diagnosis” in different disease categories.

A VUS compatible with the preliminary diagnosis was detected in 6 patients with polycystic kidney disease. A homozygous VUS in the

CRB2 gene compatible with the clinical diagnosis and a homozygous VUS in the *SLC5A2* gene incompatible with the clinical diagnosis were detected in 2 patients with a preliminary diagnosis of nephrotic syndrome. One patient with a preliminary diagnosis of Bartter syndrome was found to have a homozygous VUS in the *SLC12A1* gene. In addition, a VUS in the *COL4A3* gene was shown in a patient with a preliminary diagnosis of FSGS, which was different from the preliminary clinical diagnosis.

Discussion

As a result of the nephropathy gene panel study, which included 44 genes in 145 patients, most of whom were diagnosed with polycystic kidney disease but also with renal tubular acidosis, nephropathy, CRF, Bartter syndrome, Gitelman syndrome, Alport syndrome, FSGS, nephrocalcinosis, and nephrogenic DI, the overall genetic diagnosis rate was 48%.

In the polycystic kidney disease group, representing the largest number of patients in the cohort, family history was positive in 38% of patients, and a diagnostic yield of 58.7% was obtained. As in the literature, variants were mostly found in the *PKD1* or *PKD2* genes.^{9,10} The diagnostic yield was 72.7% in Gitelman syndrome, 66.6% in Bartter syndrome, and 45.4% in Alport syndrome. Such a high diagnostic yield could not be achieved in patient groups referred to other nephropathy clinics. This is because many genes associated with hereditary kidney disease have been identified in recent years, and the gene panel used at the time of the study was inadequate to detect other hereditary nephropathies. In a recent study, a diagnostic yield of 59% was achieved by applying a 127-gene nephropathy panel to a small cohort of 56 families.¹¹ In another study, a genetic diagnostic yield of 43% was obtained after examining a panel of 207 genes in 135 families.¹² Comparing the overall diagnostic yield in our cohort to these studies, the ratios are close.

In addition, it is hypothesized that many of the VUS representing 11% of the cohort that were not included in our genetic diagnostic statistics and that were also mentioned in **TABLE 3** may have a phenotypic effect. However, data such as functional studies, family segregation analyses, and identification of other unrelated affected individuals with the same genetic variants may change the classification of these variants in the future. Moreover, a potential disadvantage of NGS is its limited ability to detect copy number variations and we may have missed these copy number variations in this cohort. Therefore, the true rate of genetic diagnoses is likely higher than we currently report. The variants in 18 patients diagnosed with genetic disease in our cohort have not been previously reported in the literature or HGMD Professional. These variants in *AQP2*, *CLCN5*, *HNF1B*, *OCRL*, *PAX2*, *PKD1*, *PKHD1*, *SLC12A1*, *SLC12A3*, *TTC21B* genes were pathogenic and likely pathogenic variants according to ACMG classification, most of them in the *PKD1* gene. These novel variants included 4 nonsense, 5 frameshift, 3 splice region and 6 missense variants. All novel variants were considered disease-causing by at least 1 prediction tool. Functional studies on these variants data may help to ascertain the role of novel variants in disease development. These variants will contribute to the spectrum of variants in the literature. Genes with novel variants have been previously associated with several known hereditary kidney diseases in OMIM. **TABLE 4** provides information on 70 patients diagnosed with genetic disease and on variants. The novel variants are listed together in **TABLE 5**.

Pathogenic and likely pathogenic variants compatible with the preliminary clinical diagnosis were detected in 61 of 70 patients diagnosed as a result of the nephropathy gene panel study. However, variants different from the preliminary clinical diagnosis were identified in 9 patients. After retrospective reevaluation of these 9 patients, the preliminary clinical diagnoses were changed in agreement with the detected pathogenic variants. This condition, referred to as phenocopy in some studies in the literature, was frequently observed in groups of patients with hereditary kidney disease. In particular, the phenotypic overlap between Bartter and Gitelman syndromes is well known.^{13,14} Our cohort's diagnosis changed from Bartter to Gitelman and vice versa in one patient each. In addition, causal variants of Bartter syndrome were found in 2 of the referred patients with clinical diagnoses of FSGS and nephrocalcinosis. Another study reported that cohorts of patients with clinically diagnosed FSGS had varying rates of pathogenic variants in the Alport syndrome genes *COL4A3*, *COL4A4*, and *COL4A5* but not in FSGS-related genes.^{15,16} In our cohort, a pathogenic variant in the *COL4A5* gene was detected in a patient with a clinical diagnosis of FSGS.

In one study, adults awaiting renal transplantation for ESRD of unclear cause were found to have a genetic cause in 12% of cases by renal gene panel study. Since the primary etiology may affect graft survival by recurrence or rejection, it is very important in terms of renal transplantation to know the underlying renal disease for the treatment of ESRD; therefore, genetic diagnosis is very important.¹⁷ In the study cohort, genetic diagnosis was made in 4 patients with ESRD and the etiology was determined. In this way, this study helped to improve these patients' management before and after transplantation and estimate the risk of kidney disease in relatives.

Our study presents the results of diagnostic tests for hereditary kidney disease that can help clinicians in test selection for appropriate patients and in counseling patients about the possibility of obtaining a positive result with genetic testing. Hereditary kidney disease gene

panels enable differentiation of complex phenotypes and classification of patients and facilitate patient management by improving our understanding of the relevant phenotype. The gene panel used is a non-invasive, cost-effective tool for genetic diagnosis of hereditary kidney diseases. In the future, the addition of other genes related to hereditary kidney diseases will enable a higher diagnosis rate and thus more personalized treatment.

Conflict of Interest Disclosure

The authors have nothing to disclose.

REFERENCES

- Bullich G, Domingo-Gallego A, Vargas I, et al. A kidney-disease gene panel allows a comprehensive genetic diagnosis of cystic and glomerular inherited kidney diseases. *Kidney Int*. 2018;94(2):363–371. doi:10.1016/j.kint.2018.02.027.
- Gross O, Licht C, Anders HJ, et al; Study Group Members of the Gesellschaft für Pädiatrische Nephrologie. Early angiotensin-converting enzyme inhibition in Alport syndrome delays renal failure and improves life expectancy. *Kidney Int*. 2012;81(5):494–501. doi:10.1038/ki.2011.407.
- Siji A, Karthik KN, Pardeshi VC, Hari PS, Vasudevan A. Targeted gene panel for genetic testing of south Indian children with steroid resistant nephrotic syndrome. *BMC Med Genet*. 2018;19(1):200. doi:10.1186/s12881-018-0714-6.
- De Haan A, Eijgelsheim M, Vogt L, Knoers NVAM, de Borst MH. Diagnostic yield of next-generation sequencing in patients with chronic kidney disease of unknown etiology. *Front Genet*. 2019;10:1264. doi:10.3389/fgene.2019.01264.
- Renkema KY, Stokman MF, Giles RH, Knoers NVAM. Next-generation sequencing for research and diagnostics in kidney disease. *Nat Rev Nephrol*. 2014;10(8):433–444. doi:10.1038/nrneph.2014.95.
- Stenson PD, Mort M, Ball EV, et al. The human gene mutation database: 2008 update. *Genome Med*. 2009;1(1):13. doi:10.1186/gm13.
- Richards S, Aziz N, Bale S, et al. Standards and guidelines for the interpretation of sequence variants: a joint consensus recommendation of the American College of Medical Genetics and Genomics and the Association for Molecular Pathology. *Genet Med*. 2015;17(5):405–424.
- Karczewski KJ, Francioli LC, Tiao G, et al. The mutational constraint spectrum quantified from variation in 141,456 humans. *Nature*. 2020;581(7809):434–443. doi:10.1038/s41586-020-2308-7.
- Bergmann C. ARPKD and early manifestations of ADPKD: the original polycystic kidney disease and phenocopies. *Pediatr Nephrol*. 2015;30(1):15–30. doi:10.1007/s00467-013-2706-2.
- Wang T, Li Q, Shang S, et al. Identifying gene mutations of Chinese patients with polycystic kidney disease through targeted next-generation sequencing technology. *Mol Genet Genomic Med*. 2019;7(6):e720. doi:10.1002/mgg3.720.
- Mori T, Hosomichi K, Chiga M, et al. Comprehensive genetic testing approach for major inherited kidney diseases, using next-generation sequencing with a custom panel. *Clin Exp Nephrol*. 2017;21(1):63–75.
- Mallett AJ, McCarthy HJ, Ho G, et al. Massively parallel sequencing and targeted exomes in familial kidney disease can diagnose underlying genetic disorders. *Kidney Int*. 2017;92(6):1493–1506. doi:10.1016/j.kint.2017.06.013.
- Riedhammer KM, Braunisch MC, Günthner R, et al. Exome sequencing and identification of phenocopies in patients with clinically presumed hereditary nephropathies. *Am J Kidney Dis*. 2020;76(4):460–470.

14. Ashton EJ, Legran A, Benoit V, et al. Simultaneous sequencing of 37 genes identified causative mutations in the majority of children with renal tubulopathies. *Kidney Int.* 2018;93(4):961–967.
15. Becherucci F, Landini S, Cirillo L, Mazzinghi B, Romagnani P. Look alike, sound alike: phenocopies in steroid-resistant nephrotic syndrome. *Int J Environ Res Public Health.* 2020;17(22):8363. doi:10.3390/ijerph17228363.
16. Yao T, Udwan K, John R, et al. Integration of genetic testing and pathology for the diagnosis of adults with FSGS. *Clin J Am Soc Nephrol.* 2019;14(2):213–223. doi:10.2215/CJN.08750718.
17. Ottlewski I, Münch J, Wagner T, et al. Value of renal gene panel diagnostics in adults waiting for kidney transplantation due to undetermined end-stage renal disease. *Kidney Int.* 2019;96(1):222–230. doi:10.1016/j.kint.2019.01.038.

Bronchoalveolar lavage cytology in children with chronic unexplained cough and severely neurologically impaired children

Ivan Pavić, MD, PhD,^{1,2} Draženka Ezgeta Karačić, MD,³ Iva Hojsak, MD, PhD^{4,5,6}

¹Departments of Pulmonology, Allergology and Immunology, Children's Hospital Zagreb, Zagreb, Croatia, ²University of Split School of Medicine, Split, Croatia, ³Department of Cytology Children's Hospital Zagreb, Zagreb, Croatia, ⁴Referral Center for Pediatric Gastroenterology and Nutrition, Children's Hospital Zagreb, Zagreb, Croatia, ⁵University of Zagreb School of Medicine, Zagreb, Croatia, ⁶University J.J. Strossmayer School of Medicine Osijek, Osijek, Croatia. Corresponding author: Ivan Pavić; ipavic01@gmail.com

Key words: bronchoscopy; bronchoalveolar lavage; cytology; children

Abbreviations: BAL, bronchoalveolar lavage; ORO, oil red O; LLMs, lipid-laden macrophages; GERD, gastroesophageal reflux disease; MII-pH, multichannel intraluminal impedance-pH; AR, acid reflux; WAR, weakly AR; AM, alveolar macrophages; RI, reflux index; SI, symptom index; SSI, symptom sensitivity index; SAP, symptom association probability; LLI, lipid-laden index

Laboratory Medicine 2024;55:20-26; <https://doi.org/10.1093/labmed/lmad028>

ABSTRACT

Objective: We aimed to compare the cellular composition of bronchoalveolar lavage (BAL) fluids in children with chronic unexplained cough (group 1) and severely neurologically impaired children with chronic or recurrent respiratory problems (group 2) with the BAL cytology of children without pulmonary or systemic diseases (group 3).

Methods: Bronchoscopy with BAL fluid analysis was performed in all subjects. Children with respiratory symptoms underwent 24-hour multichannel intraluminal impedance monitoring.

Results: A significant difference was found between the groups in the total number of cells in BAL fluid cytology (191 [range, 24–12,747], 747 [range, 53–13,000], and 105 [range, 41–233] cells/ μ L, $P = .015$), in the percentage of neutrophils (21.2 [SD = 32.4], 49.4 [SD = 36.6], and 3.6 [SD = 2.4], $P < .001$), and in the percentage of lipid-laden macrophages (10.3 [SD = 11.4], 13.7 [SD = 15.8] and 0.44 [SD = 1.0], $P < .001$).

Conclusion: The BAL fluid cytology provides useful data for determining the cause of chronic unexplained cough and chronic or recurrent respiratory problems in severely neurologically impaired children.

Bronchoalveolar lavage (BAL) has become a valuable diagnostic tool in diagnosing and managing various pulmonary diseases in pediatric patients. Bronchoscopy with BAL in children is not considered a high-risk procedure, but it must be performed carefully and thoughtfully.¹ It is well tolerated and rarely has complications. Moreover, it is a reliable method for obtaining organ-specific specimens in children.² BAL fluid contains cellular and noncellular components whose changes reflect pathologic changes in the lung parenchyma. In addition, analysis of these components of BAL fluid could help identify various causes of respiratory symptoms in children. However, determination of reference values in healthy children is difficult due to ethical limitations and is mostly based on data from children without pulmonary or systemic disease, with normal physical examination and chest radiographs, who are scheduled to undergo elective surgery or to evaluate laryngeal stridor.³

Chronic cough is the most common underlying indication for BAL in children.⁴ It has been shown that BAL fluid from children with isolated chronic cough contained a higher percentage of neutrophils than that of the control group, which the authors attributed to underlying persistent airway inflammation.⁵ In addition, it was shown that higher neutrophil counts in BAL samples from young children with chronic cough were associated with bacterial growth, mostly typical respiratory bacteria.⁶

Although sensitivity and specificity are controversial, oil red O (ORO) staining is commonly used to detect lipid-laden macrophages (LLMs) to diagnose aspiration in children. Previously, using pH-metry alone, it was shown that LLMs were higher in children diagnosed with gastroesophageal reflux disease (GERD) than in children without GERD.^{7,8} However, little is known about these differences in children with GERD diagnosed using combined multichannel intraluminal impedance-pH (MII-pH). This may be an important issue because it has been shown that not only acid reflux (AR) but also weakly AR (WAR), which cannot be detected with pH-metry alone, can cause extraesophageal manifestations of GERD, including chronic cough.^{9,10}

Severely neurologically impaired children represent another important group in whom bronchoscopy is indicated in many cases because

these children have a higher incidence of respiratory problems that are multifactorial.¹¹ Among the many underlying causes of respiratory problems in this group of children, aspiration and inadequate cough are the most common.¹² Considering that aspiration in severely neurologically impaired children often occurs without obvious coughing or choking, this is referred to as silent aspiration.¹³ Recurrent aspiration can lead to acute aspiration pneumonia and chronic airway inflammation and damage and is a risk for bronchiectasis and respiratory failure.¹⁴ Little is known about this issue, as few studies have been conducted on this population.^{13,15,16} Data on BAL fluid cytology in severely neurologically impaired children are even sparser.

Therefore, the aim of this prospective study was to investigate the cellular composition of the BAL fluids of children with chronic unexplained cough and severely neurologically impaired children with chronic or recurrent respiratory problems and to compare the results with a population of children without pulmonary or systemic disease undergoing elective surgery. Moreover, we aimed to compare the cellular composition of BAL fluids in children with chronic unexplained cough and severely neurologically impaired children with chronic or recurrent respiratory problems with the results of 24-hour (24h) MII-pH monitoring.

Methods

All children who underwent flexible bronchoscopy and BAL at the Department of Pediatric Pulmonology, Children's Hospital Zagreb, between June 2017 and May 2022 were prospectively enrolled in the study. Inclusion criteria were chronic cough persisting for at least 2 months before study enrolment, with no proven etiology of the cough, and chronic or recurrent respiratory symptoms in severely neurologically impaired children, both of which had a possible association with GER as one of the possible causes of their unexplained respiratory symptoms. All included children had no other gastrointestinal symptoms suggestive of GER. Furthermore, patients who underwent a surgical procedure and therefore required intubation, who had no history of respiratory disease, and whose parents agreed to participate and signed an informed consent form were used as healthy controls.

Simultaneously, children with respiratory symptoms underwent 24h MII-pH monitoring, because GER or aspiration were clinically suspected as possible causes. Before enrollment into the study, the indication and procedure were explained and discussed with the child's parents and caregivers. Only children who met the inclusion criteria and whose parents or caregivers signed an informed consent form were included in the study. The study was conducted in accordance with the Declaration of Helsinki and approved by the Ethics Committee of the Children's Hospital Zagreb.

Before the procedures, all included children underwent the same diagnostic protocol, which included a complete history and physical examination by a single pediatric pulmonologist and ear, nose, and throat specialist. In addition, pulmonary function tests (for those who could cooperate during testing), radiologic and immunologic examinations, and allergy testing were performed to rule out other underlying diseases. Children with current respiratory infections, airway and other structural abnormalities, upper airway cough syndrome, suspected and proven asthma, heart disease, and known antibiotic therapy in the month before admission were excluded from the study.

All included patients were divided into 3 groups: children with chronic cough lasting at least 2 months with no proven etiology of the cough (group 1), severely neurologically impaired children with chronic or

current respiratory problems (group 2), and children without lung or systemic diseases with normal physical examination and chest radiographs who underwent elective surgery and were therefore intubated were used as a control group (group 3). Bronchoscopy was performed in all subjects, but 24h MII-pH was performed in groups 1 and 2.

Flexible bronchoscopy with BAL was performed according to the European Respiratory Society guidelines.¹⁷ Bronchoscopy and BAL were performed by the same interdisciplinary team of pediatric pulmonologists and anesthesiologists and were performed under general anesthesia (administered by inhalation or intravenously). All procedures were performed in the operating room.

The BAL was performed in the right middle lobe or selected based on findings at the time of bronchoscopy. The total cell count was determined in a Fuchs-Rosenthal counting chamber. Smears for cell differentiation were prepared by cytocentrifugation. Cell differentiation was performed by microscopy on cytospin slides after staining with May-Grünwald-Giemsa. Cell evaluation was performed by the same cytologist, who was blinded to the result of the of bronchoscopy, BAL culture, or the clinical findings of the patients, using a light microscope. An ORO staining was used to detect LLM, count them, and express them as a ratio to the total amount of alveolar macrophages (AM) (ratio [%] LLAM/AM) as previously described.¹⁸ For microbiological studies, the first noncentrifuged aliquots from BAL were used. Bronchoscopy and BAL were well tolerated in all subjects.

Twenty-four hour MII-pH monitoring was performed with an ambulatory MII-pH system (Ohmega, MMS) according to a previously published protocol.^{10,19,20}

Gastroesophageal reflux disease was defined by pH-metry as reflux index (RI) >10% in infants and >7% in older children.^{21,22} MII results were defined as abnormal if the measurement met 2 of the following 3 criteria: symptom index (SI) ≥50%, symptom sensitivity index (SSI) ≥10%, and symptom association probability (SAP) ≥95%.²³

Outcomes

The primary outcome was to determine the differences between the 3 groups in BAL findings. Secondary outcomes were to assess the correlation between BAL findings and 24h MII-pH, the difference between children with GERD and children without GERD, and the difference between children who had positive isolates in BAL and those who did not.

Statistics

The Shapiro-Wilk test revealed that the data were not normally distributed. The differences between categorical variables were assessed by a χ^2 test. The differences for noncategorical data were assessed by the nonparametric Mann-Whitney *U* test or Kruskal-Wallis test (depending on the number of groups). When needed, correction for age was performed using the multivariate analysis of variance test. Correlation analysis was performed by Pearson correlation test. All *P* values less than .05 were considered significant. Statistical analysis was performed using SPSS 26.0 statistical software.

Results

A total of 77 children were included in the study: 34 (44%) in group 1, 27 (35%) in group 2, and 16 (21%) in group 3.

The difference in demographic data and BAL characteristics are presented in **TABLE 1**.

TABLE 1. Difference between 3 groups in demographic data and bronchoalveolar lavage; post-hoc analysis

	Group 1 (n = 34)	Group 2 (n = 27)	Group 3 (n = 16)	P value
Age, median (range), y	8.6 (0.8–17.9)	4.9 (0.2–16.2)	4.3 (1.1–15.6)	.05
Sex, female/male	20/14	14/13	7/9	.815
Presence of GI symptoms, n (%)	6 (18)	19 (70)	—	<.001
Bronchoscopy, macroscopic changes, n (%)	17 (50)	25 (93)	2 (12.5)	<.001 ^a
BAL, positive isolates, n (%)	8 (24)	14 (52)	0	.001 ^a
BAL, median (range), number of cells/μL	191 (24–12,747)	747 (53–13,000)	105 (41–233)	.015 ^a
Macrophages, mean (SD), % ^b	72.1 (33.5)	47 (37.1)	92.3 (3.7)	<.001 ^c
LLM/AM ratio, mean (SD), % ^b	10.3 (11.4)	13.7 (15.8)	0.44 (1.0)	<.001 ^a
Lymphocytes, mean (SD), % ^b	3.1 (2.8)	2.7 (2.1)	3 (2.0)	.869
Monocytes, mean (SD), % ^b	1.1 (2.5)	0.9 (1.3)	1.0 (2.0)	.794
Neutrophils, mean (SD), % ^b	21.2 (32.4)	49.4 (36.6)	3.6 (2.4)	<.001 ^c
Eosinophils, mean (SD), % ^b	2.4 (9.9)	0.4 (1.2)	0.2 (0.4)	.424
Mastocytes, mean (SD), %	0	0	0	—

AM, alveolar macrophages; BAL, bronchoalveolar lavage; GI, gastrointestinal; LLM, lipid-laden macrophages.

^aSignificant between all groups.

^bCorrected for age.

^cSignificant between groups 1 and 2 and groups 2 and 3.

TABLE 2. Microorganisms isolated from bronchoalveolar lavage^a

	Group 1 (n = 8)	Group 2 (n = 14)
<i>Haemophilus influenzae</i>	2 (25.0)	4 (28.6)
<i>Haemophilus influenzae</i> ; <i>Moraxella catarrhalis</i>	1 (12.5)	1 (7.1)
<i>Moraxella catarrhalis</i>	1 (12.5)	0
<i>Pseudomonas aeruginosa</i>	1 (12.5)	4 (28.6)
<i>Pseudomonas aeruginosa</i> ; <i>Klebsiella pneumoniae</i>	0	2 (14.3)
<i>Sphingomonas paucimobills</i>	0	1 (7.1)
<i>Streptococcus pneumoniae</i>	1 (12.5)	0
<i>Streptococcus pyogenes</i>	1 (12.5)	0
<i>Achromobacter xylooxidans</i>	1 (12.5)	0
<i>Enterobacter cloacae</i>	0	2 (14.3)

^aData are given as n (%).

A significant difference was found between groups in pathological findings on bronchoscopy that was found in 50% of children in group 1, 93% in group 2, and only 12.5% in group 3 ($P < .001$). Furthermore, the highest number of children with a microbiology-positive BAL was in group 2 (52%) compared with those in group 1 (24%) and none of the children in group 3 had a microbiology-positive BAL ($P = .001$). The most frequently isolated bacteria were *Haemophilus influenzae* found alone in 6 children and in combination with *Moraxella catarrhalis* in 2; from all *H influenzae* isolates, 5 were in group 2. The second most common isolate was *Pseudomonas aeruginosa* alone found in 5 children (and in combination with *Klebsiella pneumoniae* in 2); from all *P aeruginosa* isolates, 6 out of 7 were in group 2 (TABLE 2).

TABLE 3 shows the difference in the MII-pH characteristics between groups 1 and 2.

The only significant difference was in SSI percentage, which was higher in group 2. GERD based on pH-metry was diagnosed in 7 children in total (5 in group 1), whereas GERD based on MII was found in 31 out of 61 children (18 [53%] in group 1 vs 13 [48%] in group 2, $P = .79$).

We compared BAL characteristics between children diagnosed with GERD based on the MII and children without GERD (TABLE 4). Only the percentage of LLM in BAL was significantly different between groups (median 9% [4–45] in a group with GERD vs median 4.5% [0–66] in the group without GERD; $P = .003$), for all other cells there was no significant difference.

Correlations between BAL characteristics and MII-pH are presented in TABLE 5. When we compared MII-pH characteristics between children that had microbiological isolate in BAL to children without isolate, only a significant difference was found in RI, which was higher in children who had microbiology-positive BAL fluid (median 1.2 [0–23.5] vs 3.4 [0.5–21.4]). No significant difference was found for other factors (number of GER, AR, WAR, nonacidic reflux, SI, SSI, SAP).

When we compared BAL cytology findings between children with microbiologically positive and negative BAL (TABLE 6), significant differences were found in the total number of cells (median 6579 [95–13,000] cells/μL vs 123 [24–982] cells/μL) in percentage of neutrophils (83% [9%–98%] vs 3% [0%–55%]), and in percentage of macrophages (10.5% [0%–88%] vs 92% [37%–100%]).

Discussion

Children with chronic unexplained cough and severely neurologically impaired children had a significantly higher number of cells and a higher percentage of LLM in BAL fluid than the control group of children, with the differences being more pronounced in severely neurologically impaired children. We also found a significantly higher percentage of neutrophils in severely neurologically impaired children compared with both children with chronic unexplained cough and the controls. Furthermore, the number of microbiologically positive BAL was highest

TABLE 3. Difference between group 1 and group 2 in the 24h pH-metry and multichannel intraluminal impedance

	Group 1 (n = 34)	Group 2 (n = 27)	P value
Symptoms recorded during pH-MII, n (%)	26 (76)	15 (56)	.354
Number of reflux episodes, pH-metry, median (range)	26 (1–125)	25 (0–96)	.872
RI, median (range), %	1.25 (0.1–23.5)	2.7 (0–21.3)	.093
Number of reflux episodes, impedance, median (range)	100 (25–429)	94 (33–245)	.629
Number of acidic GER, impedance, median (range)	22 (2–87)	21 (0–75)	.872
Number of weakly acidic GER, impedance, median (range)	60.5 (4–408)	68 (17–198)	.705
Number of nonacidic GER, impedance, median (range)	2 (0–132)	10 (0–53)	.255
Number of liquid GER, impedance, median (range)	21.5 (3–81)	28 (8–87)	.413
Number of mixed GER, impedance, (median, range)	26.5 (8–108)	35 (5–135)	.872
Number of gas GER, impedance, median (range)	38 (0–304)	35 (3–87)	.215
SI, median (range), %	50 (0–100)	56.8 (9.9–90.9)	.1
SSI, median (range), %	5.8 (0–98.9)	11.6 (4.3–17.6)	.004
SAP, median (range), %	98.9 (0–100)	99.9 (93.7–100)	.066
BCT, median (range)	9.1 (4.2–22.2)	9.4 (7.5–10.1)	.584
MNBI, median (range)	2168 (799–11,488)	1896 (834–9369)	.215

BCT, bolus clearance time; GER, gastroesophageal reflux; MNBI, mean nocturnal baseline impedance; pH-MII, pH metry and multichannel intraluminal impedance; RI, reflux index; SAP, symptom association probability; SI, symptom index; SSI, symptom sensitivity index.

TABLE 4. Difference between BAL cytology findings in children diagnosed with GERD based on MII and children without GERD

	GERD – MII (n = 30)	GERD + MII (n = 31)	P value
BAL, positive isolates, n (%)	8 (27%)	11 (35%)	.923
BAL, median (range), number of cells/μL	290 (35–11,350)	267 (24–13,000)	.857
Macrophages, median (range), %	87 (0–100)	63 (1–99)	.484
LLM/AM ratio, median (range), %	4.5 (0–66)	9 (4–45)	.003
Lymphocytes, median (range), %	2.5 (0–13)	2 (0–9)	.855
Monocytes, median (range), %	0 (0–13)	0 (0–5)	.324
Neutrophils, median (range), %	8.5 (0–98)	21 (0–95)	.634
Eosinophils, median (range), %	0 (0–6)	0 (0–58)	.848
Mastocytes, median (range), %	0	0	1.0

AM, alveolar macrophages; BAL, bronchoalveolar lavage; GI, gastrointestinal; GERD, gastroesophageal reflux disease; LLM, lipid-laden macrophages; MII, multichannel intraluminal impedance.

in severely neurologically impaired children. In addition, we found that GERD was diagnosed more frequently in children with respiratory symptoms using MII than pH-metry alone, confirming that not only AR but also WAR can cause GERD-related respiratory symptoms.

Previously, it was shown that the amount of lipid in alveolar macrophages, known as the lipid-laden index (LLI), was significantly increased in children with chronic respiratory symptoms, including chronic cough, compared with healthy adults.⁷ However, LLI did not correlate with total cell count or percentage of neutrophils as a marker of inflammation in the BAL fluid, suggesting that elevated LLM in children with chronic respiratory symptoms is also found in other pulmonary diseases, independent of aspiration.⁷

In a study that included 24 children with chronic cough, Ferreira and colleagues²⁴ demonstrated that atopic and nonatopic children with a chronic cough had an increased percentage of neutrophils in BAL fluid compared with the control group of children without chronic cough. They hypothesized that this could be due to an underlying inflammatory process, although microbiological analyses of the BAL fluid sample were negative for bacteria and viruses in all children studied.²⁴ However, it is

worth mentioning that they found a higher median BAL neutrophil percentage in the children with positive GERD compared with those without GERD diagnosed by pH-metry.²⁴ This could lead to the conclusion that neutrophilia of BAL fluid may be associated with the presence of GERD and airway inflammation due to aspiration of gastric contents.

Fitch et al⁵ studied 23 children with chronic unexplained cough and found a statistically significant increase in the percentage of eosinophils and neutrophils in the BAL fluid of children with chronic cough compared with the control group of children. Elevated eosinophils were not found in our study. This could be explained by the fact that we excluded all children with atopy from the study. Other possible explanations could be the different sample sizes, the age of the study participants, or the methodology used.

Recently, in a large retrospective analysis of 100 pediatric patients who underwent bronchoscopy with BAL, Gami and colleagues⁴ found that 71% of patients with a history of cough had positive ORO staining results. In addition, 42% of patients with cough showed acute inflammation on cytologic examination of BAL, whereas only 4% showed evidence of chronic inflammation. However, a higher prevalence of LLM in

TABLE 5. Correlation between BAL characteristics and the 24h pH-metry and multichannel intraluminal impedance

	Number of cells in BAL coefficient	Number of cells in BAL P value	Macrophage percentage in BAL coefficient	Macrophage percentage in BAL P value	LLM/AM percentage in BAL coefficient	LLM/AM percentage in BAL P value	Neutrophils percentage in BAL coefficient	Neutrophils percentage in BAL P value
Number of reflux episodes, pH-metry	-0.92	.497	0.05	.69	0.03	.85	-0.04	.76
RI, %	0.10	.44	-0.12	.37	0.24	.07	0.15	.28
Number of reflux episodes, impedance	-0.21	.13	0.18	.18	0.04	.79	-0.18	.18
Number of acidic GER, impedance	-0.16	.24	0.12	.38	0.04	.77	-0.09	.49
Number of weakly acidic GER, impedance	-0.13	.34	0.14	.38	0.04	.78	-0.13	.32
Number of nonacidic GER, impedance	-0.19	.17	0.14	.31	-0.04	.77	-0.19	.16
Number of liquid GER, impedance	-0.11	.42	-0.05	.7	0.08	.54	0.09	.51
Number of mixed GER, impedance	-0.16	.24	-0.02	.91	0.04	.78	-0.01	.97
Number of gas GER, impedance	-0.16	.22	0.26	.05	0	.98	-0.27	.04
SI, %	-0.01	.92	0.01	.96	0.3	.04	0.01	.97
SSI, %	-0.11	.44	0.07	.62	0.33	.02	-0.05	.75
SAP, %	0.05	.76	-0.06	.66	0.25	.08	0.07	.66

AM, alveolar macrophages; BAL, bronchoalveolar lavage; GER, gastroesophageal reflux; LLM, lipid-laden macrophages; RI, reflux index; SAP, symptom association probability; SI, symptom index; SSI, symptom sensitivity index.

TABLE 6. Difference between BAL cytology findings in children with microbiologically positive and negative BAL

	Positive isolate in BAL	Negative isolate in BAL	P value
BAL, median (range), number of cells/ μ L	6579 (95–13,000)	123 (24–982)	<.001
Macrophages, median (range), %	10.5 (0–88)	92 (37–100)	<.001
LLM/AM ratio, median (range), %	7 (0–66)	5 (0–50)	.102
Lymphocytes, median (range), %	2 (0–9)	3 (0–13)	.073
Monocytes, median (range), %	0 (0–13)	0 (0–6)	.249
Neutrophils, median (range), %	83 (9–98)	3 (0–55)	<.001
Eosinophils, median (range), %	0 (0–5)	0 (0–58)	.582
Mastocytes, median (range), %	0	0	1.0

AM, alveolar macrophages; BAL, bronchoalveolar lavage; LLM, lipid-laden macrophages.

BAL of patients with more chronic symptoms was found, suggesting the possibility that GER is a cause of cough in these patients.⁴

Sacco and colleagues,⁸ using 24h oesophageal pH monitoring and bronchoscopy with BAL in 20 children with “difficult-to-treat” respiratory symptoms and a clinical history suggestive of GERD, showed that the pH-positive children had higher percentages of neutrophils and LLMs than the pH-negative children. They hypothesized that these abnormalities of BAL cytology in children with respiratory symptoms would indicate airway inflammation and aspiration of gastric contents. However, 55% of the patients they studied had normal pH-metry findings despite a clinical picture suggestive of GERD. At this point, it should be mentioned that pH-metry is limited to the detection of AR but not WAR, which could also be associated with chronic cough. The availability of MII-pH monitoring allows detection of both AR and WAR, as well as determination of composition (liquid, gas, and liquid-gas mixture) and the level that the refluxate reaches. Little is known about

BAL cytologic findings in children with GERD diagnosed using MII-pH monitoring. In particular, we show that GERD was diagnosed more frequently based on MII than on pH-metry alone. Presumably, if pH measurement had been used alone, a high proportion of children would have been missed because none of the WAR would have been detected. The result of our study underscores the importance of MII-pH monitoring in the diagnostic workup of children with respiratory symptoms suspected to be caused by GERD. However, when pH-metry was used alone, a high percentage of GERD was diagnosed in severely neurologically impaired children, who were more likely to have gastrointestinal symptoms suggestive of GERD than children with chronic cough.

Severely neurologically impaired children often have respiratory problems that are multifactorial but are related to GERD, with the aspiration of gastric contents and direct aspiration of food or fluid due to oropharyngeal motor dysfunction.¹¹ Previously it was shown that severely neurologically impaired children have a high incidence

of respiratory tract infections, which are most severe in the subgroup of children with both GERD and direct aspiration.¹⁵ Because the authors did not perform bronchoscopy with BAL, it is not possible to compare the cytologic findings of BAL fluid to our data. Severely neurologically impaired children in our study had a high percentage of microbiologically positive BAL fluid, which corresponds significantly with the percentage of neutrophils in BAL fluid. On the other hand, we did not perform video-fluoroscopy and swallowing manometry to evaluate swallowing function to determine whether there was a higher percentage of microbiologically positive findings in the group of children with GERD and swallowing disorders. However, we used determination of the presence and percentage of LLM in BAL fluid from our patients as BAL markers to determine the presence of pulmonary aspiration. One of the potential rationales for a higher LLM/AM ratio in severely neurologically impaired children might be a lower macrophage percentage due to a higher neutrophil percentage, which might be attributed to significantly higher positive isolates in those children. Therefore, a higher LLM might not be specifically indicative of GERD or swallowing disorders only. Although it is known that LLM can be found in the BAL of children with various conditions and the utility of LLMI for diagnosing aspiration is controversial, the determination of LLM in the BAL fluid may be useful as a diagnostic test for detecting aspiration when interpreted in a clinical context.²

Previously, Nussbaum et al,²⁵ studying 115 children with chronic respiratory disease, demonstrated a good correlation between GERD and the presence of LLM in BAL fluid, suggesting aspiration as a cause of chronic lung disease. In addition, the presence of LLM in BAL fluid proved to be 85% sensitive and 80% specific for GERD in children with chronic lung disease.²⁵ The results of our study support these findings. We found that both children with chronic unexplained cough and severely neurologically impaired children diagnosed with GERD using MII had a significantly higher percentage of LLM in BAL fluid than children without GERD, suggesting that aspiration may be one of the causes of their respiratory problems.

The main potential limitation of our study, besides the limited sample size, is that the MII-pH tracings and bronchoscopy with BAL were evaluated by only 1 investigator, knowing that interpretation may vary between observers. It can be argued that we counted LLM and expressed it as a ratio to total AM rather than using the LLI scoring system. However, Kitz and colleagues,¹⁸ in their large study, compared counting LLM and expressing them as a ratio to total AM and compared this ratio with the LLI scoring method and demonstrated a high correlation between the LLAM/AM ratio and the LLI method of qualitative scoring (Pearson's $r = 0.9890$). This justifies the use of the LLAM/AM ratio for evaluation in our study because we used the same method as the cited authors. This study provides important data on the performance of MII-pH monitoring and BAL fluid analyses in specific groups of children, suggesting that GER-induced aspiration may play an important role in chronic cough and chronic or recurrent respiratory problems in severely neurologically impaired children.

In conclusion, the results of our study demonstrate that both bronchoscopy with BAL fluid cytology and MII-pH monitoring can provide valuable information in the evaluation of children with chronic unexplained cough and severely neurologically impaired children to identify a possible cause of their respiratory problems.

Conflict of Interest Disclosure

The authors have nothing to disclose.

REFERENCES

1. Wood RE. Bronchoscopy and bronchoalveolar lavage in pediatric patients. In: Wilmott RW, Deterding R, Li A, et al. eds. *Kendig's Disorders of the Respiratory Tract in Children*, 9th ed. Philadelphia: Elsevier; 2019: 134–146. e1.
2. Faro A, Wood RE, Schechter MS, et al; American Thoracic Society Ad Hoc Committee on Flexible Airway Endoscopy in Children. Official American Thoracic Society technical standards: flexible airway endoscopy in children. *Am J Respir Crit Care Med*. 2015;191:1066–1080. doi:10.1164/rccm.201503-0474ST.
3. Picinin IF, Camargos PA, Marguet C. Cell profile of BAL fluid in children and adolescents with and without lung disease. *J Bras Pneumol*. 2010;36:372–385. doi:10.1590/s1806-37132010000300016.
4. Gami A, Rinaldi K, Degefe YT, Vosoughi AS, Lee D, Maleki Z. Bronchoalveolar lavage in a pediatric population. *Am J Clin Pathol*. 2022;157:678–684. doi:10.1093/ajcp/aqab177.
5. Fitch PS, Brown V, Schock BC, Taylor R, Ennis M, Shields MD. Chronic cough in children: bronchoalveolar lavage findings. *Eur Respir J*. 2000;16:1109–1114. doi:10.1034/j.1399-3003.2000.16f15.x.
6. Asseri AA, Khattab N, Ezmigna D, Awadalla NJ, Daines C, Morgan W. Diagnostic accuracy of nasopharyngeal swab cultures in children less than five years with chronic wet cough. *Children*. 2021;8:1161. doi:10.3390/children8121161.
7. Kazachkov MY, Muhlebach MS, Livasy CA, Noah TL. Lipid-laden macrophage index and inflammation in bronchoalveolar lavage fluids in children. *Eur Respir J*. 2001;18:790–795. doi:10.1183/09031936.01.00047301.
8. Sacco O, Fregonese B, Silvestri M, Sabatini F, Mattioli G, Rossi GA. Bronchoalveolar lavage and esophageal pH monitoring data in children with "difficult to treat" respiratory symptoms. *Pediatr Pulmonol*. 2000;30:313–319. doi:10.1002/1099-0496(200010)30:4<313::aid-ppul7>3.0.co;2-h.
9. Blondeau K, Mertens V, Dupont L, et al. The relationship between gastroesophageal reflux and cough in children with chronic unexplained cough using combined impedance-pH-manometry recordings. *Pediatr Pulmonol*. 2011;46:286–294. doi:10.1002/ppul.21365.
10. Pavic I, Babic I, Cepin Bogovic J, Hojsak I. The importance of combined 24-hour multichannel intraluminal impedance-pH monitoring in the evaluation of children with suspected laryngopharyngeal reflux. *Clin Otolaryngol*. 2017;42:544–549. doi:10.1111/coa.12766.
11. Seddon PC, Khan Y. Respiratory problems in children with neurological impairment. *Arch Dis Child*. 2003;88:75–78. doi:10.1136/adc.88.1.75.
12. Proesmans M. Respiratory illness in children with disability: a serious problem? *Breathe*. 2016;12:e97–e103. doi:10.1183/20734735.017416.
13. Weir KA, McMahon S, Taylor S, Chang AB. Oropharyngeal aspiration and silent aspiration in children. *Chest*. 2011;140:589–597. doi:10.1378/chest.10-1618.
14. Fung CW, Khong PL, To R, et al. Video-fluoroscopic study of swallowing in children with neurodevelopmental disorders. *Pediatr Int*. 2004;46(1):26–30.
15. Morton RE, Wheatley R, Minford J. Respiratory tract infections due to direct and reflux aspiration in children with severe neurodisability. *Dev Med Child Neurol*. 1999;41:329–334. doi:10.1017/s0012162299000729.
16. Veugelers R, Calis EA, Penning C, et al. A population-based nested case control study on recurrent pneumonias in children with severe generalized cerebral palsy: ethical considerations of the design and

- representativeness of the study sample. *BMC Pediatr.* 2005;5:25. doi:10.1186/1471-2431-5-25.
17. de Blic J, Midulla F, Barbato A, et al. Bronchoalveolar lavage in children. ERS Task Force on bronchoalveolar lavage in children. European Respiratory Society. *Eur Respir J.* 2000;15:217–231. doi:10.1183/09031936.00.15121700.
 18. Kitz R, Boehles HJ, Rosewich M, Rose MA. Lipid-laden alveolar macrophages and pH monitoring in gastroesophageal reflux-related respiratory symptoms. *Pulm Med.* 2012;2012:673637. doi:10.1155/2012/673637.
 19. Hojsak I, Ivkovic L, Trbojevic T, et al. The role of combined 24-h multichannel intraluminal impedance-pH monitoring in the evaluation of children with gastrointestinal symptoms suggesting gastroesophageal reflux disease. *Neurogastroenterol Motil.* 2016;28:1488–1493. doi:10.1111/nmo.12846.
 20. Pavic I, Babic I, Matijasic N, Hojsak I. Combined multichannel intraluminal impedance-pH monitoring should be used to diagnose reflux-related otitis media with effusion in children. *Acta Paediatr.* 2018;107(9):1642–1647. doi:10.1111/apa.14339.
 21. Boeckxstaens GE, Smout A. Systematic review: role of acid, weakly acidic and weakly alkaline reflux in gastro-oesophageal reflux disease. *Aliment Pharmacol Ther.* 2010;32(3):334–343. doi:10.1111/j.1365-2036.2010.04358.x.
 22. Rosen R, Vandenplas Y, Singendonk M, et al. Pediatric Gastroesophageal Reflux Clinical Practice Guidelines: joint recommendations of the North American Society for Pediatric Gastroenterology, Hepatology, and Nutrition and the European Society for Pediatric Gastroenterology, Hepatology, and Nutrition. *J Pediatr Gastroenterol Nutr.* 2018;66(3):516–554. doi:10.1097/MPG.0000000000001889.
 23. Mousa HM, Rosen R, Woodley FW, et al. Esophageal impedance monitoring for gastroesophageal reflux. *J Pediatr Gastroenterol Nutr.* 2011;52(2):129–139. doi:10.1097/MPG.0b013e3181ffde67.
 24. Ferreira Fde A, Filho LV, Rodrigues JC, et al. Comparison of atopic and nonatopic children with chronic cough: bronchoalveolar lavage cell profile. *Pediatr Pulmonol.* 2007;42:857–863.
 25. Nussbaum E, Maggi JC, Mathis R, Galant SP. Association of lipid-laden alveolar macrophages and gastroesophageal reflux in children. *J Pediatr.* 1987;110:190–194. doi:10.1016/s0022-3476(87)80152-x.

Quantitative Detection of House Dust Mites–Specific IgE by Light-Initiated Chemiluminescence Assay

Xiaohui Yang, MA,^{1,*} Lisheng Zheng, MA,^{1,*} Yuanmin Sun, MA,¹ Xin Tan, MA,¹ Bei Zhang, MA,¹ Xue Li, PhD,¹ Huiqiang Li, MA¹

¹Department of Clinical Immunology, School of Medical Laboratory, Tianjin Medical University, Tianjin, China. Corresponding author: Huiqiang Li; lhq@tmu.edu.cn. *First authors.

Key words: inhalant allergens, HDM-specific IgE, light-initiated chemiluminescence assay, quantitative detection, performance, comparison

Abbreviations: WAO, World Allergy Organization; HDMs, house dust mites; SPT, skin-prick testing; FEIA, fluorescent enzyme immunoassay; LiCA, light-initiated chemiluminescence assay; CBS, carbonate buffer solution; CL, chemiluminescence; CLSI, Clinical and Laboratory Standards Institute; LoB, limit of blank; LoD, limit of detection; LoQ, limit of quantitation; Pct_B, percentile of the control specimen result distribution; RLU, relative luminescence unit; R₂, determination coefficient

Laboratory Medicine 2024;55:27–33; <https://doi.org/10.1093/labmed/lmad024>

ABSTRACT

Objective: To establish a new method for quantitative detection of house dust mite (HDM)–sIgE based on light-initiated chemiluminescence assay (LiCA).

Methods: The assay was established after optimizing the reaction conditions, and the assay performance was evaluated according to the clinical guidelines. Further, the results of LiCA were compared with those from the ELISA and ImmunoCAP methods.

Results: Coefficients of variation for repeatability ranged from 4.22% to 7.69%, and intermediate precision from 8.38% to 10.34%. The limit of blank (LoB), limit of detection (LoD), and limit of quantitation (LoQ) were 0.066 kU_A/L, 0.165 kU_A/L, and 0.171 kU_A/L, respectively. The coefficient of correlation (*r*) between the results of LiCA and ELISA was 0.9263, and the *r* between the results of LiCA and ImmunoCAP was 0.8870.

Conclusions: A HDM-sIgE quantitation assay based on LiCA was established, which could be used as a new reliable analytical tool for the determination of HDM-sIgE.

With the advancement of industrialization, the prevalence of allergic diseases is increasing worldwide, especially in newly industrialized countries such as China and India.¹ The World Allergy Organization (WAO) anaphylaxis guidelines show that 40% of the global population is affected by allergic diseases.² These diseases not only affect quality of life but also impose a huge economic burden on society.

The existence of allergens is a necessary factor for the development of allergic diseases.³ Common allergens include 2 main categories: inhalant allergens and food allergens. Dust mites are ubiquitous in our living environment and are one of the most common inhalant allergens.^{4,5} The major allergenic dust mites include house dust mites (HDMs) and *Dermatophagoides farinae* in China.⁶ More than 50% of patients with allergies are reported to have allergic symptoms to HDMs, and as many as 85% of children with allergic asthma are sensitive to HDMs.^{7,8} Early diagnosis of patients with allergies is important to avoid allergens and guide clinical treatment.

Skin-prick testing (SPT) and serum allergen-sIgE detection are the main methods for diagnosing patients who are allergic to HDMs.⁹ The serum allergen-sIgE test is widely used due to its safety, simplicity, and convenience.¹⁰ The ImmunoCAP (Thermo Fisher Scientific) system is internationally recognized as the criterion standard for the detection of singleplex allergen-sIgE, which is a fluorescent enzyme immunoassay (FEIA) method with high sensitivity and specificity.^{11,12} However, it is not widely used in China because of its high cost and long turnaround period.¹³

Light-initiated chemiluminescence assay (LiCA) is a homogeneous luminescence immunoassay based on singlet oxygen transmission.¹⁴ The method is sensitive, time-saving, wash-free, and simple to operate, all of which make it a promising alternative to existing conventional methods.¹⁵ The results of previous studies^{16–18} have successfully established LiCA for the detection of food allergen-sIgE, such as egg white-sIgE and milk protein-sIgE. After that, our team set out to investigate the feasibility of detecting inhalant allergen-sIgE and successfully established LiCA for the quantitative detection of mugwort-sIgE.¹⁹ So far, there have been no reports on LiCA-based assay for other inhalant allergen-sIgE except for mugwort. Consequently, we took HDMs as an example for exploring the feasibility of a LiCA-based method for the quantitative detection of inhalant allergen-sIgE. Also, we validated the performance of this method according to the clinical guidelines to confirm whether it meets the requirements of clinical laboratories.

Materials and Methods

Specimens

A total of 108 serum specimens were collected from Tianjin Children's Hospital, China, from March 2022 through August 2022. A total of 90 specimens were collected from patients with HDM allergies, and 18 specimens were obtained from volunteers without HDM allergies. All serum specimens were stored at -20°C before testing. A total of 85 serum specimens were detected via a capture ELISA kit, and 23 serum specimens were tested by ImmunoCAP. Serum specimens with HDM-sIgE values $\geq 0.35 \text{ kU}_A/\text{L}$ were regarded as having tested positive. In contrast, serum specimens with HDM-sIgE values $< 0.35 \text{ kU}_A/\text{L}$ were considered as having tested negative. Informed oral consent was obtained from all patients. The study procedures were designed and carried out based on the Declaration of Helsinki and were approved by the Ethics Committee of the Tianjin Children's Hospital.

Reagents and Chemicals

We purchased HDM extract from Stallergenes Greer, biotinylated goat anti-human IgE antibody from Thermo Fisher Scientific, human hemoglobin from Merck, and ProClin 300 (Merck) and bilirubin from Solarbio. Naked chemibeads and streptavidin-coated sensibeads were acquired from Beyond Biotech.

Coupling of HDM Allergens to Chemibeads

HDM allergens were coupled with chemibeads according to a standard procedure described previously.¹⁶ Briefly, the chemibeads were pretreated in carbonate buffer solution (CBS) by sonication. PBS-solubilized HDM allergens were added to CBS-suspended chemibeads. The mixture was incubated overnight at 37°C with slow stirring. The next day, 8 mg/mL NaBH_4 and 75 mg/mL glycine were added sequentially to the mixture, and the reaction mixture was rotated at room temperature. After washing, the HDM allergens-coated chemibeads were resuspended at 10 mg/mL and stored at 4°C .

Assay Principle and Procedure

The principle of LiCA for detecting HDM-sIgE was shown in [Supplementary Figure 1](#). The entire measurement procedure lasted 45 minutes. First, $25 \mu\text{L}$ of HDM allergens-coated chemibeads, $25 \mu\text{L}$ of serum specimens or calibrators, and $25 \mu\text{L}$ of biotinylated goat anti-human IgE antibody were added to a 96-well microplate. Then, we placed the microplate in a chemiluminescence analyzer (Beyond Biotech) at 37°C for 30 minutes. Next, $150 \mu\text{L}$ of streptavidin-coated sensibeads were added in the dark. Then the microplate was put back into the instrument and incubated in the dark at 37°C for 15 more minutes. Finally, the chemiluminescence (CL) signals were read by the instrument at 612 nm .

Optimization of the Reaction Conditions

The reaction system of LiCA was influenced by several factors, including the mass ratio of HDM allergens-coated chemibeads, the working concentration of the chemibeads, and the reaction buffer system. First, 3 mass ratios (20:4, 20:8, 20:16) of chemibeads were prepared. Afterward, 3 serum pools containing a high, medium, and low level of HDM-sIgE, respectively, were selected. The serum specimens from the individuals without allergies were used as negative controls. The CL signal of each

specimen was detected by LiCA, and the signal-to-noise (S/N) ratio was calculated to obtain the optimal mass ratio. The selection of serum pools and the determination of optimal conditions in the following experiments were performed in the same manner.

Next, the optimal working concentration of the chemibeads was selected by diluting them to $12.5 \mu\text{g/mL}$, $25.0 \mu\text{g/mL}$, and $50.0 \mu\text{g/mL}$. To optimize the buffer system, 4 different kinds of buffer systems, including PBS, CBS, HEPES buffer, and Tris-HCl buffer, were used in LiCA to examine all the specimens.

The pH value and concentration of HEPES buffer were further optimized because the HEPES buffer was selected as the best buffer system. Three pH values of 6.7, 7.2, and 7.7 of HEPES buffer were prepared to obtain the optimum pH value, and 3 concentrations of 0.01 M, 0.025 M, and 0.05 M of HEPES buffer were made to obtain the optimal concentration.

Surfactants contribute to opening the disulphide bonds of proteins, which expose the linear epitopes.²⁰ Therefore, 3 surfactants containing sodium deoxycholate, Triton X100, and Tween 20 were added to the buffer system separately, to explore whether they could improve the S/N ratio. After that, the content of Tween 20 in HEPES buffer was optimized: Tween 20 was used as the best surfactant. Finally, HEPES buffer containing 0.01% Tween 20, 0.05% Tween 20, and 0.1% Tween 20 were prepared to determine the appropriate amount of surfactant.

Construction of Calibration Curve

Serum specimens with HDM-sIgE concentration of $35 \text{ kU}_A/\text{L}$ (measured by the ImmunoCAP system) were selected and diluted to $17.5 \text{ kU}_A/\text{L}$, $3.5 \text{ kU}_A/\text{L}$, $0.7 \text{ kU}_A/\text{L}$, and $0.35 \text{ kU}_A/\text{L}$. Serum specimens from an individual without allergies were used, which measured $0 \text{ kU}_A/\text{L}$. All 6 calibration points were detected by LiCA. A calibration curve based on a 4-parameter logistic regression was established using the concentration and the corresponding CL signal, which could be used for quantitative conversion of the detection results.

Precision

According to Clinical and Laboratory Standards Institute (CLSI) EP5-A2, the precision was evaluated by repeatability and intermediate precision.²¹ Three serum pools, containing a high, medium, and low level of HDM-sIgE, respectively, were selected, and each specimen was tested 20 times in an analytical run to evaluate the repeatability. For intermediate precision, the same aforementioned specimens were measured 8 times per day for 5 consecutive days.

Detection Capability

We tested for the limit of blank (LoB), the limit of detection (LoD), and the limit of quantitation (LoQ), based on clinical guidelines WS/T 514-2017 and CLSI EP17-A.^{22,23} To obtain LoB, 4 serum specimens from individuals without allergies, which had each tested negative for allergens, were used as control specimens, and each specimen was measured 5 times per day for 3 consecutive days. Then, 4 serum specimens with HDM-sIgE between 1 LoB and 4 LoB were selected, and each specimen was measured 5 times a day for 3 consecutive days to get the LoD. For the LoQ, a serum specimen ($0.682 \text{ kU}_A/\text{L}$) was diluted to $0.341 \text{ kU}_A/\text{L}$, $0.171 \text{ kU}_A/\text{L}$, and $0.085 \text{ kU}_A/\text{L}$. Each concentration was tested 20 times in 1 batch.

Interference Test

The specificity of the established method was assessed by interference tests. According to WS/T 416-2013, a total of 3 serum pools, containing a high, middle, and low level of HDM-sIgE, respectively, were selected.²⁴ Different concentrations of hemoglobin (2.5 mg/mL, 5 mg/mL, 10 mg/mL), bilirubin (85.5 μ mol/L, 171 μ mol/L, 342 μ mol/L) and biotin (10 ng/mL, 20 ng/mL, 100 ng/mL) were added to the serum specimens as interfering substances. Then, the recoveries were calculated by detecting the concentrations of HDM-sIgE before and after interference.

Method Comparison

A total of 65 serum specimens were tested by LiCA and commercial ELISA kit (Hob Biotech Group), and the data obtained were analyzed for correlation. Similarly, 23 serum specimens (measured by the ImmunoCAP system) were selected to detect HDM-sIgE by LiCA, and the correlation between the 2 methods was compared.

Statistical Analysis

The concentration of HDM-sIgE in serum specimens was calculated using ELISACalc (BlueGene Biotech). All statistical analyses were performed using SPSS software, Version 25.0 (SPSS), and $P < .05$ was considered to be a statistically significant difference. We plotted 4-parameter logistic regression curves and other graphs using GraphPad Prism software, Version 9.0 (GraphPad Software).

Results

Establishment of LiCA Method for HDM-sIgE Quantitation

We prepared 3 HDM antigen-coated chemibeads with different mass ratios. The results (FIGURE 1A) showed that when the mass ratio of the chemibeads to antigen was 20:8 and 20:16, the CL signals of the specimens were comparable. FIGURE 1B showed that the S/N ratio was highest when the mass ratio was 20:8. Therefore, we chose 20:8 as the best mass ratio for chemibeads.

Then, we diluted the chemibeads to 12.5 μ g/mL, 25.0 μ g/mL, and 50.0 μ g/mL. The results showed that the S/N ratios of the 3 serum pools were not improved significantly when the concentration was 50.0 μ g/mL, but the background signals increased (Supplementary Figure 2A

and 2B). Considering the CL signals and S/N ratios, 25.0 μ g/mL was selected as the most suitable concentration of the chemibeads.

As shown in FIGURE 2A, the S/N ratio was highest when using the HEPES buffer. Therefore, we selected the HEPES buffer as the best buffer system for the subsequent experiments. After that, the pH value of the HEPES buffer was optimized. The results showed that the S/N ratio of a low positive serum pool was the highest when pH was 7.2, and the S/N ratio of a high positive serum pool was the highest when pH was 7.7 (FIGURE 2B). From the perspective of improving sensitivity, 7.2 was used as the optimum pH value of the HEPES buffer. Then, we prepared 0.01 M, 0.025 M, and 0.05 M HEPES buffer. FIGURE 2C shows that the S/N ratio of 0.01M HEPES buffer was higher than that of the other values. Finally, we chose 0.01 M HEPES buffer with pH 7.2 as the optimal reaction buffer for the LiCA detection system.

The addition of Tween 20 and sodium deoxycholate significantly increased the S/N values of high- and medium-positive serum pools. However, sodium deoxycholate did not improve the S/N values of the low-positive serum pool (FIGURE 2D). Therefore, Tween 20 was chosen as the best surfactant. The results showed that the highest S/N values were obtained for all samples when 0.01% Tween was added to the reaction buffer (FIGURE 2E), which was selected as the optimum content of surfactant in the buffer. FIGURE 3 showed the calibration curve for quantitative detection HDM-sIgE by LiCA. The curve equation was $y = 9717.05/[1 + (x/31.47)^{-0.89}] + 299.41$.

Evaluation of Clinical Performance

To evaluate precision, 3 serum pools were detected by LiCA and then the mean, SD, and CV were calculated. As shown in TABLE 1, in the repeatability study results, the CV ranged from 4.22% through 7.69%. In the intermediate precision study, the CV ranged from 8.38% through 10.34%. No matter the repeatability or intermediate precision, the CV value was less than 15%, which was considered acceptable.

The obtained LoB data were non-Gaussian distributed, and then the 60 data points were ranked to calculate the percentile of the control-specimen result distribution (Pct_B). It was required that $\alpha = 0.05$, $Pct_B = 1 - \alpha = 0.95$, and ranked position = $0.5 + (N_B \times Pct_B)$, where N_B was the total number of tests, and the arrangement of 60 test results was 57.5. Therefore, $LoB = X_{57} + 0.5(X_{58} - X_{57})$. In this study, $X_{57} = 0.056$, and $X_{58} = 0.075$, so LoB was 0.066 kU_A/L.

FIGURE 1. Optimization of mass ratio of chemibeads coated with antigen. **A**, Effect of chemibeads mass ratios on chemiluminescence (CL) signal. **B**, Effect of chemibeads mass ratios on the signal-to-noise (S/N) ratio. RLU, relative luminescence unit.

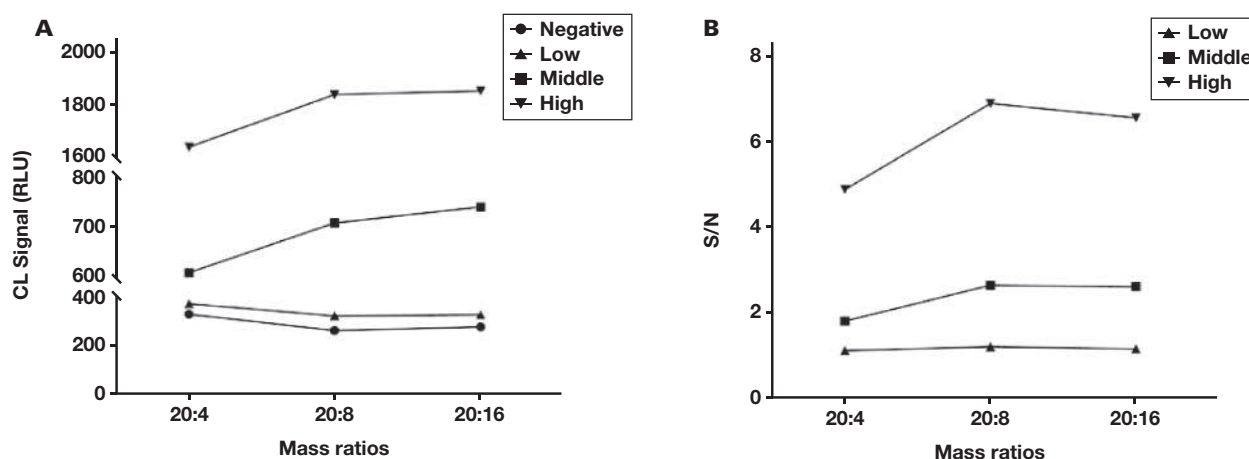


FIGURE 2. Optimization of reaction buffer system and surfactant. **A,** Comparison of the signal-to-noise (S/N) ratio of 3 serum pools in 4 reaction buffer systems. **B,** Comparison of S/N ratio of 3 serum pools in HEPES buffer with 3 pH values. **C,** Comparison of S/N ratio of 3 serum pools in HEPES buffer (pH, 7.2) with 3 concentrations. **D,** Comparison of S/N ratio of 3 serum pools in HEPES buffer (0.01 M; pH, 7.2) with 3 surfactants. **E,** Comparison of S/N ratio of 3 serum pools in Tween 20 with 3 additional specimens.

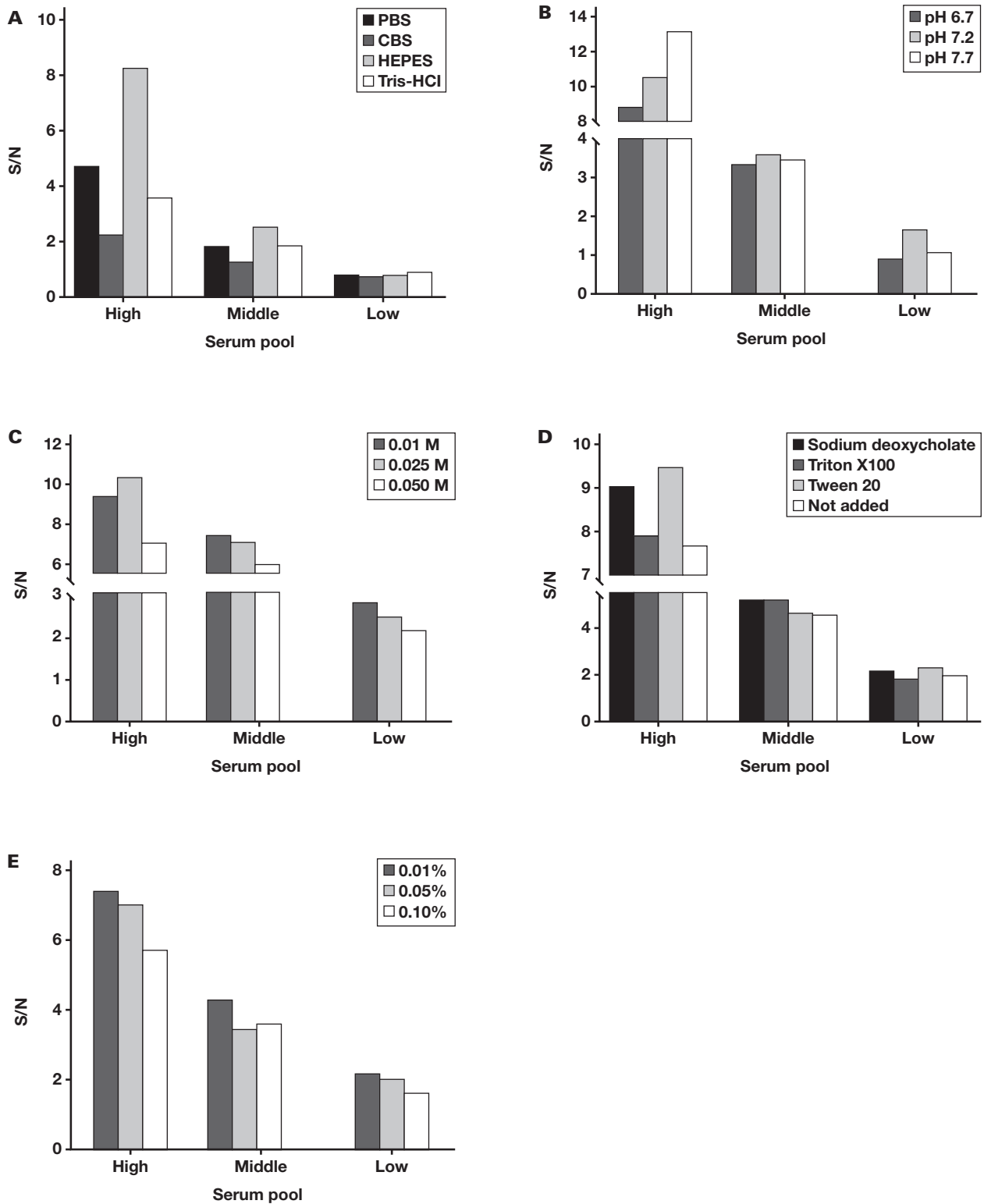


FIGURE 3. Calibration curve of light-initiated chemiluminescence (CL) assay for detecting house dust mite-sIgE ($R^2 = 1.000$).

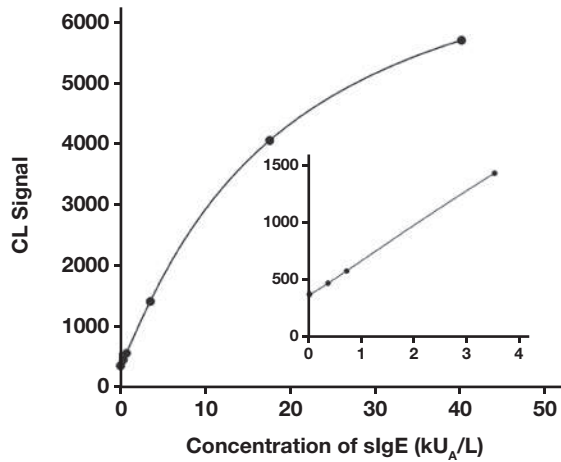


TABLE 1. Repeatability and Intermediate Precision

Serum Pool	Repeatability		Intermediate Precision	
	Mean (SD), kU _A /L	CV, %	Mean (SD), kU _A /L	CV, %
Low	0.52 (0.04)	7.69	0.58 (0.06)	10.34
Middle	3.75 (0.25)	6.67	3.70 (0.31)	8.38
High	7.35 (0.31)	4.22	7.75 (0.69)	8.90

The LoD data showed Gaussian distribution. Therefore, it was calculated according to the following formula:

$$\text{LoD} = \text{LoB} + \frac{1.645}{1 - \frac{1}{4(N-K)}} \times \text{SD}_S$$

for this study, $N = 60$, $K = 4$, and $\text{SD}_S = 0.06$, so the LoD of the method was $0.165 \text{ kU}_A/\text{L}$.

For the LoQ, the CV value was required to be less than 15% and not lower than LoD, so the LoQ of this method was $0.171 \text{ kU}_A/\text{L}$.

The specificity of the established method was evaluated by interference testing. As shown in Supplementary Table 1, the recoveries ranged from 80% to 120% when the specimens contained less than 5 mg/mL hemoglobin, less than $342 \text{ } \mu\text{mol/L}$ bilirubin, and less than 10 ng/mL biotin.

Methods Comparison

The results showed that the detection method established in this study correlated well with ELISA and ImmunoCAP. The regression equations and correlation coefficients were as follows: $y = 0.8646x + 0.2607$, $r = 0.9263$ and $y = 0.2279x + 0.2286$, $r = 0.8870$ (FIGURE 4A and 4B).

As shown in FIGURE 4C, the Bland-Altman test was applied to analyze the difference between LiCA and ELISA. The results showed that the mean deviation between LiCA and ELISA was 0.1 . Mean ($\pm 1.96 \text{ SD}$) was used as the 95% consistency limit. Thus, the lower and upper limits for the 2 methods were -2.6 and 2.8 , respectively. The number of data exceeding the lower and upper limits was 5, which means that 92.31% of the data distribution was within the acceptable range. Therefore, there

was good agreement between LiCA and ELISA, and the assay results were reliable. The same method was used to analyze the agreement between LiCA and ImmunoCAP (FIGURE 4D). The results showed that 95.65% of the data were distributed within the acceptable range. Thus, the 2 methods were correlated.

Discussion

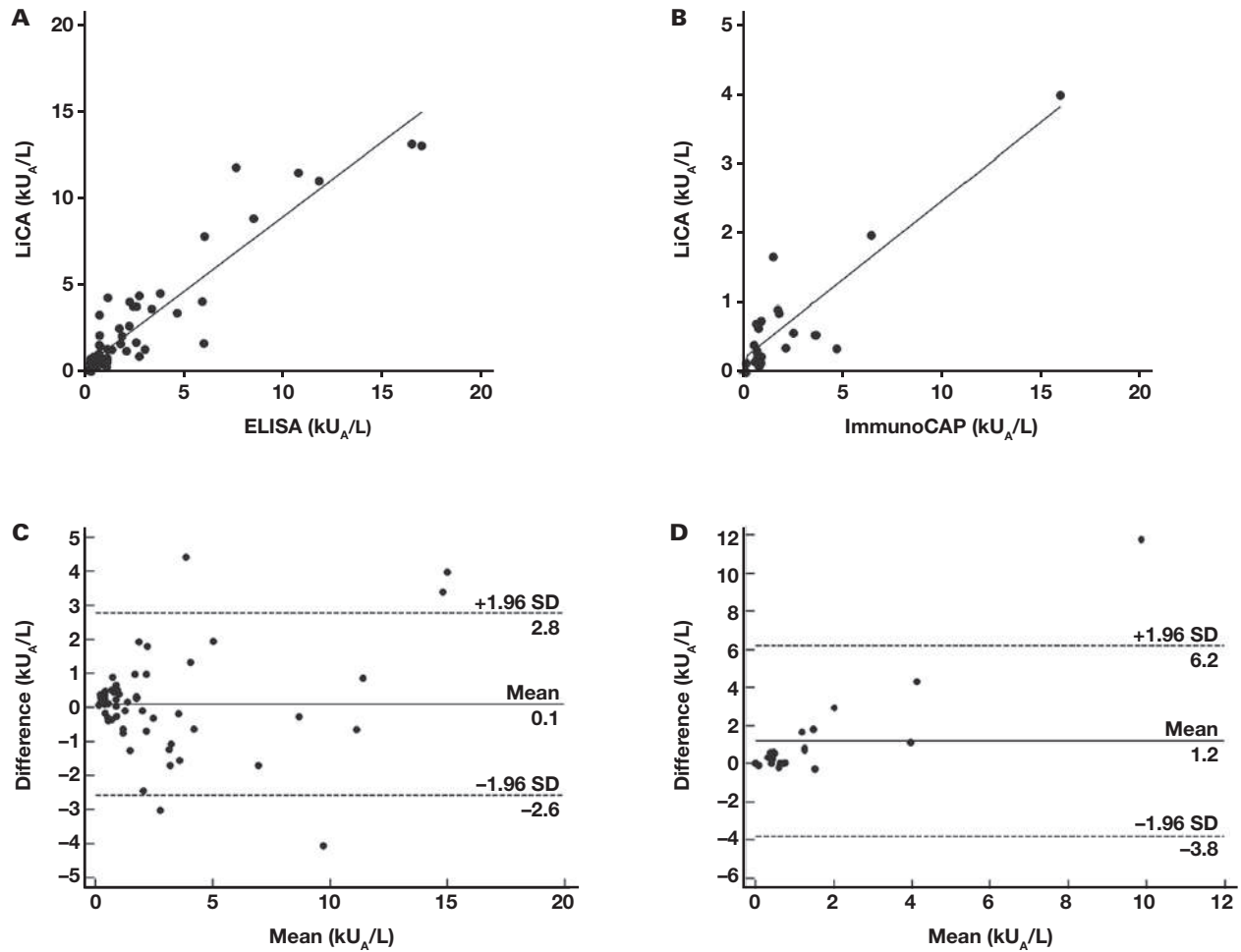
LiCA is a homogeneous immunoassay based on nanoparticles, which originated from the lumino-oxygen channel immunoassay in the 1990s.¹⁴ The method does not require washing steps, and the process can be completed within 1 hour.²⁵ The results of previous studies, such as Zhang et al.,¹⁸ have revealed that the chemibeads can provide more binding sites for allergen proteins due to their larger specific surface area, so allergen-specific IgG interference can be significantly reduced. Moreover, the reagents are simple to prepare: allergen-coated chemibeads have mature standard procedures, and biotinylated anti-human IgE antibodies and streptavidin-coated sensibeads (universal solution) are commercially available. Thus, the method is easy to commercialize and automate with domestic equipment. These advantages make LiCA suitable for allergen-sIgE detection. Therefore, a quantitative LiCA-based assay was established in this study for the detection of HDM-sIgE.

For HDM-sIgE detection, there are 2 analysis modes to select, namely the capture secondary antibody mode or the solid-phase antigen mode. The former is called the capture method; the latter is called the indirect method. In this study, the indirect LiCA analysis mode was applied. The targeting antibody preferentially binds to the solid-phase antigen, which can reduce the interference of nontarget antibodies. HDM allergens are coupled to chemibeads by chemical bonding, and allergen epitopes may be masked due to binding to aldehyde groups on the surface of the chemibeads.^{26,27} However, these masked epitopes may be exposed in a buffer system of suitable pH and ionic strength, so 4 commonly used buffer systems were prepared for the study. Based on the experimental results, 0.01 M HEPES (pH 7.2) was chosen as the best buffer system, and 0.01% Tween 20 was added to it.

As a homogeneous immunoassay, LiCA does not require separation or multiple washing steps, which eliminates the effect of washing errors. According to CLSI EP5-A2, precision is verified by repeatability and intermediate precision.²¹ The results showed that the CV values for repeatability were 4.22%, 6.67%, and 7.69% and for intermediate precision were 8.38%, 8.90%, and 10.34%. Both were acceptable in clinical practice ($<15\%$). Only $2.50 \text{ } \mu\text{L}$ of serum was used for each test, which is significantly lower than the $50 \text{ } \mu\text{L}$ used by the ImmunoCAP system ($50 \text{ } \mu\text{L}$).²⁸ Therefore, the method is suitable for specimens from infants and children. Moreover, LiCA shows excellent sensitivity because each sensibead can release 60,000 singly linear oxygen ions per second for signal amplification.²⁹

The sIgE cut-off value for allergic sensitization determined by the ImmunoCAP system is $0.35 \text{ kU}_A/\text{L}$, which is derived from the detection limit of the first assay available.³⁰ However, the results of some research³¹ have shown that the decision based on the clinical decision limit was in disagreement with the SPT. This may be partially attributed to the detection limit of the ImmunoCAP, which misses some specimens that should test positive. Moreover, this sIgE cut-off value is not suitable for all allergens. In our research findings, the LoD and LoQ of the LiCA method were $0.165 \text{ kU}_A/\text{L}$ and $0.171 \text{ kU}_A/\text{L}$, respectively. Both $0.165 \text{ kU}_A/\text{L}$ and $0.171 \text{ kU}_A/\text{L}$ were lower than $0.35 \text{ kU}_A/\text{L}$, implying that the

FIGURE 4. Methods comparison. **A**, Correlation analysis between light-initiated chemiluminescence assay (LiCA) and ELISA ($y = 0.8646x + 0.2607$; $r = 0.9263$). **B**, Correlation analysis between LiCA and ImmunoCAP ($y = 0.2279x + 0.2286$; $r = 0.8870$). ImmunoCAP is manufactured by Thermo Fisher Scientific Inc. **C**, Bland-Altman analysis between LiCA and ELISA. **D**, Bland-Altman analysis between LiCA and ImmunoCAP.



established method may be better in differentiating the specimens with positive results that have low concentrations of antibodies.

Because LiCA does not require multiple washing steps, it may be affected by interfering components in the serum specimens. Therefore, we chose hemoglobin, bilirubin, and biotin as interfering substances to evaluate the anti-interference ability of the method. The data showed that the method could tolerate 5 mg/mL bilirubin and 342 μ mol/L hemoglobin in serum specimens. Further, physiological concentrations of biotin in serum had no significant effect on the results. However, increasing the concentration of biotin resulted in a significant decrease in CL signal. Moreover, LiCA showed a statistically significant correlation with ELISA ($r = 0.9263$; $P < .001$) and ImmunoCAP ($r = 0.8870$; $P < .001$). Bland-Altman plotting demonstrated acceptable agreement between LiCA and the 2 other methods for detecting HDM-sIgE, indicating its potential clinical application in the detection of HDM-sIgE.

This study had certain limitations. First, different modes of detection (capture mode for ELISA and indirect mode for LiCA) and inconsistent results may be observed between the 2 analytical systems. Second, the small differences in HDM-sIgE levels for several specimens may be due to different allergen components, which need to be demonstrated by further studies.

In conclusion, we have successfully established an indirect LiCA for the quantitative detection of HDM-sIgE in serum. This new method improves on the shortcomings of the traditional methods, which tend to take a long time and tend to be complicated to perform. Also, the method had a good performance and met clinical laboratory standards. As a homogeneous immunoassay, there are no separation and washing steps. Therefore, LiCA can be used as a new rapid, convenient, and efficient method for HDM-sIgE quantification in medical clinics.

Supplementary Data

Supplemental figures and tables can be found in the online version of this article at www.labmedicine.com.

Acknowledgments

We thank the Clinical Laboratory of Tianjin Children's Hospital, China, for material support. This work was supported by the National Natural Science Foundation of China (81772259).

Conflict of Interest Disclosure

The authors have nothing to disclose.

REFERENCES

1. Zhang Y, Zhang L. Increasing prevalence of allergic rhinitis in China. *Allergy Asthma Immunol Res.* 2019;11(2):156–169. doi:10.4168/aaair.2019.11.2.156
2. Cardona V, Ansotegui IJ, Ebisawac M, et al. World Allergy Organization Anaphylaxis Guidance 2020. *World Allergy Organ J.* 2020;13(10):100472. doi:10.1016/j.waojou.2020.100472
3. D'Amato G, Ortega OPM, Annesi-Maesano I, D'Amato M. Prevention of allergic asthma with allergen avoidance measures and the role of exposome. *Curr Allergy Asthma Rep.* 2020;20(3):1–8. doi:10.1007/s11882-020-0901-3
4. Zhang C, Li J, Lai X, et al. House dust mite and storage mite IgE reactivity in allergic patients from Guangzhou, China. *Asian Pac J Allergy Immunol.* 2012;30(4):294–300.
5. Cheng L, Zhou W-C. Sublingual immunotherapy of house dust mite respiratory allergy in children. *Allergol Immunopathol.* 2019;47(1):85–89. doi:10.1016/j.aller.2018.02.008
6. Cao H, Liu Z. Clinical significance of dust mite allergens. *Mol Biol Rep.* 2020;47(8):6239–6246. doi:10.1007/s11033-020-05613-1
7. Wang J-Y. The innate immune response in house dust mite-induced allergic inflammation. *Allergy Asthma Immunol Res.* 2013;5(2):68–74. doi:10.4168/aaair.2013.5.2.68
8. Ye Q, Zhang T, Mao J-H. Haze facilitates sensitization to house dust mites in children. *Environ Geochem Health.* 2020;42(7):2195–2203. doi:10.1007/s10653-019-00481-6
9. Bronnert M, Mancini J, Birnbaum J, et al. Component-resolved diagnosis with commercially available *D. pteronyssinus* Der p 1, Der p 2 and Der p 10: relevant markers for house dust mite allergy. *Clin Exp Allergy.* 2012;42(9):1406–115. doi:10.1111/j.1365-2222.2012.04035.x
10. Griffiths RLM, El-Shanawany T, Jolles SRA, et al. Comparison of the performance of skin prick, ImmunoCAP, and ISAC tests in the diagnosis of patients with allergy. *Int Arch Allergy Immunol.* 2017;172(4):215–223. doi:10.1159/000464326
11. Park KH, Lee J, Sim DW, Lee SC. Comparison of Singleplex specific IgE detection immunoassays: ImmunoCAP Phadia 250 and Immulite 2000 3gAllergy. *Ann Lab Med.* 2018;38(1):23–31. doi:10.3343/alm.2018.38.1.23
12. Lambert C, Sarrat A, Bienvenu F, et al; AllergoBioNet sIgE Accreditation Interest Group. The importance of EN ISO 15189 accreditation of allergen-specific IgE determination for reliable *in vitro* allergy diagnosis. *Allergy.* 2015;70(2):180–186. doi:10.1111/all.12546
13. Shoormasti RS, Fazlollahi MR, Kazemnejad A, et al. Accuracy of immunoblotting assay for detection of specific IgE compared with ImmunoCAP in allergic patients. *Electron Physician.* 2018;10(2):6327–6332. doi:10.19082/6327
14. Ullman EF, Kirakossian H, Singh S, et al. Luminescent oxygen channeling immunoassay: measurement of particle binding kinetics by chemiluminescence. *Proc Natl Acad Sci U S A.* 1994;91(12):5426–5430. doi:10.1073/pnas.91.12.5426
15. Ullman EF, Kirakossian H, Switchenko AC, et al. Luminescent oxygen channeling assay (LOCI) sensitive, broadly applicable homogeneous immunoassay method. *Clin Chem.* 1996;42(9):1518–1526.
16. Bian Y, Liu C, She T, et al. Development of a light-initiated chemiluminescent assay for the quantitation of sIgE against egg white allergens based on component-resolved diagnosis. *Anal Bioanal Chem.* 2018;410(5):1501–1510. doi:10.1007/s00216-017-0791-y
17. Tan X, Zhang B, Zheng L, et al. Performance evaluation of a laboratory-developed light-initiated chemiluminescence assay for quantification of egg white-specific IgE. *J Clin Lab Anal.* 2022;36(7):e24544. doi:10.1002/jcla.24544
18. Zhang B, Liu D, Zheng L, et al. A light-initiated chemiluminescent assay for the detection of children's milk protein-specific IgE with excellent ability to avoid interference of specific IgG. *J Immunol Methods.* 2021;497:113110110. doi:10.1016/j.jim.2021.113110
19. Liu D, Zhang B, Zhu L, et al. A simple and rapid light-initiated chemiluminescence assay for quantitation of *Artemisia*-specific immunoglobulin E. *Int Arch Allergy Immunol.* 2022;183(5):490–497. doi:10.1159/000520511
20. Żamoć K, Wyrzykowski D, Chmurzyński L. On the effect of pH, temperature, and surfactant structure on bovine serum albumin-cationic/anionic/nonionic surfactants interactions in cacodylate buffer-fluorescence quenching studies supported by UV spectrophotometry and CD spectroscopy. *Int J Mol Sci.* 2021;23(1):41–55. doi:10.3390/ijms23010041
21. Clinical and Laboratory Standards Institute (CLSI). *Evaluation of Precision Performance of Quantitative Measurement Methods.* 2nd ed. CLSI Document EP5-A2. CLSI; 2004.
22. Clinical and Laboratory Standards Institute (CLSI). *Protocols for Determination of Limits of Detection and Limits of Quantitation Approved Guideline.* CLSI Document EP17-A. CLSI; 2004.
23. *Establishment and Verification of Detection Capability for Clinical Laboratory Measurement Procedures.* Standards Press of China; 2017.
24. *Guide to Interference Testing in Clinical Chemistry.* Standards Press of China; 2013.
25. Li J, Li S, Huang L, et al. A light-initiated chemiluminescent assay for rapid quantitation of allergen-specific IgG₄ in clinical samples. *Clin Chim Acta.* 2019;489:83–88. doi:10.1016/j.cca.2018.11.036
26. Cai Q, Zhang W-J, Zhu Q-Q, Chen Q. Influence of heat treatment on the structure and core IgE-binding epitopes of rAra h 2.02. *Food Chem.* 2016;202:404–408. doi:10.1016/j.foodchem.2016.02.004
27. Xiang Z, Chen X, Zhou X, et al. Development and application of a novel aldehyde nanoparticle-based amplified luminescent proximity homogeneous assay for rapid quantitation of pancreatic stone protein. *Clin Chim Acta.* 2022;535:120–130. doi:10.1016/j.cca.2022.08.020
28. van Hage M, Hamsten C, Valenta R. ImmunoCAP assays: pros and cons in allergology. *J Allergy Clin Immunol.* 2017;140(4):974–977. doi:10.1016/j.jaci.2017.05.008
29. Yasgar A, Jadhav A, Simeonov A, Coussens NP. AlphaScreen-based assays: ultra-high-throughput screening for small-molecule inhibitors of challenging enzymes and protein-protein interactions. *Methods Mol Biol.* 2016;1439(10):77–98. doi:10.1007/978-1-4939-3673-1_5
30. Schoos A-MM, Hansen SM, Skov FR, et al. Allergen specificity in specific IgE cutoff. *JAMA Pediatr.* 2020;174(10):993–995. doi:10.1001/jamapediatrics.2020.0944
31. Schoos A-MM, Chawes BLK, Folsgaard NV, Samandari N, Bonnellykke K, Bisgaard H. Disagreement between skin prick test and specific IgE in young children. *Allergy.* 2015;70(1):41–48. doi:10.1111/all.12523

Optimization of laboratory diagnosis of heparin-induced thrombocytopenia using HemosIL-AcuStar-HIT-IgG assay

Catherine M. Tucker, MD,¹ Ruben Rhoades, MD,² Ruchika Sharma, MD,³ Jerald Z. Gong, MD¹

¹Department of Pathology, Anatomy, and Cell Biology, Thomas Jefferson University, Philadelphia, PA, US, ²Department of Medicine, Division of Hematology, Thomas Jefferson University, Philadelphia, PA, US ³Department of Pediatrics, Division of Hematology/Oncology/BMT, Medical College of Wisconsin, Versiti Blood Research Institute, Milwaukee, WI, US. Corresponding author: Jerald Z. Gong; Jerald.gong@jefferson.edu

Key words: heparin-induced thrombocytopenia; HIT; PF4; AcuStar; ELISA; SRA

Abbreviations: HIT, heparin-induced thrombocytopenia; SRA, serotonin release assay; PF4, platelet factor 4; Ig, immunoglobulin; ELISAs, enzyme-linked immunosorbent assays; NPV, negative predictive value; FDA, US Food and Drug Administration; OD, optical density; ROC, receiver operating characteristic; AUC, area under the ROC curve; PPV, positive predictive value

Laboratory Medicine 2024;55:34-39; <https://doi.org/10.1093/labmed/lmad029>

ABSTRACT

Objective: The aim of this study was to determine an optimal cut-off value for the newly available HemosIL-AcuStar-HIT-IgG assay (AcuStar) for the diagnosis of heparin-induced thrombocytopenia (HIT).

Method: We evaluated the performance of AcuStar using serotonin release assay (SRA) as the gold standard and incorporated 4T score calculation in a cohort of suspected HIT cases. Statistical analysis was performed to determine optimal cutoff value for the diagnosis of HIT.

Result: A diagnosis of HIT can be excluded with a platelet factor 4 (PF4) value of <0.4 U/mL by AcuStar and 4T score in the low-risk category (≤ 3). All other cases will require confirmation with a functional test.

Conclusion: Our study resulted in the implementation of a diagnostic algorithm for laboratory diagnosis of HIT, which incorporates pretest calculation of 4T score and AcuStar as a screening test, with reflex confirmation by SRA. This new algorithm resulted in extended hours

of test availability and a more rapid turnaround time in reporting PF4 results.

Heparin-induced thrombocytopenia (HIT) is a clinical syndrome characterized by heparin-induced peripheral thrombocytopenia accompanied by venous or arterial thrombosis. The pathologic antibody in HIT is an immunoglobulin (Ig)G autoantibody against platelet factor 4 (PF4), which forms an immune complex with heparin and PF4. These heparin-PF4-HIT IgG complexes bind to Fc receptors on platelets, endothelial cells, and monocytes, leading to activation and ultimately pathologic thrombus formation. Heparin-induced thrombocytopenia is a rare complication of heparin therapy, occurring at a rate of approximately 0.2% to 2.7%, but more commonly in surgical patients or with the use of unfractionated heparin.^{1,2} Heparin-induced thrombocytopenia is a clinical emergency that may cause life-threatening outcomes without immediate intervention. Due to its devastating adverse clinical consequences, when HIT is suspected, heparin is discontinued immediately, even before final laboratory confirmation of HIT is obtained. Alternative anticoagulants such as direct thrombin or factor Xa inhibitors are typically used in place of heparin when HIT is suspected or confirmed.^{3,4}

Initial clinical assessment of HIT is typically conducted using various clinical scoring systems, among which the 4T score is most widely used. Calculation of the 4T score is an important assessment tool in the setting of suspected HIT.¹ The 4T score incorporates the following measures: (1) thrombocytopenia, (2) characteristic timing of thrombocytopenia, (3) presence of thrombosis or other clinical sequelae, and (4) absence of other causes of thrombocytopenia. The resulting 4T score is a pretest probability that is classified according to a point system, namely low risk (0–3 points), intermediate risk (4–5 points), and high risk (6–8 points). The negative predictive value of a low 4T score (0–3 points) can reach 99.8%, whereas the positive predictive values of intermediate and high 4T scores are more modest at 14% and 64%, respectively.⁵

Laboratory tests play a vital role in further screening and confirmation of potential HIT. Multiple screening assays with high sensitivity and prompt turnaround times are used in the evaluation of patients with suspected HIT. PF4 enzyme-linked immunosorbent assays (ELISAs) have been available for many years and are commonly used in the laboratory assessment of HIT.^{6,7} The major limitations of the ELISA

assay are its hands-on and time-consuming nature. The assay typically requires 3 to 4 hours to complete and it is difficult to incorporate the assay into the routine workflow of hematology or chemistry laboratories. The HemosIL-AcuStar-HIT-IgG assay (AcuStar) is a screening assay, newly available in the United States, that offers the advantages of rapid turnaround (40–50 minutes) and shorter hands-on time (5–10 minutes).⁸ However, previous studies have indicated that there were a high number of false-negative results associated with the manufacturer-recommended cutoff value of 1.0 U/mL.^{9–11}

Given the availability of the new AcuStar assay and the uncertainty as to which cutoff value results yield the highest negative predictive value (NPV), the goal of our study was to determine an optimal cutoff value within our laboratory. In this way, we are able to both deliver the most efficient and quality patient care and to contribute to the evolving literature on this topic. To our knowledge, this is the first study to assess the performance of the AcuStar assay in the United States.

Methods

The study was approved by the Thomas Jefferson University institutional review board. We performed a retrospective cohort study on 96 consecutive samples from patients evaluated for suspected HIT at our institution in the 2-year period from 2018 to 2020. The patient demographic data were obtained from the hospital electronic charts and reported in **TABLE 1**. Some of the study cohort cases were included and used in the initial clinical validation, which was performed as per the institutional guidelines for US Food and Drug Administration (FDA)-

cleared tests. Initial selections of the cohort included samples that were tested for PF4 ELISA, PF4 AcuStar, and serotonin release assay (SRA), and had available 4T score information. Seven samples were excluded based on the following criteria (**Supplemental Table 1**): SRA not ordered (3), SRA result not consistent (2), and values at threshold precluding a discrete quantitative result (2). A total of 89 samples were included in the final cohort. The results of samples run twice on the AcuStar and/or ELISA assay were averaged (5). The resulting 89 samples were each associated with the following data: quantitative AcuStar result, qualitative AcuStar interpretation, quantitative ELISA result, qualitative ELISA interpretation, qualitative SRA interpretation (negative, positive, borderline positive), and 4T score. The 4T scores were pulled from the electronic medical record and recalculated as needed to ensure accuracy. The performance of AcuStar was assessed in comparison to ELISA using the SRA as the gold standard.

The AcuStar assay was performed using HemosIL-AcuStar-HIT-IgG in the ACL AcuStar platform according to the manufacturer's specification (Instrumentation Laboratory). The AcuStar assay is a fully automated, quantitative/qualitative, latex-enhanced immunoassay consisting of magnetic particles coated with PF4-complexed polyvinyl sulfonate, which capture the PF4/heparin antibodies from the sample. A tracer consisting of an isoluminol-labeled anti-human IgG antibody was added, which binds to the captured PF4/heparin IgG on the particles. Reagents that trigger the luminescent reaction were then added and the emitted light was measured as relative light units by a sensor. The relative light units were directly proportional to the PF4/heparin IgG concentration in the sample. The ELISA assay was performed using the in vitro

TABLE 1. Patient demographics and 4T score according to HIT results^a

	HIT positive	HIT negative	All	P value
Patients/specimen	27 (30.3)	62 (69.7)	89 (100)	
Age, median (range), y	63 (21–82)	64 (29–91)	66 (21–91)	.447
Male	17 (63.0)	36 (58.1)	53 (59.6)	.669
Female	10 (37.0)	26 (41.9)	36 (40.4)	.669
Ethnicity				
White	23 (85.2)	39 (62.9)	62 (69.7)	.020
Black	2 (7.4)	16 (25.8)	18 (20.2)	.018
Hispanic	2 (7.4)	2 (3.2)	4 (4.5)	.461
Others	0 (0)	5 (8.1)	5 (5.6)	.024
Clinical				
Surgery	17 (63.0)	29 (46.8)	46 (51.7)	.163
ICU	23 (85.2)	51 (82.3)	74 (83.1)	.732
Type of heparin				
UFH	21 (77.8)	37 (59.7)	58 (65.2)	.196
LMWH	0 (0)	5 (8.1)	5 (5.6)	.024
Both	6 (22.2)	20 (32.3)	26 (29.2)	.325
Thrombocytopenic	27 (100)	62 (100)	89 (100)	na
Thrombosis	25 (92.6)	27 (43.5)	52 (58.4)	.000
4T score				
Low risk	1 (3.7)	14 (22.6)	15 (16.9)	.005
Intermediate risk	15 (55.6)	38 (61.3)	53 (59.6)	.622
High risk	11 (40.7)	10 (16.1)	21 (23.6)	.027

HIT, heparin-induced thrombocytopenia; ICU, intensive care unit; LMWH, low molecular weight heparin; na, not applicable; UFH, unfractionated heparin.
^aData calculated based on numbers of tested samples. Results are given as No. (%) except where noted.

diagnostic PF4 Enhanced Assay by Immucor according to the manufacturer's specification. Briefly, patient sample was added to microwells coated with PF4 complexed to polyvinyl sulfonate. After washing, an alkaline phosphatase labeled anti-human globulin reagent (anti-IgG) was added and incubated at 37°C. The substrate p-nitrophenyl phosphate was then added and the reaction was stopped after incubation for 30 minutes. The optical density was measured on the Biotek ELx800 spectrophotometer (Agilent Technologies). An optical density (OD) of ≥ 0.4 was considered positive. The SRA was performed at a reference laboratory (Versiti Blood Research Institute) using a previously described method.¹² Briefly, normal donor platelets were loaded with 14C-serotonin (Perkin Elmer), which localized to the platelet dense granules. Heat-treated patient serum was incubated with donor platelets and heparin at 37°C. After centrifugation to remove platelets, the amount of radioactivity in the supernatant was determined using a Beckman LS6500 Scintillation Counter (Beckman Coulter). The SRA was considered positive if serotonin release with low-dose (0.1 U/mL) heparin was $\geq 20\%$, and if release with high-dose (100 U/mL) heparin was $< 20\%$.

Calculation of 4T scores was based on the previously published method.¹² Four clinical parameters were scored from 0 to 2: thrombocytopenia, timing of platelet count fall, thrombosis or other sequelae, and other causes for thrombocytopenia. The scores were then added to determine the HIT risk categories as follows: 4T score 0 to 3, low risk; 4 to 5, intermediate risk; 6 to 8, high risk (TABLE 2). The 4T scores for all cases were reviewed and recalculated by one of the authors (C.M.T.). A change of 4T score was made if a discrepancy was identified between the reported 4T score and 4T score in the author's chart review.

Sample data were analyzed using MedCalc (MedCalc Software) and NCSS (NCSS) statistical software. The quantitative results of AcuStar and ELISA were compared with SRA interpretation, with 0 = negative for HIT and 1 = positive for HIT, using receiver operating characteristic (ROC) curve analysis. An ROC curve, which is a plot of the true-positive rate (sensitivity) and false-positive rate (100 – specificity) at different cutoff values, was created for AcuStar results and ELISA results. The area under the ROC curve (AUC) for the resulting graphs represented the ability of AcuStar and ELISA assays to discriminate between the disease groups (patients without HIT and patients with HIT), where an AUC of 1 represents a diagnostic assay with perfect discrimination (100% sensitivity and 100% specificity). We then analyzed a series of cutoff values for each assay, including Youden's index as calculated by MedCalc. The

NCSS Statistical Software allowed for input of our desired cutoff values of 0.2, 0.4, 0.6 (approximate Youden's index), 0.8, and 1.0 with output of sensitivity, specificity, positive predictive value (PPV), and NPV. We subsequently selected a cutoff value for AcuStar in between that would yield a sensitivity of 100% (0.2 U/mL) and that would maximally optimize both sensitivity and specificity if the test were stand-alone. We then included 4T score in combination and conducted statistical analysis using the following standard equations: sensitivity = true positives/(true positives + false negatives), specificity = true negatives/(false positives + true negatives), PPV = true positives/(true positives + false positives), and NPV = true negatives/(false negatives + true negatives).

Results

First, using ROC analysis, we found that AcuStar had a slightly higher probability of detection than ELISA for detection of HIT, with AUC values of 0.871 and 0.866, respectively. The AUC values of both assays were statistically significant ($P < .001$) and indicated excellent probability of detection for each individual assay. However, the probability of detection between the AcuStar and ELISA was not statistically significant ($P = .7362$) (Supplemental FIGURE 1). Calculated using Youden's index, the optimal cutoff value for AcuStar using ROC analysis, in the absence of additional diagnostic tests, was 0.5842. We then analyzed sensitivity, specificity, PPV, and NPV using various cutoff values of 0.2, 0.4, 0.6, 0.8, and 1.0 U/mL for the AcuStar assay. These values were increments of 0.2 from the point at which NPV was 100% (0.2 U/mL) and included Youden's index (0.6 U/mL) and the manufacturer-recommended cutoff value (1.0 U/mL) (TABLE 3). Sensitivity and NPV were 100% at a cutoff value of 0.2 U/mL. Similarly, we analyzed sensitivity, specificity, PPV, and NPV at cutoff values of 0.2, 0.4, 0.6, 0.8, and 1.0 OD for the ELISA assay. Sensitivity and NPV were 100% at a cutoff value of 0.4 OD using the ELISA assay. This cutoff value for the FDA-cleared ELISA assay was determined by the manufacturer and was used in our laboratory.

We then incorporated 4T score in the analysis, which ranged from 2 to 8 in our cohort. We correlated 3 categories of 4T scores (low, intermediate, high) with the AcuStar and SRA results and created a clinical algorithm to triage suspected HIT patients. Using SRA as the gold standard, we analyzed negative predictive values of the 3 categories of 4T scores in combination with the AcuStar assay using the predetermined cutoffs. We determined that an AcuStar value of 0.4 U/mL was the optimal

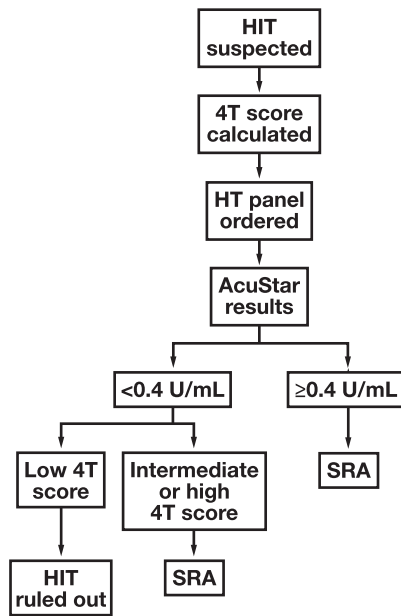
TABLE 2. 4T grading process, including description and points associated with each category

Thrombocytopenia	Platelet count fall $> 50\%$ and platelet nadir ≥ 20	+2
	Platelet count fall 30%–50% or platelet nadir 10–19	+1
	Platelet count fall $< 30\%$ or platelet nadir < 10	+0
Timing of platelet count fall	Clear onset of platelet count fall between days 5–10 or platelet count fall ≤ 1 day (heparin exposure within 30 days)	+2
	Probable platelet count fall between days 5–10, onset of platelet count fall after day 10, or platelet count fall ≤ 1 day (heparin exposure 30–100 days ago)	+1
	Platelet count fall < 4 days without recent exposure	+0
Thrombosis or other sequelae	New thrombosis or skin necrosis, acute systemic reaction post-IV heparin bolus	+2
	Progressive or recurrent thrombosis, non-necrotizing skin lesions, suspected thrombosis	+1
	None	+0
Other causes of thrombocytopenia	None apparent	+2
	Possible	+1
	Definite	+0

cutoff value (TABLE 4). Using 0.4 U/mL as the cutoff for AcuStar assay in combination with 4T score, the NPV reached 100%. A lower cutoff value would increase the number of unnecessary reflexed confirmative SRA tests, delaying final diagnosis. A higher cutoff would result in reduced NPV and therefore potentially miss rare cases of true HIT. With these results, we proposed a diagnostic algorithm incorporating 4T score with AcuStar as a screening assay and determined the optimal criteria for reflex to SRA (FIGURE 1).

When comparing AcuStar and ELISA using the cutoff values of 0.4 U/mL for AcuStar and 0.4 OD for ELISA, both tests had comparable overall sensitivity, specificity, PPV, and NPV. However, ELISA appeared to

FIGURE 1. Diagnostic algorithm used in our laboratory, consisting of 4T score calculation and reflex testing based on a cutoff value of 0.4 U/mL using the AcuStar assay. HIT, heparin-induced thrombocytopenia; SRA, serotonin release assay.



perform slightly better in sensitivity whereas AcuStar performed better in specificity in the low-risk group (TABLES 4 and 5). The overall NPV for ELISA was excellent at 100%, whereas AcuStar had a slightly lower overall NPV at 95%. The lower NPV by AcuStar was caused by 2 false-negative cases in the intermediate risk group (TABLES 4 and 5). Seventy-one cases showed concordant results between ELISA and AcuStar, whereas 18 cases were discordant. Of the discordant cases, AcuStar interpretation was positive and ELISA was negative in 1 case, and the final SRA interpretation was negative. Of the remaining 17 cases in which the AcuStar interpretation was negative and the ELISA interpretation was positive, the final SRA was negative in 11 cases, positive in 3 cases, borderline positive in 1 case, and not consistent in 2 cases (Supplemental Table 2).

Discussion

HemosIL-AcuStar-HIT-IgG chemiluminescent immunoassay (AcuStar) is a recently available semi-automated screening test for HIT. Compared with the widely used ELISA test, AcuStar has the advantage of fast turnaround time and is easy to perform with a high level of automation. These advantages allow clinical laboratories to perform tests within more extended hours, which is critical in managing suspected HIT patients.⁸ However, although a cutoff value was established by the manufacturer, multiple studies have shown increased numbers of false-negative results and as such, various cutoff values were proposed.^{9–14} A consensus optimal cutoff value has not yet been established.

Nearly all previous studies of the AcuStar assay were from European groups.^{9–14} In a study of 87 suspected HIT cases, Van Hoecke et al⁹ found 100% sensitivity and 100% NPV by AcuStar using the manufacturer's recommended cutoff value (1.0 U/mL), which is in contrast to our results of 77.8% and 87.8% respectively. The study used a flow cytometry-based functional confirmative test by assessing platelet surface expression of CD62p. Marchetti et al¹⁰ determined an algorithm for ruling HIT in or out, in which the authors combined pretest probability (4T score) with first- and second-line assays. The authors commented that there were a high number of false-negative results using the manufacturer-recommended

TABLE 3. Sensitivity, specificity, positive predictive value (PPV), and negative predictive value (NPV) for the AcuStar assay using various cutoff values of 0.2, 0.4, 0.6, 0.8, and 1.0 U/mL and serotonin release assay as the gold standard

Cutoff value, U/mL	Sensitivity (95% CI), %	Specificity (95% CI), %	PPV (95% CI), %	NPV (95% CI), %
0.2	100 (87.2–100)	50 (37.0–63.0)	46.55 (33.3–60.1)	100 (88.8–100)
0.4	88.9 (70.8–97.7)	59.7 (46.5–72.0)	49.0 (34.4–63.7)	92.5 (79.6–98.4)
0.6	85.2 (66.3–95.8)	67.7 (54.7–79.1)	53.5 (37.7–68.8)	91.3 (79.2–97.6)
0.8	77.8 (57.7–91.4)	67.7 (54.7–79.1)	51.2 (35.1–67.1)	87.5 (74.8–95.3)
1.0	77.8 (57.7–91.4)	69.4 (56.4–80.4)	52.5 (36.1–68.5)	87.8 (75.2–95.4)

TABLE 4. Sensitivity, specificity, positive predictive value (PPV), and negative predictive value (NPV) for the AcuStar assay using 0.4 U/mL as cutoff value with incorporation of the 3 risk groups of 4T score

HIT risk by 4T score	Sensitivity, % (No. of cases)	Specificity, % (No. of cases)	PPV, % (No. of cases)	NPV, % (No. of cases)
Low (n = 19)	75.0 (3/4)	60.0 (9/15)	33.3 (3/9)	100 (10/10)
Intermediate (n = 49)	91.1 (10/11)	42.1 (16/38)	40.0 (10/25)	91.7 (22/24)
High (n = 21)	100 (11/11)	60.0 (6/10)	73.3 (11/15)	100 (6/6)
All cases (n = 89)	92.3 (24/26)	49.2 (31/63)	49.0 (24/49)	95.0 (38/40)

HIT, heparin-induced thrombocytopenia.

TABLE 5. Sensitivity, specificity, positive predictive value (PPV), and negative predictive value (NPV) for the enzyme-linked immunosorbent assay using 0.4 OD as cutoff value with incorporation of the 3 risk groups of 4T score

HIT risk by 4T score	Sensitivity, % (No. of cases)	Specificity, % (No. of cases)	PPV, % (No. of cases)	NPV, % (No. of cases)
Low (n = 19)	100 (4/4)	26.7 (4/15)	28.6 (4/14)	100 (5/5)
Intermediate (n = 49)	100 (11/11)	55.3 (21/38)	39.3 (11/28)	100 (21/21)
High (n = 21)	100 (11/11)	60.0 (6/10)	73.3 (11/15)	100 (6/6)
All cases (n = 89)	100 (26/26)	49.2 (31/63)	45.6 (26/57)	100 (32/32)

HIT, heparin-induced thrombocytopenia.

cutoff value of 1.0 U/mL, with a sensitivity of 80.8%. They were unable to exclude HIT in the presence of a low or intermediate pretest probability unless the assay cutoff was <0.13 U/mL. Althaus et al¹¹ compared the performance of AcuStar and ELISA using the heparin-induced platelet activation assay as the confirmative test. The study identified an optimal cutoff of 0.57 U/mL with sensitivity of 98.1%, PPV of 66.2%, and NPV of 99.7%. Using the proposed cutoff value, the authors concluded that optimal compromise (trade-off) was reached between sensitivity and specificity. Vianello et al¹⁴ used ROC analysis to determine an optimal cutoff value of 1.13 U/mL for AcuStar. The authors reported sensitivity and specificity of 95% and 98%, respectively. However, the NPV was not analyzed in their study.

To date, there are no HIT screening tests that offer both high PPV and high NPV. Studies have shown that higher PF4 values by AcuStar were associated with higher probability of having HIT.¹⁵ However, a higher cutoff value will invariably decrease the NPV with an increased rate of false-negative cases. Because the potential clinical consequences of HIT are severe, a high NPV (ideally 100%) from a screening test is essential to ensure that all HIT patients are properly identified, although this inevitably allows some degree of sacrifice of PPV. Several studies, including ours, have observed that variable numbers of false-negative cases were observed when using the manufacturer's recommended cutoff of 1.0 U/mL.^{6,10} We designed our experiments using variable cutoff values starting from 0.2 U/mL with 0.2 U/mL increments and assessed the screening power of each category separately. We found that when using AcuStar alone, the most optimal cutoff was 0.2 U/mL, which had an NPV of 100%. However, this cutoff also had the lowest specificity and PPV. When factoring in the result of the 4T score, the optimal cutoff of AcuStar increased to 0.4 U/mL. This still allowed an NPV of 100% with increased specificity and PPV. Further increasing the AcuStar cutoff to 0.6 U/mL or above did not provide 100% NPV even with the combination of 4T score. Similar results were observed by Warkentin et al.¹⁶ They had reported 100% NPV on AcuStar using the same cutoff of 0.4 U/mL and only 1 (of 448 patients total) false-negative using the manufacturer's recommended cutoff (1.0 U/mL). This single HIT-positive patient had an intermediate risk 4T score.

We have determined that HIT can be ruled out (NPV of 100%) with the combination of 4T score of ≤ 3 combined and AcuStar value of <0.4 U/mL. SRA confirmation is not necessary in this group of patients and the clinical management of heparin anticoagulation may safely continue. If either 4T ≥ 4 or AcuStar ≥ 0.4 U/mL, confirmation by SRA is needed to further rule in or rule out HIT, along with relevant clinical information. In the author's institution's experience, using this algorithm, 9.0% of suspected HIT cases were ruled out by screening test, as compared with 4.5% by ELISA using a similar algorithm (data not shown). Although high percentages of SRA tests in suspected HIT cases are still necessary for both tests, AcuStar can be used in more extended

laboratory hours in our institution (7 days a week), which shortens the waiting time for results when tests are requested in off-hours and on weekends. This allows more rapid clinical decision-making for these patients.¹⁷ By implementing this newly available screening assay, we are able to provide improved patient care while simultaneously conserving healthcare resources.

Our study has certain strengths and limitations. Our retrospective cohort represents all patients with possible or suspected HIT at our institution within a certain timeframe; thus, it is most representative of a hospital-based clinical practice. The design of our study also facilitates an accurate assessment of 4T scores. Initial 4T scores as part of the PF4 order set were determined by ordering providers, which were frequently prone to subjective and objective errors due to interobserver variability. In this study, all the 4T scores were first obtained from the patient chart followed by central review by one of the authors (C.M.T.) to confirm the accuracy of the scores. If the scores were deemed inaccurate, the newly calculated scores were used for the final data. It is worth noting that, although our algorithm provides 100% NPV in our patient population, an additional testing parameter such as immature platelet fraction (IPF), PF4-dependent P-selectin expression assay (PEA), or heparin-induced multiple electrode aggregometry (HIMEA) may be helpful or indicated depending on the clinical setting. The algorithm should therefore be adjusted as needed if applied in other laboratories. Our study is limited by the number of subjects included in the cohort, which was relatively low as compared with some of the larger studies. This may affect the calculation of prevalence of HIT in the population, thus affecting NPV. Future studies including a larger cohort over a longer period of time may mitigate these effects, as would future studies determining prevalence of HIT in our institution or within the general local population.

In conclusion, our study assessed the performance of an automated HIT screening test in a large tertiary care hospital in the United States and evaluated the diagnostic feasibility of HIT using the manufacturer-recommended cutoff value of 1.0 U/mL. We compared the AcuStar assay with the traditional ELISA assay and used SRA as the gold standard. We further incorporated 4T score in the diagnostic algorithm. We conclude that a combination of AcuStar <0.4 U/mL and 4T score of ≤ 3 (low-risk category) had an NPV of 100% and SRA confirmation is not needed. SRA confirmation was still necessary in the remaining patients. Based on our results, we have created a diagnostic algorithm using the 4T score, AcuStar, and SRA, which was subsequently implemented in our institution. The implementation of the diagnostic algorithm using the AcuStar provided fast turnaround time, extended hours of test availability, and delivered more efficient and quality patient care.

Acknowledgments

These data were presented as an abstract and poster at USCAP 2021.

Funding

The study was partially supported by a grant from Instrument Laboratory.

Conflict of Interest Disclosure

The authors have nothing to disclose.

REFERENCES

1. Martel N, Lee J, Wells PS. Risk for heparin-induced thrombocytopenia with unfractionated and low-molecular-weight heparin thromboprophylaxis: a meta-analysis. *Blood*. 2005;106(8):2710–2715. doi:10.1182/blood-2005-04-1546.
2. Warkentin TE, Levine MN, Hirsh J, et al. Heparin-induced thrombocytopenia in patients treated with low-molecular-weight heparin or unfractionated heparin. *N Engl J Med*. 1995;332(20):1330–1335. doi:10.1056/NEJM199505183322003.
3. Cuker A, Arepally GM, Chong BH, et al. American Society of Hematology 2018 guidelines for management of venous thromboembolism: heparin-induced thrombocytopenia. *Blood Adv*. 2018;2(22):3360–3392. doi:10.1182/bloodadvances.2018024489.
4. McKenzie SE, Sachais BS. Advances in the pathophysiology and treatment of heparin-induced thrombocytopenia. *Curr Opin Hematol*. 2014;21(5):380–387. doi:10.1097/MOH.0000000000000066.
5. Cuker A, Gimotty PA, Crowther MA, Warkentin TE. Predictive value of the 4Ts scoring system for heparin-induced thrombocytopenia: a systematic review and meta-analysis. *Blood*. 2012;120(20):4160–4167. doi:10.1182/blood-2012-07-443051.
6. Jousset E, Guery EA, Nougier C, et al. Prospective evaluation of two specific IgG immunoassays (HemosIL AcuStar HIT-IgG and HAT45G) for the diagnosis of heparin-induced thrombocytopenia: a Bayesian approach. *Int J Lab Hematol*. 2020;43:468–476. doi:10.1111/ijlh.13404.
7. Husseinzadeh HD, Gimotty PA, Pishko AM, et al. Diagnostic accuracy of IgG-specific versus polyspecific enzyme-linked immunoassays in heparin-induced thrombocytopenia: a systematic review and meta-analysis. *J Thromb Haemost*. 2017;15(6):1203–1212.
8. Nagler M, Cuker A. Profile of instrumentation laboratory's HemosIL® AcuStar HIT-Ab (PF4-H) assay for diagnosis of heparin-induced thrombocytopenia. *Expert Rev Mol Diagn*. 2017;17(5):419–426. doi:10.1080/14737159.2017.1304213.
9. Van Hoecke F, Devreese K. Evaluation of two new automated chemiluminescent assays (HemosIL® AcuStar HIT-IgG and HemosIL® AcuStar HIT-Ab) for the detection of heparin-induced antibodies in the diagnosis of heparin-induced thrombocytopenia. *Int J Lab Hematol*. 2012;34(4):410–416. doi:10.1111/j.1751-553X.2012.01413.x.
10. Marchetti M, Barelli S, Zermatten MG, et al. Rapid and accurate Bayesian diagnosis of heparin-induced thrombocytopenia. *Blood*. 2020;135(14):1171–1184. doi:10.1182/blood.2019002845.
11. Althaus K, Hron G, Strobel U, et al. Evaluation of automated immunoassays in the diagnosis of heparin induced thrombocytopenia. *Thromb Res*. 2013;131(3):e85–e90. doi:10.1016/j.thromres.2013.01.005.
12. Sheridan D, Carter C, Kelton JG. A diagnostic test for heparin-induced thrombocytopenia. *Blood*. 1986;67(1):27–30.
13. Lo GK, Warkentin TE, Sigouin CS, et al. Evaluation of pretest clinical score (4T's) for the diagnosis of heparin-induced thrombocytopenia in two clinical settings. *J Thromb Haemost*. 2006;4(4):759–765.
14. Vianello F, Sambado L, Scarparo P, et al. Comparison of three different immunoassays in the diagnosis of heparin-induced thrombocytopenia. *Clin Chem Lab Med*. 2015;53(2):257–263. doi:10.1515/cclm-2014-0809.
15. Marashi-Sabouni Z, Vayne C, Ibrahim-Kosta M, et al. Clinical validation of immunoassay HemosIL AcuStar HIT-IgG (PF4-H) in the diagnosis of heparin-induced thrombocytopenia. *J Thromb Thrombol*. 2021;52:601–609.
16. Warkentin TE, Sheppard J-AI, Linkins L-A, Arnold DM, Nazy I. High sensitivity and specificity of an automated IgG-specific chemiluminescence immunoassay for diagnosis of HIT. *Blood*. 2018;132(12):1345–1349. doi:10.1182/blood-2018-04-847483.
17. Dykes KC, Johnson CA, Gong JZ, et al. Bleeding and thrombotic adverse events in hospitalized patients under empiric treatment for suspected heparin-induced thrombocytopenia while awaiting confirmatory testing. *Clin Appl Thromb/Hematost*. 2021;27:1–6.

Diagnostic value of dual-fluorescence staining in bacterial vaginosis

Cui Li,^{1,*} Zhongliang Duan,^{1,*} Jing Zhang,² Jing Gao,¹ Chunmei Ying¹

¹Clinical Laboratory, Obstetrics and Gynecology Hospital of Fudan University, Shanghai, China, ²Shanghai University of Medicine & Health Sciences, Shanghai, China. Corresponding author: Chunmei Ying; ycmzh2012@163.com.

*Contributed equally.

Key words: dual-fluorescence stain; bacterial vaginosis; diagnostic value; Gram stain; epidemiology

Abbreviations: BV, bacterial vaginosis; VVC, *Candida* vaginitis; TV, *Trichomonas* vaginitis; LIS, laboratory information system

Laboratory Medicine 2024;55:40-44; <https://doi.org/10.1093/labmed/lmad034>

ABSTRACT

Objective: The aim of this study was to investigate the epidemiology of bacterial vaginosis (BV) in Shanghai, China, and to explore the value of a dual-fluorescence staining method in the diagnosis of BV.

Methods: Specimens were collected from women with vaginitis at the Obstetrics and Gynecology Hospital of Fudan University from January 2020 to December 2021, and the proportions of various vaginitis types (such as *Candida* vaginitis, *Trichomonas*, and bacterial vaginitis) were analyzed statistically. To explore the diagnostic value of dual-fluorescence staining for BV, we first executed a dual-fluorescence staining method to analyze the vaginal secretions of 265 patients, then confirmed our diagnoses by consulting clinical physicians and by using Nugent scoring of Gram staining.

Results: There were 16,905 patients who were diagnosed with vaginitis over the previous 2 years, with a median age of 32 (minimum age of 9 years and maximum of 84 years). Of these patients, we noted 10,887 cases (64.40%) of BV. Our staining results revealed that the dual-fluorescence method was consistent with Gram staining in the diagnosis of BV, with a *P* value of less than .001 using a χ^2 test and a consistency kappa value of 0.896. Compared with Gram staining, the dual-fluorescence staining method required an acceptable time (2.2 min vs 2.5 min, respectively) and exhibited different visual effects (green and yellow vs purple and red, respectively).

Conclusion: Dual-fluorescence staining for the detection of bacterial diseases of the vagina exhibited acceptable consistency with Gram staining and performed well with respect to dyeing time, stability, and the interpretation of results. We argue that this method should be used in outpatient services.

Bacterial vaginosis (BV) encompasses disorders of vaginal bacterial communities or pathogen infections caused by a diminution in the abundance or the complete disappearance of *Lactobacillus* and an elevation in the abundance of anaerobic or facultative anaerobic bacteria.¹ Common pathogens include facultative anaerobes (eg, *Gardnerella vaginalis*), anaerobes (*Prevotella*, *Campylobacter*, *Bacteroidetes*, *Atopourella vaginalis*), *Ureaplasma urealyticum*, and *Mycoplasma hominis*.² Bacterial vaginosis is one of the most common infectious vaginal diseases in women of childbearing age, and it primarily occurs in sexually active women. There are many complications associated with BV, including pelvic inflammatory disease, gynecological infection, infertility, and abnormal pregnancy,³ and BV pathogens are complexed with many other pathogens. The disease has a high recurrence rate after treatment⁴ that can cause serious harm to female reproductive health.⁵ Symptoms of BV are often atypical, and its diagnosis is easily missed. The incidence of BV varies by countries and regions due to the diversity of patients, races, and diagnostic methods,⁶ and its incidence is high in part due to concurrence with immunodeficiency disease.⁷ Approximately 11% of women undergoing physical examinations are infected with BV, and 36%–60% of outpatients are infected with BV in China according to 1 report;⁸ however, epidemiological data regarding BV in China are lacking.

Rapid and accurate diagnosis of BV using vaginal secretions is an important prerequisite for appropriate clinical treatment, particularly with outpatients. The Gram staining method is relatively accurate but time-consuming. The stain colors (purple and red) are not easily distinguished for some technicians, and their identification partially depends on the technique used by each technician. Thus, Gram staining is not suitable for outpatient testing. Examination of vaginal microbial chips is another diagnostic method,⁹ but it is relatively expensive. A novel method therefore needs to be sought that is easy to perform, requires less time than the Gram staining method, and is inexpensive. Dual-fluorescence staining is one such newly developed method that applies direct microscopic examination using a fluorescence microscope that can store photomicrographs and allows collective reporting for direct clinical review.

There are currently few reports on the application and resulting data of this technique in the routine analysis of vaginal secretions. For this study, we therefore analyzed the advantages and disadvantages of a dual-fluorescence staining system in the detection of BV by comparing it with the classical Gram staining method for the detection of BV.

Materials and Methods

Sources of Specimens and Clinical Data

Specimens from outpatient vaginitis patients in the Department of Gynecology at the Obstetrics and Gynecology Hospital of Fudan University from January 2020 to December 2021 were collected for analysis, including the proportions of various vaginitis types—*Candida* vaginitis (VVC), *Trichomonas* vaginitis (TV), and BV. Bacterial vaginosis was diagnosed by exploiting a clinical and laboratory vaginal microbial chip and confirmed by gynecologists. We also collected derived data and clinical information. The microbial chip method, BD Affirm VPIII Microbial Identification Test (Affirm, BD), has been widely used in our hospital. The main principle is based on the principle of nucleic acid hybridization. The specimens were cracked, combined with a probe analysis card including capture probe and chromogenic probe, and interpreted according to the chromogenic results. Bacterial vaginosis was associated with increase of *Gardnerella vaginalis* in this method.

Finally, 16,905 patients were enrolled in this study for clinical data analysis, and we selected 265 random specimens from them for method comparison.

Gram staining and dual-fluorescence staining were used to analyze vaginal secretions of patients. We subsequently compared the sensitivity, specificity, consistency, time, and visual effects of the novel staining technique with Gram staining to illustrate the diagnostic value of the novel method. For Gram staining, Nugent score was used to diagnose BV, with the Nugent score no less than 7. As dual-fluorescence staining is a morphological method, the Nugent score was also used to diagnose BV, with the Nugent score no less than 7.

This study complied with the principles of the Declaration of Helsinki and was approved by the Ethics Committee of the Obstetrics and Gynecology Hospital of Fudan University.

Principles of Dual-Fluorescence Staining

This modality uses fluorescent dyes to stain DNA, RNA, dextran, and peptidoglycan in vaginal secretion samples such that each target component displays a different color under a specific wavelength of fluorescence excitation. The combination of the fluorescent stains with methyl green as a counterstain significantly improved the coloration of cell structures.¹⁰ This compound staining method also clarified the morphologies of epithelial cells, leukocytes, bacilli, cocci, *Candida*, and *Trichomonas* under a fluorescence microscope, thus allowing convenient observation and evaluation.

Materials, Equipment, and Reagents

We used an OLYMPUS CX series microscope and fluorescence analysis system, an automatic dye machine (Minomics) and a dual-fluorescence staining solution (Medomics Medical Technology), ordinary glass slides, cover slips, 0.9% normal saline, and a thermostatically controlled heater.

Sample Testing Process

Operation of the Microscopy System

We set the serial number and other relevant indices and connected the microscopy system to a laboratory information system (LIS).

Preparation of Patient Information

Patient information was input to the LIS.

Preparation of Specimens

We placed vaginal secretions onto a microslide, dried the specimen with a heater, cooled the specimen, and inserted it into the dyeing machine for automatic staining under green light. We subsequently removed the microslide when the green light flashed, coverslipped it, dried it with absorbent paper, and proceeded with our analysis.

Microscopic Examination

Vaginal secretions were stained and the morphological types of different bacteria were observed under a microscope ($\times 1000$, oil immersion, OLYMPUS CX23). We selected at least 2 images to provide for an appropriate field of vision and analyzed and stored them; a laboratory technician ultimately reviewed the report and transmitted it to the LIS.

Statistical Analysis

Continuous variables are presented as means \pm SD or median and interquartile range according to their normality of distribution (as assessed with the Shapiro-Wilk test). We used the χ^2 test for categorical data, and the Mann-Whitney *U* test was applied to compare data that did not follow a normal distribution. Data were analyzed using SPSS 19 software (SPSS) and GraphPad Prism 7 (GraphPad). The kappa consistency test and paired χ^2 test were adopted to compare the difference between the 2 staining methods: a kappa greater than or equal to 0.75 was considered to exhibit acceptable consistency, a kappa greater than or equal to 0.4 and less than 0.75 was considered generally consistent, and a kappa less than 0.4 was considered to show poor consistency. A *P* value $< .05$ denoted statistical significance.

Results

Clinical Information

There were 16,905 patients in this study, with a median age (interquartile range) of 32 years (27, 41); the youngest was 9 years of age and the oldest was 84 years old. Among the total 16,905 patients with vaginitis, we noted only 3 with all 3 types of vaginitis, accounting for 0.02%, whereas there were 126 cases (0.75%) with both BV and TV, one case with TV and VVC (0.01%), and 2521 cases (14.91%) with BV and VVC. Regarding infection with only a single type of vaginitis, we observed 230 cases (1.36%) with TV, 3137 cases (18.56%) with VVC, and 10,887 cases (64.40%) with BV. Importantly, there were 5204 patients (30.78%) who were re-infected with vaginitis 6 months later. Thus, vaginitis is certainly worthy of serious consideration in the clinic, especially with respect to BV (TABLE 1).

Comparisons of Diagnostic Value Between Gram Staining and Dual-Fluorescence Staining Methods

To compare the dual-fluorescence staining method with Gram staining, we evaluated 265 specimens that were additionally diagnosed via clinical and laboratory examinations of vaginal microbial chips and confirmed

by gynecologists. Representative characteristics and results are shown in **FIGURE 1** and **TABLE 2**.

Dual-fluorescence staining revealed 215 cases of BV, whereas there were 206 cases of BV detected by the Gram-staining method; our

analysis showed a P value of less than .001 by χ^2 test and a kappa value of 0.896 for consistency. Our results thus reflected favorable consistency between double-fluorescence staining and Gram staining in the diagnosis of BV. Comparison of the 2 methods regarding acceptable time (2.2 min vs 2.5 min, respectively), different visual effects (distinguishing green from yellow vs purple from red, respectively) and other characteristics are shown in **TABLE 3**.

TABLE 1. Percentages of patients (n = 16,905) with different types of vaginitis

Types	No. (%) of patients
TV + BV + VVC	3 (0.02)
TV + BV	126 (0.75)
TV + VVC	1 (0.01)
BV + VVC	2521 (14.91)
TV	230 (1.36)
WC	3137 (18.56)
BV	10,887 (64.40)

BV, bacterial vaginosis; TV, *Trichomonas vaginitis*; VVC, *Candida vaginitis*.

Discussion

With the increasing attention paid to women's health in the modern society, the concept of involvement of female reproductive tract microecology in the onset of disease has achieved heightened recognition. Pathogen infection or an imbalance in local flora may precipitate related gynecological and pregnancy-related diseases.^{11,12} Examination of vaginal secretions is currently the most routine clinical detection method used to observe the vaginal environment. Patients with BV often show significant changes in the dominant flora of the vaginal environment. As shown in our study, over 64.40% of vaginitis patients

FIGURE 1. Views of dual-fluorescence staining (A and B) and Gram staining (C and D) in the diagnosis of bacterial vaginosis. A, Epithelial cells and *Lactobacillus* in the BV-negative group. B, The clue cells are in the BV-positive group. Gram-negative (C) and Gram-positive (D) bacteria were observed under a microscope (x1000, oil immersion).

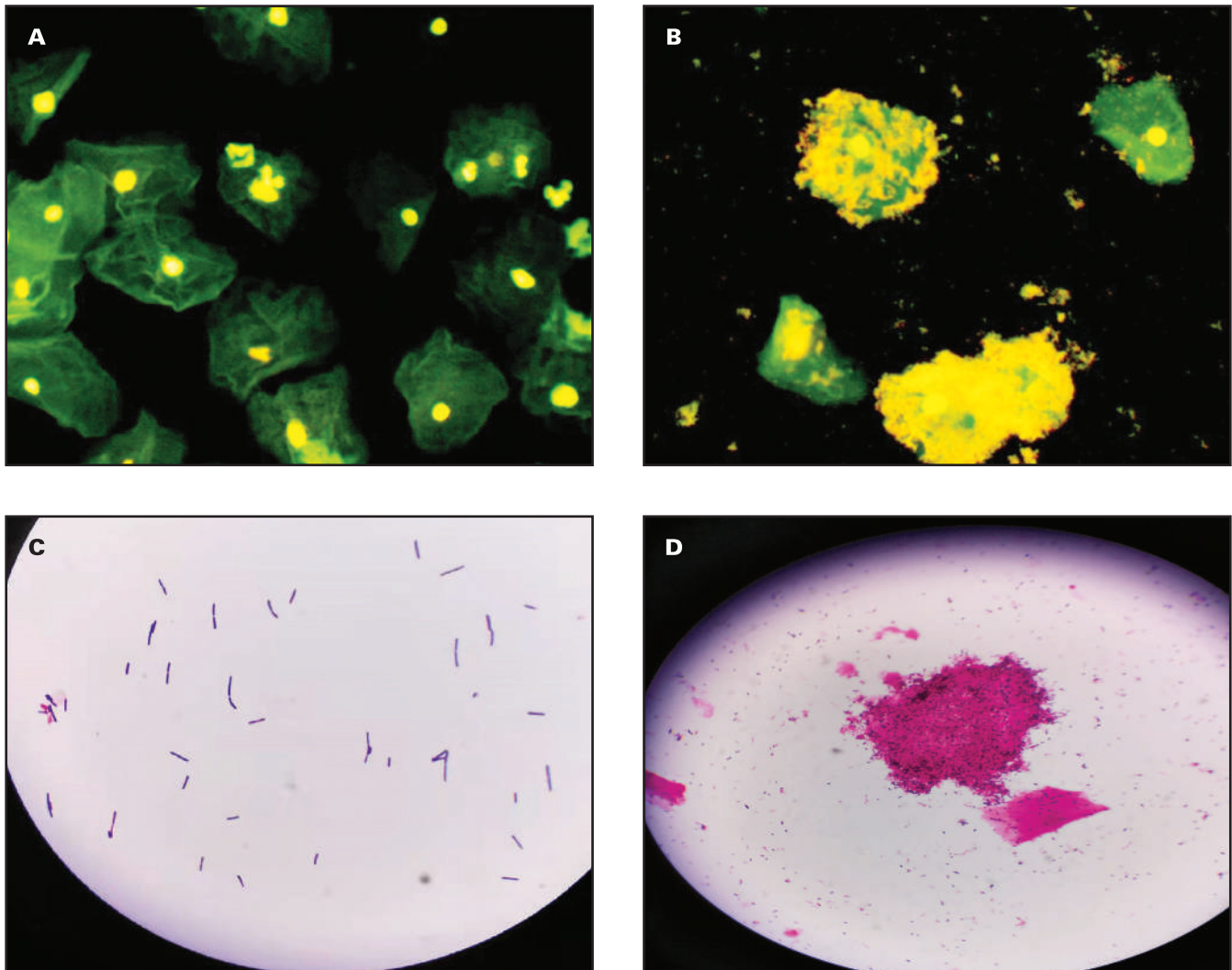


TABLE 2. Comparison of dual-fluorescence staining and Gram staining in the diagnosis of bacterial vaginosis

	Gram staining		Total
	Positive	Negative	
Dual-fluorescence staining			
Positive	206	9	215
Negative	0	50	50
Total	206	59	265

TABLE 3. Comparison and correlation between dual-fluorescence staining and Gram staining

	Gram staining	Dual-fluorescence staining
Testing time (min)	2.5	2.2
Color	Purple vs red	Yellow vs green
Sensitivity ^a		100.00%
Specificity ^a		84.75%
Consistency kappa value ^a		0.896 ^b
Pearson correlation coefficient ^a		0.901 ^b

^aCompared or correlated with Gram staining.

^b $P < .001$.

manifested BV, with the youngest at 9 years of age and the oldest at 84 years. Thus, BV is certainly worthy of receiving greater attention in the clinic.

The Amsel standard is the clinical gold standard for the diagnosis of BV. Diagnostic BV is defined as positivity for at least 3 of the following 4 clinical features: primary positivity for clue cells (ie, the number of clue cells over 20% of the total number of vaginal epithelial cells); a positive reaction on the amine test; a pH value of vaginal secretions > 4.5 ; and vaginal secretions that are homogeneous, thin, and grayish white, and have positivity for clue cells.¹³ Nugent scoring of Gram staining is the laboratory gold standard for the diagnosis of BV. To an extent, our novel method combined the evidence of positive clue cells within the Amsel criteria with the characteristics of microflora distribution using the Nugent score.

In addition to the above diagnostic criteria, there are other methods used for the diagnosis of BV as a clinical reference in China and elsewhere. For example, Hay-Ison scoring has been implemented, as have graded Gram-stain smears of vaginal secretions.^{14,15} In terms of molecular diagnosis, nucleic acid detection of *Gardnerella* has been implemented in BV, including the Affirm VPIII and Aptima BV assays, which revealed a sensitivity of 78%–100%. There are also some functional assays used for the detection of BV. For example, regarding the detection of the anaerobic bacterial metabolite sialidase, we suggest that functional detection be combined with morphological detection results, and when the functional and morphological results are inconsistent, we suggest that the morphological detection results prevail.

Our novel dual-fluorescence staining method allowed clear differentiation among epithelial cells, leukocytes, bacilli, cocci, *Candida*, and *Trichomonas* under the fluorescence microscope; this is convenient for microscopic observation and evaluation. Moreover, dyeing and electronic reporting can be completed within 2 min after mastery of the technique, showing robust operational capability for outpatient departments. This method has the advantages of simple operation, rapid detection, and acceptable observation and identification of pathogenic microorganisms after staining. In addition, we were able to circumvent

the effects of interference from contamination in samples such as blood, semen, and basal-layer cells on detection results; accuracy and detection rates were thus effectively improved. However, after comparative analysis and practical operational experience, we also found that there were certain interfering factors that affected this method; for example, specimens need to be sent for inspection immediately after being collected. If delayed (such as by over 2 h), abnormal results could be obtained. The location of specimen collection is also critical to obtaining appropriate samples, and a sufficient number of specimens need to be collected. The uniformity of the vaginal smear also has an impact on the results, as the smear cannot be too thick.

This method was first used in an outpatient setting for quick testing; however, it could be widely used in the clinical laboratory, pathology department, and molecular laboratory. According to its principle, this method could also be used to examine many other materials, such as peritoneal fluid.

To summarize, BV accounts for 64.40% of vaginitis in China. Dual-fluorescence staining for the detection of BV manifested good consistency with the Gram-staining method while showing advantages in dyeing time, stability, and the interpretation of results. Thus, we postulate that dual-fluorescence staining as a novel modality is worth pursuing in outpatient gynecology departments and other clinical laboratories.

Conclusion

Vaginitis is certainly worthy of serious consideration in the clinic, especially with respect to BV. Dual-fluorescence staining for the detection of bacterial vaginal diseases showed acceptable consistency with Gram staining and performed well with respect to dyeing time, stability, and interpretation of results. We therefore argue that this modality should be used by outpatient services.

Acknowledgments

We thank LetPub (www.letpub.com) for its linguistic assistance during the preparation of this manuscript.

Funding

This work was supported by grants from the National Natural Science Foundation of China (No. 81873970 to C.Y. and No. 82102469 to Z.D.).

Conflict of Interest Disclosure

The authors have nothing to disclose.

REFERENCES

- Schwebke JR. New concepts in the etiology of bacterial vaginosis. *Curr Infect Dis Rep*. 2009;11:143–147. doi: 10.1007/s11908-009-0021-7
- Yuan D, Chen W, Qin J, et al. Associations between bacterial vaginosis, candida vaginitis, trichomonas vaginalis, and vaginal pathogenic community in Chinese women. *Am J Transl Res*. 2021;13:7148–7155.
- Redelinghuys MJ, Ehlers MM, Dreyer AW, et al. Normal flora and bacterial vaginosis in pregnancy: an overview. *Crit Rev Microbiol*. 2016a;42:352–363. doi: 10.3109/1040841X.2014.954522

4. Bradshaw CS, Morton AN, Hocking J, et al. High recurrence rates of bacterial vaginosis over the course of 12 months after oral metronidazole therapy and factors associated with recurrence. *J Infect Dis*. 2006;193:1478–1486. doi: [10.1086/503780](https://doi.org/10.1086/503780)
5. Doerflinger SY, Throop AL, Herbst-Kralovetz MM. Bacteria in the vaginal microbiome alter the innate immune response and barrier properties of the human vaginal epithelia in a species-specific manner. *J Infect Dis*. 2014;209:1989–1999. doi: [10.1093/infdis/jiu004](https://doi.org/10.1093/infdis/jiu004)
6. Kenyon C, Colebunders R, Crucitti T. The global epidemiology of bacterial vaginosis: a systematic review. *Am J Obstet Gynecol*. 2013;209:505–523. doi: [10.1016/j.ajog.2013.05.006](https://doi.org/10.1016/j.ajog.2013.05.006)
7. Torrone EA, Morrison CS, Chen PL, et al. Prevalence of sexually transmitted infections and bacterial vaginosis among women in sub-Saharan Africa: an individual participant data meta-analysis of 18 HIV prevention studies. *PLoS Med*. 2018;15:e1002511. doi: [10.1371/journal.pmed.1002511](https://doi.org/10.1371/journal.pmed.1002511)
8. Fan A, Yue Y, Geng N, et al. Aerobic vaginitis and mixed infections: comparison of clinical and laboratory findings. *Arch Gynecol Obstet*. 2013;287:329–335. doi: [10.1007/s00404-012-2571-4](https://doi.org/10.1007/s00404-012-2571-4)
9. Cartwright CP, Lembke BD, Ramachandran K, et al. Comparison of nucleic acid amplification assays with BD affirm VPIII for diagnosis of vaginitis in symptomatic women. *J Clin Microbiol*. 2013;51:3694–3699. doi: [10.1128/JCM.01537-13](https://doi.org/10.1128/JCM.01537-13)
10. Zipper H, Brunner H, Bernhagen J, et al. Investigations on DNA intercalation and surface binding by SYBR Green I, its structure determination and methodological implications. *Nucleic Acids Res*. 2004;32:e103. doi: [10.1093/nar/gnh101](https://doi.org/10.1093/nar/gnh101)
11. Liu X, Xiao Y, Zhang H, et al. Comparison of vaginal flora in patients with spontaneous abortion and women with normal first-trimester. *Reprod Dev Med*. 2018;2:150. doi: [10.4103/2096-2924.248490](https://doi.org/10.4103/2096-2924.248490)
12. Redelinghuys MJ, Ehlers MM, Dreyer AW, et al. Normal flora and bacterial vaginosis in pregnancy: an overview. *Crit Rev Microbiol*. 2016b;42:352–363. doi: [10.3109/1040841X.2014.954522](https://doi.org/10.3109/1040841X.2014.954522)
13. Sherrard J, Wilson J, Donders G, et al. 2018 European (IUSTI/WHO) International Union against sexually transmitted infections (IUSTI) World Health Organisation (WHO) guideline on the management of vaginal discharge. *Int J STD AIDS*. 2018;29:1258–1272. doi: [10.1177/0956462418785451](https://doi.org/10.1177/0956462418785451)
14. Chawla R, Bhalla P, Chadha S, et al. Comparison of Hay's criteria with Nugent's scoring system for diagnosis of bacterial vaginosis. *Biomed Res Int*. 2013;2013:365194. doi: [10.1155/2013/365194](https://doi.org/10.1155/2013/365194)
15. Forsum U, Jakobsson T, Larsson PG, et al. An international study of the interobserver variation between interpretations of vaginal smear criteria of bacterial vaginosis. *APMIS*. 2002;110:811–818. doi: [10.1034/j.1600-0463.2002.1101107.x](https://doi.org/10.1034/j.1600-0463.2002.1101107.x)

Vitamin D Status in Palindromic Rheumatism: A Propensity Score Matching Analysis

Alireza Khabbazi, MD,¹ Maryam Mahmoudi, MD,¹ Kamal Esalatmanesh, MD,² Masoomeh Asgari-Sabet, MD,¹ and Azam Safary, PhD¹

¹Connective Tissue Diseases Research Center, Tabriz University of Medical Sciences, Tabriz, Iran; ²Department of Internal Medicine, Faculty of Medicine, Kashan University of Medical Sciences, Kashan, Iran. Corresponding author: Azam Safary, PhD; azamsafary@yahoo.com

Key words: palindromic rheumatism, prerheumatoid arthritis, autoimmunity, vitamin D, ELISA, propensity-score matching

Abbreviations: VDR, vitamin D receptor; TLRs, Toll-like receptors; TH1, T-helper 1; T_{Reg}, regulatory T cells; PR, palindromic rheumatism; SS, systemic sclerosis; BD, Behçet disease; PSM, propensity score matching; PIP, proximal interphalangeal; MCP, metacarpophalangeal; MTP, metatarsophalangeal; RF, rheumatoid factor; anti-CCP, anti-cyclic citrullinated peptide; anti-MCV, anti-modified citrullinated vimentin

Laboratory Medicine 2024;55:45-49; <https://doi.org/10.1093/labmed/lmad032>

ABSTRACT

Objective: To determine whether there is a correlation between vitamin D levels and palindromic rheumatism (PR) as an at-risk phenotype of rheumatoid arthritis (RA).

Methods: A total of 308 participants were enrolled in this cross-sectional study. We recorded their clinical characteristics and performed propensity-score matching (PSM). Serum 25(OH)D₃ levels were determined via enzyme-linked immunosorbent assay.

Results: Our PSM resulted in 48 patients with PR and 96 matched control individuals. The multivariate regression analysis we performed after the PSM did not show a significant increase in PR risk in patients with vitamin D deficiency/insufficiency. There was no significant correlation between levels of 25(OH)D₃ and frequency/duration of attacks, number of joints affected, and duration of symptoms before diagnosis ($P \geq .05$). Mean (SD) serum levels of 25(OH)D₃ in patients with and without progression to RA were 28.7 (15.9) ng/mL and 25.1 (11.4) ng/mL, respectively.

Conclusion: Based on the results, we found no clear association between vitamin D serum levels and the risk, severity, and rate of PR progressing into RA.

Vitamin D is a steroid hormone primarily known for its action on bone formation and its regulation of calcium/phosphate homeostasis in the human body. However, vitamin D also has extraskelatal functions, the most important of which is the immunomodulatory effect on the immune system.^{1,2} Vitamin D is primarily synthesized in the skin as cholecalciferol (vitamin D₃) and then converted to 25(OH)D₃ in the liver by 25 α -hydroxylase. Subsequently, it is converted to the main bioactive form 1,25(OH)₂D₃ in the kidneys by 1 α -hydroxylase.³ Regarding the multiple functions of vitamin D in several physiological processes such as bone formation, immunity, cellular growth, and cellular differentiation,¹ several studies⁴⁻⁹ have been conducted in recent years to evaluate the role of vitamin D deficiency in different diseases.

The level of 1,25(OH)₂D₃ modulates the immune system by binding to the vitamin D receptor (VDR) expressed on antigen-presenting cells and activating T and B cells. This action leads to widespread changes in immune-system functions, such as the expression of Toll-like receptors (TLRs), reduction of the expression levels of T-helper 1 (TH1) cytokines (eg, IL-12, IL-16, IL-8, TNF- α , and IFN- γ), increase in the expression level of T-helper 2 (TH2) cytokines (eg, IL-4, IL-5, IL-10), and differentiation of regulatory T cells (T_{Reg}). Eventually, this process shifts immune system activity from proinflammatory to tolerogenic status.¹⁰⁻¹²

Although 25(OH)D₃ is not the active form of vitamin D, it was introduced as the best marker of vitamin D status in the clinical setting and research due to its long half-life (2-3 weeks).¹³ The optimal serum level of 25(OH)D₃ is measured at ~30-50 ng/mL, and the value of ~20-30 ng/mL is defined as vitamin D insufficiency. A serum level 25(OH)D₃ <20 ng/mL is considered to indicate vitamin D deficiency.¹⁴

Palindromic rheumatism (PR) is an autoimmune rheumatic disease (ARD) characterized by self-resolving attacks of arthritis and periartthritis that usually lasts a few hours to a few days. PR is considered an at-risk phenotype for rheumatoid arthritis (RA), and many physicians believe it is a variant of RA.¹⁵⁻¹⁷ PR may progress to chronic arthritis, mainly RA, in 10%-70% of patients.¹⁷⁻¹⁹ The findings of multiple observational studies unequivocally confirmed the association between vitamin D deficiency and increased risk and severity of ARD, including RA, systemic lupus erythematosus (SLE), seronegative spondyloarthropathic manifestations, systemic sclerosis (SS), inflammatory myopathies, vasculitis and Behçet disease (BD).²⁰⁻²² The results of the CARMA study²³ showed that serum levels 25(OH)D₃ in patients with RA, psoriatic arthritis, ankylosing spondylitis, SS, and SLE were ~8-10 ng/mL, indicating an increased risk of vitamin D deficiency in patients, compared with the control group.

In a study conducted by our research team in patients with BD who had a relapsing-remitting disease such as PR, serum level 25(OH)D₃ was detected at ~13.5 ng/mL, which was lower than in healthy control individuals.²² Also, some study reports^{21,24–26} indicated lower serum 25(OH)D₃ levels in patients with RA, revealing an association between 25(OH)D₃ serum levels and RA activity. However, the causal role of vitamin D in RA is not fully understood yet. In the current study, we aimed to assess the vitamin D status and the potential association between serum levels of 25(OH)D₃ and the clinical characteristics, severity, and rate of progression to RA in patients with PR.

Methods

Study Design and Participants

This cross-sectional study was conducted at the Connective Tissue Diseases Research Center. A total of 48 consecutive patients newly diagnosed with PR and 260 healthy controls were included between March 2018 and May 2022. The inclusion criteria were age ≥16 years, diagnosis of PR according to Guerne and Weisman criteria,²⁷ having active disease, and being treatment-naïve. The exclusion criteria were having illnesses including impaired renal and liver function, thyroid and/or parathyroid disorders, diabetes mellitus, and other inflammatory diseases and malignant neoplasms; having taken vitamin D supplements during the past 6 months; having taken anticonvulsants during the past 3 months; using sunscreen; and being pregnant. The research ethics committees approved the study protocol; written informed consent was obtained from all participants, according to the Declaration of Helsinki guidelines.

The demographic information, body mass index (BMI), and the smoking history of participants were collected by direct oral interviews. The clinical and laboratory characteristics of the patients were recorded at cohort entry. People who had smoked daily for more than 6 months were considered to be smokers.¹⁹ In the PR group, smokers were defined as those who had started smoking before the onset of their disease attacks. We divided the smokers into 2 groups, namely, current smokers and past smokers. For this analysis, current and past smokers were combined into the category of ever smokers.

PR severity was evaluated by the frequency of disease attacks, the duration of attacks, and the number of joints affected in each attack.²⁰ We collected 5 mL of venous blood from each participant at cohort entry after 12 hours of overnight fasting. The serum specimens were separated from whole blood and were kept at -70°C until biochemical analysis. Serum level 25(OH)D₃ concentration was determined by commercially available enzyme-linked immunosorbent assay (ELISA) kits according to the manufacturer-provided recommendations, using an ELISA plate reader (Model stat fax 2100; Awareness Technologies). Serum 25(OH)D₃ values <30 ng/mL were considered to indicate vitamin D insufficiency, and values of <10 ng/mL were classified as vitamin D deficiency.¹⁴

Statistical Analysis

We used SPSS software, version 22 (IBM) for statistical analyses. Kolmogorov-Smirnov testing was used to assess the normal distribution of data. Variables were displayed as numbers (percentages), mean (SD), or median (25%–75% interquartile range). Patients and control groups were compared using χ^2 testing, independent-sample *t* testing, or Mann-Whitney *U* testing. To reduce the heterogeneity between

the studied groups, propensity score matching (PSM) analyses were performed. Matching was achieved by considering age, sex, BMI, and smoking status. We selected 2 healthy controls for each patient with PR (ratio, 2:1).

After PSM, a multivariate analysis was performed, with PR as the main outcome variable; vitamin D deficiency or insufficiency as the main predictor variable; and age, sex, and BMI as covariates. In the next step, the correlation between the number of tender joints, frequency of disease attacks, duration of attacks, and disease duration with 25(OH)D₃ serum level values was assessed via Spearman testing. *P* < .05 was considered statistically significant.

Results

A total of 308 participants, 48 patients with PR, and 260 healthy controls were enrolled in the current study. The baseline demographic, clinical, and laboratory characteristics of participants are shown in **TABLE 1**. At the cohort entry, the median duration of symptoms in patients with PR was 12 months. PSM resulted in 48 patients with PR and 96 matched controls. There was no significant difference in the demographic characteristics of the participants after PSM (*P* ≥ .05) (**TABLE 2**).

TABLE 1. Demographic, Clinical, and Laboratory Characteristics of Participants

Parameter	PR Group (n = 48)	Control Group (n = 260)
Female, No. (%)	26 (51.4)	159 (61.2)
Age at cohort entry, y, mean (SD)	42.7 (9.1)	38.7 (11.9)
BMI, kg/m ² , mean (SD)	26.8 (4.8)	27.2 (4.9)
Ever smokers, No. (%)	8 (16.7)	31 (11.9)
Disease duration, mo, median (IQR)	12 (6–39)	—
Frequency of disease attacks, wk, median (IQR)	1.5 (1–4)	—
Duration of attacks, d, median (IQR)	2 (1–3)	—
Joints, No. (%)	1 (2.1)	—
Involved body parts, No. (%)		—
Knees	33 (68.8)	
Wrists	27 (56.2)	
Shoulders	25 (52.1)	
Hand PIP joints	23 (47.9)	
Elbows	20 (41.7)	
MCP joints	18 (37.5)	
Ankles	18 (37.5)	
MTP joints	9 (18.8)	
Hips	4 (8.3)	
Periarticular parts	16 (33.3)	
Autoantibodies, No. (%)		—
RF	25 (52.1)	
Anti-CCP	28 (58.3)	
Anti-MCV	35 (72.9)	
25(OH)D ₃ serum levels (ng/mL), mean (SD)	25.6 (12.2)	26.1 (13.2)

anti-CCP, anti-cyclic citrullinated peptide; anti-MCV; anti-modified citrullinated vimentin; BMI, body mass index; MCP, metacarpophalangeal; MTP, metatarsophalangeal; PR, palindromic rheumatism; PIP, proximal interphalangeal; RF, rheumatoid factor.

TABLE 2. Demographic Characteristics of Participants After PSM^a

Variable	PR Group (n = 48)	Control Group (n = 96)	P Value
Age, y, mean (SD)	42.7 (9.1)	41.9 (9.7)	.65
Female, No. (%)	26 (54.2)	52 (54.2)	.55
BMI, kg/m ² , mean (SD)	26.8 (4.8)	27.9 (4.7)	.13
Smokers, No. (%)	8 (16.7)	15 (15.6)	.17
25(OH)D ₃ (ng/mL), mean (SD)	25.6 (12.2)	25.8 (13.3)	.95
Vitamin D status, No. (%)			.79
Sufficient	14 (29.2)	24 (25.0)	
Insufficient	14 (29.2)	28 (29.1)	
Deficient	20 (41.7)	46 (47.9)	

BMI, body mass index; PR, palindromic rheumatism; PSM, propensity score matching.
^aPercentages may not total 100 because of rounding.

TABLE 3. Multivariate Regression Analysis of the Association Between Vitamin D Deficiency and PR After PSM

Variable	Healthy Control Group		
	OR	95% CI	P Value
Model (age, sex, smoking status, BMI)	—	—	—
Vitamin D deficiency (reference)	—	—	—
Vitamin D sufficiency	0.79	0.36–1.73	.55

BMI, body mass index; PR, palindromic rheumatism; PSM, propensity score matching.

TABLE 4. Correlation Between 25(OH)D₃ Serum Levels and Clinical Characteristics of Palindromic Rheumatism

Variable	Pearson Correlation	P Value
Frequency of attacks	0.210	.20
Duration of attacks	0.014	.93
No. of joints affected	−0.109	.51
Duration of symptoms at cohort entry	0.135	.41

We measured the serum level of 25(OH)D₃ in all participants using the ELISA method (TABLE 2). A multivariate regression analysis after PSM, after adjustment for age, sex, BMI, and smoking status, did not show a significant increase in the risk of PR in patients with vitamin D deficiency/insufficiency (TABLE 3). Subsequently, we assessed the correlation between 25(OH)D₃ serum levels and disease-severity measures in patients with PR. Based on the results, there was no significant correlation between serum levels of 25(OH)D₃ and frequency of disease attacks, duration of attacks, number of joints involved, and duration of symptoms before diagnosis ($P \geq .05$; TABLE 4).

To assess the correlation between vitamin D status and risk of PR progression to RA, we compared 25(OH)D₃ serum levels in patients whose disease had progressed to RA and had not progressed to RA. The mean (SD) values in those patient groups were 28.7 (15.9) ng/mL and 25.1 (11.4) ng/mL, respectively; there was no significant difference ($P = .35$).

Discussion

Despite numerous studies that reported low vitamin D levels in patients with RA and other acute respiratory distress syndromes (ARDSs), our findings did not show a significant difference in 25(OH)D₃ levels in the PR

and control groups. Also, a significant association between serum 25(OH)D₃ levels and the severity of PR was not detected. In explaining this contradiction, it should be noted that despite the clear evidence on the association between vitamin D status and the risk and severity of RA,²⁵ the role of vitamin D deficiency in the onset and early progression of RA is less clear.

Similar to our study findings, several reports underlined a poor association between vitamin D deficiency and various ARDs. In an analytical, retrospective, cross-sectional study conducted by de la Torre Lossa and coworkers² on 100 patients with RA, no significant correlations were found between serum vitamin D level and disease activity ($P = .60$) or other determining variables. In another study reported on by Cen et al,²⁴ no correlations were found between serum levels of 25(OH)D and disease activity among 116 patients with RA; however, serum 25(OH)D levels in the RA group were significantly lower (mean [SD], 35.99 [12.59] nmol/L) than those in the normal group (54.35 [8.20] nmol/L; $P < .05$). Besides, no correlation between serum 25(OH)D levels with disease activity or functional status have been reported by Pakchotanon et al²⁸ in Thai patients with RA.

Also, although many experts believe that PR is a variant of RA and is a transitional state leading to RA, some researchers consider PR and RA to be 2 different diseases. The results of imaging studies have revealed that the pattern of inflammation in RA and that in PR are different. Mankia et al²⁹ performed ultrasonography of joints in 31 patients with PR during attacks of the disease. They showed that true synovitis was presented only in 23% of patients and that inflammation was extracapsular in most patients, unlike RA. Also, the results of genetic studies, such as those in the study by Cañete et al,³⁰ supported that inflammation-related disease mechanisms play a role in the pathogenesis of PR. Cuervo et al³¹ divided PR-like arthritis according to the *MEFV* gene and RF/ACPA status into 4 subgroups. They revealed that in patients with *MEFV*⁺ and RF/ACPA[−], attacks can be controlled with colchicine.

In a study by Khabbazi et al,³² it was shown that PR is not a pre-RA state, and during a mean follow-up of 33 months, PR progressed to RA in only 9% of patients. In the current study, we have focused on the serum concentrations of 25(OH)D₃; however, there are multiple reports that other vitamin D metabolites such as 1,25(OH)₂D₃ affect the immune system at the molecular level. It has been shown^{33,34} that 1,25(OH)₂D₃ promotes tolerogenic dendritic cell function and regulates the balance of Th1/Th2 cells.³⁵ Also, it can suppress TH17 cells^{36–38} and promotes T_{Reg} function.^{10,39}

In addition, the importance of VDR gene expression, methylation, and polymorphisms in ARD has been indicated in various study reports.^{20,40–42}

The lack of association between 25(OH)D₃ levels and PR may be related to different VDR expressions in patients with PR. Therefore, it is likely that the measurement of serum 25(OH)D₃ provides only limited insight into the potential impact of vitamin D on a complex disease such as PR. It should be highlighted that serum levels of 25(OH)D can be easily affected by several factors, including geographical region, ethnic group(s), the season in which specimens are collected, age, sex, genetic variants, use of sunblock products, photosensitivity, dress, use of glucocorticoids, and use of immunosuppressant drugs to treat related diseases.

To our knowledge, this study is the first quantitative analysis in the literature of the vitamin D status in PR, measuring 25(OH)D₃ levels in a relatively large number of patients with PR at disease diagnosis and before starting treatment. The main limitation of our study was that we did not assess 1,25(OH)₂D₃ levels and VDR expression in patients with PR. Future studies should be conducted to focus on the analysis of multiple vitamin D metabolites and VDR in PR.

Conclusion

The correlation between lower vitamin D levels, more severe clinical manifestations of ARDS, and disease-activity index is controversial, and researchers studying this association have reported contrasting findings. This study showed no significant and clear association between serum levels of 25(OH)D₃ and the risk, severity, and rate of progression of PR to RA. Further comprehensive clinical studies and follow-up programs are needed, to evaluate this concept and to determine the possible association of vitamin D in the activity, severity, and development of PR autoimmune disease.

Acknowledgments

We acknowledge the cooperation of the Clinical Research Development Unit of Imam Reza General Hospital at Tabriz University of Medical Sciences, Iran. This study was approved by the Institutional Review Board and Research Ethics Committees of Kashan University of Medical Sciences, Kashan, Iran (IR.KAUMS.MEDNT.REC.1401.080), and all methods were performed under the relevant guidelines and regulations.

The current study was funded by Connective Tissue Diseases Research Center at Tabriz University of Medical Sciences (grant No. 69502) to A.K. A.S. was supported by grant No. 0000-0002-8997-2003 and A.K. by grant No. 0000-0002-9482-6967.

The data supporting the findings of this study are available on request from the corresponding author.

Conflict of Interest Disclosure

The authors have nothing to disclose

REFERENCES

- Aslam MM, John P, Bhatti A, Jahangir S, Kambh MI. Vitamin D as a principal factor in mediating rheumatoid arthritis-derived immune response. *Biomed Res Int*. 2019;2019:3494937. doi:10.1155/2019/3494937
- de la Torre Lossa P, Álvarez MM, Guzmán MdCG, Martínez RL, Acosta CR. Vitamin D is not useful as a biomarker for disease activity in rheumatoid arthritis [in Spanish]. *Reumatol Clin (Engl Ed)*. 2020;16(2 pt 1):110–115.
- Lin Z, Li W. The roles of vitamin D and its analogs in inflammatory diseases. *Curr Top Med Chem*. 2016;16(11):1242–1261. doi:10.2174/1568026615666150915111557
- Verstuyf A, Carmeliet G, Bouillon R, Mathieu C. Vitamin D: a pleiotropic hormone. *Kidney Int*. 2010;78(2):140–145. doi:10.1038/ki.2010.17
- Souberbielle J-C, Body J-J, Lappe JM, et al. Vitamin D and musculoskeletal health, cardiovascular disease, autoimmunity and cancer: recommendations for clinical practice. *Autoimmun Rev*. 2010;9(11):709–715.
- Gatenby P, Lucas R, Swaminathan A. Vitamin D deficiency and risk for rheumatic diseases: an update. *Curr Opin Rheumatol*. 2013;25(2):184–191. doi:10.1097/BOR.0b013e32835cfc16
- Brance ML, Brun LR, Lioi S, et al. Vitamin D levels and bone mass in rheumatoid arthritis. *Rheumatol Int*. 2015;35(3):499–505. doi:10.1007/s00296-014-3071-6
- Guan Y, Hao Y, Guan Y, Bu H, Wang H. The effect of vitamin D supplementation on rheumatoid arthritis patients: a systematic review and meta-analysis. *Front Med (Lausanne)*. 2020;7:596007. doi:10.3389/fmed.2020.596007
- Silva MRM, Barros WMA, Silva MLD, et al. Relationship between vitamin D deficiency and psychophysiological variables: a systematic review of the literature. *Clinics*. 2021;76:e3155. doi:10.6061/clinics/2021/e3155
- Jeffery LE, Burke F, Mura M, et al. 1,25-Dihydroxyvitamin D₃ and IL-2 combine to inhibit T cell production of inflammatory cytokines and promote development of regulatory T cells expressing CTLA-4 and FoxP3. *J Immunol*. 2009;183(9):5458–5467. doi:10.4049/jimmunol.0803217
- Lotfi F, Akbarzadeh-Khiavi M, Lotfi Z, et al. Micronutrient therapy and effective immune response: a promising approach for management of COVID-19. *Infection*. 2021;49:1133–1147. doi:10.1007/s15010-021-01644-3
- Aranow C. Vitamin D and the immune system. *J Investig Med*. 2011;59(6):881–886.
- Giannini S, Giusti A, Minisola S, et al. The immunologic profile of vitamin D and its role in different immune-mediated diseases: an expert opinion. *Nutrients*. 2022;14(3):473. doi:10.3390/nu14030473
- Iruretagoyena M, Hirigoyen D, Naves R, Burgos PI. Immune response modulation by vitamin D: role in systemic lupus erythematosus. *Front Immunol*. 2015;6:513. doi:10.3389/fimmu.2015.00513
- Mankia K, Emery P. Palindromic rheumatism as part of the rheumatoid arthritis continuum. *Nat Rev Rheumatol*. 2019;15(11):687–695. doi:10.1038/s41584-019-0308-5
- Katz SJ, Russell AS. Palindromic rheumatism: a pre-rheumatoid arthritis state? *J Rheumatol*. 2012;39(10):1912–1913. doi:10.3899/jrheum.120995
- Sanmartí R, Haro I, Cañete JD. Palindromic rheumatism: a unique and enigmatic entity with a complex relationship with rheumatoid arthritis. *Expert Rev Clin Immunol*. 2021;17(4):375–384. doi:10.1080/1744666X.2021.1899811
- Ahn JK, Hwang J, Seo GH. Incidence and risk of developing rheumatic diseases in 19,724 patients with palindromic rheumatism in South Korea: a nationwide population-based study. *Joint Bone Spine*. 2021;88(3):105128. doi:10.1016/j.jbspin.2020.105128
- Ellingwood L, Schieir O, Valois MF, et al. Palindromic rheumatism frequently precedes early rheumatoid arthritis: results from an incident cohort. *ACR Open Rheumatol*. 2019;1(10):614–619. doi:10.1002/acr2.11086
- He X-J, Ding Y, Xiang W, Dang X-Q. Roles of 1,25(OH)₂D₃ and vitamin D receptor in the pathogenesis of rheumatoid arthritis and systemic lupus erythematosus by regulating the activation of CD4⁺ T cells and the PKCδ/ERK signaling pathway. *Cell Physiol Biochem*. 2016;40(3-4):743–756. doi:10.1159/000453135
- Charoenngam N. Vitamin D and rheumatic diseases: a review of clinical evidence. *Int J Mol Sci*. 2021;22(19):10659. doi:10.3390/ijms221910659
- Khabbazi A, Ghojatzadeh M, Hajebrahimi S, Nikniaz Z. Relationship between vitamin D level and Bechcet's disease activity: a systematic

- review and meta-analysis. *Int J Vitam Nutr Res.* 2020;90(5-6):527–534. doi:10.1024/0300-9831/a000542
23. Urruticoechea-Arana A, Martín-Martínez MA, Castañeda S, et al. Vitamin D deficiency in chronic inflammatory rheumatic diseases: results of the cardiovascular in rheumatology [CARMA] study. *Arthritis Res Ther.* 2015;17(1):1–10.
 24. Cen X, Liu Y, Yin G, Yang M, Xie Q. Association between serum 25-hydroxyvitamin D level and rheumatoid arthritis. *Biomed Res Int.* 2015;2015:913804. doi:10.1155/2015/913804
 25. Lee YH, Bae S-C. Vitamin D level in rheumatoid arthritis and its correlation with the disease activity: a meta-analysis. *Clin Exp Rheumatol.* 2016;34(5):827–833.
 26. Hajjaj-Hassouni N, Mawani N, Allali F, et al. Evaluation of vitamin D status in rheumatoid arthritis and its association with disease activity across 15 countries: “The COMORA Study”. *Int J Rheumatol.* 2017;2017:5491676. doi:10.1155/2017/5491676
 27. Panfili FM, Roversi M, D’Argenio P, et al. Possible role of vitamin D in Covid-19 infection in pediatric population. *J Endocrinol Invest.* 2021;44(1):27–35. doi:10.1007/s40618-020-01327-0
 28. Pakchotanon R, Chaiamnuay S, Narongroeknawin P, Asavatanabodee P. The association between serum vitamin D Level and disease activity in Thai rheumatoid arthritis patients. *Int J Rheum Dis.* 2016;19(4):355–361. doi:10.1111/1756-185X.12222
 29. Mankia K, D’Agostino M-A, Wakefield RJ, et al. Identification of a distinct imaging phenotype may improve the management of palindromic rheumatism. *Ann Rheum Dis.* 2019;78(1):43–50. doi:10.1136/annrheumdis-2018-214175
 30. Cañete JD, Arostegui JI, Queiró R, et al. An unexpectedly high frequency of *MEFV* mutations in patients with anti-citrullinated protein antibody-negative palindromic rheumatism. *Arthritis Rheum.* 2007;56(8):2784–2788. doi:10.1002/art.22755
 31. Cuervo A, Sanmartí R, Ramírez J, et al. Palindromic rheumatism: evidence of four subtypes of palindromic-like arthritis based in either *MEFV* or rheumatoid factor/ACPA status. *Joint Bone Spine.* 2021;88(6):105235. doi:10.1016/j.jbspin.2021.105235
 32. Khabbazi A, Mirza-Aghazadeh-Attari M, Goli MT, et al. Is palindromic rheumatism a pre-rheumatoid arthritis condition? Low incidence of rheumatoid arthritis in palindromic rheumatism patients treated with tight control strategy. *Reumatol Clin (Engl Ed)* 2021;17(1):7–11. doi:10.1016/j.reuma.2019.01.002
 33. Anderson AE, Swan DJ, Wong OY, et al. Tolerogenic dendritic cells generated with dexamethasone and vitamin D3 regulate rheumatoid arthritis CD4⁺ T cells partly via transforming growth factor-β1. *Clin Exp Immunol.* 2017;187(1):113–123. doi:10.1111/cei.12870
 34. Bscheider M, Butcher EC. Vitamin D immunoregulation through dendritic cells. *Immunology.* 2016;148(3):227–236. doi:10.1111/imm.12610
 35. Zhang Z, Chen F, Li J, et al. 1,25(OH)₂D₃ suppresses proinflammatory responses by inhibiting Th1 cell differentiation and cytokine production through the JAK/STAT pathway. *Am J Transl Res.* 2018;10(8):2737–2746.
 36. Nistala K, Adams S, Cambrook H, et al. Th17 plasticity in human autoimmune arthritis is driven by the inflammatory environment. *Proc Natl Acad Sci U S A.* 2010;107(33):14751–14756. doi:10.1073/pnas.1003852107
 37. van Hamburg JP, Asmawidjaja P, Davelaar N, et al. Th17 cells, but not Th1 cells, from patients with early rheumatoid arthritis are potent inducers of matrix metalloproteinases and proinflammatory cytokines upon synovial fibroblast interaction, including autocrine interleukin-17A production. *Arthritis Rheumatol.* 2011;63(1):73–83. doi:10.1002/art.30093
 38. Zhou L, Wang J, Li J, et al. 1,25-dihydroxyvitamin D3 ameliorates collagen-induced arthritis via suppression of Th17 cells through miR-124 mediated inhibition of IL-6 signaling. *Front Immunol.* 2019;10:178. doi:10.3389/fimmu.2019.00178
 39. Jeffery LE, Qureshi OS, Gardner D, et al. Vitamin D antagonises the suppressive effect of inflammatory cytokines on CTLA-4 expression and regulatory function. *PLoS One.* 2015;10:e0131539. doi:10.1371/journal.pone.0131539
 40. Hitchon CA, Sun Y, Robinson DB, et al. Vitamin D receptor polymorphism rs2228570 (Fok1) is associated with rheumatoid arthritis in North American natives. *J Rheumatol.* 2012;39(9):1792–1797. doi:10.3899/jrheum.120387
 41. Kolahi S, Khabbazi A, Khodadadi H, et al. Vitamin D receptor gene polymorphisms in Iranian Azary patients with Behçet’s disease. *Scand J Rheumatol.* 2015;44(2):163–167. doi:10.3109/03009742.2014.945477
 42. Shirvani SS, Nouri M, Sakhinia E, et al. The expression and methylation status of vitamin D receptor gene in Behçet’s disease. *Immun Inflamm Dis.* 2019;7(4):308–317. doi:10.1002/iid3.275

Elevated methemoglobin levels in patients treated with high-dose hydroxocobalamin

Martinus Dyrud, DO, FCCP¹, Jianli Niu, MD, PhD¹, Lisa Kohler, PharmD¹

¹Memorial Cardiac & Vascular Institute, Memorial Healthcare System, Hollywood, FL, US. Corresponding author: Martinus Dyrud; MDyrud@mhs.net

Key words: hydroxocobalamin; methemoglobin; carboxyhemoglobin; arterial blood gas analysis; oximetry assay

Abbreviations: OHCbl, hydroxocobalamin; MetHb, methemoglobin; tHb, total hemoglobin; COHb, carboxyhemoglobin; HbO₂, oxyhemoglobin; PaO₂, arterial oxygen partial pressure; PaCO₂, arterial CO₂ partial pressure; SaO₂, arterial oxygen saturation; ABG, arterial blood gas

Laboratory Medicine 2024;55:50-55; <https://doi.org/10.1093/labmed/lmad037>

ABSTRACT

Objective: The aim of this study was to assess the impact of hydroxocobalamin (OHCbl) infusion on arterial blood gas and oximetry values in patients with vasoplegic syndrome.

Methods: Blood samples collected from 95 patients receiving OHCbl infusion were assayed using the ABL90 FLEX Plus blood gas analyzer for the concentration of methemoglobin (MetHb), total hemoglobin (tHb), carboxyhemoglobin (COHb), arterial oxygen saturation (SaO₂), arterial oxygen partial pressure (PaO₂), and arterial carbon dioxide partial pressure (PaCO₂). Interference of OHCbl on these variables was evaluated using the measured difference between the preinfusion and postinfusion samples.

Results: Blood MetHb (%) measured after the infusion of OHCbl (5g) were significantly higher than the baseline levels, with a median of 4.8 (IQR, 3.0–6.5) versus 1.0 (IQR, 1.0–1.2) ($P < .001$). Blood COHb (%) increased from a median of 1.3 (IQR, 1.0–1.8) to 1.7 (IQR, 1.3–2.2) ($P < .001$) following the OHCbl infusion. No differences were seen in median levels of tHb, PaO₂, PaCO₂, and SaO₂ between pre- and post-OHCbl treatment.

Conclusion: The presence of OHCbl in blood clearly interfered with the oximetry measurements of the hemoglobin component fractions by falsely increasing the levels of MetHb and COHb. Blood levels of MetHb and COHb cannot be reliably determined by the co-oximetry when OHCbl is known or suspected.

The use of high-dose hydroxocobalamin (OHCbl) has become more frequent in clinical practice, with no significant adverse events reported, even with doses as high as 30 g within 24 hours.¹ Hydroxocobalamin is currently marketed under the trade name Cyanokit (BTG International) and has become the antidote of choice in cyanide poisoning in the United States, replacing amyl nitrate, sodium nitrate, and sodium thiosulfate.^{2,3} A side effect of OHCbl administration is rapid, sustained, and significant increase in blood pressure, which is proportional to dosing of OHCbl, affecting 18% of those receiving a 5 g dose and 28% of those receiving a 10 g dose.^{4,5} This side effect of high-dose OHCbl is now being exploited for its utility as a potential therapy for the treatment of vasoplegia and severe refractory hypotension,⁶ particularly in the setting of cardiac surgery following cardiopulmonary bypass.⁷⁻⁹

Although high-dose OHCbl has been proven to be beneficial to the treatment of vasoplegic syndrome, there are increasing reports that high-dose OHCbl administration may also cause elevated levels of methemoglobin (MetHb), which can interfere with serum and urine laboratory colorimetric assays of certain parameters such as clinical chemistry, hematology, coagulation, and urine parameters.¹⁰⁻¹² There are no comprehensive clinical reviews that evaluate the effects of high-dose OHCbl on arterial blood gas (ABG) and oximetry measurements in patients with vasoplegic syndrome. In this study, we describe the first case series measurements of ABG and oximetry related to high-dose OHCbl treatment for patients with vasoplegic syndrome. Furthermore, we investigated and report on the potential interference effects of high-dose OHCbl on several ABG and oximetry values, with primary interest in MetHb, total hemoglobin (tHb), carboxyhemoglobin (COHb), arterial oxygen saturation (SaO₂), arterial oxygen partial pressure (PaO₂), and arterial carbon dioxide partial pressure (PaCO₂).

Methods

Study Population and Setting

This was a retrospective chart review of all consecutive adult patients aged ≥ 18 years who were hospitalized in the Memorial Healthcare System, Hollywood, FL, between May 1, 2017, and December 31, 2020, who received OHCbl administration for the treatment of refractory vasoplegic syndrome. Patients were excluded if (1) OHCbl was ordered but never verified as given; (2) dose was given but did not have the requisite pre- or post-ABG with oximetry within 48 hours before and within 48 hours after receiving the OHCbl. Any repeated doses given

to patients were not excluded, with any number of subsequent doses acceptable. This study was approved by the institutional review board of the Memorial Healthcare System with a waiver of informed consent (MHS.2021.057).

Data Collection and Definitions

Data involved in this study were extracted from electronic medical records. We collected individual baseline demographic data (age, gender) and ABG and oximetry values, including pH, PaCO₂, PaO₂, COHb, MetHb, and tHb. The OHCbl order time, dispense time, administration time, and doses were also collected.

The Cyanokit (BTG International) for intravenous infusion was standardized to consist of 1 vial containing 5 g lyophilized OHCbl dark red crystalline powder for injection, which is reconstituted with 200 mL of a diluent with normal saline solution for a final concentration of 25 mg/mL. The starting dose of OHCbl for patients was 5 g administered as an intravenous infusion over 15 minutes and could be followed by repeated doses, if desired, depending on the clinical response. We maximized our data collection by accepting baseline ABG with oximetry measurements within 48 hours prior to dose being given, although selected results that were closest to the time of OHCbl administration. Similarly, we included any blood gas and oximetry results within 48 hours after OHCbl administration, although selected the results that were soonest after the dose was given.

All blood samples were run on the ABL90 FLEX PLUS blood gas analyzer (Radiometer Medical) calibrated with internal reference standards. The oximeter analysis provided values of tHb (grams per deciliter) and percentage levels of COHb and MetHb. This instrument is a hospital clinical laboratory grade self-calibrating co-oximeter with accuracy of detection of MetHb and COHb of $\pm 0.5\%$ -1%, depending on range. If an ABG was run without co-oximetry, the particular dose or sample was excluded from data analysis.

Outcome Measures

The main outcomes of the study were to examine changes in tHb, COHb, and MetHb values in blood after high-dose OHCbl administration and determine whether OHCbl administration interferes with ABG and oximetry values. Interference in measurements was defined as differences in the measured and test results that were caused by OHCbl administration. The magnitude of interference was deemed clinically acceptable if the difference between the pre- and post-samples was within $\pm 2\%$ (absolute) for MetHb and COHb fractions and within ± 1.0 g/dL for tHb. The relation of these altered measurement values with the measured MetHb levels were assayed. In addition, a subanalysis of 20 patients with a single dose of OHCbl administration was performed to trace MetHb levels and determine the time of MetHb level returned to the pre-drug baseline level.

Statistical Analysis

Quantitative result was reported as mean with SD or median with IQR, as appropriate. Variables were tested for normality of distribution using a Kolmogorov-Smirnov test. Differences in ABG and oximetry values before and after the OHCbl administration were compared using nonparametric Mann-Whitney *U* test. The MetHb levels across different dose groups were compared using 2-way analysis of variance with Tukey's post hoc test. The MetHb levels were classified into 1 of 3 severity grades ($<5\%$, 5%-10%, and $\geq 10\%$), and the relationship between the grade of

MetHb elevation and ABG/oximetry values were analyzed by a nonparametric Kruskal-Wallis test. The Spearman rank correlation coefficient was used to determine whether a relationship between variables existed. All statistical tests were 2-sided and $P < .05$ was considered statistically significant. Data were analyzed using SPSS version 28 (SPSS).

Results

A total of 95 patients who received OHCbl were analyzed. Median age of the study patients was 60 years (IQR, 54-70) and 73 patients (77%) were male. Of the 95 patients, 65 patients (68%) received 1 dose, 21 patients (22%) received 2 doses, 5 patients (5%) received 3 doses, 3 patients (3%) received 4 doses, and 2 patients (2%) received 5 doses; and no patient received more than 5 doses.

Effect of OHCbl Administration on Blood MetHb Levels

As shown in **FIGURE 1**, the baseline MetHb level was approximately $1.1\% \pm 0.3\%$ of total hemoglobin with a median of 1.0% (IQR, 1%-1.2%). After 1 dose of 5 g OHCbl, MetHb level increased to $5.2\% \pm 0.5\%$ ($P < .001$) with a median of 4.8% (IQR, 3.0%-6.5%), except for 2 patients who had no change in their MetHb values. The MetHb increase was as high as 13.1% in 1 patient. We performed a subgroup analysis of the patients who received multiple doses of OHCbl and found that significantly elevated MetHb levels were observed at all doses used in the study (all $P < .001$; **FIGURE 1B**), whereas changes in MetHb levels were not significantly different across the doses of OHCbl given ($P = .117$; **FIGURE 1B**).

In a subanalysis of 20 patients who had repeated follow-up ABG samples post-OHCbl, the median time of the MetHb value returning to the baseline level was 105 hours (IQR, 59-132 hours). An example of the approximate time course of the MetHb levels following OHCbl infusion as obtained in 1 patient is shown in **FIGURE 1C**. The concentration of MetHb was found to reach levels above 5.0% within 3 hours following OHCbl infusion then declined gradually and returned to the baseline level by approximately 60 hours post-OHCbl infusion in that particular example.

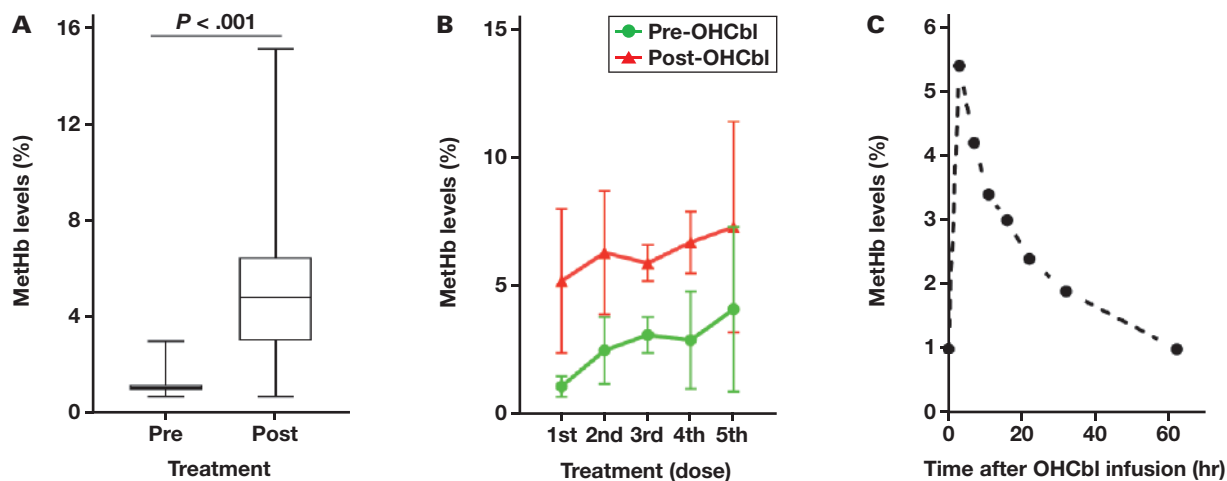
Effect of OHCbl Administration on the Measurements of Non-MetHb Values

FIGURE 2 shows the measurements of tHb, COHb, PaO₂, PaCO₂, and SaO₂ before and after OHCbl infusion. Prior to OHCbl infusion, the mean COHb level was $1.4\% \pm 0.5\%$ with a median of 1.3% (IQR, 1.0%-1.8%). After OHCbl (5 g) infusion, COHb level increased to $1.8\% \pm 0.7\%$ with a median of 1.7% (IQR, 1.3%-2.2%), which was significantly higher than the level of the pretreatment ($P < .001$) (**FIGURE 2B**). The tHb concentrations before and after OHCbl infusion were similar in the study subjects (9.9 ± 2.2 g/dL vs 9.9 ± 2.1 g/dL; $P = .868$) (**FIGURE 2A**). The PaO₂, PaCO₂, and SaO₂ measurements in the subjects were not different before or after OHCbl treatment (**FIGURE 2C-2E**).

OHCbl Interference with MetHb, COHb, and tHb Measurements

FIGURE 3 shows the absolute changes of MetHb, COHb, and tHb in patients who received one dose (5 g) OHCbl. Of the 95 patients studied, 27 patients (28%) presented with the magnitude of interference within $\pm 2\%$ and 68 patients (72%) with interference of $>2\%$ for MetHb, whereas the magnitude of interference for COHb was within $\pm 2\%$ in all

FIGURE 1. Hydroxocobalamin (OHCbl) administration increases blood methemoglobin (MetHb) values. A, Box plots showing the effect of OHCbl administration on MetHb levels in blood samples, measured the percentage of MetHb pre- and post-OHCbl administration. The box indicates the interquartile range (IQR), whereas lower and upper bars correspond to the minimum and maximum nonoutlier values of the data distribution. Outliers are defined as values outside 1.5 times the IQR from the box. The center line indicates the median value. B, Changes of the measured MetHb values with different dosing of OHCbl administration. C, Time course of the MetHb levels in the blood following OHCbl infusion obtained in 1 patient.



patients (FIGURE 3A). Of the 95 patients studied, 70 (74%) presented with interference of ± 1 g/dL for tHb, and 26% of patients ($n = 25$) had a magnitude of interference of > 1 or < 1 g/dL for tHb (FIGURE 3B).

Relationship Between MetHb Level and Blood Gas and Oximetry Values

Increases in MetHb values were classified into 3 severity levels: mild increase being $< 5\%$, moderate increase of $5\% - 10\%$, and severe increase of $> 10\%$. We performed a subgroup analysis to determine the difference of blood gas (PaCO_2 , SaO_2) and oximetry values (tHb, COHb) among the different concentration increases in MetHb levels (FIGURE 4). There was a significant difference in the levels of tHb and COHb across the different levels of MetHb (Kruskal–Wallis tests, $P = .004$ and $P < .0001$, respectively) (FIGURE 4A and 4B). There was a weak negative relationship between MetHb concentration and tHb level (Spearman coefficient = -0.293 , $P = .0041$), whereas there was a significant positive relationship between MetHb and COHb (Spearman coefficient = 0.565 , $P < .0001$). There was no difference in the levels of PaCO_2 across the different concentration of MetHb groups (Kruskal–Wallis test, $P = .385$), whereas SaO_2 level appeared to be different across the different concentration of MetHb groups (Kruskal–Wallis test, $P = .022$) (FIGURE 4C and 4D), which was significantly different in the values of SaO_2 between the MetHb $> 10\%$ and the MetHb $< 5\%$ groups ($P = .0278$). There was a weak positive relationship between the MetHb concentration and SaO_2 level (Spearman coefficient = 0.324 , $P = .0014$), with no significant relationship between MetHb and PaO_2 level (Spearman coefficient = -0.135 , $P = .193$).

Discussion

The main finding of this study is that OHCbl administration significantly affects the arterial blood oximetry values in patients with vasoplegic syndrome. This phenomenon has been observed in several case reports with poisoning,^{13–15} but this study is the first comprehensive investigation of

a relatively large number of patients with hemodynamic failure since the first report using OHCbl as a rescue therapy for the treatment of refractory vasodilatory shock in 2014.⁷ Results from our study demonstrate a baseline MetHb value of 1.1% in these patients, with an average rise to 5.2% after 5 g OHCbl administration accompanied by a significant increase in COHb level with an average rise to 1.7% . By subgroup analysis, we found a strong positive correlation between the concentrations of COHb and MetHb as measured by the ABL90 FLEX PLUS blood gas analyzer. The SaO_2 values were found to positively correlate with the level of MetHb, and no significant correlation was observed between the PaCO_2 values and the level of MetHb. This is the first study to identify such correlations. Thus, OHCbl interferes with the determination of MetHb and COHb by the ABL90 FLEX PLUS blood gas analyzer.

The question of whether MetHb elevation after OHCbl was artifactual versus true methemoglobinemia was not part of this study but is interesting to consider.

From a strictly clinical standpoint, despite showing MetHb level elevation after OHCbl administration, the level of MetHb in our study did not reach any level $> 13\%$, well below critical or symptomatic methemoglobinemia levels. This would suggest that even with single or multiple doses of OHCbl, the MetHb levels do not rise to levels that would be defined as more than “mild.” Therefore, even if the MetHb level elevation observed in our study and others was real and not an artifact, it would be of limited clinical significance. Additionally, true methemoglobinemia in nonsevere or mild forms is often difficult to establish and would require investigation of more subtle clinical features, which was not part of this study. However, we did find that the SaO_2 remained in the normal range in our patients despite significant MetHb elevation, which is suggestive that the rise in MetHb in our study was an artifact and not real.

From the standpoint of determining whether MetHb and COHb elevation is a result of colorimetric interference on measurements, this was not determined by our study, as only the ABL machines were used. The ABL90 FLEX PLUS machines that were used in our study have been previously investigated by Pamidi et al¹¹ and were shown

FIGURE 2. Impact of hydroxocobalamin (OHCbl) administration on the measurements of total hemoglobin (tHb), carboxyhemoglobin (COHb), arterial oxygen partial pressure (PaO₂), arterial carbon dioxide partial pressure (PaCO₂), and arterial oxygen saturation (SaO₂) values assayed by the ABL90 FLEX PLUS blood gas analyzer. Boxplots show the measured values of pre- and post-OHCbl treatment samples for tHb (A), COHb (B), PaO₂ (C), PaCO₂ (D), and SaO₂ (E). The box indicates the interquartile range (IQR), whereas lower and upper bars correspond to the minimum and maximum non-outlier values of the data distribution. Outliers are defined as values outside 1.5 times the IQR from the box. The center line indicates the median value.

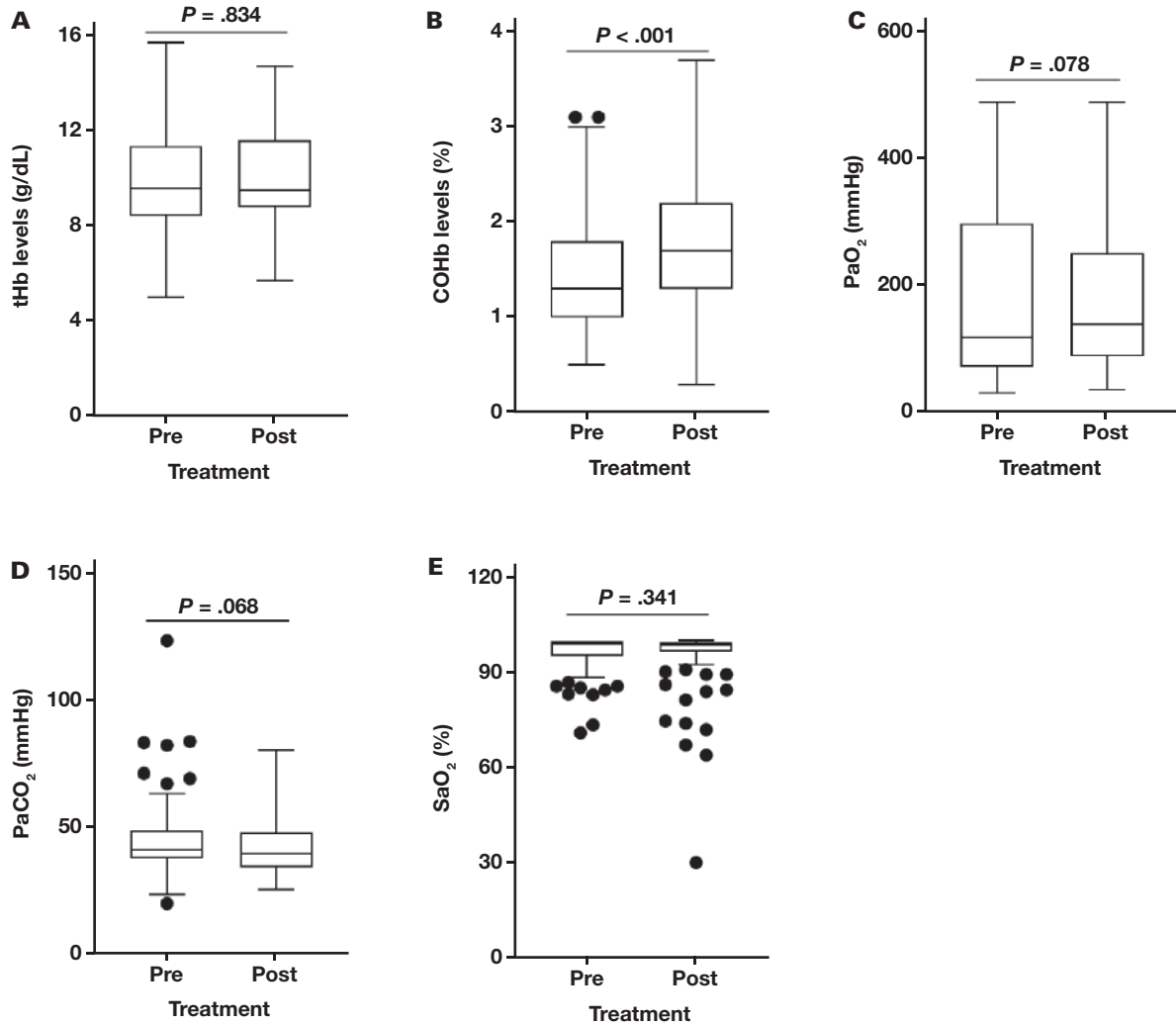


FIGURE 3. Hydroxocobalamin (OHCbl) interferes with the measurements of methemoglobin (MetHb), carboxyhemoglobin (COHb), and total hemoglobin (tHb). Percentages of patients with the interference of $\pm 2\%$ (absolute) for MetHb and COHb fractions (A) and of ± 0.5 g/dL for tHb (B) are shown.

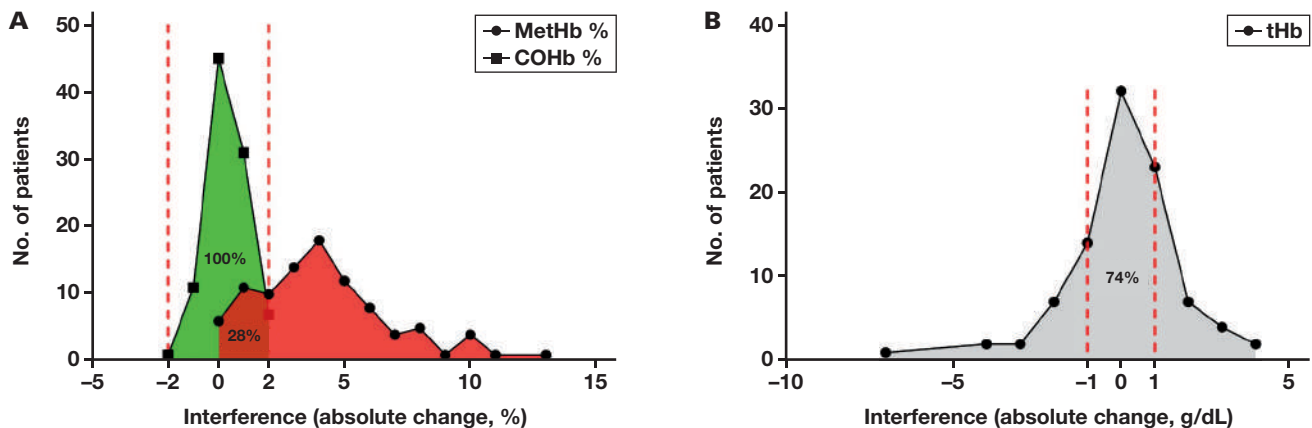
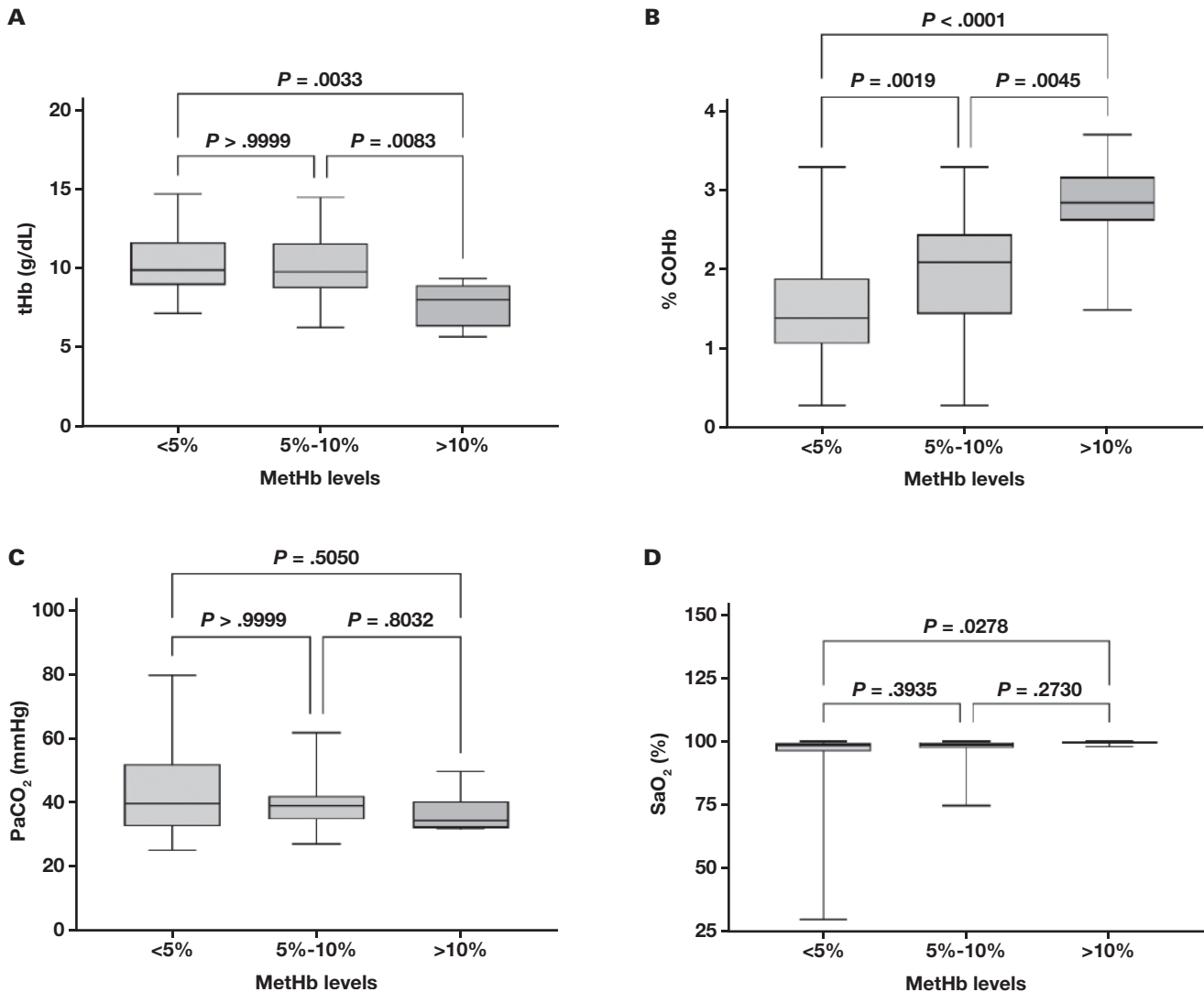


FIGURE 4. Relationship between the methemoglobin (MetHb) values and the measured total hemoglobin (tHb), carboxyhemoglobin (COHb), carbon dioxide partial pressure (PaCO₂), and arterial oxygen saturation (SaO₂) values. The MetHb levels were classified into 1 of 3 severity grades (<5%, 5%-10%, and ≥10%), and the relationship between the MetHb level by grade and the measured tHb (A), COHb (B), PaCO₂ (C), and SaO₂ (D) were analyzed by nonparametric Kruskal–Wallis tests.



to exhibit significant variability of MetHb measurements after OHCbl when compared with the GEM Premier 4000 and Siemen's Rapidpoint 405 analyzers. The highest amount of discrepancy in measurements was observed on the ABL line of machines in the Pamidi study. This discrepancy between different manufacturer's machines is curious, as the basic physical properties of each measured compound to absorb or reflect light within the 475 nm-655 nm wavelength spectrum should be consistent, even if affected by the red pigment of OHCbl. As only the ABL line of machines was used in our study, we cannot comment further on variation between different manufacturers of these machines. Nevertheless, hardware, software, or chemical components related to the photometry light source, varying software that drives the light source, and varying algorithms that interpret the measurements are involved. Other contributing factors may include but are not limited to (1) blood lysing solutions and their propensity for "foaming," (2) process control solution, solution pack, or cassette, (3) reagent type and reagent shelf

life, (4) "intelligent quality management system" in some devices, and (5) machine calibration.

Regarding tHb, data presented in **FIGURE 3B** do not suggest an interference pattern for tHb in the presence of OHCbl; rather, there is an inverse correlation between tHb values and the level of MetHb. In **FIGURE 4A**, the value of tHb is shown to be significantly lower in patients with a MetHb level of >10% than those with a MetHb level of <5% and those with MetHb level of 5%-10%. As percentage of MetHb was calculated by dividing the concentration of MetHb by the concentration of tHb, the presence of the same concentration of MetHb after OHCbl infusion in an anemic patient would represent a higher percentage of MetHb. Thus, the underlying medical conditions in these patients (eg, anemia) might contribute to this observation.

In regard to those patients who had repeat doses of OHCbl, the change in the concentration of MetHb was not detected in a dose-dependent manner. We observed that despite repeated dosing of OHCbl, elevated

concentration of MetHb did not correlate. It appears that the patients who received repeated doses of OHCbl had a less pronounced increase in MetHb level if they received their dose during the time when the previous dose was still circulating. This decremental rise in MetHb values is likely reflective of the early repeat dosing of OHCbl within 24 to 48 hours following the initial dose. Essentially, the repeat OHCbl dose was given before the MetHb value had returned to baseline, thereby not allowing enough “wash-out time” before the repeat dose. This indicates that the repeat doses were given in the period of time in which the MetHb values were high and still had not decreased significantly toward their baseline. As this was a retrospective study, we did not have standardized times that the pre- and post-samples were measured in relation to the time the OHCbl was given, limiting our data somewhat. This finding suggests that the MetHb level acts as a surrogate qualitative marker for presence of circulating OHCbl but not necessarily as a quantitative marker of OHCbl levels.

In the subanalysis of the 20 patients who received 1 dose OHCbl and had repeated follow-up samples post-OHCbl, the median time required to return to prior baseline value of MetHb was 105 hours (IQR, 59–132 hours). Anecdotally, after OHCbl administration, the urine of patients will stay a “red wine” color for up to 1 week after drug administration. One could imply from this urine discoloration that the serum retains a similar pigmentation change, thereby effecting arterial blood oximetry measurements. As a surrogate, the clearing of urine may coincide with the clearing of MetHb in co-oximetry measurements; however, urine color or color intensity was not accounted for in this study.

There are several limitations to our study. First, this study was limited by its retrospective nature, and some patients receiving OHCbl infusion were not included due to the lack of data analyzed, most notably the lack of oximetry in the blood gas analysis. Second, sampling intervals for ABG/oximetry were not consistent, as results obtained in patients were not in the same time windows following the administration of OHCbl. Therefore, differences in the time of sampling may have affected our results, although we aimed to correct for these differences by selecting the blood gas results that were soonest before or after the OHCbl was given. Also, we only used 1 type of blood gas machine in our study, limiting the ability to compare results between different machine manufacturers. Finally, the concentration of OHCbl presented in the blood was not estimated because it is not possible to measure OHCbl concentration in conventional laboratories.

Conclusion

Our findings clearly demonstrate that OHCbl administration interferes with the determination of the hemoglobin component fractions in whole blood by the ABL90 FLEX PLUS blood gas analyzer by increasing the measured MetHb and COHb fractions. These errors may potentially influence clinical decision making and thus affect patient outcomes. Our findings highlight that when OHCbl is known to be present, blood MetHb and CoHb cannot be reliably determined by the ABL90 FLEX PLUS blood gas analyzer.

Availability of Data and Materials

The dataset is available from the corresponding author on reasonable request.

Conflict of Interest Disclosure

The authors have nothing to disclose.

REFERENCES

1. DesLauriers CA, Burda AM, Wahl M. Hydroxocobalamin as a cyanide antidote. *Am J Ther*. 2006;13:161–165. doi:10.1097/01.mjt.0000174349.89671.8c
2. Bronstein AC, Spyker DA, Cantilena LR Jr, et al. 2011 Annual report of the American Association of Poison Control Centers' National Poison Data System (NPDS): 29th annual report. *Clin Toxicol*. 2012;50:911–1164. doi:10.3109/15563650.2012.746424
3. Mowry JB, Spyker DA, Brooks DE, et al. 2014 Annual Report of the American Association of Poison Control Centers' National Poison Data System (NPDS): 32nd annual report. *Clin Toxicol*. 2015;53:962–1147. doi:10.3109/15563650.2015.1102927
4. Uhl W, Nolting A, Golor G, et al. Safety of hydroxocobalamin in healthy volunteers in a randomized, placebo-controlled study. *Clin Toxicol*. 2006;44:17–28.
5. Uhl W, Nolting A, Gallemann D, et al. Changes in blood pressure after administration of hydroxocobalamin: relationship to changes in plasma cobalamins-(III) concentrations in healthy volunteers. *Clin Toxicol*. 2008;46:551–579; discussion 576. doi:10.1080/15563650701829763
6. Gerth K, Ehring T, Braendle M, et al. Nitric oxide scavenging by hydroxocobalamin may account for its hemodynamic profile. *Clin Toxicol*. 2006;44:29–36. doi:10.1080/15563650600811805
7. Roderique JD, VanDyck K, Holman B, et al. The use of high-dose hydroxocobalamin for vasoplegic syndrome. *Ann Thorac Surg*. 2014;97:1785–1786. doi:10.1016/j.athoracsur.2013.08.050
8. Burnes ML, Boettcher BT, Woehlick HJ, et al. Hydroxocobalamin as a rescue treatment for refractory vasoplegic syndrome after prolonged cardiopulmonary bypass. *J Cardiothorac Vasc Anesth*. 2017;31:1012–1014. doi:10.1053/j.jvca.2016.08.019
9. Armour S, Armour TK, Joppa WR, et al. Use of hydroxocobalamin (vitamin B12a) in patients with vasopressor refractory hypotension after cardiopulmonary bypass: a case series. *Anesth Analg*. 2019;129:e1–e4. doi:10.1213/ANE.0000000000003648
10. Curry SC, Connor DA, Raschke RA. Effect of the cyanide antidote hydroxocobalamin on commonly ordered serum chemistry studies. *Ann Emerg Med*. 1994;24:65–67. doi:10.1016/s0196-0644(94)70164-4
11. Pamidi PV, DeAbreu M, Kim D, et al. Hydroxocobalamin and cyanocobalamin interference on co-oximetry based hemoglobin measurements. *Clin Chim Acta*. 2009;401:63–67. doi:10.1016/j.cca.2008.11.007
12. Beckerman N, Leikin SM, Aitchinson R, et al. Laboratory interferences with the newer cyanide antidote: hydroxocobalamin. *Semin Diagn Pathol*. 2009;26:49–52. doi:10.1053/j.semdp.2008.12.008
13. Denninghoff K, Walter FG, Langa AJ, et al. Spectrophotometry of hydroxocobalamin and hemoglobin reveals production of an unanticipated methemoglobin variant. *Clin Toxicol*. 2008;46:545–550. doi:10.1080/15563650701846270
14. Lee J, Mukai D, Kreuter K, et al. Potential interference by hydroxocobalamin on cooximetry hemoglobin measurements during cyanide and smoke inhalation treatments. *Ann Emerg Med*. 2007;49:802–805. doi:10.1016/j.annemergmed.2006.11.016
15. Jiwani AZ, Beberta VS, Cancio LC. Acquired methemoglobinemia after hydroxocobalamin administration in a patient with burns and inhalation injury. *Clin Toxicol*. 2018;56:370–372. doi:10.1080/15563650.2017.1377838

Quantitative Value of Bacteria Associated with Leukocytes in Differential Diagnosis of Lower Respiratory Tract Infection in Children, in Comparison to Sputum Culture and Procalcitonin

Guoqiang Zhang,¹ Yihui Yao,¹ Ying Gao,¹ Xiaolu Yu,¹ and Jiabin Fang¹

¹Zhongshan Hospital, Medical College of Xiamen University, Xiamen, China.
Corresponding author: Guoqiang Zhang; zgq2127@163.com

Key words: lower respiratory tract infection, children, bacterial number, differential diagnosis, sputum culture, mycoplasma

Abbreviations: LRTI, lower respiratory tract infection; PCT, procalcitonin; OIF, oil immersion field

Laboratory Medicine 2024;55:56-61; <https://doi.org/10.1093/labmed/lmad035>

ABSTRACT

Background: The mortality and morbidity rates in children with lower respiratory tract infection (LRTI) remain high.

Objective: To describe the number of bacteria that is associated with leukocytes in differential diagnosis of bacterial, mycoplasma, and viral LRTI in children.

Methods: Sputum smears were Gram stained for counting single-morphology bacteria associated with leukocytes. The differential diagnostic values of bacterial number were assessed in children with LRTI.

Results: The area under the receiver operating characteristic (ROC) curve was 0.95 for bacterial number in the differential diagnosis of bacterial infection from mycoplasma and viral infections. The area under the ROC curve was 0.62 for procalcitonin and 0.94 for bacterial number in the differential diagnosis of bacterial infection from mycoplasma infection.

Conclusion: The number of bacteria associated with leukocytes in sputum was valuable and rapid in differential diagnosis of bacterial infection in children with suspected bacterial, mycoplasma, and viral LRTI.

Lower respiratory tract infection (LRTI) is a common disease in children, in whom mortality and morbidity resulting from the disease remain

high. The main pathogens causing LRTI in children are bacteria, viruses, and *Mycoplasma pneumoniae*.¹ Rapid differential diagnosis of different types of pathogens causing LRTI is helpful for precise treatment, selection of narrow spectrum-sensitive antibiotics, reduction of adverse drug reactions, and improvement in therapeutic effect.

Procalcitonin (PCT) increased in bacterial and mycoplasma infection but was not increased or only slightly increased in viral infections. PCT has been widely used as a biomarker for differential diagnosis between broadly bacterial infection and viral infection.² However, PCT cannot effectively distinguish bacterial infection from *M pneumoniae* infection, and some severe viral infections are still indistinguishable from bacterial infections.³⁻⁶

Sputum culture is the routine method for laboratory diagnosis of bacterial LRTI. Sputum specimens are liable to be contaminated by oropharyngeal secretions. As a result, the growth of normal oropharyngeal flora will reduce the specificity of the results, and the growth of a large number of normal flora will lower the detection rate of pathogenic bacteria, especially fastidious bacteria. At the same time, dominating pathogens may be colonized in the upper respiratory tract, such as *Streptococcus pneumoniae* and *Haemophilus influenzae*, which were often misjudged as pathogens in the culture results.^{7,8}

Sputum Gram stain is a rapid, simple, and low-cost method to establish the presence of an infection and to identify a microbiological etiology; however, its role in the diagnosis of LRTI remains controversial. The disadvantage of sputum smear is that it requires a highly skilled microbiologist to interpret the results. The qualified sputum specimens were screened by Gram-stain microscopy for culture.^{9,10}

The positional relationship of bacteria with leukocytes and squamous epithelial cells can indicate whether the bacteria originated from the upper respiratory tract or the lower respiratory tract, which provides direction in the interpretation of culture results.^{11,12} However, the relationship between the number of bacteria associated with leukocytes and the occurrence of infection still needs further study. The purpose of this study is to analyze the values of bacterial number in rapid differential diagnosis of pediatric patients with respiratory tract infection caused by bacteria, viruses, and *M pneumoniae*, and to compare these values with PCT testing and sputum culture results.

Materials and Methods

Specimens

In 12 months, a total of 249 qualified sputum and PCT blood specimens were collected from hospitalized pediatric patients with LRTI in Zhongshan Hospital, a teaching hospital in southern China. **FIGURE 1** presents the sex and age distribution of these 249 pediatric patients. All cases of LRTI adopted in this study were diagnosed as follows: 38 viral infections based on clinical symptoms, imaging and serology; 87 bacterial infections based on clinical symptoms, imaging, and bacterial culture; 102 *M pneumoniae* infections by clinical symptoms, imaging, serology, and nucleic acid testing; and 22 mixed infections based on clinical symptoms, imaging, serology, bacterial culture, and nucleic acid testing results.

Microscopic Examination

Sputum smears were dried and fixed before Gram staining. The sputum smears were Gram stained for counting the single-morphology bacteria associated with leukocytes. The number of squamous epithelial cells and leukocytes in the $\times 100$ (low-power) field were counted and their average values calculated. According to the criteria of sputum squamous epithelial cells < 10 per $\times 100$ field and leukocytes > 25 per $\times 100$ field,^{10,13} specimens were judged as acceptable sputum specimens. When more than one type of bacteria was associated with leukocytes, the most abundant bacteria were counted. The criteria for bacteria quantity grade are as follows: 0, no bacteria found; 1+, less than 1 per oil immersion field (OIF); 2+, 1 to 5/OIF; 3+, 6 to 30/OIF; and 4+, > 30 per OIF.

Sputum Culture

All of the acceptable sputum specimens were immediately inoculated on sheep blood agar, chocolate agar, and MacConkey agar and incubated at 35°C in 5% CO₂. The culture plates were read after 18–24 hours, and

the negative culture plates were read again after extended incubation for 24 hours.

PCT Assay

Blood specimens were collected for PCT detection by electrochemiluminescence from patients during the period in which they had a high fever. The blood specimens were anticoagulated with EDTA-3K and sent to the laboratory for assay in time to process them. The clinical laboratory where PCT values were examined has achieved ISO15189 accreditation.

Statistical Analysis

Statistical analyses were performed using Stata software, version 16 for Windows. *t* testing was used for comparing the mean value of PCT in 2 different types of infection. Logistic regression analyses were performed to evaluate the power of PCT and the number of bacteria in differential diagnosis among bacteria, viruses, and mycoplasma infection. Their diagnostic capabilities were evaluated by receiver operating characteristic (ROC) analysis. The agreement between sputum culture and bacterial number was calculated using kappa statistics.

Results

Difference of PCT Concentrations among Patients with Bacterial, Mycoplasma, and Viral Infections, and the Differential Diagnostic Values

The distribution of PCT concentration among 249 patients with LRTI is shown in **FIGURE 2**. The mean values and ranges are presented in **TABLE 1**.

The PCT values were significantly different (*t* testing, $P < .05$) between patients with viral infection and broadly bacterial infection

FIGURE 1. Sex and age distribution of patients.

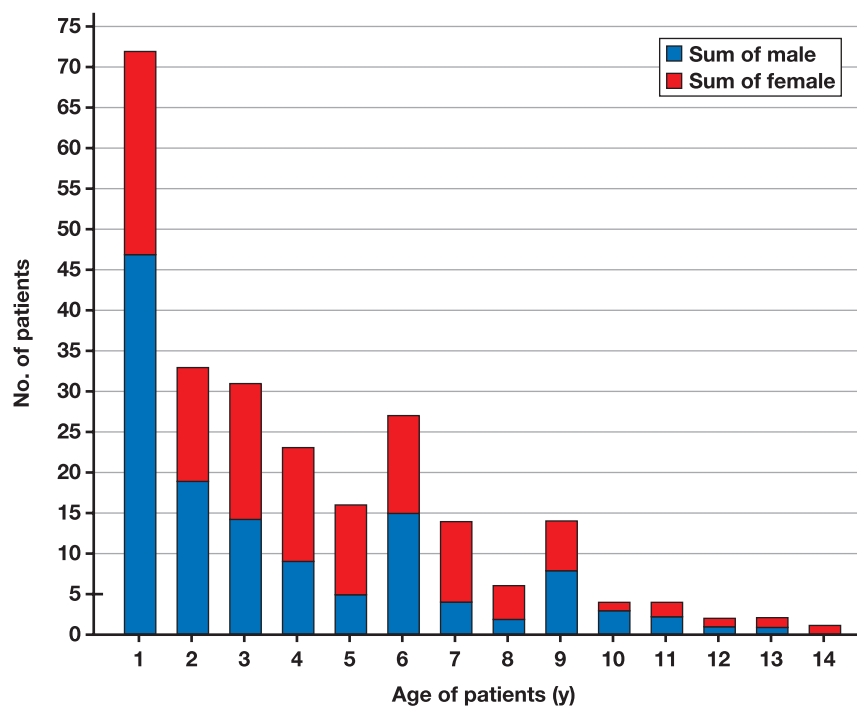
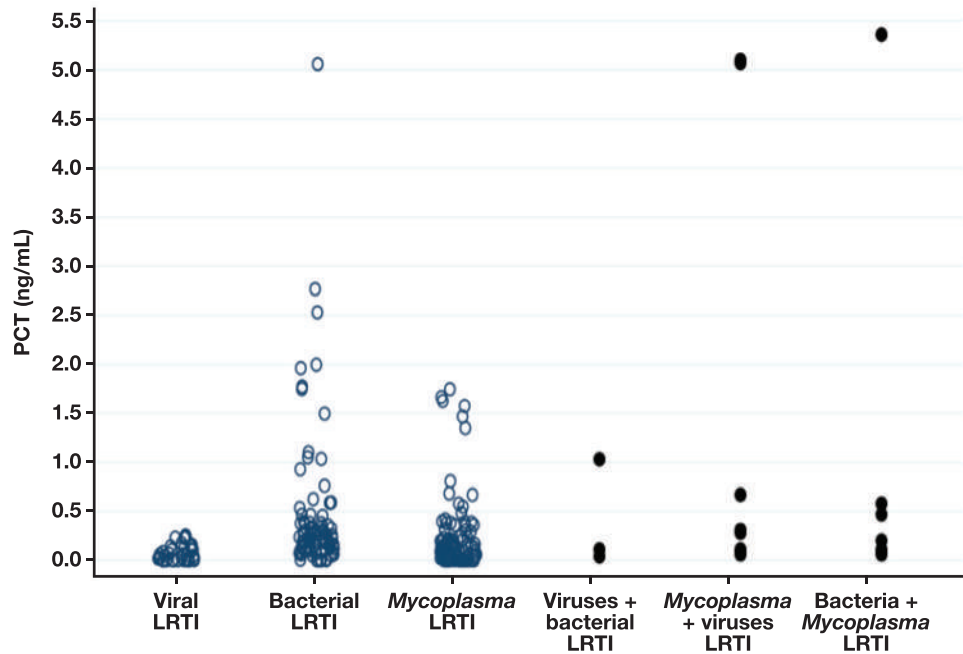


FIGURE 2. Individual values of procalcitonin (PCT) in the different patient groups. LRTI, lower respiratory tract infection.**TABLE 1.** Distribution of PCT, Sputum Culture, and Numbers of Bacteria in Different Groups of Patients

Cases	Mean PCT (SD) (ng/mL)	PCT range (ng/mL)	Bacteria, No.									
			Culture +					Normal flora				
			0	1+	2+	3+	4+	0	1+	2+	3+	4+
Viral LRTI (n = 38)	0.06 (0.02)	0.02–0.15	1	3	0	0	0	8	14	11	1	0
Bacterial LRTI (n = 87)	0.44 (0.75)	0.05–5.10	0	0	25	53	5	0	0	1	3	0
Mycoplasma LRTI (n = 102)	0.25 (0.36)	0.03–1.74	2	3	0	0	0	51	25	15	6	0
Viral + bacterial LRTI (n = 3)	0.39 (0.55)	0.04–1.03	0	0	1	2	0	0	0	0	0	0
Viral + mycoplasma LRTI (n=10)	1.18 (2.06)	0.06–5.15	0	0	0	0	0	6	4	0	0	0
Bacterial + mycoplasma LRTI (n = 9)	0.78 (1.73)	0.06–5.36	0	0	2	6	0	0	0	0	1	0

LRTI, lower respiratory tract infection; PCT, procalcitonin; +, positive.

(including bacterial infection, mycoplasma infection, and mixed infection of bacteria + virus, bacteria + mycoplasma, and virus + mycoplasma). When PCT was taken as a biomarker for differential diagnosis of broadly bacterial infection from viral infection, the area under the ROC curve was 0.89 (FIGURE 3A). At the cutoff value of 0.07 ng/mL for PCT, the sensitivity and specificity for differential diagnosis were 85.78% and 73.68%, respectively. However, although PCT was used as a biomarker for differential diagnosis of bacterial infection from viral and mycoplasma infections, the area under the ROC curve was only 0.68 (FIGURE 3B).

The Distribution and Differentially Diagnostic Values of Bacterial Number

All of the sputum specimens were screened using smear microscopy, and sputum specimens were judged as acceptable specimens when squamous epithelial cells were <10 per low magnification ($\times 100$) and leukocytes >25 per $\times 100$ field. FIGURE 4A shows the microscopic appearance of an unacceptable specimen under the $\times 100$ field. The

sputum specimen smears were Gram stained for counting the single-morphology bacteria accompanied with leukocytes (FIGURE 4B).¹² TABLE 1 shows the distribution of bacterial number in the sputum of patients with LRTI.

The area under the ROC curve was 0.95 when the bacterial number was recorded and examined as a biomarker for differential diagnosis of bacterial infection from viral and mycoplasma infections (FIGURE 3C). The sensitivity and specificity for bacterial infection diagnosis were 5.05% and 100%, respectively, at the cutoff point of 4+ for bacterial number, 70.71% and 95.33% at the cutoff point of 3+, 100% and 78% at the cutoff point of 2+, and 100% and 45.33% at the cutoff point of 1+. Binary logistic regression analysis was used to assess the bacterial number as a risk factor associated with bacterial infection. The analysis results showed that bacterial number (OR, 116.77; $P < .001$) was significantly associated with bacterial infection among patients with bacterial and viral infection; and in patients with bacterial, viral, and mycoplasma infections, bacterial number (OR, 18.00; $P < .001$) was significantly associated with bacterial infection.

FIGURE 3. Receiver operating characteristic (ROC) curves. A, Procalcitonin (PCT) in the differential diagnosis of broadly bacterial infection from viral infections (area under the curve [AUC] = 0.89). B, PCT in the differential diagnosis of bacterial infection from viral and mycoplasma infections (AUC = 0.68). C, Bacterial number (ROC area = 0.95) and PCT (ROC area = 0.68) in the differential diagnosis of bacterial infection from viral and mycoplasma infections. D, Bacterial number (ROC area = 0.94) and PCT (ROC area = 0.62) in the differential diagnosis of bacterial infection from mycoplasma infections.

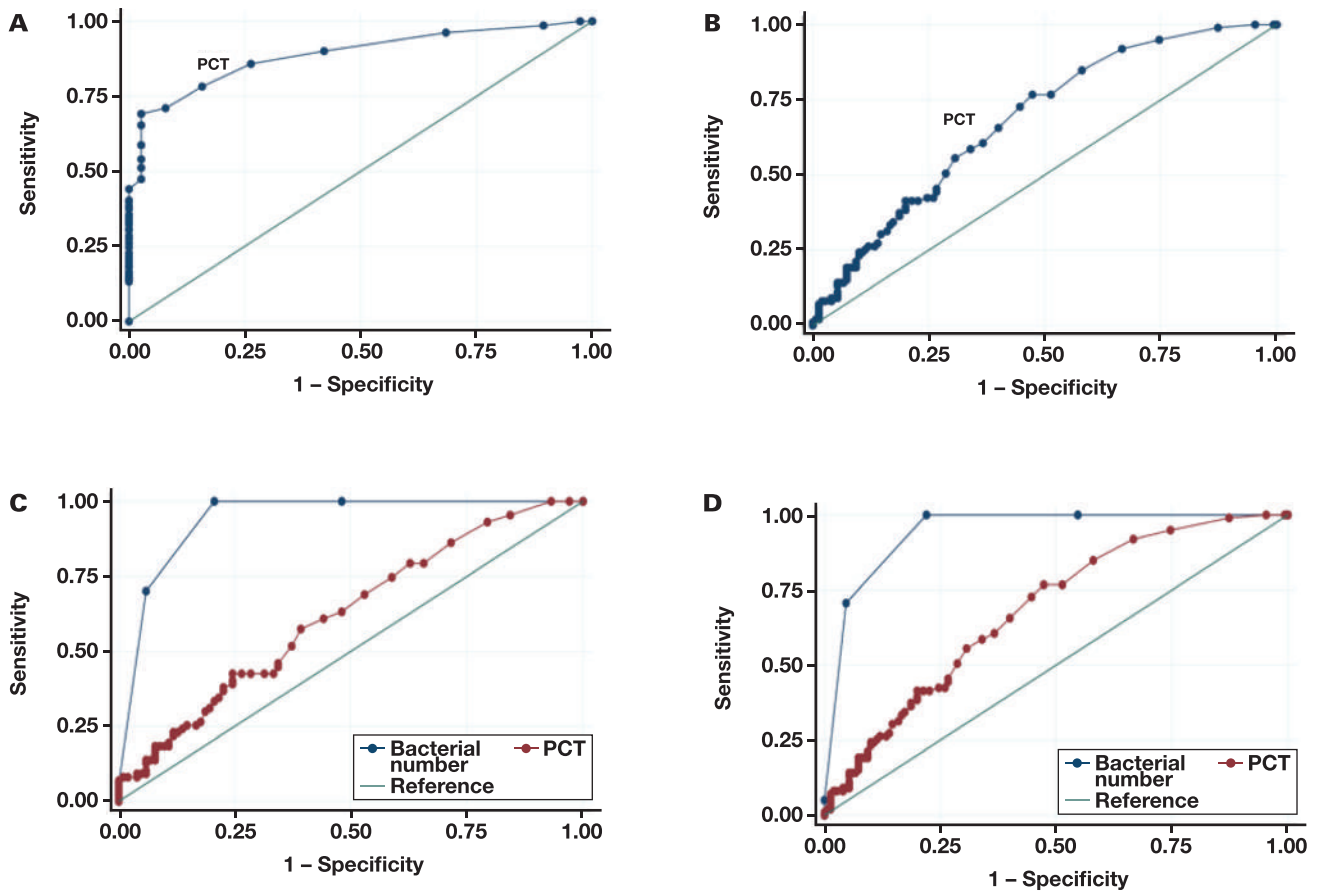
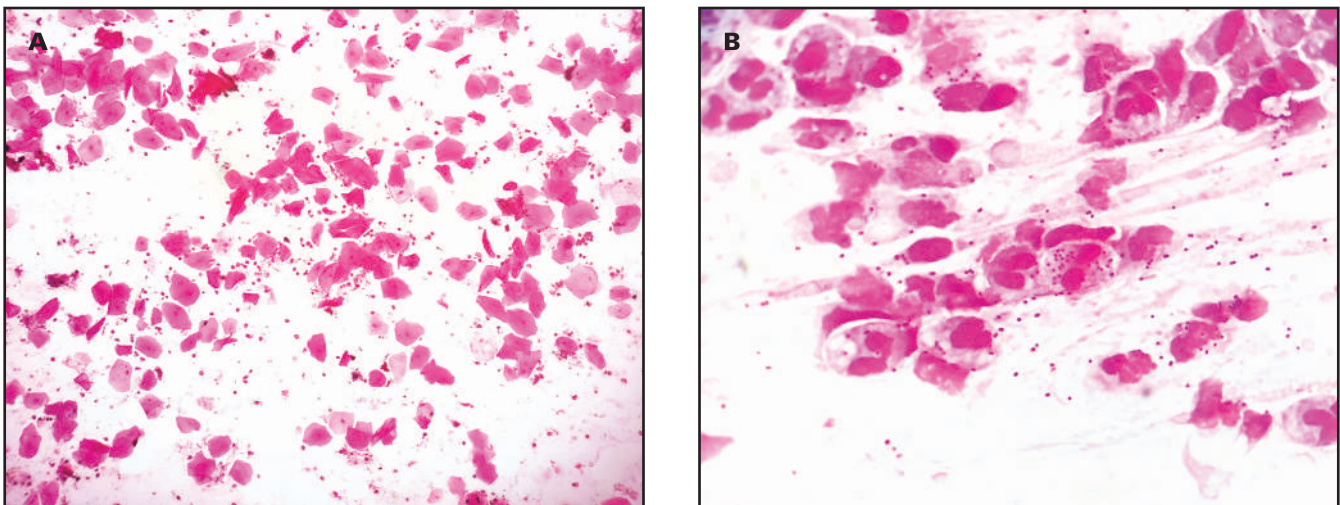


FIGURE 4. Photomicrographs of sputum Gram stains. A, Large proportion of squamous epithelial cells at low power ($\times 100$). B, *Moraxella catarrhalis* associated with leukocytes at high power ($\times 1000$).



PCT and Bacterial Number in Discriminating Bacterial Infection from Mycoplasma Infection

The mean PCT of 87 patients with bacterial LRTIs and 102 patients with mycoplasma LRTIs were 0.44 ng/mL and 0.25 ng/mL, respectively, which were statistically significantly different (t test; $P < .05$). The logistic-regression analyses showed that PCT (OR, 1.26; $P = .69$) was insignificantly associated with bacterial infection in differential diagnosis between bacterial infection and mycoplasma infection; however, bacterial number (OR, 14.89; $P < .001$) was significantly associated with bacterial infection. The area under the ROC curve was 0.62 for PCT and 0.94 for bacterial number (FIGURE 3D). The sensitivity and specificity for differential diagnosis of bacterial infection from mycoplasma infection was 57.47% and 60.78%, respectively, at the cutoff level of 0.15 ng/mL for PCT, and 100% and 79.41%, respectively, at the cutoff level of 2+ for bacterial number.

Comparison between Sputum Culture and Bacterial Number

The sputum-culture results of 249 pediatric patients were as follows: 52 cases of *S pneumoniae*, 33 cases of *H influenzae*, 13 cases of *Moraxella catarrhalis*, 1 case of *Staphylococcus aureus*, 1 case of *Klebsiella pneumoniae*, 3 mixed cases of *S pneumoniae* and *H influenzae*, and 146 cases of normal flora. The agreement between sputum culture and bacterial number was calculated using kappa statistics. The kappa value was 0.67 at the cutoff level of 2+ for bacterial number.

Discussion

Viruses, bacteria, and mycoplasma are the dominant pathogens that cause LRTI infection in children.^{1,14} The rapid differential diagnosis of infections caused by these 3 different pathogens is of great significance for the diagnosis and treatment of LRTI in children. PCT has been a useful component of a comprehensive clinical assessment and supports treatment decisions in pediatric LRTI.⁴ Blood marker PCT values increase in bacterial and mycoplasma LRTI in children.¹⁵

In the findings of this study, the mean PCT of 87 cases of bacterial LRTI was 0.44 ng/mL, and the range was 0.05–5.1 ng/mL. The mean PCT of 102 mycoplasma cases was 0.25 ng/mL, ranging from 0.03 to 1.74 ng/mL. As a result, PCT cannot effectively distinguish bacterial infection from mycoplasma infection. On the other hand, the detection of pathogen is particularly important for diagnosis of patients with bacterial LRTI when their PCT concentration is less than 0.5 ng/mL.²

Although the PCT value increased, it was uncertain whether it was bacterial infection or mycoplasma infection according to PCT level. There was a statistically significant difference in mean PCT between mycoplasma and bacterial LRTI (t test; $P < .05$); however, the area under the ROC curve was 0.62, close to 0.5, which could not discriminate the 2 infections effectively. And the area under the ROC curve was 0.94 for bacterial number in the differential diagnosis of bacterial infection from mycoplasma infection. The results of logistic-regression analyses revealed that bacterial number (OR, 18; $P < .001$) was significantly associated with bacterial infection among patients with bacterial, viral, and mycoplasma infection. The area under the ROC curve was 0.95 for bacterial number in the differential diagnosis of bacterial infection from viral and mycoplasma infections. The sensitivity and specificity for bacterial infection diagnosis were 100% and 78%, respectively, at the cutoff point of 2+ for bacterial number.

Sputum-bacteria culture is a conventional method for diagnosis of bacterial LRTI.^{16–18} Bacteriological examination of the specimens

obtained from the lower respiratory tract is challenging for medical microbiologists. Distinguishing whether the isolated pathogenic bacteria represent true causes of LRTI or are only colonized bacteria of the upper respiratory tract is often difficult.

Sputum specimens are contaminated by the oropharyngeal flora, which may include potential pathogens. Also, dominating pathogens may be colonized in the upper respiratory tract, such as *S pneumoniae* and *H influenzae*, which were often misjudged as pathogens in the culture results.^{7,8} Sputum bacterial culture is more time-consuming to process, generally needing 2 days to report, which is not suitable for rapid diagnosis. However, if qualified sputum specimens can be collected, it is possible to quickly predict potential pathogens by detecting bacteria associated with leukocytes in sputum.

The kappa value was 0.67 for the agreement between sputum culture and bacterial number in this study. Kappa values between 0.61 and 0.80 are considered to reflect good agreement.¹⁹ The results of our kappa analysis result showed that bacterial number is in good agreement with sputum bacteria culture. Bacterial number is more advantageous than sputum cultures for rapid diagnosis of bacterial infections; however, antimicrobial susceptibility tests are still needed for the acquired resistant strains. The deficiency of this study is that there is still a lack of criterion standard methods for the diagnosis of bacterial LRTI.

Conclusions

PCT has 2 shortcomings for the differential diagnosis of LRTI. First, viral infection is indistinguishable from bacterial infection when PCT level is low; second, bacterial infection cannot be differentially diagnosed from mycoplasma infection while the PCT value is increased.

In our cohort, the bacterial number was significantly different among patients with bacterial, mycoplasma, and viral infections. The results of ROC curve analysis showed that bacterial infection can be effectively differentially diagnosed from mycoplasma and viral infection via bacterial number. At the same time, the agreement between sputum culture and bacterial number was good. In conclusion, the number of bacteria associated with leukocytes in sputum was valuable information, which was rapidly determined in the differential diagnosis of bacterial infection in children with suspected cases of bacterial, mycoplasma, and viral LRTI.

Conflicts of Interest Disclosure

The authors have nothing to disclose.

REFERENCES

1. Michelow I, Olsen K, Lozano J, et al. Epidemiology and clinical characteristics of community-acquired pneumonia in hospitalized children. *Pediatrics*. 2004;113(4):701–707.
2. Gilbert DN. Use of plasma procalcitonin levels as an adjunct to clinical microbiology. *J Clin Microbiol*. 2010;48(7):2325–2329. doi:10.1128/JCM.00655-10
3. Moulin F, Raymond J, Lorrot M, et al. Procalcitonin in children admitted to hospital with community acquired pneumonia. *Arch Dis Child*. 2001;84(4):332–336. doi:10.1136/adc.84.4.332
4. Baumann P, Baer G, Bonhoeffer J, et al. Procalcitonin for diagnostics and treatment decisions in pediatric lower respiratory tract infections. *Front Pediatr*. 2017;5:183. doi:10.3389/fped.2017.00183
5. Schuetz P, Wirz Y, Sager R, et al. Procalcitonin to initiate or

- discontinue antibiotics in acute respiratory tract infections. *Cochrane Database Syst Rev*. 2017;10(10):CD007498. doi:10.1002/14651858.CD007498.pub3
6. Wu G, Wu G, Wu S, Wu H. Comparison of procalcitonin guidance-administered antibiotics with standard guidelines on antibiotic therapy in children with lower respiratory tract infections: a retrospective study in China. *Med Princ Pract*. 2017;26(4):316–320.
 7. de Steenhuijsen Piters WAA, Sanders EAM, Bogaert D. The role of the local microbial ecosystem in respiratory health and disease. *Philos Trans R Soc London Ser B*. 2015;370(1675):20140294. doi:10.1098/rstb.2014.0294
 8. Popova G, Boskovska K, Arnaudova-Danevska I, Smilevska-Spasova O, Jakovska T. Sputum quality assessment regarding sputum culture for diagnosing lower respiratory tract infections in children. *Open Access Maced J Med Sci*. 2019;7(12):1926–1930. doi:10.3889/oamjms.2019.551
 9. Wong LK, Barry AL, Horgan SM. Comparison of 6 different criteria for judging the acceptability of sputum specimens. *J Clin Microbiol*. 1982;16(4):627–631. doi:10.1128/jcm.16.4.627-631.1982
 10. Murdoch DR, Morpeth SC, Hammitt LL, et al. Microscopic analysis and quality assessment of induced sputum from children with pneumonia in the PERCH study. *Clin Infect Dis*. 2017;64(suppl 3):S271–S279.
 11. Heineman HS, Chawla JK, Lopton WM. Misinformation from sputum cultures without microscopic examination. *J Clin Microbiol*. 1977;6(5):518–527. doi:10.1128/jcm.6.5.518-527.1977
 12. Boerner DF, Zwadyk P. The value of the sputum grams stain in community-acquired pneumonia. *JAMA*. 1982;247(5):642–645.
 13. Geckler RW, Gremillion DH, McAllister CK, Ellenbogen C. Microscopic and bacteriological comparison of paired sputa and transtracheal aspirates. *J Clin Microbiol*. 1977;6(4):396–399. doi:10.1128/jcm.6.4.396-399.1977
 14. Kumar S, Garg I, Sethi G. Serological and molecular detection of *Mycoplasma pneumoniae* in children with community-acquired lower respiratory tract infections. *Diagn Microbiol Infect Dis*. 2019;95(1):5–9.
 15. Wen J, Su Y, Sun H, Zhang H, Li H. The combination of initial markers to predict refractory *Mycoplasma pneumoniae* pneumonia in Chinese children: a case control study. *Respir Res*. 2021;22:89. doi:10.1186/s12931-020-01577-9
 16. Del Rio-Pertuz G, Gutiérrez JF, Triana AJ, et al. Usefulness of sputum gram stain for etiologic diagnosis in community-acquired pneumonia: a systematic review and meta-analysis. *BMC Infect Dis*. 2019;19(1):403. doi:10.1186/s12879-019-4048-6
 17. Shimoda M, Saraya T, Yonetani S, et al. The significance of bacterial engulfment in Gram-stained sputum in patients with respiratory infections. *Medicine*. 2018;97:e0150. doi:10.1097/MD.00000000000010150
 18. Gunasekaran J, Saksena R, Jain M, Araki K, Taizawa H. Can sputum gram stain be used to predict lower respiratory tract infection and guide empiric antimicrobial treatment: experience from a tertiary care hospital. *J Microbiol Methods*. 2019;166(14):105731. doi:10.1016/j.mimet.2019.105731
 19. Cohen J. A coefficient of agreement for nominal scales. *Educ Psychol Meas*. 1960;20(1):37–46. doi:10.1177/001316446002000104

Whole-exome sequencing reveals a likely pathogenic *LMNA* variant causing hypertrophic cardiomyopathy

Mohammad Mahdavi, MD,¹ Neda Mohsen-Pour, PhD,² Majid Maleki, MD,³ Serwa Ghasemi, PhD,¹ Avis Tabib, MD,⁴ Golnaz Houshmand, MD,¹ Niloofer Naderi, MSc,³ Tannaz Masoumi, MSc,¹ Hamidreza Pouraliakbar, MD,¹ Samira Kalayinia, PhD³✉

³Cardiogenetic Research Center and ⁴Heart Valve Diseases Research Center, ¹Rajaie Cardiovascular Medical and Research Center, Iran University of Medical Sciences, Tehran, Iran, ²Department of Genetics and Molecular Medicine, Zanjan University of Medical Sciences, Zanjan, Iran. Corresponding author: Samira Kalayinia; samira.kalayi@yahoo.com

Key words: hypertrophic cardiomyopathy; whole-exome sequencing; *LMNA*; pathogenic; genetic; heterogeneity

Abbreviations: HCM, hypertrophic cardiomyopathy; WES, whole-exome sequencing; MRI, magnetic resonance imaging

Laboratory Medicine 2024;55:62-70; <https://doi.org/10.1093/labmed/Imad038>

ABSTRACT

Objective: We studied the clinical and molecular features of a family with hypertrophic cardiomyopathy (HCM).

Background: A very heterogeneous disease affecting the heart muscle, HCM is mostly caused by variants in the proteins of sarcomeres. The detection of HCM pathogenic variants can affect the handling of patients and their families.

Methods: Whole-exome sequencing (WES) was performed to assess the genetic cause(s) of HCM in a consanguineous Iranian family.

Results: Missense likely pathogenic variant c.1279C>T (p.Arg427Cys) within exon 7 of the *LMNA* gene (NM_170707) was found. The segregations were confirmed by polymerase chain reaction–based Sanger sequencing.

Conclusions: Variant c.1279C>T (p.Arg427Cys) in the *LMNA* gene seemed to have been the cause of HCM in the family. A few *LMNA* gene variants related to HCM phenotypes have been recognized so far. Identifying HCM genetic basis confers significant opportunities to understand how the disease can develop and, by extension, how this progression can be arrested. Our study supports WES effectiveness for first-tier variant screening of HCM in a clinical setting.

Introduction

Hypertrophic cardiomyopathy (HCM) is the most common genetic heart disease, estimated at 1:500 in the general population.^{1,2} It is defined by asymmetric left ventricular hypertrophy, diastolic heart failure, cardiac fibrosis, cardiomyocyte disarray, and sudden cardiac death.³⁻⁵ Hypertrophic cardiomyopathy is the primary cause of sudden cardiac death in competitive athletes and young adults.⁶ It is an autosomal dominant Mendelian disease; however, some cases are defined by de novo variants and, less frequently, autosomal recessive inheritance.⁷ Hypertrophic cardiomyopathy is generally considered a genetically heterogeneous disease with variable phenotypic manifestations and incomplete penetrance, posing diagnostic and prognostic challenges. The first chromosomal location was mapped in 1989,⁸ since which time variants in numerous genes causing HCM have been reported. Various genome-wide association investigations have identified many sarcomeric gene variants related to HCM phenotypes in multiple large affected families, including *MYH7*, *MYL3*, *MYL2*, *MYBPC3*, *TNNI3*, *TNNT2*, *ACTC1*, *TTN*, and *TPM1*.⁹⁻¹⁵ Other genes such as *ACTN2*, *CSRP3*, *MYOZ2*, *TNNC1*, *NEXN*, *PLN*, and *TTR* play a role; nevertheless, they do not definitively cause the disease.¹⁶ For pathogenic variants in other genes, evidence is either insufficient or nonexistent.¹⁷⁻¹⁹ Approximately 20% to 30% of patients with HCM have sarcomere gene variants and are considered or assumed to be pathogenic.²⁰⁻²³ It is, however, worthy of note that sarcomeric genes have been gradually expanded to nonsarcomeric ones.^{18,24} Indeed, isolated and sporadic HCM cases with probands who have no family history of HCM and do not carry known HCM variants may account for up to 40% of all patients with this heart disease.²⁵ Consequently, sarcomere dysfunction seems to be an essential component but not the needed initiating event in the pathogenesis of HCM. The etiology of HCM seems multifactorial rather than strictly genetic,^{17,21} as families and patients with the same genetic variants are mostly found with a wide range of disease manifestations.^{17,26}

The *LMNA* gene (OMIM *150330) encodes the lamin A/C protein, an integral component of the nuclear membrane, that can maintain nuclear stability. It also has been reported to be involved in the structural integrity of the entire cell through interactions with the cytoskeleton, nuclear lamina, and extracellular matrix.^{27,28} There is a link between *LMNA* variants and dilated cardiomyopathy, with *LMNA* variants causing one-third of heritable patients to have dilated cardiomyopathy.²⁹ Nonetheless, associations between *LMNA* variants and HCM have also been previously reported, suggesting the crucial effect of *LMNA* on the

development of the disease. An incomplete penetrance pattern is found in families with heterozygous *LMNA* variants, which implies that several sporadic cases reported in earlier investigations could be a consequence of incomplete penetrance.³⁰

The high level of allelic and locus heterogeneity as a characteristic of HCM can necessitate sequence analysis of the entire coding area of multiple genes, which is a costly and time-consuming process through conventional methods.^{31,32} Next-generation sequencing is a high-throughput method by comparison with classical sequencing methods, and not only does it allow a rapid analysis of many genes in a more affordable manner³²⁻³⁴ but also it provides a unique opportunity for the early detection of at-risk individuals before clinical diagnosis. The identification of the HCM genetic basis creates significant opportunities for differentiating genetic sarcomeric HCM from phenocopies such as athlete's heart, hypertensive heart disease, and metabolic or storage disorders.¹⁴

Here, we describe a consanguineous Iranian family with HCM of unknown cause. Via whole-exome sequencing (WES) analysis on the proband's genome, we found missense variant c.1279C>T in *LMNA* (NM_170707), leading to a cysteine-for-arginine substitution at position 427 (p.Arg427Cys), which segregated with the disease in the family.

Materials and Methods

Ethics Approval and Consent to Participate

This study was performed following the principles of the Declaration of Helsinki and approved by the ethics committee of Rajaie Cardiovascular Medical and Research Center (IR.RHC.REC.1400.098). The subjects gave informed written consent for participation in the study and the publication of this report.

Family Recruitment and Clinical Characteristics

Three generations of an Iranian family were recruited for this study (FIGURE 1A). Eight members of the pedigree, consisting of 2 affected (FIGURE 1A: II-4 and III-1) and 6 healthy individuals (FIGURE 1A: II-1, II-2, I II-3, I II-5, II-6, and III-2) who consented to study participation, were evaluated. The clinical and demographic information of the studied pedigree, including family history and clinical symptoms, was collected from the database at Rajaie Cardiovascular Medical and Research Center.

Echocardiography and cardiovascular magnetic resonance showed no evidence of cardiomyopathy in all the unaffected members. The proband (III-1) was an 8-year-old boy who suffered from heart murmurs and was referred for genetic testing at this age. He also experienced clinical symptoms such as breathlessness, fatigue, and chest tightness following exercise. The proband (III-1) had been diagnosed with extreme cardiac wall thickening and cardiomyopathy. Elevated levels of lactic acid and pyruvate were reported in blood biochemistry evaluation. According to the available reports, the proband (III-1) did not suffer from Pompe disease (MIM #232300) nor did he have a pathogenic variant in the molecular genetic evaluation of the *GAA* gene.

The proband (FIGURE 1A: III-1) had a healthy brother (FIGURE 1A: III-2, 2 years old). The proband's father (FIGURE 1A: II-3) and mother (FIGURE 1A: II-4) were clinically unaffected with no symptoms. Evidence of diabetes and high blood cholesterol levels (FIGURE 1A: I-1),

as well as dysentery and intestinal infections (FIGURE 1A: II-7), was reported in the family. Other clinical information was unavailable.

Echocardiography

The first diagnostic echocardiography (GE Vivid S60 cardiovascular ultrasound machine, cardiac sector probe 3Sc-RS [1.3-4.5 MHz]) was performed on the proband (III-1) at the age of 4 years and was repeated every 6 to 12 months. Sequential segmental analysis was performed on cardiovascular anatomy in different image orientations using 2D images, color Doppler, continuous-wave Doppler, and M-mode.

Cardiovascular Magnetic Resonance

Cardiac magnetic resonance (1.5T MAGNETOM, Avanto, Siemens Healthcare) was performed on the proband (III-1) at the age of 4 years for diagnosis and 4 years afterward for follow-up. The standard protocol was performed, including steady-state free precession cine imaging in the long- (4-, 2-, and 3-chamber) and short-axis cine views and the right ventricular outflow view. After the administration of 0.15 mol/kg of gadoterate meglumine (gadolinium-DOTA, Dotarem, Guerbet), early and late gadolinium enhancement images of the short-axis stack and the 3 long-axis views were obtained in magnitude and phase-sensitive inversion recovery reconstructions.

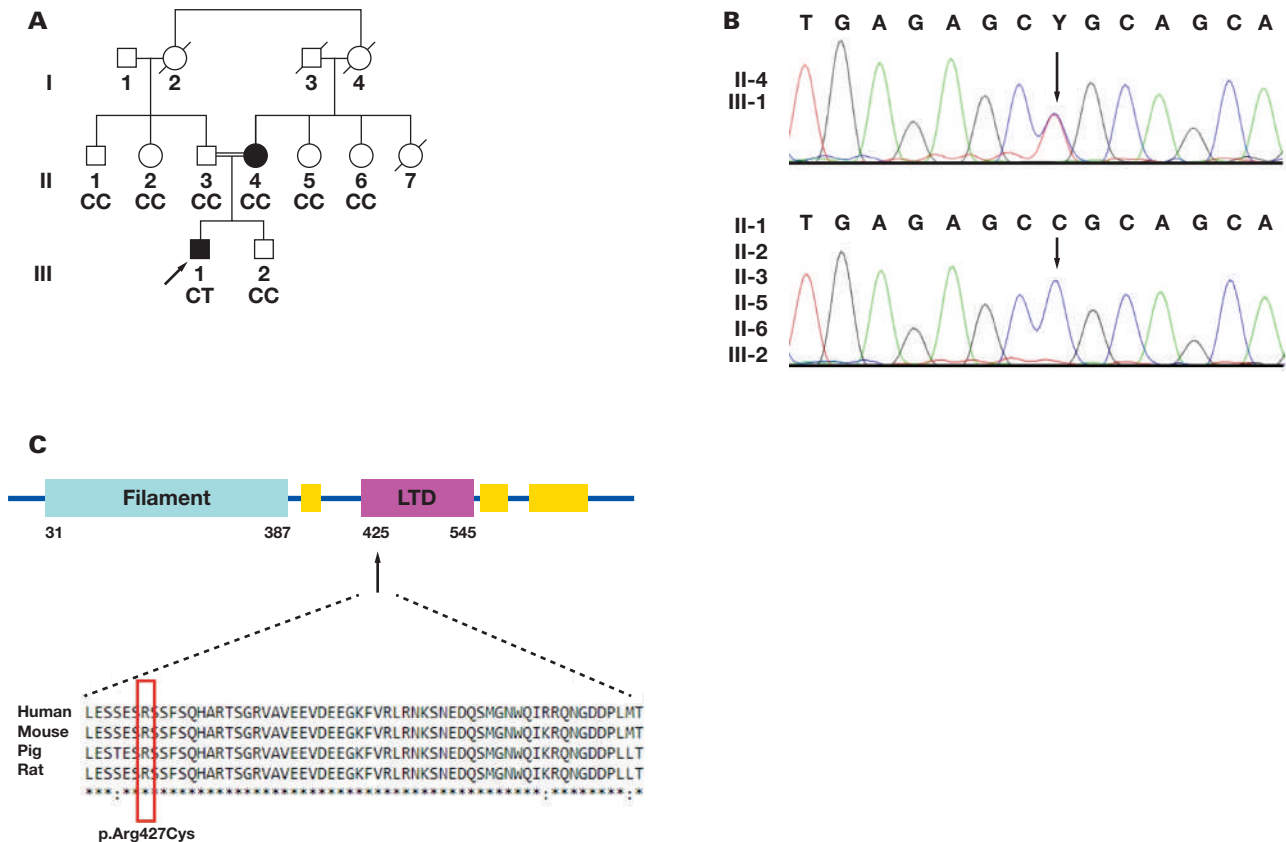
WES and Bioinformatics Analysis

WES was performed on the proband's genomic DNA. Fragmented DNA was captured using an Agilent SureSelect Exome Capture kit (Agilent). Thereafter, paired-end sequencing of Exon-Enriched Libraries was carried out on the Illumina HiSeq 4000 (Macrogen). The alignment of the sequencing reads to the human genome reference (hg19/NCBI) was done using the BWA (v07.17) tool,³⁵ with 98.8% quality and 99% region coverage. Variant calling was performed on the mapping result file (binary alignment map) by applying the GATK (v4.1.4.1) tool. Duplicates were marked and removed with the aid of SAMtools (in the GATK package)³⁶; then, SNP/INDEL calling was done. The annotated variants were prioritized and filtered by considering the minor allele frequency (>0.05) of 1000 Genomes Project and ExAc databases.³⁷ Bioinformatics analysis was performed to evaluate the pathogenicity score of the candidate variants. Prediction software tools, namely MutationTaster, SIFT, PolyPhen-2, PROVEAN, CADD, and GERP++, were applied. The variant predicted as pathogenic in at least 3 tools was considered for subsequent validation and segregation analysis.

Variant Validation

The putative pathogenic variant was verified by polymerase chain reaction and Sanger sequencing. Specific forward (5'CTTGTGATGTTTCAGAGCTGGCT3') and reverse (5'TGTGGAGGAGATATACAGGCTCAC3') primers were designed using Primer3 (v.04.0) (<http://bioinfo.ut.ee/primer3-0.4.0/>). DNA extraction was performed using our in-house method of salting out. The polymerase chain reaction test was carried out on a SimpliAmp Thermal Cycler (Thermo Fisher Scientific) with 1.5 mmol/L of MgCl₂, 10 pmol/L of primers, 200 ng of DNA, 200 mmol/L of dNTP, and 1 U of Taq DNA polymerase (Amplicon). The incubation schedule was 95°C for 5 minutes, followed by 32 amplification cycles (30 seconds at 95°C, 30 seconds at 63°C, and 30 seconds at 72°C), and the product was sequenced on an ABI Sequencer 3500XL PE (Applied Biosystems) in our center.

FIGURE 1. The image depicts the pedigree, sequencing chromatograms, LMNA protein structure, and conservation analysis in a family affected by hypertrophic cardiomyopathy due to a variant in *LMNA*. **A,** The pedigree of the affected family is presented herein. The arrow indicates the proband, the squares indicate the male family members, the circles indicate the female family members, the symbols with a strikethrough indicate the deceased cases, the open symbols indicate the unaffected individuals, and the solid symbols indicate the affected cases. **B,** The image illustrates the results of the Sanger sequencing analysis of the c.1279C>T variant. The heterozygous variant causes a missense substitution (p.Arg427Cys). The genotype of the *LMNA* variant is shown under each person examined (CC: wild type; CT: heterozygous for the variant). The proband (III-1) and his mother (II-4) carry the c.1279C>T (p.Arg427Cys) variant in a heterozygous status. The variant is absent in the unaffected members of the pedigree (II-1, II-2, II-3, II-5, II-6, and III-2). The black arrow indicates the location of the mutated nucleotide. **C,** The images show the amino acid evolutionary conservation analysis by CLUSTALW (<https://www.genome.jp/tools-bin/clustalw>). The recognized mutated site of *LMNA* is greatly conserved among species and is localized in the LTD domain of the *LMNA* protein.



Homology Modeling and Docking

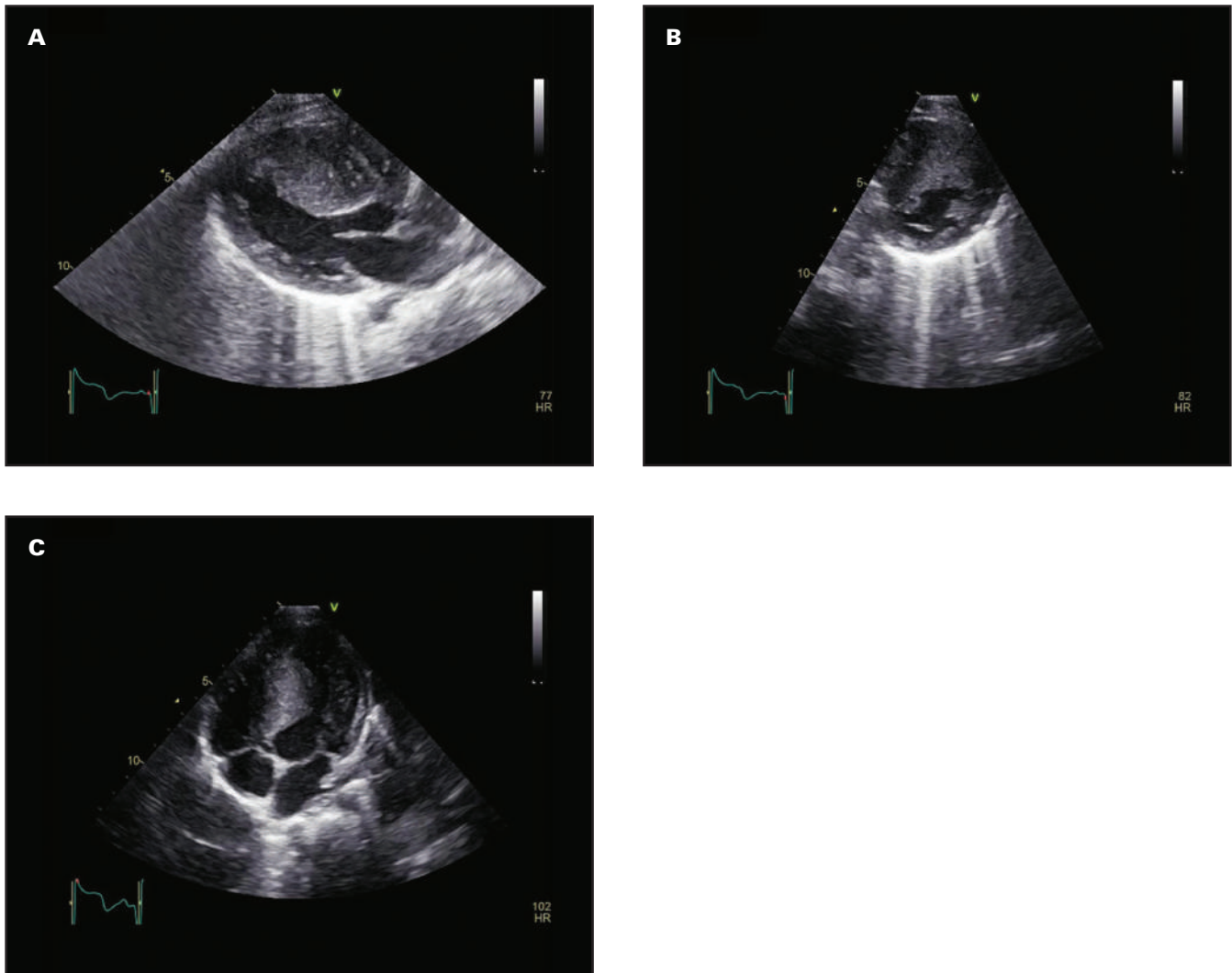
Lamin A/C and Cellular Signaling

Lamin A/C can bind Smad antagonists, namely MAN1 (inner nuclear membrane protein Man1) and PP2A (protein phosphatase 2A activator). Lamin A/C-PP2A and lamin A/C-MAN1 complexes reduce the Smad pathway through dephosphorylation and sequestering, respectively, and subsequently inhibit transforming growth factor-beta (TGF- β) signaling.³⁸ TGF- β regulates differentiation, proliferation, and apoptosis in many cell types.³⁹ Blocking TGF- β signaling diminishes the proliferation and expression of downstream myocyte targets and, thus, leads to less hypertrophy.⁴⁰ The results of a previous study indicated that lamin variants increased TGF- β activity via the Smad-dependent pathway in mice.⁴¹ Another investigation on mice with HCM showed that TGF- β activated the canonical Smad-dependent pathway.⁴²

Docking of LMNA with MAN1 Proteins

With the aid of the RCSB Protein Data Bank (PDB) (<https://www.rcsb.org/>), human lamin A/C (PDB: 7CRG) and MAN1 (2CH0) were downloaded. Mutant lamin A/C (R427C) was created with the SWISS-MODEL Homology-Modeling Server (<https://swissmodel.expasy.org/>).⁴³⁻⁴⁷ The structures of the proteins were corrected with ViewerLite (v.1.5.1). Briefly, polar hydrogens were added, and water molecules and ligands were deleted. Energy minimization was performed using the YASARA Energy Minimization Server (<http://www.yasara.org/minimizationserver.htm>).⁴⁸ The 3D structures of the compounds were imported as an SCE file into the YASARA View to deliver low-energy structures of the compounds and then saved in PDB file format. The protein-protein docking of the modeled normal lamin A/C and mutant lamin A/C (R427C) with the MAN1 protein (PDB: 2CH0) was performed using the HADDOCK Web Server (<https://wenmr.science.uu.nl/haddock2.4/>),^{49,50}

FIGURE 2. The proband's (III-1) echocardiography results are presented herein. The parasternal long-axis (A) and short-axis (B) images of the left ventricle demonstrate asymmetric septal hypertrophy (ASH). C, The apical 4-chamber view demonstrates ASH with a reversed septal curvature.



which is very efficient in protein-protein docking. Data visualization was accomplished using PyMOL (v.2.5.2),⁵¹ and the interactions of all the compounds across the interface were checked with the DIMPLOT program, implemented in LigPlus+ (v.2.2.4).⁵²

Results

Echocardiography Findings

The first echocardiography on the proband (III-1) at the age of 4 years in 2016 revealed asymmetric septal hypertrophy with reversed septal curvature (maximum thickness = 18 mm), mild dynamic outflow obstruction, mild mitral regurgitation due to the systolic anterior motion of the mitral valve, and supernormal left ventricular systolic function (ejection fraction = 75%). Additionally, mitral inflow signals revealed abnormal diastolic function, whereas right ventricular function was normal. The last echocardiographic study, in 2020, illustrated a maximum thickness of 28 mm for the interventricular septum. Moreover, there was no significant change in the function of the left and right ventricles and the

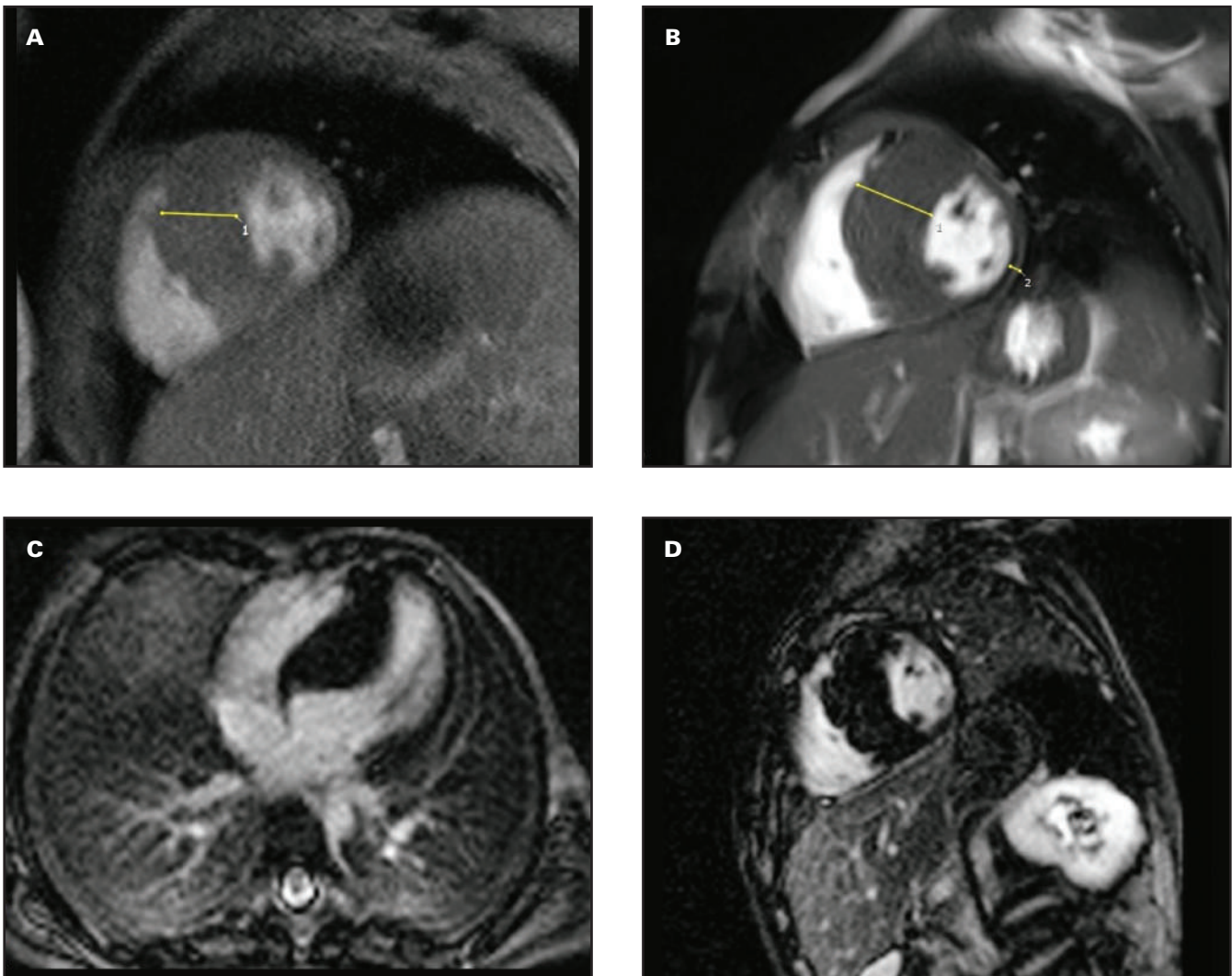
severity of left ventricular outflow obstruction and mitral regurgitation (FIGURE 2).

Cardiovascular Magnetic Resonance Findings

In 2016, cardiovascular magnetic resonance on the proband (III-1) at the age of 4 years revealed left ventricular asymmetric hypertrophy in the basal to mid-septal wall with a maximum thickness of 18 mm compared with a thickness of 3 mm in the lateral wall. The modality also demonstrated systolic anterior motion of the mitral valve, accelerated flow in the left ventricular outflow tract (Supplementary Videos 1 and 2), supernormal left ventricular systolic function (ejection fraction = 75%), and a right ventricular ejection fraction of 65%. Late gadolinium enhancement images showed no evidence of replacement fibrosis in the myocardium. Based on the clinical and imaging findings, the cardiomyopathy phenotype was defined as HCM.

The subsequent cardiovascular magnetic resonance study, performed 4 years later at follow-up, showed a significant increase in left ventricular wall thickness to a maximum of 28 mm at the mid-septal portion in comparison with the 2016 study (FIGURE 3A and 3B), the systolic

FIGURE 3. The image presents the cardiac magnetic resonance imaging findings of the proband (III-1) with hypertrophic cardiomyopathy caused by the c.1279C>T (p.Arg427Cys) variant. A and B, The images present the short-axis static images of the end-diastolic phase, showing maximal thickness in the mid-left ventricular level in the years 2016 and 2020, respectively. C and D, Late gadolinium images in the 4-chamber long- and short-axis views, obtained in the year 2020, show no evidence of enhancement and replacement fibrosis in the myocardium.



anterior motion of the mitral valve, and accelerated flow in the left ventricular outflow tract. Additionally, there was no significant change in left and right ventricular ejection fractions. The late gadolinium enhancement images yielded no evidence of replacement fibrosis (FIGURE 3C and 3D).

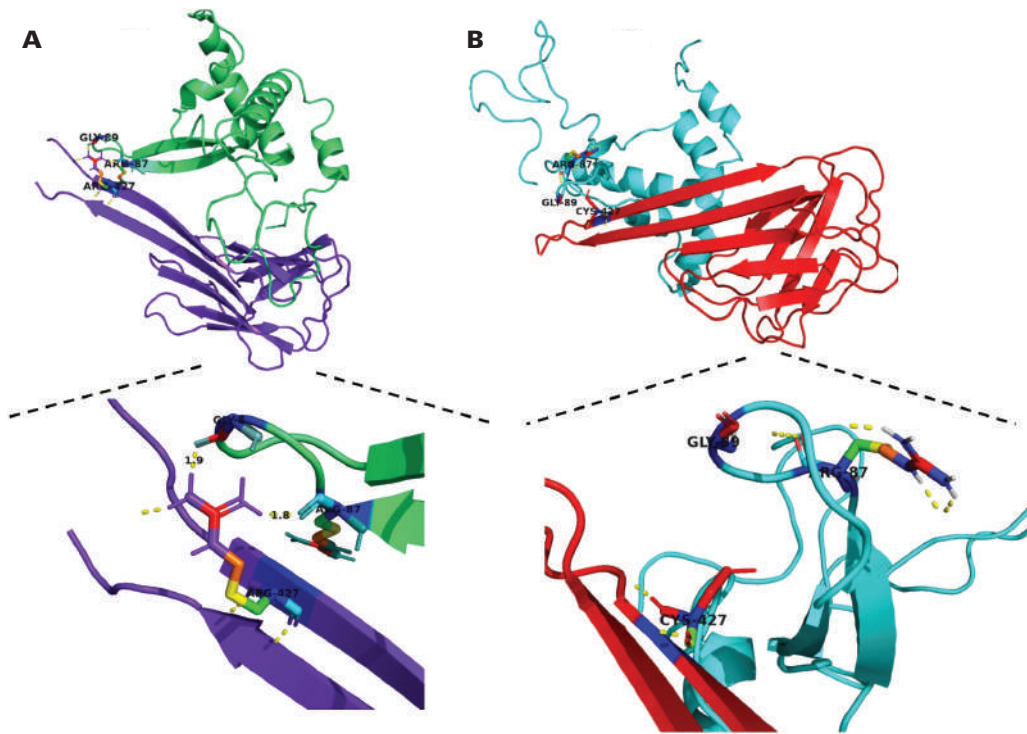
Molecular Analysis

The known C>T pathogenic heterozygous variant at nucleotide position c.1279 (transcript name: NM170707) in *LMNA* exon 7 was identified through WES. This variant resulted in arginine replacement at the 427th amino acid position with cysteine (p.Arg427Cys). This variant was verified in the proband by Sanger sequencing (FIGURE 1A: III-1), whereas it was not found in the proband's father (FIGURE 1A, II-3) or brother (FIGURE 1A: III-2). Although the mother (FIGURE 1A, II-4) of the proband (III-1) did not have clinical symptoms, she had the same pathogenic variant (*LMNA* c.1279C>T [p.Arg427Cys]) and the magnetic resonance imaging (MRI) result indicated that she also had HCM

(Supplementary File 3). The other pedigree members studied, comprising the healthy individuals (II-1, II-2, II-5, and II-6), lacked the variant (FIGURE 1B). Previous research has shown that amino acid Arg427 is located in the LTD domain of the LMNA protein (FIGURE 1C), and amino acid Arg427 is greatly conserved in several species (FIGURE 1C). According to the American College of Medical Genetics and Genomics 2015,⁵³ c.1279C>T is interpreted as a likely pathogenic variant (ie, criteria: PM1, PM2, PP2, PP3, and PP4). The missense substitution variant was considered disease causing by MutationTaster, SIFT, PolyPhen-2, PROVEAN, CADD (Phred = 27.6), and GERP++ (5.7).

Docking studies were performed between the normal and mutant forms of lamin A/C and MAN1. Among the clusters resulting from the docking experiments, the first one, which had the least root mean square deviation of the structure, was better than the others. The top complex structures for the normal and mutant forms of lamin A/C in interaction with MAN1, reductions in the HADDOCK score, changes in electrostatic energy, and the buried surface area for the interaction between

FIGURE 4. Lamin A/C and MAN1 complexes are illustrated herein. **A**, The image shows normal lamin A/C in interaction with MAN1. Lamin A/C and MAN1 are shown in purple and green, respectively. **B**, Mutant lamin A/C is illustrated in interaction with MAN1. Lamin A/C and MAN1 are shown in red and cyan, respectively. RMSD, root-mean-square deviation.



HADDOCK results	Normal Lamin A/C and MAN1	Mutant Lamin A/C and MAN1
HADDOCKscore	-69.4 +/- 8.1	-80.8 +/- 12.5
RMSD	0.8 +/- 0.5	1.8 +/- 1.3
Van der Waals energy	-51.3 +/- 3.7	-25.3 +/- 6.7
Electrostatic energy	-94.8 +/- 16.0	-251.8 +/- 92.1
Buried surface area	1452.7 +/- 38.2	1265.2 +/- 146.8
z-score	-1.1	-1.9

the normal and mutant forms of lamin A/C with MAN1 are depicted in **FIGURE 4**. The HADDOCK score for the interaction between normal lamin A/C and MAN1 was -69.4 ± 8.1 , whereas it was significantly reduced for the interaction between mutant lamin A/C and MAN1 (the HADDOCK score = -80.8 ± 12.5). Electrostatic energy reduction was significant in the interaction between normal lamin A/C and MAN1 (electrostatic energy = -94.8 ± 16.0) and between mutant lamin A/C and MAN1 (electrostatic energy = -251.8 ± 92.1). The buried surface area exhibited a more pronounced change between these 2 conditions (normal lamin A/C and MAN1 = 1452.7 ± 38.2 and mutant lamin A/C and MAN1 = 1265.2 ± 146.8). Changes in the position of MAN1 in interaction with mutant lamin A/C in comparison with normal lamin A/C are shown in **FIGURE 5**.

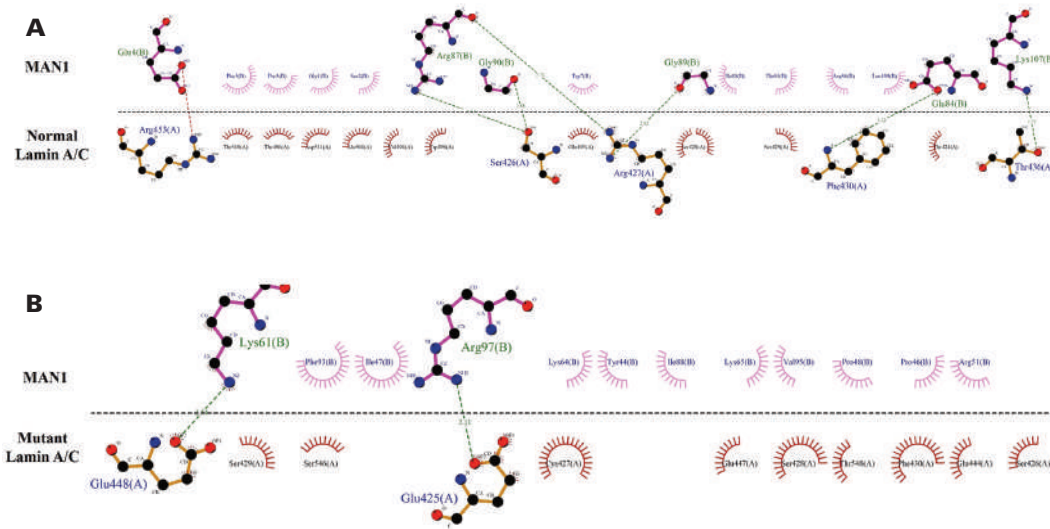
Discussion

The genetic heterogeneity of HCM is highly diverse. Because of this marked allelic heterogeneity and the high frequency of novel individual variants,^{54,55} limited data are available on genotype-phenotype relationships.⁵⁵⁻⁵⁷ Although HCM is known as a disease of the sarcomere, variable penetrance in families who have the same genetic variants can challenge the notion of a monogenic origin for HCM and

instead imply a multifactorial cause. Several patients and families with HCM are left without a definite molecular genetic diagnosis.⁵⁸ Further, large-scale genome sequencing investigations have offered little or no evidence of a relationship between HCM and several genes already reported as its cause, suggesting a sarcomere-independent mechanism for cardiomyocyte hypertrophy.⁵⁹ Cardiac imaging techniques such as cardiac MRI and echocardiography are used to diagnose HCM, which mostly presents as asymmetrical septal hypertrophy.^{5,60} Accordingly, we performed exhaustive clinical and genetic evaluations, including cardiovascular magnetic resonance, echocardiography, and WES, on our proband (III-1) and succeeded in establishing a diagnosis of HCM via these workups. The proband (**FIGURE 1A**: III-1) had a wall thickness of 28 mm, whereas a clinical diagnosis of HCM is based on a maximum wall thickness of ≥ 15 mm.

Assessments of genotype-phenotype associations have confirmed that essentially there is compatibility between any wall thickness and the existence of an HCM mutant gene; however, a high prevalence of sudden death is observed in patients with thicker walls.^{61,62} According to previous research, genetic testing is suitable for any level of hypertrophy.⁶³

Positioned on chromosome 1q22, *LMNA* encodes 2 main lamin A/C isoforms as major nuclear protein components in mammals and acts

FIGURE 5. The interacted surfaces of normal (A) and mutant (B) lamin A/C with MAN1 are presented herein.

as a meshwork structure. Recently, certain disease phenotypes called “laminopathies” have been associated with variants in *LMNA*, ranging from accelerated aging diseases to striated muscle diseases such as cardiomyopathy and muscular dystrophy.^{64,65} In general, the *LMNA* gene has exhibited a high level of conservation throughout evolution. In this study, we investigated *LMNA* protein interactions. Our protein-protein interaction analysis suggested that variant p.Arg427Cys could diminish hydrogen bonds and hydrophobic surfaces in lamin A/C and MAN1, thereby lessening the binding affinity of Smad to the complex given that MAN1 is an indirect inactivator of Smad in the TGF- β pathway. Hence, this variant can result in increased TGF- β activity in myocytes, followed by myocyte hypertrophy.

In this study, we detected candidate variant *LMNA* c.1279C>T (p.Arg427Cys) in a family with HCM using next-generation sequencing. We found that the proband (III-1) carried a heterozygous c.1279C>T (p.Arg427Cys) variant in the *LMNA* gene associated with HCM. Interestingly, the pathogenic variant *LMNA* c.1279C>T (p.Arg427Cys) was also identified in the proband’s (III-1) mother (II-4), who showed no clinical symptoms; however, MRI indicated she also had HCM. No family history of HCM was reported in the proband’s (III-1) family, and DNA was not available for further genetic assessment of the remaining family members. Surprisingly, although the majority of missense variants in the *LMNA* gene are particularly linked to dilated cardiomyopathy, there are few reports of *LMNA* variants leading to phenotypes consistent with HCM. Furthermore, the relationship between *LMNA* gene variants and extremely variable clinical manifestations is complicated and not sufficiently elucidated. The 2 novel *LMNA* variants, namely c.1772G>T (p.Cys591Phe) and c.1930C>T (p.Arg 644Cys) located at exon 11, show pleiotropic effects, with variant carriers causing several cardiomyopathies such as HCM and dilated cardiomyopathy.^{66,67} These findings imply external factors as possible pathogenic co-drivers for the development of the disease.⁵⁹ Caux et al⁶⁸ reported a heterozygous variant in exon 2: a CGG-for-CTG transversion at *LMNA* codon 133 (R133L), resulting in an arginine-for-leucine substitution in a patient with insulin-resistant diabetes, HCM with aortic valve involvement, and generalized lipoatrophy. Francisco et al⁶⁹ described a 64-year-old

woman with HCM harboring the variant c.1718C>T (p.Ser573Leu) in *LMNA* exon 11. The patient suffered from severe symptomatic ventricular hypertrophy and left ventricular outflow tract obstruction with severe dyslipidemia, diabetes, and obesity.

The clinical utility of genetic testing is limited by challenges in identifying variants of unknown significance, the absence of consistent genotype-phenotype correlations, and inadequate knowledge regarding all genes involved in HCM.²³ On the other hand, genetic testing for HCM provides essential clinical data for family screening and disease outcomes, albeit the yield is variable.⁷⁰ In a retrospective assessment of 285 cases with the pathogenic variants of sarcomere protein genes causing HCM with no diagnostic criteria for HCM, nearly 50% developed HCM during 15 years of follow-up.⁷¹ Therefore, it is essential to identify cases with the pathogenic variants of HCM and provide proper follow-up testing, even for asymptomatic cases.

The existing literature contains a dearth of data on the spectrum and clinical characteristics of the causal genetic variants of HCM in Iranians. To the best of our knowledge, this investigation is the first report regarding *LMNA* pathogenesis as causative of HCM in Iranians. We recommend WES as the most cost-effective first-line genetic assay to identify the causal genetic variants of HCM or the diseases misdiagnosed as HCM.

Conclusions

Although it has been demonstrated that HCM is primarily a disease affecting the sarcomere, its genetic basis is highly varied, and the association between a single variant and a particular typical phenotype has yet to be elucidated. Furthermore, sarcomere variants are associated with other diseases affecting cardiac function and structure. Nonsarcomeric gene variants have also been linked with HCM. Genetic assessment is appropriate for precision medicine in HCM and is essential for optimal treatment strategies, genetic counseling, and clinical management of the carriers of *LMNA* variants in families with HCM. In this study, we used WES and found a heterozygous variant in the *LMNA* gene related to the HCM phenotype, thereby demonstrating the utility of this approach for the timely and precise detection of the genetic causes of such diseases.

Supplementary Material

Supplementary material is available at *Laboratory Medicine* online.

Acknowledgments

Our sincere gratitude goes to the family members who participated in this study. This research was funded by Rajaie Cardiovascular Medical and Research Center, Tehran, Iran.

Conflict of Interest Disclosure

The authors have nothing to declare.

Data Availability

The datasets generated or analyzed during the current study are available in the ClinVar repository [<https://www.ncbi.nlm.nih.gov/clinvar/variation/200943/>]. The submission ID of the variant in ClinVar is as follows: LMNA (NM_170707.4): c.1279C>T (p.Arg427Cys): VCV000200943.18.

REFERENCES

1. Semsarian C, Ingles J, Maron MS, Maron BJ. New perspectives on the prevalence of hypertrophic cardiomyopathy. *J Am Coll Cardiol*. 2015;65(12):1249–1254.
2. Maron MS, Hellawell JL, Lucove JC, Farzaneh-Far R, Olivetto I. Occurrence of clinically diagnosed hypertrophic cardiomyopathy in the United States. *Am J Cardiol*. 2016;117(10):1651–1654.
3. Bonow R. Hypertrophic cardiomyopathy: past, present... and future. *Trends Cardiovasc Med*. 2014;25(1):65–66.
4. Maron BJ, Ommen SR, Semsarian C, Spirito P, Olivetto I, Maron MS. Hypertrophic cardiomyopathy: present and future, with translation into contemporary cardiovascular medicine. *J Am Coll Cardiol*. 2014;64(1):83–99.
5. Khaleghparast S, Maleki A, Taghavi S, et al. Hospital facilities at home for heart failure patients. *Iran Heart J*. 2020;21(1):34–44.
6. Maron BJ, Olivetto I, Spirito P, et al. Epidemiology of hypertrophic cardiomyopathy-related death: revisited in a large non-referral-based patient population. *Circulation*. 2000;102(8):858–864.
7. Sabater-Molina M, Pérez-Sánchez I, Hernández DRJ, Gimeno J. Genetics of hypertrophic cardiomyopathy: a review of current state. *Clin Genet*. 2018;93(1):3–14.
8. Jarcho JA, McKenna W, Pare JP, et al. Mapping a gene for familial hypertrophic cardiomyopathy to chromosome 14q1. *N Engl J Med*. 1989;321(20):1372–1378.
9. Seidman CE, Seidman JJC. Identifying sarcomere gene mutations in hypertrophic cardiomyopathy: a personal history. *Circ Res*. 2011;108(6):743–750.
10. Thierfelder L, Watkins H, MacRae C, et al. α -Tropomyosin and cardiac troponin T mutations cause familial hypertrophic cardiomyopathy: a disease of the sarcomere. *Cell*. 1994;77(5):701–712.
11. Watkins H, Ashrafian H, Redwood C. Inherited cardiomyopathies. *N Engl J Med*. 2011;364(17):1643–1656.
12. Geisterfer-Lowrance AA, Kass S, Tanigawa G, et al. A molecular basis for familial hypertrophic cardiomyopathy: a β cardiac myosin heavy chain gene missense mutation. *Cell*. 1990;62(5):999–1006.
13. Watkins H, MacRae C, Thierfelder L, et al. A disease locus for familial hypertrophic cardiomyopathy maps to chromosome 1q3. *Nat Genet*. 1993;3(4):333–337.
14. Bonaventura J, Polakova E, Vejtasova V, Veselka J. Genetic testing in patients with hypertrophic cardiomyopathy. *Int J Mol Sci*. 2021;22(19):10401.
15. Mahdavi M, Mohsen-Pour N, Maleki M, et al. Whole-exome sequencing identified compound heterozygous variants in the TTN gene causing Salih myopathy with dilated cardiomyopathy in an Iranian family. *Cardiol Young*. 2021;32(9):1–6.
16. Teekakirikul P, Kelly MA, Rehm HL, Lakdawala NK, Funke B. Inherited cardiomyopathies: molecular genetics and clinical genetic testing in the postgenomic era. *J Mol Diagn*. 2013;15(2):158–170.
17. Ingles J, Goldstein J, Thaxton C, et al. Evaluating the clinical validity of hypertrophic cardiomyopathy genes. *Circ Genom Precis Med*. 2019;12(2):e002460.
18. Walsh R, Buchan R, Wilk A, et al. Defining the genetic architecture of hypertrophic cardiomyopathy: re-evaluating the role of non-sarcomeric genes. *Eur Heart J*. 2017;38(46):3461–3468.
19. Walsh R, Offerhaus JA, Tadros R, Bezzina C. Minor hypertrophic cardiomyopathy genes, major insights into the genetics of cardiomyopathies. *Nat Rev Cardiol*. 2021;19(3):1–17.
20. Akhtar M, Elliott PJG. Practice. The genetics of hypertrophic cardiomyopathy. *Glob Cardiol Sci Pract*. 2018;2018(3):36.
21. Maron BJ, Maron MS, Maron BA, Loscalzo J. Moving beyond the sarcomere to explain heterogeneity in hypertrophic cardiomyopathy: JACC review topic of the week. *J Am Coll Cardiol*. 2019;73(15):1978–1986.
22. Maron BJ. Clinical course and management of hypertrophic cardiomyopathy. *N Engl J Med*. 2018;379(7):655–668.
23. Gruner C, Ivanov J, Care M, et al. Toronto hypertrophic cardiomyopathy genotype score for prediction of a positive genotype in hypertrophic cardiomyopathy. *Circ Cardiovasc Genet*. 2013;6(1):19–26.
24. Lopes LR, Syrris P, Guttman OP, et al. Novel genotype–phenotype associations demonstrated by high-throughput sequencing in patients with hypertrophic cardiomyopathy. *Heart*. 2015;101(4):294–301.
25. Ingles J, Burns C, Bagnall RD, et al. Nonfamilial hypertrophic cardiomyopathy: prevalence, natural history, and clinical implications. *Circ Cardiovasc Genet*. 2017;10(2):e001620.
26. Manrai AK, Funke BH, Rehm HL, et al. Genetic misdiagnoses and the potential for health disparities. *N Engl J Med*. 2016;375(7):655–665.
27. Broers JL, Peeters EA, Kuijpers HJ, et al. Decreased mechanical stiffness in LMNA–/– cells is caused by defective nucleocytoskeletal integrity: implications for the development of laminopathies. *Hum Mol Genet*. 2004;13(21):2567–2580.
28. Lee H, Adams WJ, Alford PW, et al. Cytoskeletal prestress regulates nuclear shape and stiffness in cardiac myocytes. *Exp Biol Med*. 2015;240(11):1543–1554.
29. Fatkin D, MacRae C, Sasaki T, et al. Missense mutations in the rod domain of the lamin A/C gene as causes of dilated cardiomyopathy and conduction-system disease. *N Engl J Med*. 1999;341(23):1715–1724.
30. Vytopil M, Ricci E, Russo AD, et al. Frequent low penetrance mutations in the Lamin A/C gene, causing Emery Dreifuss muscular dystrophy. *Neuromuscul Disord*. 2002;12(10):958–963.
31. Bortot B, Athanasakis E, Brun F, et al. High-throughput genotyping robot-assisted method for mutation detection in patients with hypertrophic cardiomyopathy. *Diagn Mol Pathol*. 2011;20(3):175–179.
32. Fokstuen S, Munoz A, Melacini P, et al. Rapid detection of genetic variants in hypertrophic cardiomyopathy by custom DNA resequencing array in clinical practice. *J Med Genet*. 2011;48(8):572–576.
33. Meder B, Haas J, Keller A, et al. Targeted next-generation sequencing for the molecular genetic diagnostics of cardiomyopathies. *Circ Cardiovasc Genet*. 2011;4(2):110–122.
34. Kalayinia S, Goodarzynejad H, Maleki M, Mahdih N. Next generation sequencing applications for cardiovascular disease. *Ann Med*. 2018;50(2):91–109. doi:10.1080/07853890.2017.1392595
35. Li H, Durbin R. Fast and accurate long-read alignment with Burrows–Wheeler transform. *Bioinformatics*. 2010;26(5):589–595. doi:10.1093/bioinformatics/btp698
36. DePristo MA, Banks E, Poplin R, et al. A framework for variation discovery and genotyping using next-generation DNA sequencing data. *Nat Genet*. 2011;43(5):491–498. doi:10.1038/ng.806

37. Karczewski KJ, Francioli LC, Tiao G, et al; Genome Aggregation Database Consortium. The mutational constraint spectrum quantified from variation in 141,456 humans. *Nature*. 2021;590(7846):E53–E53. doi:10.1038/s41586-020-03174-8
38. Andrés V, González JM. Role of A-type lamins in signaling, transcription, and chromatin organization. *J Cell Biol*. 2009;187(7):945–957. doi:10.1083/jcb.200904124
39. Dittmer TA, Misteli T. The lamin protein family. *Genome Biol*. 2011;12(5):2221–2214. doi:10.1186/gb-2011-12-5-222
40. Teekakirikul P, Padera RF, Seidman JG, Seidman CE. *Hypertrophic Cardiomyopathy: Translating Cellular Cross Talk into Therapeutics*. Rockefeller University Press; 2012.
41. Gerace L, Tapia O. Messages from the voices within: regulation of signaling by proteins of the nuclear lamina. *Curr Opin Cell Biol*. 2018;52(1):14–21. doi:10.1016/j.ceb.2017.12.009
42. Teekakirikul P, Eminaga S, Toka O, et al. Cardiac fibrosis in mice with hypertrophic cardiomyopathy is mediated by non-myocyte proliferation and requires TGF- β . *J Clin Invest*. 2010;120(10):3520–3529. doi:10.1172/JCI42028
43. Waterhouse A, Bertoni M, Bienert S, et al. SWISS-MODEL: homology modelling of protein structures and complexes. *Nucleic Acids Res*. 2018;46(W1):W296–W303. doi:10.1093/nar/gky427
44. Bienert S, Waterhouse A, de Beer TA, et al. The SWISS-MODEL Repository—new features and functionality. *Nucleic Acids Res*. 2017;45(D1):D313–D319. doi:10.1093/nar/gkw1132
45. Guex N, Peitsch MC, Schwede T. Automated comparative protein structure modeling with SWISS-MODEL and Swiss-PdbViewer: a historical perspective. *Electrophoresis*. 2009;30(S1):S162–S173. doi:10.1002/elps.200900140
46. Studer G, Rempfer C, Waterhouse AM, Gumienny R, Haas J, Schwede T. QMEANDisCo—distance constraints applied on model quality estimation. *Bioinformatics*. 2020;36(6):1765–1771. doi:10.1093/bioinformatics/btz828
47. Bertoni M, Kiefer F, Biasini M, Bordoli L, Schwede T. Modeling protein quaternary structure of homo- and hetero-oligomers beyond binary interactions by homology. *Sci Rep*. 2017;7(1):1–15.
48. Krieger E, Joo K, Lee J, et al. Improving physical realism, stereochemistry, and side-chain accuracy in homology modeling: four approaches that performed well in CASP8. *Proteins Struct Funct Bioinf*. 2009;77(S9):114–122. doi:10.1002/prot.22570
49. Honorato RV, Koukos PI, Jiménez-García B, et al. Structural biology in the clouds: the WeNMR-EOSC ecosystem. *Front Mol Biosci*. 2021;8(2):708–712.
50. Van Zundert G, Rodrigues J, Trellet M, et al. The HADDOCK2.2 web server: user-friendly integrative modeling of biomolecular complexes. *J Mol Biol*. 2016;428(4):720–725. doi:10.1016/j.jmb.2015.09.014
51. Seeliger D, de Groot BL. Ligand docking and binding site analysis with PyMOL and Autodock/Vina. *J Comput Aided Mol Des*. 2010;24(5):417–422.
52. Wallace AC, Laskowski RA, Thornton JM. LIGPLOT: a program to generate schematic diagrams of protein-ligand interactions. *Protein Eng Des Sel*. 1995;8(2):127–134.
53. Richards S, Aziz N, Bale S, et al. Standards and guidelines for the interpretation of sequence variants: a joint consensus recommendation of the American College of Medical Genetics and Genomics and the Association for Molecular Pathology. *Genet Med*. 2015;17(5):405–424. doi:10.1038/gim.2015.30
54. Charron P, Arad M, Arbustini E, et al. Genetic counselling and testing in cardiomyopathies: a position statement of the European Society of Cardiology Working Group on Myocardial and Pericardial Diseases. *Eur Heart J*. 2010;31(22):2715–2726.
55. Maron BJ, Maron MS, Semsarian C. Genetics of hypertrophic cardiomyopathy after 20 years: clinical perspectives. *J Am Coll Cardiol*. 2012;60(8):705–715.
56. Alfares AA, Kelly MA, Mcdermott G, et al. Results of clinical genetic testing of 2,912 probands with hypertrophic cardiomyopathy: expanded panels offer limited additional sensitivity. *Genet Med*. 2015;17(11):880–888.
57. Ingles J, Burns C, Barratt A, Semsarian C. Application of genetic testing in hypertrophic cardiomyopathy for preclinical disease detection. *Circ Cardiovasc Genet*. 2015;8(6):852–859.
58. Koskenvuo J, Leivo K, Vanninen S, et al. P6325 JPH2 p.(Thr161Lys) is a Finnish founder mutation associating to hypertrophic cardiomyopathy with or without systolic heart failure and conduction abnormalities. *Eur Heart J*. 2018;39(suppl_1):ehy566–eP6325.
59. Chou C, Chin M. Pathogenic mechanisms of hypertrophic cardiomyopathy beyond sarcomere dysfunction. *Int J Mol Sci*. 2021;22(16):8933.
60. Cirino AL, Ho C.J.G. *Familial Hypertrophic Cardiomyopathy Overview*. University of Washington; 1993; vol 2008.
61. Maron BJ, Niimura H, Casey SA, et al. Development of left ventricular hypertrophy in adults with hypertrophic cardiomyopathy caused by cardiac myosin-binding protein C gene mutations. *J Am Coll Cardiol*. 2001;38(2):315–321.
62. Niimura H, Bachinski LL, Sangwatanaroj S, et al. Mutations in the gene for cardiac myosin-binding protein C and late-onset familial hypertrophic cardiomyopathy. *N Engl J Med*. 1998;338(18):1248–1257.
63. Maron BJ, McKenna WJ, Danielson GK, et al. American College of Cardiology/European Society of Cardiology clinical expert consensus document on hypertrophic cardiomyopathy: a report of the American College of Cardiology Foundation Task Force on Clinical Expert Consensus Documents and the European Society of Cardiology Committee for Practice Guidelines. *J Am Coll Cardiol*. 2003;42(9):1687–1713.
64. Capell BC, Collins F. Human laminopathies: nuclei gone genetically awry. *Nat Rev Genet*. 2006;7(12):940–952.
65. Colombo MG, Botto N, Vittorini S, Paradossi U, Andreassi M. Clinical utility of genetic tests for inherited hypertrophic and dilated cardiomyopathies. *Cardiovasc Ultrasound*. 2008;6(1):1–10.
66. Araújo-Vilar D, Lado-Abeal J, Palos-Paz F, et al. A novel phenotypic expression associated with a new mutation in LMNA gene, characterized by partial lipodystrophy, insulin resistance, aortic stenosis and hypertrophic cardiomyopathy. *Clin Endocrinol*. 2008;69(1):61–68.
67. Mercuri E, Brown S, Nihoyannopoulos P, et al. Extreme variability of skeletal and cardiac muscle involvement in patients with mutations in exon 11 of the lamin A/C gene. *Muscle Nerve*. 2005;31(5):602–609.
68. Caux F, Dubosclard E, Lascols O, et al. A new clinical condition linked to a novel mutation in lamins A and C with generalized lipodystrophy, insulin-resistant diabetes, disseminated leukomelanodermic papules, liver steatosis, and cardiomyopathy. *J Clin Endocrinol Metab*. 2003;88(3):1006–1013.
69. Francisco ARG, Gonçalves IS, Veiga F, Pedro MM, Pinto FJ, Brito D. Complex phenotype linked to a mutation in exon 11 of the lamin A/C gene: hypertrophic cardiomyopathy, atrioventricular block, severe dyslipidemia and diabetes. *Rev Port Cardiol*. 2017;36(9):669e661–669e664.
70. Musunuru K, Hershberger RE, Day SM, et al. Genetic testing for inherited cardiovascular diseases: a scientific statement from the American Heart Association. *Circ Genom Precis Med*. 2020;13(4):e000067.
71. Lorenzini M, Norrish G, Field E, et al. Penetration of hypertrophic cardiomyopathy in sarcomere protein mutation carriers. *J Am Coll Cardiol*. 2020;76(5):550–559.

Metagenomic next-generation sequencing for the identification of infections caused by Gram-negative pathogens and the prediction of antimicrobial resistance

Yang-Hua Xiao, MM,^{1,3} Zhao-Xia Luo, MM,³ Hong-Wen Wu, MD,² De-Rong Xu, MD,¹ and Rui Zhao, MD¹ 

¹Department of Clinical Laboratory, Medical Center of Burn Plastic and Wound Repair, and ²Department of Medical Instruments, The First Affiliated Hospital of Nanchang University, Nanchang, China; ³School of Public Health, Nanchang University, Nanchang, China. Corresponding author: Rui Zhao; zhaoruisc@163.com

Key words: metagenomic next-generation sequencing; Gram-negative bacterial infections; antibiotic resistance; cytokines

Abbreviations: mNGS, metagenomic next-generation sequencing; GNB, Gram-negative bacteria; CMTs, conventional microbiological tests; AST, antimicrobial susceptibility testing; PCR, polymerase chain reaction; BALF, bronchoalveolar lavage fluid; CSF, cerebrospinal fluid; CLSI, Clinical and Laboratory Standards Institute; IL, interleukin; IFN, interferon; TNF, tumor necrosis factor; WBC, white blood cell count; CRP, C-reactive protein; SAA, serum amyloid A; PCT, procalcitonin; AK, amikacin; TOB, tobramycin; GEN, gentamicin; FEP, cefepime; CRO, ceftriaxone; CFP, cefoperazone; IPM, imipenem; MEM, meropenem; TZP, piperacillin-tazobactam; AMP, ampicillin; CAZ, ceftazidime; CIP, ciprofloxacin; LEV, levofloxacin; TMP-SMZ, sulfamethoxazole/trimethoprim

Laboratory Medicine 2024;55:71-79; <https://doi.org/10.1093/labmed/lmad039>

ABSTRACT

Objective: The aim of this study was to evaluate the efficacy of metagenomic next-generation sequencing (mNGS) for the identification of Gram-negative bacteria (GNB) infections and the prediction of antimicrobial resistance.

Methods: A retrospective analysis was conducted on 182 patients with diagnosis of GNB infections who underwent mNGS and conventional microbiological tests (CMTs).

Results: The detection rate of mNGS was 96.15%, higher than CMTs (45.05%) with a significant difference ($\chi^2 = 114.46$, $P < .01$). The pathogen spectrum identified by mNGS was significantly wider than CMTs. Interestingly, the detection rate of mNGS was substantially higher than that of CMTs (70.33% vs 23.08%, $P < .01$) in patients with but not without antibiotic exposure. There was a significant positive correlation between mapped reads and pro-inflammatory cytokines (interleukin-6 and interleukin-8). However, mNGS failed to predict antimicrobial resistance

in 5 of 12 patients compared to phenotype antimicrobial susceptibility testing results.

Conclusions: Metagenomic next-generation sequencing has a higher detection rate, a wider pathogen spectrum, and is less affected by prior antibiotic exposure than CMTs in identifying Gram-negative pathogens. The mapped reads may reflect a pro-inflammatory state in GNB-infected patients. Inferring actual resistance phenotypes from metagenomic data remains a great challenge.

Gram-negative bacteria (GNB) can infect almost all systems of the human body, including the respiratory, circulatory, and neurological systems, causing pneumonia, bacteremia, and meningitis, as well as eliciting life-threatening inflammatory reactions.^{1,2} Gram-negative bacteria (such as *Klebsiella pneumoniae*, *Pseudomonas aeruginosa*, and *Acinetobacter baumannii*) are more often associated with severe sepsis than Gram-positive bacteria.² Endotoxin derived from GNB is a powerful cytokine inducer that can trigger auto-amplificatory loops in monocytes and macrophages following activation.³ Excessive production of cytokines may cause a cytokine storm and contribute to death in patients with sepsis.^{3,4} The current research mainly focuses on the early identification of GNB infections to prevent patients from developing sepsis and septic shock.⁵ However, infections caused by GNB are practically indistinguishable from those with other etiologies due to the wide variety of clinical presentations.¹ Conventional microbiological culture is the gold standard for the etiological diagnosis of GNB infections, and phenotypic antimicrobial susceptibility testing (AST) is helpful to guide clinical treatment.⁶ Despite this, conventional microbial culture cannot meet the demands of GNB infection diagnosis due to its time consumption, requirements for pure cultures, few available detection targets, and high initial concentration of bacteria.⁷⁻⁹ Thus, clinicians usually adopt empirical broad-spectrum therapy before the etiological test results are available, which might contribute to the emergence of antibiotic resistance.^{10,11} Infections by multidrug-resistant GNB may result in prolonged hospitalization and unacceptably high mortality rates.¹² Therefore, timely and accurate microbiological results are essential to initiate targeted antibiotic treatment.

Metagenomic next-generation sequencing (mNGS) is a novel and promising molecular approach that combines genome sequencing technologies with bioinformatics approaches.¹³ The development of mNGS

has revolutionized the routine identification of pathogens in microbiology laboratories. As a high-throughput sequencing technology, mNGS has high sensitivity, short turnaround time, and a wide range of detectable pathogens.¹⁴ Metagenomic next-generation sequencing can theoretically identify all pathogens at the species level of bacteria by a single test and is less affected by prior antibiotic exposure.^{15,16} Furthermore, mNGS not only can detect antimicrobial resistance and virulence genes but also allows inferring genetic features in pathogen genomes, thus providing genetic evidence to facilitate epidemiologic studies.^{16,17} However, there have been very few reports on the application of mNGS in identifying Gram-negative pathogens and predicting antimicrobial resistance.

This study assessed the effectiveness of mNGS for the diagnosis of patients with GNB infections and compared the results with conventional microbiological tests (CMTs). The correlations between the mapped reads with inflammatory biomarker concentrations were explored. In addition, we also evaluated the accuracy of using mNGS to predict antimicrobial resistance in clinical practice.

Materials and Methods

Study Population and Samples

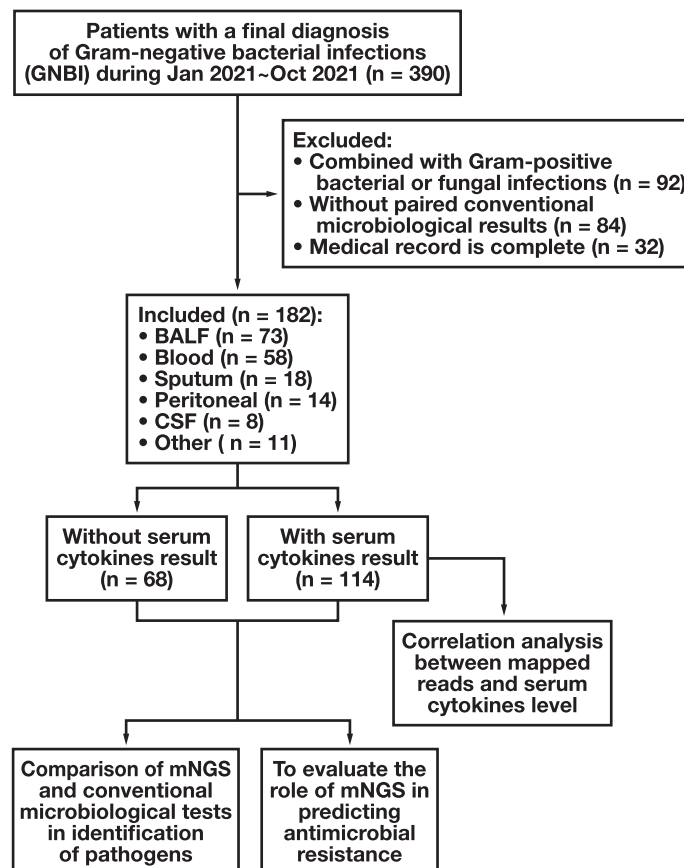
The study involved 390 cases with a final diagnosis of GNB infection at the First Affiliated Hospital of Nanchang University (Nanchang, China) during the period from January 2021 to October 2021. Using our exclusion criteria (FIGURE 1), we excluded 92 cases with combined

Gram-positive bacterial and fungal infections, 84 in which conventional microbiological tests and mNGS were not conducted at the same time, and 32 cases of incomplete information. Finally, a total of 182 patients were included for further analysis. Only 1 specimen was collected from each patient and split into 2 aliquots for mNGS and conventional microbiological testing. Specimens included bronchoalveolar lavage fluid (n = 73), blood (n = 58), sputum (n = 18), peritoneum (n = 14), cerebrospinal fluid (n = 8), urine (n = 4), pus (n = 4), pleural (n = 2), and marrow (n = 1). The final diagnosis of GNB infections was based on all laboratory testing and a longitudinal review of the patient's clinical characteristics. Data on the 182 patients' demographic characteristics and clinical laboratory findings were collected from their medical records. Serum cytokines were measured in 114 of 182 patients, and the correlation between mapped reads and serum cytokine concentrations was analyzed. Data was collected in a nonselective and continuous manner. Ethics approval was given by the institutional review board of the First Affiliated Hospital of Nanchang University.

Conventional Microbiological Tests

Conventional microbiological tests included Gram staining, bacteriological cultures, bacterial endotoxin testing, and serum tube agglutination test. For the blood specimens, blood was collected using aerobic and anaerobic blood culture bottles and incubated in the BacT/ALERT 3D Microbial Detection System (bioMérieux). All other specimens were collected in sterile containers from each patient according to standard procedures. Specimens were then immediately transported to an

FIGURE 1. Flowchart of this study. BALF, bronchoalveolar lavage fluid; CSF, cerebrospinal fluid; mNGS, metagenomic next-generation sequencing.



in-house microbiology laboratory (Department of Clinical Laboratory, The First Affiliated Hospital of Nanchang University) for pathogen testing. Routine separation media (sheep blood agar, chocolate agar, and Mueller-Hinton agar plates) were used for isolation of organisms under aerobic (37°C, 5% CO₂ for 24 h) and anaerobic conditions. Bacterial isolates were further identified by VITEK2 COMPACT system (bioMérieux).

Metagenomic Next-Generation Sequencing and Bioinformatics Analysis

Total DNA was extracted by using a DNA extraction kit (Hugo Biotech), as described in the manufacturer's protocol. The extracted nucleic acid samples were used for the construction of DNA libraries. Libraries were constructed through DNA fragmentation, end repair, adapter ligation, and polymerase chain reaction (PCR) amplification. The quality and concentration of the DNA libraries were assessed using the Qubit 4 Fluorometer (Thermo Fisher Scientific) and Agilent 2100 Bioanalyzer (Agilent Technologies). Libraries were sequenced using the NextSeq 550Dx (Illumina Technologies).

Trimmomatic was used to remove low-quality and duplicate reads, adapter contamination, and reads shorter than 50 bp from raw sequence data.¹⁸ High-quality sequencing data were generated by subtracting data consistent with the human reference genome (hg19) using the Burrows-Wheeler alignment tool (<http://bio-bwa.sourceforge.net/>). The remaining data (clean reads) were categorized using a customized database containing genome sequences of bacteria, fungi, viruses, and parasites (refseq database from NCBI). The strict criteria for positive results were as follows: mNGS discovered a bacterium (species level) with a 10-fold higher coverage rate than any other microorganism.¹⁹ Antibiotic resistance genes were identified from metagenomic data using PathoFact (<https://pathofact.lcsb.uni.lu>).²⁰ The identity measures the similarity between the microbial sequence and the reference sequence. The total reads, microbial reads, mapped reads (stringent mapped reads number at the species level), genomic coverage, drug resistance genes, and identity were included in the mNGS report.

Antimicrobial Susceptibility Testing

The minimal inhibitory concentrations of amikacin, tobramycin, gentamicin, cefepime, ceftriaxone, cefoperazone, imipenem, meropenem, piperacillin-tazobactam, ampicillin, ceftazidime, ciprofloxacin, levofloxacin, and sulfamethoxazole-trimethoprim were determined using the broth microdilution methodology. Antimicrobial susceptibility was determined according to Clinical and Laboratory Standards Institute (CLSI) M100 guidelines (2020). The strains *Escherichia coli* (ATCC 25922) and *Pseudomonas aeruginosa* (ATCC 27853) were used as quality controls.

Cytokine Assessment

Expression levels of serum cytokine (interleukin [IL]-1 β , IL-2, IL-4, IL-5, IL-6, IL-8, IL-10, IL-17, IL- α , IL- γ , tumor necrosis factor [TNF]- α) were determined by flow cytometer (ACEA NovoCyt flow cytometer, ACEA Bioscience) according to the manufacturer's protocol. The data were compared to the standard curve and analyzed using NovoExpress software (1.3.0, ACEA Biosciences). We present serum cytokine data as median (interquartile range), and values below the minimum detectable concentrations are defined as 0 pg/mL.

Statistical Analysis

Comparative analysis between mNGS and CMTs was performed using the Pearson χ^2 test. Relationships between the mapped reads and serum cytokine concentration were investigated by the Spearman correlation method. Data analyses were conducted using SPSS 25.0 software (SPSS), and a 2-tailed value of $P < .05$ was considered significant.

Results

Patient Characteristics

A total of 182 patients with a final diagnosis of GNB infections were enrolled; 67.58% (123/182) were male and 32.42% (59/182) were female, and the average age was 58.02 \pm 17.86 years (TABLE 1). Among the basic illnesses, hypertension (50 cases), diabetes (19 cases) and chronic liver diseases (19 cases) were the most prevalent. The most common primary clinical symptoms were fever (40.11%), cough (24.18%), and chest congestion (18.13%). A total of 114 patients underwent serum cytokine assay. The clinical laboratory characteristics of these 114 patients are shown in TABLE 1.

Comparison of Pathogen Detection Between mNGS and CMTs

Among the 182 GNB infections cases, only 48 (26.37%) were detected by culture. When culture was combined with other microbiological tests, 82 (45.05%) cases were detected. However, mNGS could provide pathogen detection rate up to 96% (175/182, FIGURE 2A). There was a statistically significant difference between mNGS and CMTs ($\chi^2=114.46$, $P < .01$). As for Gram-negative pathogen identification, mNGS identified more pathogens (31 vs 13) than CMTs (FIGURE 2B). The most common detected pathogenic bacteria were *K pneumoniae* (65 cases), *A baumannii* (49 cases), *P aeruginosa* (42 cases), *Stenotrophomonas maltophilia* (41 cases), and *E coli* (38 cases), with <10 total isolates of other pathogens in our samples. There were 19 and 1 pathogens identified only by mNGS and CMTs, respectively. This suggests that the pathogen spectrum detected by mNGS was significantly wider than that of the CMT. The clinical information of the 182 patients and comparison of the pathogens identified by mNGS and CMTs are shown in Supplementary Table S1.

The Effect of Prior Antibiotic Exposure on Pathogen Detection Rates

Among the 182 GNB infection patients, 129 of 182 (70.88%) patients were exposed to antibiotics before undergoing the mNGS test and CMTs, whereas the remaining patients were not exposed. There was no significant difference in the detection rate between mNGS and CMTs in nonexposed patients (25.82% vs 21.98%, $P = .076$). However, the detection rate of mNGS was significantly higher in infections with prior antibiotic use than CMTs (70.33% vs 23.08%, $P < .01$; FIGURE 2C), indicating that mNGS testing was less affected by prior antibiotic exposure.

Association Between Mapped Reads and Serum Cytokine Level Alterations in Patients With GNB Infections

White blood cell count (WBC), C-reactive protein (CRP), serum amyloid A (SAA), procalcitonin (PCT), and serum cytokine (including IL-2, IL-4, IL-5, IL-6, IL-8, IL-10, IL-17, IL-1 β , INF- α , INF- γ , TNF- α) were detected

TABLE 1. Demographics and clinical characteristics of 182 patients

Characteristics	Count
Patient demographics (n = 182)	
Sex, n (%)	
Male	123 (67.58)
Female	59 (32.42)
Age, y	58.02 ± 17.86 ^a
Primary clinical symptoms, n (%)	
Fever	73 (40.11)
Cough	44 (24.18)
Chest congestion	33 (18.13)
Dizziness	28 (15.38)
Shortness of breath	19 (10.44)
Basic illness, n (%)	
Hypertension	50 (27.47)
Diabetes	19 (10.44)
Chronic liver diseases	19 (10.44)
Chronic lung diseases	14 (7.69)
Chronic kidney diseases	10 (5.49)
Previous history of tuberculosis	7 (3.85)
Autoimmunity disease	3 (1.65)
Laboratory test	
White blood cell count, 10 ⁹ /L	10.70 ± 6.83 ^a
C-reactive protein, mg/L	77.16 ± 70.03 ^a
Serum amyloid A, mg/L	160.72 ± 137.53 ^a
Procalcitonin, ng/mL	0.71 (0.25, 7.12) ^b
Interleukin-1β, pg/mL	2.83 (1.16, 12.44) ^b
Interleukin-2, pg/mL	1.67 (0.52, 2.60) ^b
Interleukin-4, pg/mL	1.21 (0.84, 1.58) ^b
Interleukin-5, pg/mL	2.07 (0.43, 5.17) ^b
Interleukin-6, pg/mL	29.10 (13.58, 107.51) ^b
Interleukin-8, pg/mL	21.03 (8.11, 53.91) ^b
Interleukin-10, pg/mL	2.45 (1.43, 5.10) ^b
Interleukin-17, pg/mL	4.96 (2.23, 9.72) ^b
Interferon-α, μg/mL	1.82 (1.11, 3.53) ^b
Interferon-γ, μg/mL	7.07 (2.23, 16.09) ^b
Tumor necrosis factor-α, pg/mL	1.82 (0.83, 3.44) ^b

^aMean ± SD.^bMedian (interquartile range).

in this study. We performed a correlation analysis between mapped reads and inflammatory biomarker concentrations. As shown in [Supplementary Table S2](#), no correlation was found between mapped reads and WBC, CRP, SAA, PCT, IL-2, IL-4, IL-5, IL-10, IL-17, IL-1β, INF-α, INF-γ, and TNF-α. However, the mapped reads were positively correlated with IL-6 ($r^2 = 0.239$, $P = .010$) and IL-8 ($r^2 = 0.319$, $P = .001$) ([FIGURE 3](#)).

The Accuracy of mNGS Predicting Antimicrobial Resistance Based on Resistance Genes

To determine the accuracy of mNGS in predicting antimicrobial resistance, we selectively enrolled 12 patients with corresponding AST results. We analyzed the consistency between predicted antimicrobial

resistance by mNGS and the results of broth microdilution AST according to CLSI interpretive guidelines. The mNGS-based antimicrobial resistance predictions were obtained by performing a PathoFact analysis (see Materials and Methods). A total of 15 resistance genes (*aac(6)-ib-cr*, *aada2*, *aph(3)-ia*, *aph(6)-id*, *bla*_{CTX-M-14}, *bla*_{OXA-100}, *bla*_{OXA-50}, *bla*_{OXA-66}, *bla*_{OXA-70}, *bla*_{TEM-185}, *bla*_{SHV-11}, *bla*_{PAO}, *sul1*, *sul2*, and *qnrS1*) were detected in 9 strains ([TABLE 2](#)). The enzymes encoded by *aada2*, *aph(3)-ia*, and *aph(6)-id* were the aminoglycoside-modifying enzymes, which can phosphorylate, adenylate, or acetylate aminoglycoside antibiotics (amikacin [AK], tobramycin [TOB], gentamicin [GEN]). *aac(6)-ib-cr* is a plasmid-mediated drug resistance gene that confers resistance to quinolones and aminoglycosides.^{21,22} The enzymes encoded by *bla*_{CTX-M-14}, *bla*_{OXA-100}, *bla*_{OXA-50}, *bla*_{OXA-66}, *bla*_{OXA-70}, *bla*_{TEM-185}, *bla*_{SHV-11}, and *bla*_{PAO} were β-lactamase, which can hydrolyze penicillin (ampicillin [AMP], piperacillin-tazobactam [TZP]), cephalosporin (cefepime [FEP], ceftriaxone [CRO], cefoperazone [CFP], ceftazidime [CAZ]), and carbapenems (imipenem [IPM], meropenem [MPM]).²³ *sul1* and *sul2* are sulfonamide resistance genes. *QnrS1*, located in pX39-8, confers a plasmid-mediated quinolone resistance.²⁴

The results of antimicrobial resistance predicted by mNGS in 12 individuals were compared to phenotypic AST ([TABLE 2](#)). Seven patients (patients 7, 21, 33, 37, 72, 77, and 100) had an excellent match of antimicrobial resistance results from mNGS and AST. However, mNGS results were partially matched with AST results in 5 of 12 patients (patients 2, 13, 38, 58, and 120). The pathogen of patient 2 was *A baumannii*; it had the *aph(3)-ia*, *bla*_{TEM-185} gene, which suggests resistance to aminoglycoside and β-lactam, whereas AST results showed that it was also resistant to ciprofloxacin (CIP) and levofloxacin (LEV). The pathogen of patients 13 and 58 was *P aeruginosa* and *K pneumoniae*, respectively; patient 13 had the *bla*_{OXA-50} gene with an identity of 78%, and patient 58 had the *qnrS1*, *bla*_{SHV-11}, and *sul2* genes. According to the prediction results of mNGS, both patients 13 and 58 were not resistant to aminoglycoside, whereas AST results showed that they were resistant to aminoglycoside. The pathogen of patients 38 and 120 was *A baumannii* and *S maltophilia*; patient 38 had *aph(6)-id* and *sul2* genes, and patient 120 had *aph(6)-id* and *sul2* genes. The mNGS results suggested that 2 patients were resistant to aminoglycoside and sulfonamide, whereas the AST results showed that there was also resistance to β-lactams and quinolones.

Discussion

The application of mNGS to identify Gram-negative pathogens and predict drug resistance is rarely reported. This study evaluated the efficiency of mNGS in pathogen detection and drug resistance prediction of GNB infections. We first compared Gram-negative pathogen detection by mNGS and CMTs in a pairwise manner and found that mNGS outperformed CMTs in several aspects. The pathogen spectrum identified by mNGS was significantly wider than that of the CMTs. Metagenomic next-generation sequencing can detect the majority of pathogens in GNB-infected patients compared to CMTs (96.15% vs 45.05%). There was a statistically significant difference ($\chi^2 = 114.46$, $P < .01$) between mNGS and CMTs. Our finding was similar to previous research.^{25–27} Gu et al²⁵ observed that the sensitivity and specificity of mNGS were 79.2% and 90.6% for bacteria, respectively. Zeng et al²⁶ evaluated the role of mNGS in the etiological diagnosis of patients with infective endocarditis. Compared to culture-based detection, mNGS

FIGURE 2. Clinical applications of metagenomic next-generation sequencing (mNGS) for the identification of Gram-negative bacteria (GNB) infections. **A,** Proportion of patients with pathogens that were identified by mNGS and conventional microbiological tests (CMTs). **B,** A total of 32 pathogens were detected by mNGS and CMTs in GNB-infected patients with their associated frequencies represented in histograms. **C,** The influence of prior antibiotic exposure on pathogen detection rates.

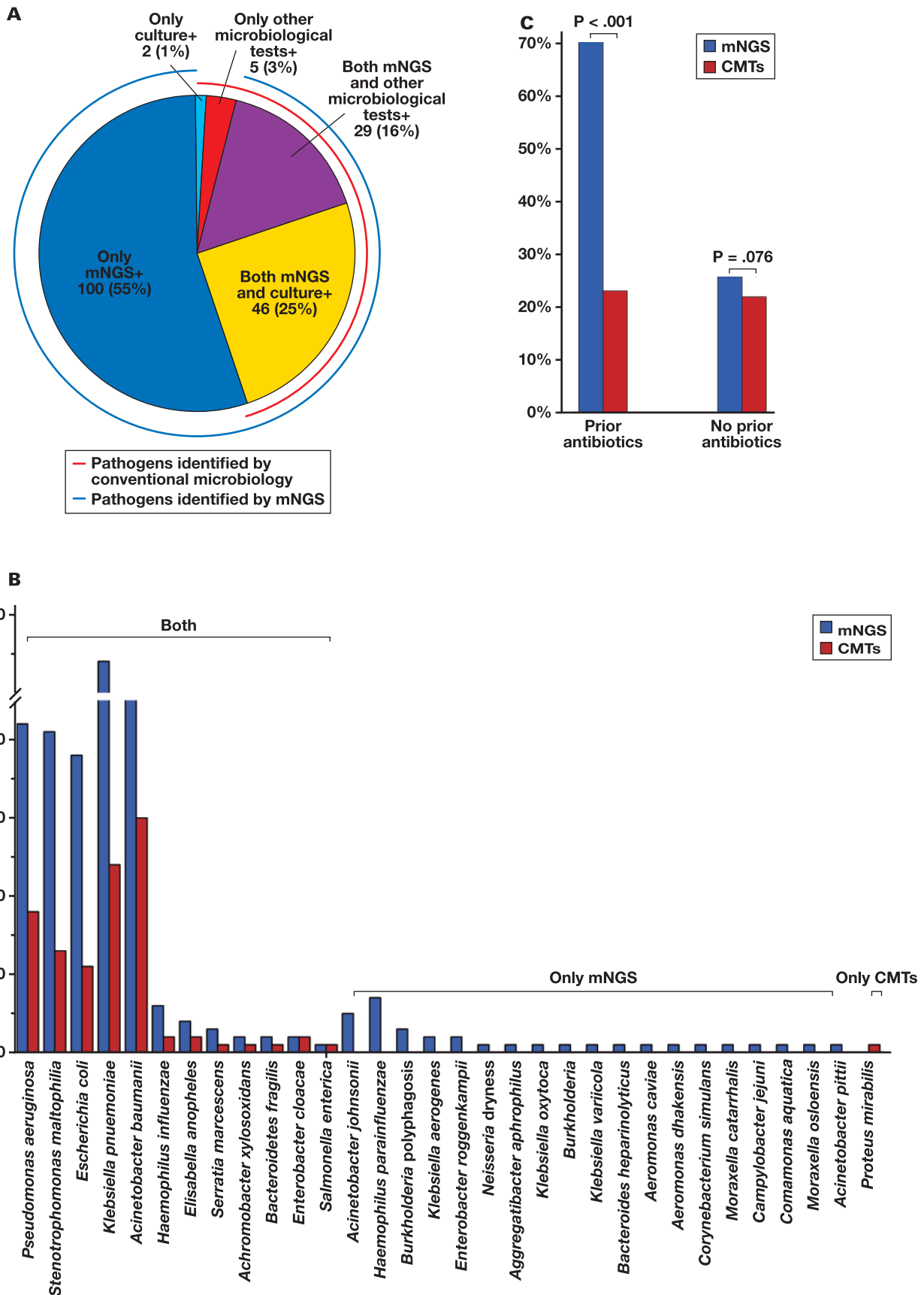
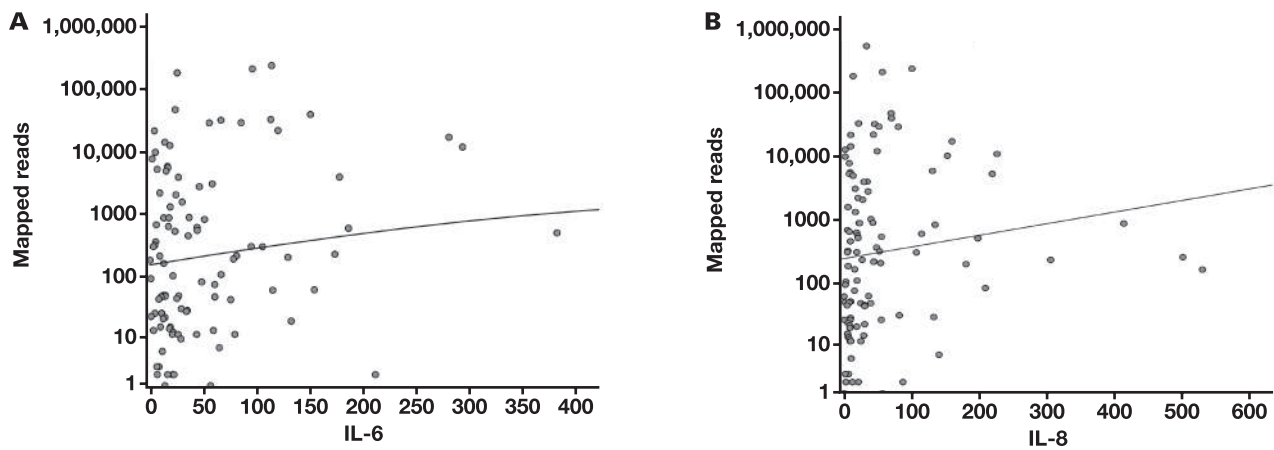


FIGURE 3. Increased level of serum cytokines are correlated with mapped reads in the Gram-negative bacteria infection patients. **A,** Interleukin (IL)-6 was positively correlated with mapped reads ($r^2 = 0.239$; $P = .01$). **B,** IL-8 was positively correlated with mapped reads ($r^2 = 0.319$; $P = .001$).



displayed higher pathogen detection rate (85.9% vs 45.2%) in infective endocarditis patients. Tang et al²⁷ enrolled 16 patients with suspected infections who had primary immunodeficiency disease. Metagenomic next-generation sequencing detected pathogens in 93.75% of samples compared with 68.75% for conventional methods and 31.25% for culture and also detected an extra 18 pathogenic microorganisms. These studies suggest that mNGS is increasingly being used in clinical laboratories and that it performs well in identifying pathogens in a multitude of clinical settings.

The administration of broad-spectrum antibiotics before sampling, either orally or intravenously, might lead to false-negative conventional microbiological results.²⁸ Wang et al²⁹ reported that antibiotic treatment prior to sampling reduced the sensitivity of conventional microbiological culture. To explore whether prior antibiotic exposure can affect conventional microbiological results, we divided patients into 2 groups according to whether they had received antibiotic treatment before sampling. Interestingly, the detection rate of mNGS was significantly better than that of CMTs (70.33% vs 23.08%, $P < .01$) in patients with prior antibiotic exposure, but there was no significant difference in the nonexposed group, indicating that mNGS was less affected by prior antibiotic exposure. This is consistent with previous reports.^{15,30} An mNGS test may be more valuable to patients who have been exposed to antibiotics or whose conventional microbiological results were negative.

Cytokines are the key regulators of inflammatory responses. As rapid and convenient indicators for assessing the body's inflammation status, serum cytokines have received much scientific attention regarding the diagnosis and treatment of infectious diseases.³¹ Previous studies reported the IL-6 level in patients with bacterial infection was much higher than those with nonbacterial infection.³² Xu et al³³ found the levels of IL-6, IL-10, and TNF- α in patients with Gram-negative bacteremia were significantly higher than those in patients with Gram-positive bacteremia. The cytokine signatures were helpful to distinguish between Gram-positive and Gram-negative bacterial infections. In this study, inflammatory biomarkers were tested in 144 patients. Lourault et al³⁴ reported a significant positive correlation between mapped reads and the bacterial load in blood, kidneys, and liver. Mapped reads may reflect pathogen load to some extent. Thus, we performed a correlation analysis between mapped reads and inflammatory biomarker concentrations

to determine whether a signature of inflammatory biomarkers could be correlated with mapped reads in GNB infections. We observed that mapped reads were positively correlated with IL-6 ($r^2 = 0.239$, $P = .010$) and IL-8 levels ($r^2 = 0.319$, $P = .001$). Interestingly, IL-6 and IL-8 are proinflammatory cytokines, indicating that mapped reads may reflect a proinflammatory state and inform which patients could be treated more aggressively for ongoing inflammatory responses.

In addition to pathogen identification, another clinical utility of mNGS is the identification of genetic determinants of antimicrobial resistance by comparing pathogen metagenome data with antibiotic resistance database.³⁵ However, there have been limited studies of mNGS being used to infer an actual resistance phenotype.^{36,37} To evaluate the accuracy of mNGS in predicting antimicrobial resistance, we selectively enrolled 12 patients with corresponding AST results. This study found 7/12 (58.33%) of mNGS results were consistent with the results given by AST. In the remaining 5 patients, mNGS failed to predict antimicrobial resistance identified by AST as resistant to antibiotic. There are a number of reasons for this finding: (1) The antimicrobial resistance prediction tool is based on existing antibiotic resistance gene databases. These databases (which include CARD, ARDB, and UNIPROT)³⁸⁻⁴⁰ have limitations when it comes to clinical diagnosis; many drugs' resistance information is incomplete, and some have not been phenotypically verified in clinical isolates. In addition, emerging resistance genes cannot be updated and managed promptly in databases. (2) It ignores other potential drug resistance mechanisms such as modifications of the antimicrobial target, mutations in rRNA or regulatory elements, lipopolysaccharide modification, gene expression changes, and activation of efflux systems,^{41,42} particularly in *A baumannii* and *P aeruginosa*. (3) The detection of antibiotic resistance genes requires extremely high sequencing depth. Incomplete genome coverage results in insufficient sequence reads for identification of antibiotic resistance genes. Inferring actual resistance phenotypes from metagenomic data remains a big challenge. Therefore, we do not recommend clinicians directly prescribe medication based on mNGS results alone. Rational antibiotic treatment should be based on phenotypic AST results.

This study was strengthened by evaluating mNGS in the real-world practice of detecting Gram-negative pathogens and predicting

antimicrobial resistance. However, there were limitations. First, the numbers of each specimen type tested is limited. Second, only 12 cases were selected to evaluate the accuracy of mNGS in predicting antimicrobial resistance. This is because the accuracy of mNGS in predicting antimicrobial resistance can be assessed only when the bacterial culture is positive. In this study, the positive detection rate of culture was only 26.37% (48/182). This partly explains why only 12 isolates were tested. Third, the pathogens detected by mNGS were not all validated by quantitative PCR; thus, there might be false-positive results. Nevertheless, our results shed new light on the applicability of mNGS in diagnosing GNB infections and suggest that clinical mNGS testing is effective in the diagnosis of GNB infections.

In summary, this study enhances our knowledge of the application of mNGS in GNB infections. Metagenomic next-generation sequencing has a higher detection rate, a wider pathogen spectrum, and is less affected by prior antibiotic exposure than CMTs in identifying Gram-negative pathogens. The mapped reads may reflect a proinflammatory state and inform which patients with GNB infection could be treated more aggressively for ongoing inflammatory responses. However, the real-world role of the mNGS in predicting antimicrobial resistance is limited given the incompleteness of resistance gene databases, the diversity of bacterial resistance mechanisms, and sequencing depth. The continuous expansion of resistance gene databases will be required. In the future, mNGS may play a greater role in the diagnosis and drug resistance analysis of GNB infections.

Supplementary Material

Supplementary material is available at *Laboratory Medicine* online .

Funding

This work was supported by the National Natural Science Fund of China (grant number 82260085).

Conflict of Interest Disclosure

The authors have nothing to declare.

REFERENCES

- Oliveira J, Reygaert WC. *Gram Negative Bacteria*. StatPearls; 2022.
- Abe R, Oda S, Sadahiro T, et al. Gram-negative bacteremia induces greater magnitude of inflammatory response than Gram-positive bacteremia. *Crit Care*. 2010;14:R27. doi:10.1186/cc8898
- Cavaillon J-M. Exotoxins and endotoxins: inducers of inflammatory cytokines. *Toxicon*. 2018;149:45–53. doi:10.1016/j.toxicon.2017.10.016
- Munford RS. Severe sepsis and septic shock: the role of gram-negative bacteremia. *Annu Rev Pathol*. 2006;1:467–496. doi:10.1146/annurev.pathol.1.110304.100200
- Andersson M, Östholm-Balkhed Å, Fredrikson M, et al. Delay of appropriate antibiotic treatment is associated with high mortality in patients with community-onset sepsis in a Swedish setting. *Eur J Clin Microbiol Infect Dis*. 2019;38:1223–1234. doi:10.1007/s10096-019-03529-8
- Idelevich EA, Becker K. How to accelerate antimicrobial susceptibility testing. *Clin Microbiol Infect*. 2019;25:1347–1355 doi:10.1016/j.cmi.2019.04.025
- Zhang P, Chen Y, Li S, et al. Metagenomic next-generation sequencing for the clinical diagnosis and prognosis of acute respiratory distress syndrome caused by severe pneumonia: a retrospective study. *PeerJ*. 2020;8:e9623. doi:10.7717/peerj.9623
- Banerjee R, Humphries R. Rapid antimicrobial susceptibility testing methods for blood cultures and their clinical impact. *Front Med*. 2021;8:635831. doi:10.3389/fmed.2021.635831
- Humphries RM. Update on susceptibility testing: genotypic and phenotypic methods. *Clin Lab Med*. 2020;40:433–446. doi:10.1016/j.cll.2020.08.002
- Cunha CB, Opal SM. Antibiotic stewardship: strategies to minimize antibiotic resistance while maximizing antibiotic effectiveness. *Med Clin North Am*. 2018;102:831–843. doi:10.1016/j.mcna.2018.04.006
- Tamma PD, Aitken SL, Bonomo RA, et al. Infectious Diseases Society of America Guidance on the treatment of extended-spectrum beta-lactamase producing Enterobacterales (ESBL-E), carbapenem-resistant Enterobacterales (CRE), and *Pseudomonas aeruginosa* with difficult-to-treat resistance (DTR-P. aeruginosa). *Clin Infect Dis*. 2021;72:e169–e183. doi:10.1093/cid/ciaa1478
- Cerceo E, Deitelzweig SB, Sherman BM, et al. Multidrug-resistant gram-negative bacterial infections in the hospital setting: overview, implications for clinical practice, and emerging treatment options. *Microb Drug Resist*. 2016;22:412–431.
- Li N, Cai Q, Miao Q, et al. High-throughput metagenomics for identification of pathogens in the clinical settings. *Small Methods*. 2021;5:2000792. doi:10.1002/smt.202000792
- Zhang Y, Cui P, Zhang H-C, et al. Clinical application and evaluation of metagenomic next-generation sequencing in suspected adult central nervous system infection. *J Transl Med*. 2020;18:199. doi:10.1186/s12967-020-02360-6
- Miao Q, Ma Y, Wang Q, et al. Microbiological diagnostic performance of metagenomic next-generation sequencing when applied to clinical practice. *Clin Infect Dis*. 2018;67:S231–S240. doi:10.1093/cid/ciy693
- Haslam DB. Future applications of metagenomic next-generation sequencing for infectious diseases diagnostics. *J Pediatric Infect Dis Soc*. 2021;10:S112–S117.
- Gwinn M, MacCannell D, Armstrong GL. Next-generation sequencing of infectious pathogens. *JAMA*. 2019;321:893–894. doi:10.1001/jama.2018.21669
- Xu Y, Kang L, Shen Z, et al. Dynamics of severe acute respiratory syndrome coronavirus 2 genome variants in the feces during convalescence. *J Genet Genomics*. 2020;47:610–617. doi:10.1016/j.jgg.2020.10.002
- Langelier C, Zinter MS, Kalantar K, et al. Metagenomic sequencing detects respiratory pathogens in hematopoietic cellular transplant patients. *Am J Respir Crit Care Med*. 2018;197:524–528. doi:10.1164/rccm.201706-1097LE
- de Nies L, Lopes S, Busi SB, et al. PathoFact: a pipeline for the prediction of virulence factors and antimicrobial resistance genes in metagenomic data. *Microbiome*. 2021;9:49. doi:10.1186/s40168-020-00993-9
- Mana HA, Sundararaju S, Eltai NO, et al. Low-level amikacin resistance induced by AAC(6′)-Ib and AAC(6′)-Ib-cr in extended-spectrum β-lactamase (ESBL)-producing Enterobacterales isolated from urine in children. *J Glob Antimicrob Resist*. 2021;26:42–44. doi:10.1016/j.jgar.2021.04.026
- Raherison S, Jove T, Gaschet M, et al. Expression of the gene in class 1 integrons. *Antimicrob Agents Chemother*. 2017;61:e02704–16.
- Carvalho I, Chenouf NS, Carvalho JA, et al. Multidrug-resistant *Klebsiella pneumoniae* harboring extended spectrum β-lactamase encoding genes isolated from human septicemias. *PLoS One*. 2021;16:e0250525. doi:10.1371/journal.pone.0250525
- Tavio MM, Jacoby GA, Hooper DC. QnrS1 structure-activity relationships. *J Antimicrob Chemother*. 2014;69:2102–2109. doi:10.1093/jac/dku102
- Gu W, Deng X, Lee M, et al. Rapid pathogen detection by metagenomic next-generation sequencing of infected body fluids. *Nat Med*. 2021;27:115–124. doi:10.1038/s41591-020-1105-z

26. Zeng X, Wu J, Li X, et al. Application of metagenomic next-generation sequencing in the etiological diagnosis of infective endocarditis during the perioperative period of cardiac surgery: a prospective cohort study. *Front Cardiovasc Med*. 2022;9:811492. doi:10.3389/fcvm.2022.811492
27. Tang W, Zhang Y, Luo C, et al. Clinical application of metagenomic next-generation sequencing for suspected infections in patients with primary immunodeficiency disease. *Front Immunol*. 2021;12:696403. doi:10.3389/fimmu.2021.696403
28. Zhu J, Xia H, Tang R, et al. Metagenomic next-generation sequencing detects pathogens in endophthalmitis patients. *Retina*. 2022;42:992–1000.
29. Wang K, Li P, Lin Y, et al. Metagenomic diagnosis for a culture-negative sample from a patient with severe pneumonia by nanopore and next-generation sequencing. *Front Cell Infect Microbiol*. 2020;10:182. doi:10.3389/fcimb.2020.00182
30. Hu H-L, Guo L-Y, Wu H-L, et al. Evaluation of next-generation sequencing for the pathogenic diagnosis of children brain abscesses. *J Infect*. 2019;78:323–337. doi:10.1016/j.jinf.2019.01.003
31. Hocum Stone L, Oppler SH, Nugent JL, et al. Serum cytokine profiles in healthy nonhuman primates are blunted by sedation and demonstrate sexual dimorphism as detected by a validated multiplex immunoassay. *Sci Rep*. 2021;11:2340.
32. Wang D, Lai M, Song H, et al. Integration of interleukin-6 improves the diagnostic precision of metagenomic next-generation sequencing for infection in immunocompromised children. *Front Microbiol*. 2022;13:819467. doi:10.3389/fmicb.2022.819467
33. Xu X-J, Tang Y-M, Liao C, et al. Inflammatory cytokine measurement quickly discriminates gram-negative from gram-positive bacteremia in pediatric hematology/oncology patients with septic shock. *Intensive Care Med*. 2013;39:319–326. doi:10.1007/s00134-012-2752-4
34. Lourdault K, Matsunaga J, Haake DA. High-throughput parallel sequencing to measure fitness of *Leptospira interrogans* transposon insertion mutants during acute infection. *PLoS Negl Trop Dis*. 2016;10:e0005117. doi:10.1371/journal.pntd.0005117
35. Gu W, Miller S, Chiu CY. Clinical metagenomic next-generation sequencing for pathogen detection. *Annu Rev Pathol*. 2019;14:319–338. doi:10.1146/annurev-pathmechdis-012418-012751
36. Sanabria AM, Janice J, Hjerde E, et al. Shotgun-metagenomics based prediction of antibiotic resistance and virulence determinants in *Staphylococcus aureus* from periprosthetic tissue on blood culture bottles. *Sci Rep*. 2021;11:20848. doi:10.1038/s41598-021-00383-7
37. Wilson MR, Sample HA, Zorn KC, et al. Clinical metagenomic sequencing for diagnosis of meningitis and encephalitis. *N Engl J Med*. 2019;380:2327–2340. doi:10.1056/NEJMoa1803396
38. Alcock BP, Raphenya AR, Lau TTY, et al. CARD 2020: antibiotic resistance surveillance with the comprehensive antibiotic resistance database. *Nucleic Acids Res*. 2020;48:D517–D525.
39. Liu B, Pop M. ARDB--antibiotic resistance genes database. *Nucleic Acids Res*. 2009;37:D443–D447.
40. UniProt Consortium T. UniProt: the universal protein knowledgebase. *Nucleic Acids Res*. 2018;46:2699.
41. Munita JM, Arias CA. Mechanisms of antibiotic resistance. *Microbiol Spectr*. 2016;4:15.
42. Grumaz S, Stevens P, Grumaz C, et al. Next-generation sequencing diagnostics of bacteremia in septic patients. *Genome Med*. 2016;8:73. doi:10.1186/s13073-016-0326-8

Identification and analysis of a clinically isolated strain of *Halomonas* based on whole-genome sequencing and comparative genomics

Pinjia Wang, PhD,¹ and Chengbin Xie, MD^{2,3} 

¹School of Laboratory Medicine, Chengdu Medical College, Chengdu, China, ²Department of Laboratory Medicine, Sichuan Provincial Maternity and Child Health Care Hospital, Chengdu, China, ³Department of Laboratory Medicine, Women's and Children's Hospital Affiliated to Chengdu Medical College, Chengdu, China. Corresponding author: Chengbin Xie; chengbinxie@foxmail.com

Key words: *Halomonas*; blood; whole-genome sequencing; species identification; comparative genomics

Abbreviations: ANI, average nucleotide identity; dDDH, DNA-DNA hybridization; NCBI, National Center for Biotechnology Information; rRNA, ribosomal RNA; tRNA, transfer RNA; COG, Clusters of Orthologous Groups of Proteins; KEGG, Kyoto Encyclopedia of Genes and Genomes; PGAP, Pan-genome Analysis Pipeline; BRIG, BLAST Ring Image Generator; HGT, horizontal gene transfer

Laboratory Medicine 2024;55:80-87; <https://doi.org/10.1093/labmed/lmad040>

ABSTRACT

Objective: The aim of this study was to identify the species of a *Halomonas* strain isolated from a neonatal blood sample and to understand the potential pathogenicity and characteristic genes of the strain.

Methods: The genomic DNA of strain 18071143 (identified as *Halomonas* by matrix-assisted laser desorption/ionization time of flight-mass spectrometry and the 16S ribosomal RNA (rRNA) gene sequence) was sequenced using Nanopore PromethION platforms. The average nucleotide identity (ANI) and digital DNA-DNA hybridization (dDDH) were calculated using the complete genome sequences of the strain. Comparative genomic analyses were performed on strain 18071143 and 3 strains of *Halomonas* (*Halomonas stevensii* S18214, *Halomonas hamiltonii* KCTC 22154, and *Halomonas johnsoniae* KCTC 22157) that were associated with human infections and had high genomic similarity to strain 18071143.

Results: Phylogenetic, ANI, and dDDH similarity analyses based on genome sequence indicated that strain 18071143 belonged to the species *H. stevensii*. Similarities exist between strain 18071143 and

the other 3 *Halomonas* strains in terms of gene structure and protein function. Nonetheless, strain 18071143 has greater potential for DNA replication, recombination, repair, and horizontal transfer.

Conclusion: Whole-genome sequencing holds great promise for accurate strain identification in clinical microbiology. In addition, the results of this study provide data for understanding *Halomonas* from the perspective of pathogenic bacteria.

Halomonas is a genus of Gram-negative moderately halophilic/halotolerant bacteria, which generally thrive in saline or hypersaline environments. The pathogenicity of these bacteria, used primarily for industrial purposes, was not initially recognized, but case reports related to human disease subsequently emerged. The bacteria were first reported as a human pathogen in 2000 when a woman contracted *Halomonas venusta* after being bitten by a fish while diving.¹ In a study searching for bacterial DNA signatures in patients with unexplained deaths and critical illnesses, an unspecified *Halomonas* organism was found in the blood of a patient.² Berger et al³ described a case of an outbreak of *Halomonas phocaensis* bacteremia in a neonatal intensive care unit in Tunisia. Stevens et al⁴ isolated 3 new species of *Halomonas* from the blood of patients and environmental specimens in a dialysis center. Yeo et al⁵ presented a case report of peritoneal dialysis-related peritonitis due to *Halomonas*. The most recent case report was for purulent lymphadenitis caused by *Halomonas* in October 2022.⁶ A review of cases of infections caused by *Halomonas* found that the majority of types were bacteremia.⁷ The reason for this may be that blood is usually sterile, and *Halomonas* exists in pure culture as a pathogen, which can be readily identified. In other samples contaminated by normal flora, such as feces or sputum, the growth of the *Halomonas* is often overlooked.

In 2018, a Gram-negative bacillus strain 18071143 was isolated from the blood of a neonatal patient at the Sichuan Provincial Maternity and Child Health Care Hospital of China. The species of this clinical isolate could not be identified by conventional biochemical identification methods. The strain was characterized as *Halomonas hamiltonii* by matrix-assisted laser desorption/ionization time of flight mass spectrometry. Furthermore, the 16S rRNA gene sequence (GenBank accession number MZ097522) was identified using the EzBioCloud 16S database (<https://www.ezbiocloud.net/>), and the bacterium was

determined to be *H hamiltonii*, with the highest similarity of 99.93%, followed by *Halomonas stevensii* (99.50%) and *Halomonas johnsoniae* (99.57%) (Supplementary File S1). Although the above identification rate was higher than 99.0%, the separation rate between different species was less than 0.8%, and therefore the bacterium could not be identified at the species level according to Clinical and Laboratory Standards Institute guidelines.⁸

A review of the literature shows that *H stevensii*, *H johnsoniae*, and *H hamiltonii* have repeatedly appeared in events related to human diseases.^{4–7,9,10} They were all newly discovered in the same event in 2010 and were considered as 3 separate species of the genus *Halomonas* based on phenotype and DNA-DNA hybridization.¹⁰ *H stevensii* S18214 was isolated from a renal care patient's blood. *H hamiltonii* KCTC 22154 was isolated from the drain of a dialysis machine. *H johnsoniae* KCTC 22157 was isolated from a dialysis machine's waste handling option port. At the genomic level, it is of great interest to know what the similarities and differences are between strain 18071143 and these 3 strains of *Halomonas* that share a highly similar 16S rRNA gene sequence with it.

In view of the above, the purpose of this study was 2-fold: first, to determine the species of strain 18071143 using whole-genome sequencing technology. Second, to discover the similarities and differences between strain 18071143 and the 3 *Halomonas* species mentioned above based on comparative genomics. The results of this study may provide basic data for public health interventions targeting *Halomonas*, a potentially pathogenic bacterium.

Materials and Methods

Genomic DNA Extraction

Genomic DNA of *Halomonas* species strain 18071143 was prepared using QIAGEN Genomic-tip kits (QIAGEN) following the manufacturer's instructions. The harvested DNA was qualified and quantified by agarose gel electrophoresis, a NanoDrop One spectrophotometer (NanoDrop Technologies), and a Qubit 2.0 Fluorometer (Life Technologies).

Sequencing

Whole-genome sequencing of strain 18071143 was performed with the Nanopore PromethION platform (Biomarker Technologies). Canu v1.5 was used to assemble the sequences. Pilon v1.22 was used to improve the draft genome assemblies by correcting bases. The complete genome sequence of strain 18071143 has been deposited in the National Center for Biotechnology Information (NCBI) GenBank under the accession number CP078120.1 and in the Sequence Read Archive under the accession number PRJNA743705. Whole-genome sequences for *H stevensii* S18214, *H johnsoniae* KCTC22157, and *H hamiltonii* KCTC22154 have been obtained from the NCBI GenBank nucleotide database.

Gene Prediction and Annotation

Gene prediction in bacterium was performed using Glimmer v3.02 software. Prediction of ribosomal RNA and transfer RNA (tRNA) contained in the genome was carried out with Barrnap v 0.4.2 and tRNAscan-SE v1.3.1 software, respectively. The software IslandPath-DIMOB v 1.0.0 was used to predict the genomic islands in the genome of strain 18071143. The software IslandPath-DIMOB v 1.0.4 and PhiSpy v4.2.19 were used to predict genomic islands and prophages in the genome of strain 18071143, respectively. Virulence gene profiling was carried

out by BLAST against the Virulence Factor Database (<http://www.mgc.ac.cn/VFs/>). The predicted coding sequences were annotated from databases such as Clusters of Orthologous Groups of Proteins (COG), Kyoto Encyclopedia of Genes and Genomes (KEGG), etc, using the sequence matching tool BLAST. Briefly, each set of query proteins was aligned with the databases, and annotations of best-matched subjects (e-value <10⁻⁵) were obtained for gene annotation.

Genome Sequence Similarity Analysis

The average nucleotide identity (ANI) values and digital DNA-DNA hybridization (dDDH) values between strain 18071143 and *H hamiltonii*, *H stevensii*, and *H johnsoniae* were calculated. The ANI was calculated using the OrthoANIu algorithm using the online web server EZGenome (<https://www.ezbiocloud.net/tools/ani>).^{11,12} The dDDH values were calculated with the Genome-to-Genome Distance Calculator version 3.0 (<http://ggdc.dsmz.de/>), and the results were interpreted with the recommended formula 2.^{13,14} The whole genome-based taxonomic analysis was carried out using the type strain genome server (<https://tygs.dsmz.de>). The phylogenomic tree was constructed using FastME 2.1.6.1 from the Genome BLAST Distance Phylogeny.¹⁵ All pairwise genome comparisons for phylogenomic inference were performed using Genome BLAST Distance Phylogeny, and intergenomic distances were calculated using the algorithm "trimming" and distance formula d5.¹³ Branch support was inferred from 100 pseudo-bootstrap replicates each. The trees were rooted at the midpoint.

Comparative Genomic Analysis

The genomic collinearity between strain 18071143 and *H hamiltonii*, *H stevensii*, and *H johnsoniae* was performed using Mummer v3.23. The number of genes annotated in each strain at the COG's Function category level was compared. A core-pan-genome analysis was performed by Pan-genome Analysis Pipeline (PGAP) v1.2.1 using the GeneFamily method with the default parameters setting. Comparative genome visualization was achieved using the BLAST Ring Image Generator (BRIG).¹⁶ The Fisher exact test was used to compare differences in the number of core and unique genes in combination with the results of pan-genomic analysis and COG annotation. The unique genes of strain 18071143 were analyzed for KEGG pathway enrichment and compared statistically using the Fisher exact test. The Benjamini and Hochberg correction method was chosen to calibrate *P* values and control for false positives in enrichment results. When the corrected *P* value was less than .05, this KEGG pathway was considered to have a significant enrichment.

Results and Discussion

General Genome Features of Strain 18071143

The final assembled genome length of strain 18071143 is 3.86 Mb. It consists of only 1 replicon, namely 1 chromosome (60.38% guanine-cytosine [GC] content). The genome is predicted to contain 3556 putative protein-coding genes, 18 rRNAs, and 62 tRNAs. A total of 12 genomic islands were predicted, with a total length of 167,146 bp representing 4.3% of the total genome length, which was below the average of 10.1% for 157 bacterial chromosomes.¹⁷ By comparing the protein sequences of the predicted genes with the Virulence Factor Database, it was found that strain 18071143 encodes some putative virulence factors that were

associated with adherence (flagella and type IV pili), antiphagocytosis (capsule biosynthesis and regulation), iron uptake (pyochelin and yersiniabactin), secretion system, etc (Supplementary File S2). These features support its ability to colonize different niches from the environment to humans.

Determination of Species Type

ANI is widely used in the classification and identification of bacteria by calculating the ANI value of 2 prokaryotic genome sequences. The ANI values were calculated between strain 18071143 and *H. hamiltonii*, *H. stevensii*, and *H. johnsoniae* using the OrthoANIu algorithm. It was found that all three *Halomonas* species had ANI values higher than 96%. These values were higher than the 95% to 96% determined to delineate the different species.¹⁸ In addition, dDDH is another metric of relatedness computed using whole genomes. In dDDH, the highest matching score was obtained with *H. stevensii* (79.70%). The gold standard threshold for species boundaries is generally considered to be a dDDH of 70%.¹⁹ Therefore, the analysis of the whole-genome sequence showed that strain 18071143 was more closely related to *H. stevensii*. TABLE 1 lists the results of ANI calculations and dDDH of the strain 18071143 compared with other related species. FIGURE 1 shows a phylogenetic tree based on genome sequencing with the strain 18071143 and the other species of the genus *Halomonas*. As shown in FIGURE 1, 4 strains of *Halomonas* are phylogenetically close, and strain 18071143 shows stronger evolutionary relatedness to *H. stevensii* S18214.

TABLE 1. Genome sequence similarity between the strain 18071143 against *Halomonas stevensii*, *H. johnsoniae*, and *H. hamiltonii*

Species	ANI (%) ^a	dDDH (%) ^b
<i>Halomonas stevensii</i> S18214	97.68	79.70
<i>Halomonas johnsoniae</i> KCTC22157	96.66	69.20
<i>Halomonas hamiltonii</i> KCTC22154	96.00	66.70

^aUsing the EzBioCloud server (<https://www.ezbiocloud.net/>).

^bUsing the Genome-to-Genome Distance Calculator server (<http://ggdc.dsmz.de/>).

Given the above, it is more likely that strain 18071143 belongs to the *H. stevensii* species. This was also confirmed by the genomic collinearity between strain 18071143 and the other 3 *Halomonas* species, *H. stevensii*, *H. johnsoniae*, and *H. hamiltonii*, whose results indicated that strain 18071143 exhibited higher sequence identity to *H. stevensii* (Supplementary Figure S1).

Comparative Genomic Analysis

The genome of strain 18071143 was compared with those of the above 3 *Halomonas* species to further understand the similarities and differences in gene structure. The final assembly of 4 strains of *Halomonas* showed that genomes were similar in size, GC content, and the number of protein-coding genes (TABLE 2). Four bacteria were compared by BLAST analysis using the BRIG program considering strain 18071143 genome as the reference sequence (FIGURE 2). The BRIG alignment makes it clear that most regions of the 3 *Halomonas* species' genomes are conserved compared with the reference strain 18071143. A few regions appear to have little or no similarity, which could be the result of acquisition/deletion/rearrangement or horizontal gene transfer (HGT). Genomic islands and prophages play an important role in HGT. The outermost circle in FIGURE 2 shows the distribution of genomic islands and prophages in the genome of strain 18071143, the exact locations of which are shown in Supplementary Files S3 and S4. The largest gap in the circle is just right of the location of the longest prophages in strain 18071143 genome.

To compare the functional distribution of the 4 *Halomonas* strains, categories of COG were analyzed. As expected, the most abundant functional groups were function unknown (S in FIGURE 3A). Aside from that nondeterministic group, the largest COG group was the amino acid transport and metabolism (E), followed by inorganic ion transport and metabolism (P), and transcription (K), whose average genes were 283, 250, and 216, respectively (FIGURE 3A; Supplementary File S5). The COG group that differed most among the 4 strains was replication, recombination, and repair (L), with strain 18071143 having the most genes, followed by *H. stevensii* S18214. The difference in the number of genes contained in the L group between these 2 strains was, however, still statistically significant (Fisher exact test, $P < .01$; FIGURE 3B). We

FIGURE 1. Phylogenetic tree based on genome data. Tree inferred with FastME 2.1.6.1 from Genome BLAST Distance Phylogeny approach distances calculated from genome sequences under the algorithm “trimming” and distance formula d5. Strain 18071143 is in red. The numbers at the nodes indicate the bootstrap probabilities of the particular branch. The tree was visualized with iTOL (<https://itol.embl.de/>).

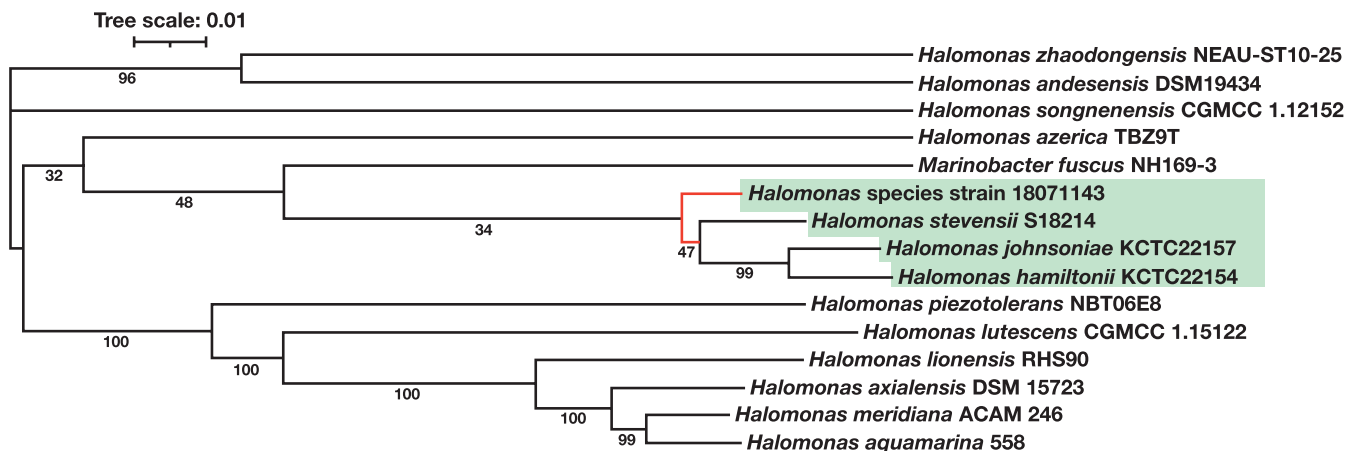


TABLE 2. Genome component comparison among 4 strains of *Halomonas*

Strain	<i>Halomonas</i> sp 18071143	<i>H. stevensii</i> S18214	<i>H. hamiltonii</i> KCTC 22154	<i>H. johnsoniae</i> KCTC 22157
NCBI reference sequence	NZ_CP078120.1	NZ_AJTS000000000.1	NZ_BMXN000000000.1	NZ_BMX000000000.1
Genome size (Mb)	3.86	3.69	3.93	3.82
GC content (%)	60.4	60.2	60.1	60.1
CDS ^a	3556	3429	3612	3515
rRNA ^b	18	16	6	13
tRNA ^c	61	56	57	57

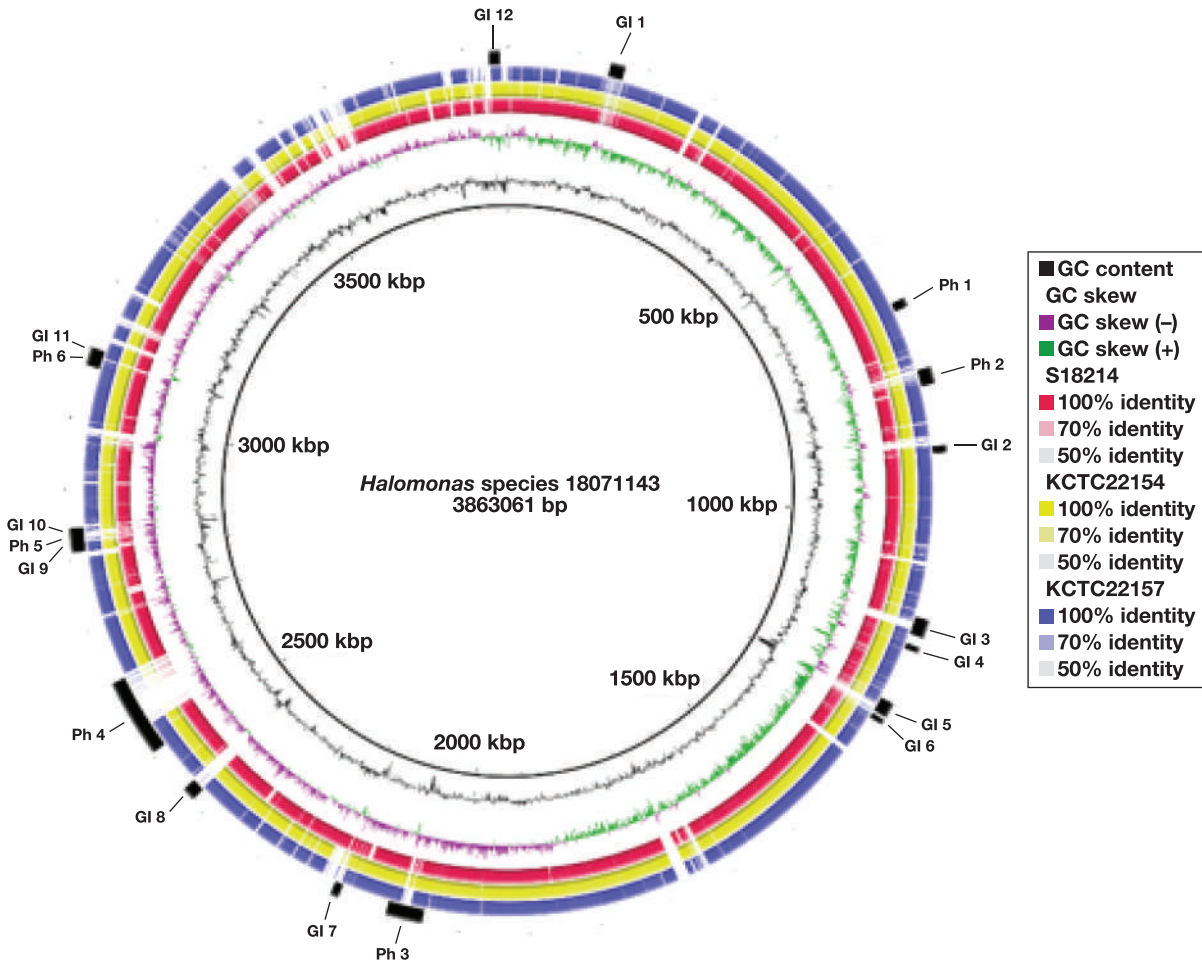
CDS, coding sequences; GC, guanine-cytosine; NCBI, National Center for Biotechnology Information; rRNA, ribosomal RNA; tRNA, transfer RNA

^aData from analysis of Glimmer v 3.02.

^bData from analysis of Barrnap v 0.4.2.

^cData from analysis of tRNAscan-SE v1.3.1.

FIGURE 2. Comparison of *Halomonas* sp 18071143 genome with 3 other *Halomonas* strains. The comparison was visualized using the BLAST Ring Image Generator. The strain 18071143 genome was used as the reference sequence. The 3 inner rings show the DNA size, guanine-cytosine (GC) content, and GC skew of the reference genome. The 3 outer rings show regions of the comparison genomes that matched the reference genome. From inside to outside, the comparison genomes are: *H. stevensii* S18214, *H. hamiltonii* KCTC 22154, and *H. johnsoniae* KCTC 22157. The color intensity in each ring represents the BLAST match identity (%) based on the similarity to the reference genome. Gaps in the circles represent regions of low or no similarity. The outermost circle indicates the location of the genomic island and prophage regions (designated as GI and Ph, respectively) in strain 18071143 genome.



performed Spearman correlation analysis on 4 strains based on the COG functional categories, and all 4 strains were highly correlated with each other ($P < .001$) (Supplementary File S6). Additionally, compared with the correlation between the other 2 strains, strain 18071143 showed

the highest correlation with *H. stevensii* S18214, with a correlation coefficient of 0.9935 (FIGURE 4).

A core-pan-genome analysis was performed using all 4 *Halomonas* strains genome sequences. The results revealed that there were 4410

FIGURE 3. Comparisons of Clusters of Orthologous Groups of Proteins (COG) functional categories. **A**, COG function comparison of *Halomonas stevensii* S18214, *H hamiltonii* KCTC 22154, *H johnsoniae* KCTC 22157, and *Halomonas* sp 18071143. The x-axis indicates the number of genes, the y-axis indicates the taxonomic name of the COG function, and each bar indicates each strain. **B**, Differential analysis of COG functional categories between *H stevensii* S18214 and *Halomonas* sp 18071143. The y-axis indicates the name of the function at different classification levels and the x-axis indicates the percentage value of the abundance of a particular function for that strain, with different colors indicating different strains. *P* values are on the right.

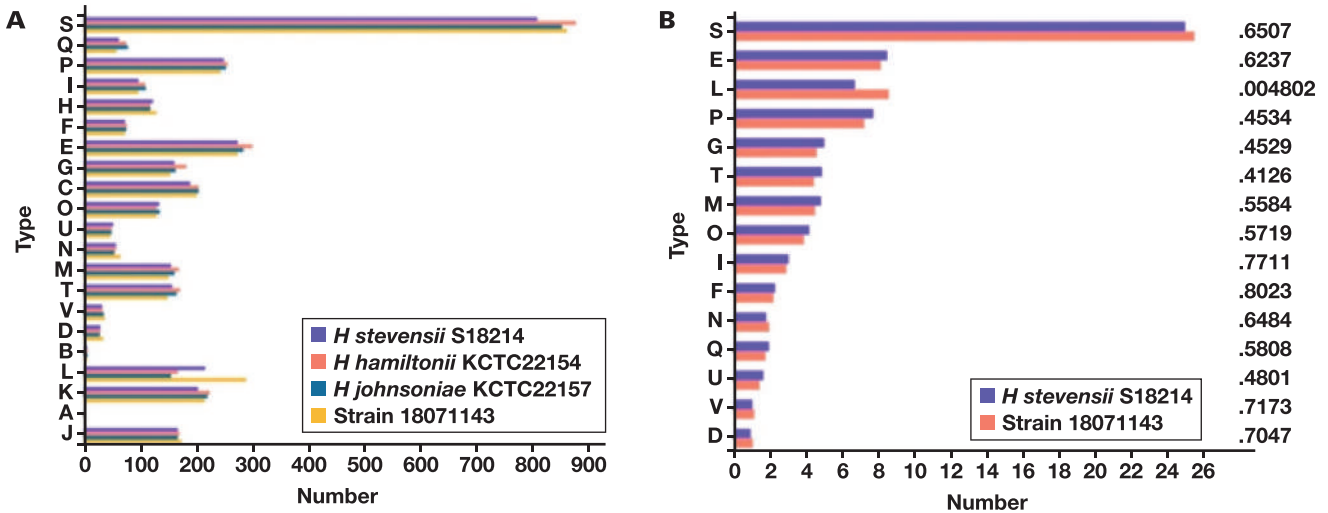
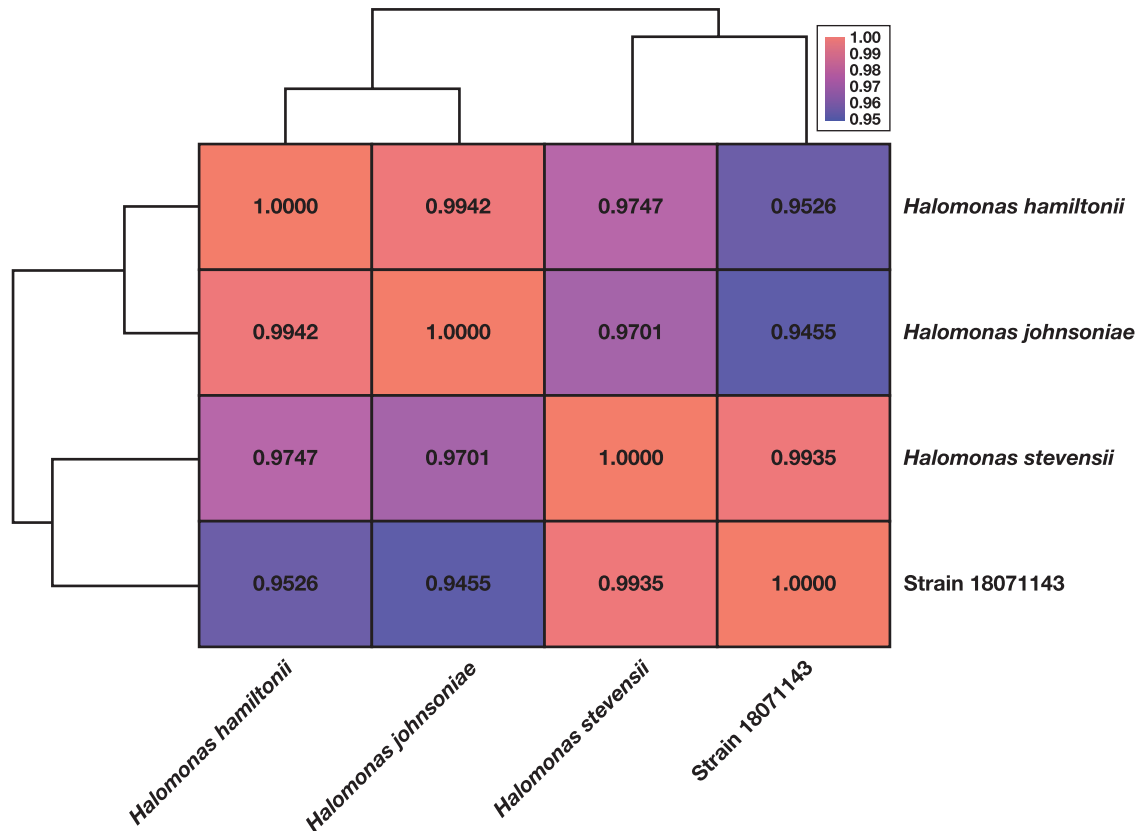


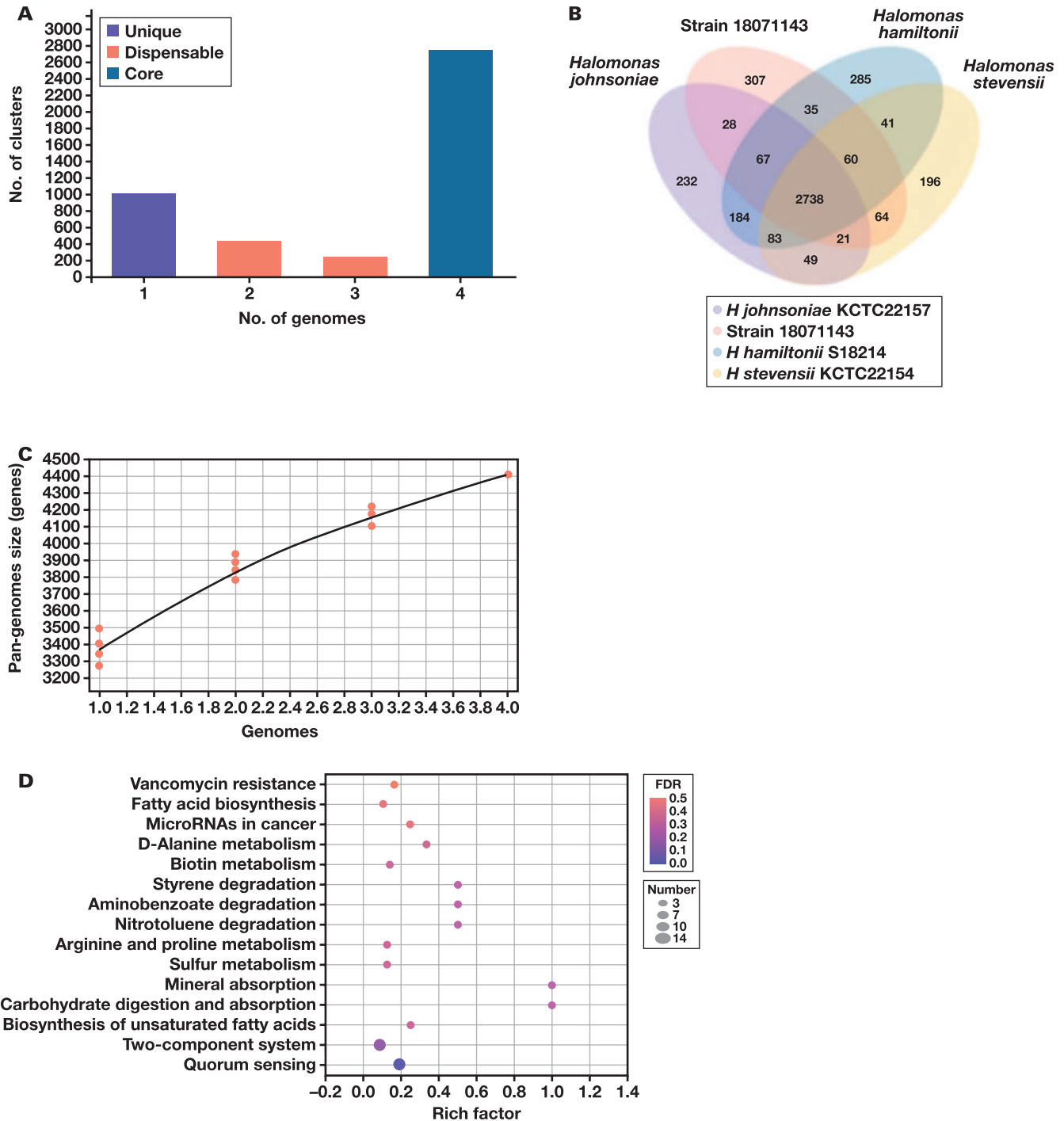
FIGURE 4. Spearman correlation analysis on four strains based on the Clusters of Orthologous Groups of Proteins (COG) functional categories. On the right and bottom side of the figure are the sample names, and on the left and top side are the sample clusters. The different colored squares represent the high or low correlation between the 2 samples, and the middle number is the correlation coefficient.



nonredundant proteins (14,100 genes) in total (pan-genome), among them, 2738 proteins (11,351 genes) were shared among all 4 analyzed genomes (core genome). The ratio of the core and pan-genome size was

found to be 0.62; thus, the core forms 62% of the pan-genome, revealing the high similarity of the 4 strains of *Halomonas* (FIGURE 5A; Supplementary File S7). We compared the distribution of core genes and unique

FIGURE 5. The pan-genome of 4 *Halomonas* strains. **A**, Categorization of the pan-genome into unique, dispensable, and core gene clusters. **B**, Venn diagram of the unique, dispensable, and core gene clusters of the pan-genome. **C**, Estimation of the sizes of the pan-genome. Genomes were resampled in all possible combinations of 1 through 4 and the number of pan-genome genes is reported as dots. The pan-genome curve was modeled by fitting the power-law regression formula $y = A \times B + C$ ($y = 1656.306 \times 0.348 + 1720.147$). The pan-genome is closed or open according to the B value. If $0 < B < 1$, the pan-genome is open, and if $B < 0$ or $B > 1$, it is closed. **D**, Top 15 enriched Kyoto Encyclopedia of Genes and Genomes (KEGG) pathways of unique genes in strain 18071143 genome. The x-axis represents the rich factor, and the y-axis shows the name of the KEGG pathway. The greater the rich factor, the higher the degree of enrichment. The false discovery rate (FDR) ranges from 0 to 1 and the closer it is to 0, the more significant the enrichment.



genes in COG functional categories. It was found that in addition to the abundance of unique genes in the function unknown (S) was much higher than that of the core genes, it also had an advantage in the transcription (K), replication, recombination and repair (L), and defense mechanisms (V) groups. The abundance of core genes in the cell wall/membrane/envelope biogenesis (M), translation, ribosomal structure and biogenesis (J), signal transduction mechanisms (T), posttranslational modification, protein turnover, chaperones (O), coenzyme transport and metabolism (H), and lipid transport and metabolism (I) groups was much higher than that of the unique genes (Supplementary Figure S2 and File S8). When the number of genes in the pan-genome was plotted against the number of genomes using PGAP calculation, the obtained B value of 0.348 (FIGURE 5C), suggesting that the pan-genome was open, experiencing frequent evolutionary changes through gene gains and losses or HGT for efficient environmental adaptations. Extensive HGT is associated with open pan-genomes.²⁰ According to FIGURE 5B, strain 18071143 and *H stevensii* S18214 are most closely related, sharing the most total proteins (165) outside the core and having the most proteins shared between only these 2 populations (84). Strain 18071143 has a higher proportion of unique proteins, with 307 proteins. Subsequently, KEGG pathway mapping of strain 18071143 unique genes was carried out. As shown in FIGURE 5D, the significantly enriched pathways (top 15) of strain 18071143 unique genes including quorum sensing, 2-component system, RNA transport, and biosynthesis of unsaturated fatty acids (Supplementary File S9).

Conclusions

The availability of whole-genome sequence determination has greatly facilitated the identification of rare pathogenic bacteria and the improved understanding of their genome structure and function. In the specific case of *Halomonas* species strain 18071143 isolated from the blood of a newborn, our study aimed to reveal the species type and genomic assets of this strain. Phylogenetic, ANI, and dDDH similarity analyses based on genome sequences indicated that strain 18071143 belonged to species *H stevensii*. Pan-genome analysis of 4 *Halomonas* species strains associated with the human disease showed that the strain-specific genes were only a small proportion of each strain. We found that *H hamiltonii*, *H stevensii*, and *H johnsoniae*, despite being distinct species, had similarities in gene structure and protein function, suggesting that these 3 species of *Halomonas* associated with human infection events share similar genetic characteristics. We also found that strain 18071143 had more genes related to DNA replication, recombination, repair capacity, and horizontal transfer than other strains. Overall, more research should be conducted on the pathogenic potential of this genus.

Supplementary Material

Supplementary material is available at *Laboratory Medicine* online.

Acknowledgments

We thank Shanghai Major Biomedical Technology for assistance with some of the bioinformatics analyses.

Funding

C.X. was supported by the JINGYING Talent Program of Sichuan Provincial Maternity and Child Health Care Hospital and the Science and Technology Project of Chengdu Science and Technology Bureau (2021-

YF05-00260-SN). P.W. was supported by the Natural Science Foundation of the School of Laboratory Medicine of Chengdu Medical College (JYZK202206).

Conflict of Interest Disclosure

The authors have nothing to disclose.

REFERENCES

1. von Graevenitz A, Bowman J, Del Notaro C, et al. Human infection with *Halomonas venusta* following fish bite. *J Clin Microbiol*. 2000;38:3123–3124. doi:10.1128/JCM.38.8.3123-3124.2000
2. Nikkari S, Lopez FA, Lepp PW, et al. Broad-range bacterial detection and the analysis of unexplained death and critical illness. *Emerg Infect Dis*. 2002;8:188–194. doi:10.3201/eid0802.010150
3. Berger P, Barguelli F, Raoult D, et al. An outbreak of *Halomonas phocaeensis* sp. nov. bacteraemia in a neonatal intensive care unit. *J Hosp Infect*. 2007;67:79–85. doi:10.1016/j.jhin.2007.06.018
4. Stevens DA, Hamilton JR, Johnson N, et al. *Halomonas*, a newly recognized human pathogen causing infections and contamination in a dialysis center: three new species. *Medicine*. 2009;88:244–249. doi:10.1097/MD.0b013e3181aede29
5. Yeo SH, Kwak JH, Kim YU, et al. Peritoneal dialysis-related peritonitis due to *Halomonas hamiltonii*: a first case report. *Medicine*. 2016;95:e5424. doi:10.1097/MD.0000000000005424
6. Uejima Y, Oh-Ishi T, Kitajima I, et al. Purulent lymphadenitis due to *Halomonas hamiltonii*: a case report. *Int J Infect Dis*. 2022;125:145–148. doi:10.1016/j.ijid.2022.10.032
7. Kim KK, Lee JS, Stevens DA. Microbiology and epidemiology of *Halomonas* species. *Future Microbiol*. 2013;8:1559–1573. doi:10.2217/fmb.13.108
8. Clinical and Laboratory Standards Institute. Interpretive criteria for identification of bacteria and fungi by targeted DNA sequencing. In: *CLSI Standard MM18*. 2nd ed. Clinical and Laboratory Standards Institute; 2018.
9. Stevens DA, Kim KK, Johnson N, et al. *Halomonas johnsoniae*: review of a medically underappreciated genus of growing human importance. *Am J Med Sci*. 2013;345:335–338. doi:10.1097/MAJ.0b013e31825600de
10. Kim KK, Lee KC, Oh HM, et al. *Halomonas stevensii* sp. nov., *Halomonas hamiltonii* sp. nov. and *Halomonas johnsoniae* sp. nov., isolated from a renal care centre. *Int J Syst Evol Microbiol*. 2010;60:369–377. doi:10.1099/ijms.0.004424-0
11. Lee I, Ouk Kim Y, Park SC, et al. OrthoANI: an improved algorithm and software for calculating average nucleotide identity. *Int J Syst Evol Microbiol*. 2016;66:1100–1103. doi:10.1099/ijsem.0.000760
12. Yoon SH, Ha SM, Lim J, et al. A large-scale evaluation of algorithms to calculate average nucleotide identity. *Anton Leeuw*. 2017;110:1281–1286. doi:10.1007/s10482-017-0844-4
13. Meier-Kolthoff JP, Auch AF, Klenk HP, et al. Genome sequence-based species delimitation with confidence intervals and improved distance functions. *BMC Bioinf*. 2013;14:60. doi:10.1186/1471-2105-14-60
14. Meier-Kolthoff JP, Carbasse JS, Peinado-Olarte RL, et al. TYGS and LPSN: a database tandem for fast and reliable genome-based classification and nomenclature of prokaryotes. *Nucleic Acids Res*. 2022;50:D801–D807. doi:10.1093/nar/gkab902.
15. Lefort V, Desper R, Gascuel O. FastME 2.0: a comprehensive, accurate, and fast distance-based phylogeny inference program. *Mol Biol Evol*. 2015;32:2798–2800. doi:10.1093/molbev/msv150
16. Alikhan NF, Petty NK, Ben Zakour NL, et al. BLAST Ring Image Generator (BRIG): simple prokaryote genome comparisons. *BMC Genom*. 2011;12:402. doi:10.1186/1471-2164-12-402

17. Yoon SH, Hur CG, Kang HY, et al. A computational approach for identifying pathogenicity islands in prokaryotic genomes. *BMC Bioinf.* 2005;6:184. doi:[10.1186/1471-2105-6-184](https://doi.org/10.1186/1471-2105-6-184)
18. Kim M, Oh HS, Park SC, et al. Towards a taxonomic coherence between average nucleotide identity and 16S rRNA gene sequence similarity for species demarcation of prokaryotes. *Int J Syst Evol Microbiol.* 2014;64:346–351. doi: [10.1099/ijs.0.059774-0](https://doi.org/10.1099/ijs.0.059774-0).
19. Ashok Kumar J, Vinaya Kumar K, Avunje S, et al. Phylogenetic relationship among brackish water *Vibrio* species. *Evol Bioinform Online.* 2020;16. doi:[10.1177/1176934320903288](https://doi.org/10.1177/1176934320903288)
20. Golicz AA, Bayer PE, Bhalla PL, et al. Pangenomics comes of age: from bacteria to plant and animal applications. *Trends Genet.* 2020;36:132–145. doi:[10.1016/j.tig.2019.11.006](https://doi.org/10.1016/j.tig.2019.11.006)

Can lipid mediators and free fatty acids guide acute coronary syndrome diagnosis and treatment?

Gulbahar Uzun, MD¹, Aslihan Unal, MD², Ibrahim Basarici, MD³, Murathan Kucuk, MD³, Levent Donmez, MD⁴, Cahit Nacitarhan, MD⁵, Sebahat Özdem, MD¹

Departments of ¹Medical Biochemistry, ²Emergency Medicine, ³Cardiology, ⁴Public Health, and ⁵Clinical Pharmacology, Akdeniz University Medical Faculty, Antalya, Turkey. Corresponding author: Sebahat Özdem; ozdem@akdeniz.edu.tr

Key words: acute coronary syndrome; fatty acids; inflammation; lipid mediators

Abbreviations: MI, myocardial infarction; MUFA, monounsaturated fatty acid; SFA, saturated fatty acids; ACS, acute coronary syndrome; CAD, coronary artery disease; ALA, alpha-linolenic acid; AA, arachidonic acid; EPA, eicosapentaenoic acid; DHA, docosahexaenoic acid; USAP, unstable angina pectoris; HDL, high-density lipoprotein; LDL, low-density lipoprotein; hs, high sensitive; D9D, delta 9-desaturase; D6D, delta 6-desaturase; PUFA, polyunsaturated fatty acids; CRP, C-reactive protein; CV, coefficient of variation

Laboratory Medicine 2024;55:88-95; <https://doi.org/10.1093/labmed/lmad042>

ABSTRACT

Objective: The aim of this study was to investigate fatty acids, lipid mediator levels, and the desaturase index rates on different acute coronary syndrome types and their possible relationship with routine lipid parameters.

Methods: The study included 81 patients with myocardial infarction (MI), 20 patients with unstable angina pectoris, and 31 healthy people. Fatty acids, CD59, lipoxin A4, 8-isoprostane, serum lipids, albumin, C-reactive protein (CRP), and high sensitive troponin levels were measured in all participants.

Results: When the fatty acid groups were evaluated as a ratio of albumin, MUFA/albumin and SFA/albumin ratios were significantly higher in the MI group compared to the control group. Although CD59 and lipoxin A4 levels were higher in the control group, there was no significant differences between the groups. When lipoxin A4/CRP and CD59/CRP ratios were evaluated, the results were significantly lower than those in the control group.

Conclusion: Lipid mediators may be useful in treating atherosclerosis by contributing to the resolution of inflammation.

Introduction

Acute coronary syndrome (ACS) is an emergency situation characterized by unstable atheromatous plaque and impaired myocardial perfusion, based generally on atherosclerotic coronary artery disease (CAD), which in turn may lead to myocardial infarction (MI) or cardiac death.¹

Atherosclerosis, which is the underlying cause of cardiovascular diseases, has been defined as an inflammatory disease of the vascular wall.²⁻⁴ Some atherosclerotic lesions result in ACS, whereas some disappear in time. Resolution of the inflammation minimizes the tissue or organ damage.⁴ New locally effective, endogenous autocooids that provide the resolution (lipoxins, resolvins, protectins, and maresins) have been specified as pre-resolving lipid mediators.⁵ Recently, essential fatty acids have been shown to have beneficial effects in many diseases.⁶ It has been stated that the balance of these fatty acids is important and reflects the risk of cardiovascular disease.⁷ Linoleic acid and alpha-linolenic acid (ALA) are omega-6 and omega-3 fatty acids, respectively,⁸ and are transformed into arachidonic acid (AA) and eicosapentaenoic acid (EPA), docosahexaenoic acid (DHA) in the body, respectively.^{8,9} AA may be transformed into the proinflammatory prostaglandin, leukotriene, and thromboxane A₂, as well as lipoxins that are facilitative in the resolution process, whereas EPA and DHA may be transformed into these anti-inflammatory lipid mediators.⁹

The aim of this study was to investigate fatty acids, which have pro-inflammatory and anti-inflammatory effects, and lipid mediator (protectin, lipoxin, 8-isoprostane) levels and the desaturase index rates on different ACS types (MI and unstable angina pectoris [USAP]), and their possible relationship with routine lipid parameters.

Materials and Methods

Case Selection

The study included 81 patients with MI diagnosed according to European Society of Cardiology, American College of Cardiology, American Heart Association, and World Heart Federation criteria and 20 patients with USAP who were admitted to the Emergency Unit of Akdeniz University Hospital with acute chest pain or other symptoms suggestive of ACS, and who were older than 18 years of age. The control group included 31 healthy volunteers selected in accordance with the age and sex distribution of the patient group.

Exclusion Criteria

The exclusion criteria were cardiogenic shock, severe hepatic disorder, <18 years of age, duration of >24 hours after symptom onset, renal

insufficiency (serum creatinine level >1.5 mg/dL), valve disorder, hypertrophic cardiomyopathy, severe systemic hypertension (cystolic >180 mmHg, diastolic >110 mmHg), refractory ventricular arrhythmia, history of recent MI (<4 weeks), recent myocardial revascularization surgery (<4 weeks), history of recent percutaneous coronary intervention (<2 weeks), congestive cardiac failure diagnosis or symptoms, severe noncardiovascular diseases (infection, sepsis, immunological or inflammatory diseases, malignancies, cerebrovascular disease), history of organ transplantation or awaiting transplantation, regular use of vitamin, antioxidant, nonsteroid anti-inflammatory, anticoagulant drugs, hormone replacement therapy, major trauma, and pregnancy.

Fatty acids, lipid mediators (CD59, lipoxin A4, 8-isoprostane), serum lipids (total cholesterol, high-density lipoprotein [HDL], low-density lipoprotein [LDL]), triglyceride, albumin, C-reactive protein (CRP), and high sensitive (hs)-troponin levels were measured in all participants in both the study and the control groups.

The study was accepted by the Scientific Research Projects Coordination Department of Akdeniz University with the number 2012.04.0103.007 and was approved by Clinical Research Ethical Committee of Akdeniz University Faculty of Medicine with the number 02.04.2012/45 (B.30.2.AKD.0.20.05.06/35). Written informed consent was obtained from all participants or their relatives.

Sample Collection and Storage

Venous blood samples were collected from patients who had presented to the emergency unit within 24 hours after the onset of symptoms, into gel biochemistry, EDTA, citrated coagulation, and 2 mL EDTA hemogram tubes. The samples were centrifuged at 4°C, 2500g for 4 minutes; serum and plasma were separated and kept at -80°C until analysis.

The hs-troponin T levels were measured in serum samples using the Roche Elecsys 2010 instrument via the electrochemiluminescence immunological assay method (Roche Diagnostics). The lower reading limit of the kit used is 3 pg/mL; the upper reading limit is 10,000 pg/mL. Total cholesterol, HDL cholesterol, LDL cholesterol, triglyceride, albumin, and CRP levels were measured in serum samples using the Roche cobas 8000 instrument (Roche Diagnostics). Non-HDL cholesterol was calculated by subtracting HDL cholesterol from total cholesterol. The 8-isoprostane level was measured using the Cayman kit (Cayman Chemical; the specificity of the kit for 8-iso prostaglandin F2 α was 100%) in plasma samples, protectin (CD59) level was measured using the CUSABIO kit (Cusabio; the intra-assay CV of the kit was <8% and the inter-assay CV <10%, the measurement range of the kit was 2.35 ng/mL to 150 ng/mL in serum samples, and the lipoxin A4 level was measured using the EIAab kit (EIAab Science; the measurement range of the kit was 31.2 pg/mL to 2000 pg/mL) in plasma samples via enzyme-linked immunosorbent assay method. Fatty acids were studied in the Shimadzu gas chromatography–mass spectrometer instrument in plasma samples.

The desaturase index is calculated by dividing the fatty acid formed by the desaturase to the first fatty acid that reacts. Calculations of the desaturases were as follows: delta 9-desaturase-18 (D9D-[18]) index: C18:1n9/C18:0; delta 9-desaturase-16 (D9D-[16]) index: C16:1n7/C16:0; and delta 6-desaturase (D6D) index: C18:3n6/C18:2n6.¹⁰

Statistical Analysis

The data obtained in the study were analyzed using GraphPad Prism 5 and SPSS for windows 11.0 program packages. The data were presented as number, percentage, and arithmetic mean \pm SD. The Student *t* test was used for intergroup comparisons, Pearson correlation analysis was used to evaluate the correlation between variables, and the multiple regression analysis was used to investigate the relationship between dependent and independent variables. The significance level was accepted as *P* < .05.

Results

Distribution of sex and age within groups are summarized in **TABLE 1**. No statistical difference was present between MI, USAP, and control groups with regard to age and gender (*P* > .05). It was observed that 80% to 85% of the patients in the MI and USAP groups were male.

The hs-troponin T values were 859.10 \pm 1815.00 pg/mL in the MI group, 44.79 \pm 82.60 pg/mL in the USAP group, and 5.81 \pm 2.39 pg/mL in the control group. A statistically significant difference was determined in serum hs-troponin T levels between the MI and the USAP groups (*P* < .05), between the MI and the control groups (*P* = .01), and between the USAP and the control groups (*P* = 0.01).

The serum lipid profiles of the groups were compared and the parameters with significant differences are summarized in **TABLE 2**.

Lipoxin A4 (pg/mL) levels were measured as 71.48 \pm 43.85 pg/mL in the MI group, 77.12 \pm 52.97 pg/mL in the USAP group, and 82.46 \pm 82.79 pg/mL in the control group. The CD59 levels were 5.94 \pm 3.24 ng/mL, 5.44 \pm 4.51 ng/mL, and 6.34 \pm 3.14 ng/mL in the MI, USAP, and the control groups, respectively. The 8-isoprostane levels were 107.20 \pm 253.60 pg/mL, 26.89 \pm 16.47 pg/mL, and 43.02 \pm 36.96 pg/mL in the MI, USAP, and the control groups, respectively. The lipid mediator levels were compared and 8-isoprostane was observed to be significantly higher in the MI group than in the USAP and the control groups (*P* = .012 and *P* = .006, respectively). Lipoxin A4 and CD59 parameters were higher in the control group; however, the difference was not significant between the groups (*P* > .05) (**FIGURE 1**).

Plasma percentages of EPA, DHA, AA, SFA, MUFA, polyunsaturated fatty acids (PUFA) and AA/EPA, SFA/albumin, MUFA/albumin, PUFA/albumin rates, desaturase indexes, and the parameters with significant differences have been presented in **TABLE 3**.

The CD59/CRP ratio was significantly lower in the MI group (27.59 \pm 35.80) than in the control group (95.82 \pm 146.40) (*P* = .0002). No

TABLE 1. Age and sex distribution of the groups^a

Groups	Sex		Total	Age, y (Mean \pm SD)
	Female	Male		
MI	16	65	81	60.2 \pm 12.6
USAP	3	17	20	59.3 \pm 14.2
Control	7	24	31	56.1 \pm 11.4

^aThere was no statistical difference between myocardial infarction (MI), unstable angina pectoris (USAP), and control groups with regard to age and sex (*P* = .05).

TABLE 2. Lipid parameters levels in MI, USAP, and control groups^a

	MI group			USAP group			Control group		
	Men (n = 65)	Women (n = 16)	Total (n = 81)	Men (n = 17)	Women (n = 3)	Total (n = 20)	Men (n = 24)	Women (n = 7)	Total (n = 31)
Total cholesterol (mg/dL)	200.10 ± 41.76	202.6010 ± 24.07	200.610 ± 38.79 ^b	177.9010 ± 36.65	196.0010 ± 8.18	180.610 ± 34.38	196.3010 ± 28.38	201.3010 ± 32.26	197.410 ± 28.81
HDL cholesterol (mg/dL)	39.7110 ± 9.11 ^c	45.510 ± 9.72	40.8510 ± 9.46 ^d	41.0010 ± 9.38 ^c	60.6710 ± 4.04	43.9510 ± 11.3	45.0810 ± 9.03 ^c	64.5710 ± 15.33	49.4810 ± 13.34
LDL cholesterol (mg/dL)	138.5010 ± 36.98	141.3010 ± 24.26	13910 ± 34.72 ^b	110.4010 ± 33.60	120.3010 ± 11.37	111.910 ± 31.2 ^e	131.0010 ± 27.69	121.310 ± 29.07	128.810 ± 27.82
Non-HDL cholesterol (mg/dL)	160.4010 ± 42.49	157.1010 ± 22.03	159.810 ± 39.2 ^b	136.9010 ± 39.03	135.310 ± 5.86	136.710 ± 35.87	151.2010 ± 29.93	136.7010 ± 29.75	147.910 ± 30.02
Total cholesterol / HDL	5.2910 ± 1.59	4.5910 ± 0.89	5.1610 ± 1.51 ^f	4.5710 ± 1.50	3.2410 ± 0.15	4.3710 ± 1.46	4.5510 ± 1.32 ^g	3.2310 ± 0.72	4.310 ± 1.33
Triglyceride (mg/dL)	187.5010 ± 95.22	189.4010 ± 50.63	187.910 ± 87.95 ^h	217.9010 ± 130.50	156.710 ± 34.36	208.810 ± 122.4 ^h	133.910 ± 55.29	86.8610 ± 56.35	123.310 ± 58.12

^aData are presented as mean ± SD.

^bTotal cholesterol, low-density lipoprotein (LDL), and non-HDL cholesterol levels were found to be statistically significantly higher in the MI group than in the USAP group ($P = .037$, $P = .002$, and $P = .018$, respectively).

^cHigh-density lipoprotein (HDL) levels were found to be lower in males than in females in the myocardial infarction (MI), unstable angina pectoris (USAP), and control groups ($P = .027$, $P = .0024$, and $P = .00019$, respectively).

^dHDL levels were statistically significantly lower in the MI group than in the control group ($P = .0002$).

^eLDL levels were significantly lower ($P < .05$) and triglyceride levels were significantly higher in the USAP group than in the control group ($P = .0015$).

^fTotal cholesterol/HDL levels were significantly higher in the MI group than in the control and USAP groups ($P = .004$ and $P = .039$, respectively).

^gTotal cholesterol/HDL levels in the control group were found to be significantly higher in males than in females ($P = .017$).

^hThe triglyceride levels were statistically significantly higher in the MI group than in the control group ($P = .00025$).

FIGURE 1. Lipid mediator (lipoxin A4 [A], CD59 [B], and 8-isoprostane [C]) levels in myocardial infarction (MI), unstable angina pectoris (USAP), and control groups (mean ± SD). 8-Isoprostane was observed to be significantly higher in the MI group than in the USAP and the control groups ($P = .012$ and $P = .006$, respectively). Lipoxin A4 and CD59 parameters were higher in the control group; however, the difference was not significant between the groups ($P = .05$).

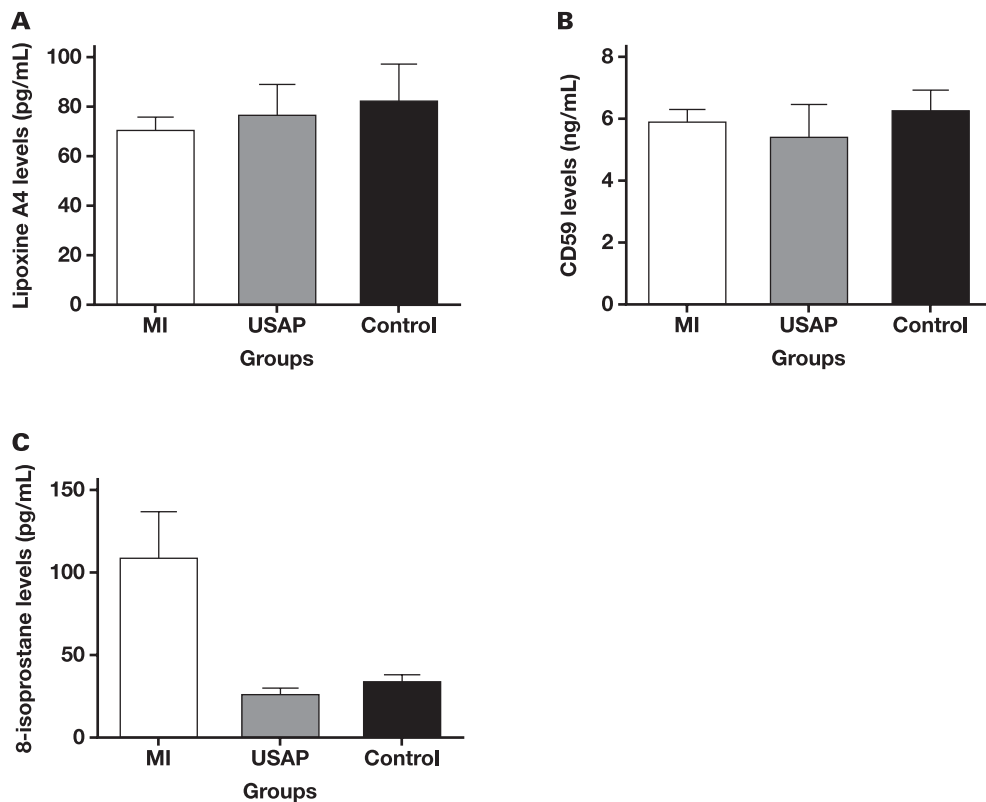


TABLE 3. Albumin, CRP, fatty acids, fatty acid groups, fatty acid groups/albumin, and desaturase index ratios of study groups^a

	MI group			USAP group			Control group		
	Men (n = 65)	Women (n = 16)	Total (n = 81)	Men (n = 17)	Women (n = 3)	Total (n = 20)	Men (n = 24)	Women (n = 7)	Total (n = 31)
Albumin (g/dL)	4.51 ± 0.31 ^b	4.27 ± 0.39	4.46 ± 0.34 ^c	4.50 ± 0.39	4.48 ± 0.35	4.49 ± 0.38	4.90 ± 0.30	4.80 ± 0.34	4.88 ± 0.31
CRP (mg/dL)	1.47 ± 3.12	1.19 ± 1.88	1.42 ± 2.99 ^d	0.91 ± 2.06	0.41 ± 0.19	0.84 ± 1.90	0.30 ± 0.29	0.05 ± 0.04 ^e	0.24 ± 0.28
EPA (%)	3.45 ± 2.83	3.18 ± 2.42	3.39 ± 2.75	3.40 ± 3.22	5.60 ± 1.10	3.73 ± 3.08	3.14 ± 2.37	4.35 ± 2.58	3.41 ± 2.43
DHA (%)	0.55 ± 0.33	0.51 ± 0.38	0.54 ± 0.34	0.58 ± 0.25	0.46 ± 0.13	0.56 ± 0.24	0.56 ± 0.47	0.74 ± 0.48	0.60 ± 0.47
AA (%)	1.66 ± 2.42	2.02 ± 2.73	1.73 ± 2.47	1.52 ± 1.87	0.02 ± 0.00	1.30 ± 1.81	1.67 ± 2.47	1.67 ± 2.79	1.66 ± 2.49
AA/EPA	16.85 ± 53.15	18.78 ± 58.20	17.23 ± 53.81	47.47 ± 84.32	0.004 ± 0.001	40.35 ± 79.31	9.77 ± 34.57	1.35 ± 2.75	7.86 ± 30.50
AA/DHA	2.56 ± 4.13	3.88 ± 6.05	2.82 ± 4.56	2.87 ± 3.94	0.05 ± 0.01	2.45 ± 3.76	2.23 ± 3.67	1.52 ± 2.33	2.07 ± 3.39
SFA (%)	37.00 ± 2.92	38.04 ± 2.25	37.21 ± 2.82	37.61 ± 3.49	36.47 ± 1.13	37.44 ± 3.26	38.39 ± 7.12	35.59 ± 2.14	37.76 ± 6.42
MUFA (%)	25.46 ± 4.58 ^f	28.40 ± 4.37	26.04 ± 4.66	25.13 ± 4.99	22.71 ± 2.47	24.76 ± 4.74	21.90 ± 10.46	25.83 ± 5.68	22.82 ± 9.62
PUFA (%)	7.15 ± 2.07	7.38 ± 1.23	7.19 ± 1.92	6.80 ± 2.05	7.20 ± 1.47	6.86 ± 1.95	6.69 ± 2.59	8.33 ± 1.95	7.06 ± 2.53
Omega-3 fatty acids (%)	4.12 ± 2.76	3.76 ± 2.33	4.04 ± 2.68	4.07 ± 3.12	6.08 ± 0.97	4.37 ± 3.04	3.76 ± 2.29	5.14 ± 2.44	4.07 ± 2.36
SFA/albumin	8.25 ± 0.86 ^g	8.99 ± 1.07	8.40 ± 0.95 ^g	8.41 ± 1.00	8.18 ± 0.40	8.38 ± 0.94	7.88 ± 1.68	7.43 ± 0.45	7.75 ± 1.20
MUFA/albumin	5.68 ± 1.08 ^f	6.71 ± 1.19	5.88 ± 1.18 ^h	5.57 ± 0.96	5.13 ± 0.95	5.51 ± 0.94	4.51 ± 2.18	5.39 ± 1.16	4.53 ± 2.10
PUFA/albumin	1.59 ± 0.48	1.74 ± 0.30	1.62 ± 0.45	1.53 ± 0.54	1.62 ± 0.41	1.55 ± 0.51	1.36 ± 0.54	1.72 ± 0.32	1.46 ± 0.55
D9D-(16) index	0.003 ± 0.002 ⁱ	0.004 ± 0.003	0.003 ± 0.002	0.002 ± 0.003	0.001 ± 0.000	0.002 ± 0.002	0.006 ± 0.012	0.003 ± 0.002	0.005 ± 0.011
D9D-(18) index	2.93 ± 0.74	3.10 ± 0.49	2.96 ± 0.69	2.86 ± 0.66	2.62 ± 0.45	2.83 ± 0.63	2.86 ± 0.61	2.72 ± 0.61	2.83 ± 0.60
D6D index	0.042 ± 0.020	0.049 ± 0.033	0.043 ± 0.023 ⁱ	0.038 ± 0.018	0.029 ± 0.025	0.037 ± 0.018	0.036 ± 0.028	0.020 ± 0.029	0.032 ± 0.029

AA, arachidonic acid; CRP, C-reactive protein; DHA, docosahexaenoic acid; D9D, delta 9-desaturase; D6D, delta 6-desaturase; EPA, eicosapentaenoic acid; MI, myocardial infarction; MUFA, monounsaturated fatty acid; PUFA, polyunsaturated fatty acids; SFA, saturated fatty acids; USAP, unstable angina pectoris

^aData are presented as mean ± SD.

^bAlbumin levels in the MI group were significantly higher in males than in females ($P = .011$).

^cAlbumin levels were significantly lower in the MI group than in the control group ($P < .00001$).

^dCRP levels were significantly higher in the MI group than in the control group ($P = .033$).

^eCRP levels in the control group were significantly higher in females than in males ($P = .037$).

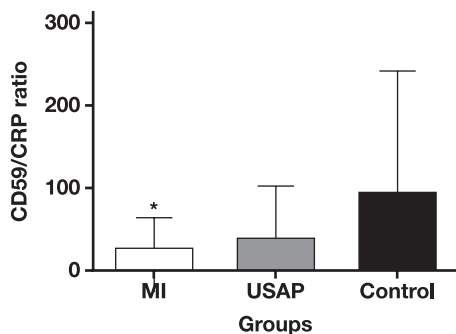
^fMUFA levels, SFA/albumin and MUFA/albumin rates, and D9D-16 index in the MI group were significantly lower in males than in females ($P = .023$, $P = .0043$, $P = .0013$, and $P = .01$, respectively).

^gThe SFA/albumin ratio of the MI group was significantly higher than that of the control group ($P = .003$).

^hThe MUFA/albumin ratio of the MI group was significantly higher than that of the control group ($P < .0001$).

ⁱThe D6D index of the MI group was significantly higher than that of the control group ($P = .039$).

FIGURE 2. CD59/CRP levels in myocardial infarction (MI), unstable angina pectoris (USAP), and control groups. The CD59/CRP ratio was significantly lower in the MI group than in the control group ($*P = .0002$ as compared with control group). No difference was observed between the MI and the USAP groups or the USAP and the control groups ($P = .05$).



difference was observed between the MI and the USAP (41.68 ± 60.43) groups or the USAP and the control groups (FIGURE 2).

In the study groups, lipoxin A4 level per CRP was observed to be significantly lower in the MI group than in the control group ($P = .0026$),

whereas it was again lower in the MI group than in the USAP group, although it was not significant ($P = .059$).

The relation of the total percentages of omega-3 fatty acids (EPA + DHA + ALA) in the MI group with other parameters and the correlations (P values and coefficient of correlations) are presented in TABLE 4.

The MUFA/SFA ratio in the MI group was observed to be positively and significantly correlated to the triglyceride levels ($P = .001$, $r = 0.357$).

The PUFA/SFA ratio was positively correlated with HDL in the MI group ($P = .004$, $r = 0.319$), whereas it was negatively correlated with the presence of diabetes mellitus ($P = .009$, $r = -0.290$), total cholesterol/HDL ($P = .012$, $r = -0.279$), and triglyceride levels ($P = .004$, $r = -0.317$).

The relationship between the activity index of the D9D-(18) enzyme, which has a role in the metabolic pathway of oleic acid, a MUFA, and other parameters was investigated, and a positive correlation was observed with total cholesterol ($P = .016$, $r = 0.266$), non-HDL cholesterol ($P = .013$, $r = 0.276$) and more significantly, with triglyceride ($P < .0001$, $r = 0.487$).

The lipoxin A4 values in the MI group were positively correlated with percent DHA ($P = .042$ and $r = 0.226$), and negatively correlated with the number of stents installed in the patient ($P = .03$ and $r = 0.281$). The 8-isoprostane values were positively correlated with the number of stents implanted in the patient ($P = .002$ and $r = 0.387$).

TABLE 4. Correlation table of MI group total % omega-3 fatty acids with other parameters^a

Parameters	P value	Coefficient of correlations (r)
Total cholesterol (mg/dL)	.0064	-0.300
LDL (mg/dL)	.025	-0.249
Non-HDL cholesterol (mg/dL)	.0035	-0.324
Total cholesterol/HDL	.0099	-0.285
Triglyceride (mg/dL)	.006	-0.302
AA (%)	<.0001	-0.745
MUFA (%)	.0029	-0.327

AA, AA, arachidonic acid; MUFA, monounsaturated fatty acid

^aTotal % omega-3 fatty acids (alpha-linolenic acid [ALA] + eicosapentaenoic acid [EPA] + Docosahexaenoic acid [DHA]).

The CD59 values in the MI group were observed to be negatively correlated to albumin and triglyceride levels ($P = .005$, $r = -0.310$ and $P = .028$, $r = -0.244$, respectively).

Although the AA/DHA ratios were higher in the MI and the USAP groups than in the control group, no significant difference was determined ($P = .05$).

When the MI group was divided into 2 groups of <60 and >60 years of age, the CD59 levels were observed to be 5.11 ± 2.66 ng/mL in the younger group and 6.94 ± 3.61 ng/mL in the older group, where the difference was significant ($P = .007$). The 8-isoprostane levels were observed to be 54.5 ± 103.0 pg/mL in the younger group and 169.90 ± 350.4 pg/mL in the older group. Although the 8-isoprostane levels were higher in the older group, the difference was not statistically significant ($P = .051$). No statistical difference was observed between the younger and the older MI groups with regard to the remaining parameters.

Discussion

Coronary artery disease (CAD) and its common complication ACS are major causes of morbidity and mortality worldwide.¹¹ The relationship between ACS and dyslipidemias, inflammation, and oxidative stress are the most common relationships investigated.

The inflammation observed in the process of atherosclerosis generally resolves spontaneously and tissue hemostasis is provided. This resolution is a complex active situation provided by the mediators synthesized during the early phase of acute inflammation.¹² These molecules, referred to as pro-resolving lipid mediators, are lipoxins, resolvins, and protectins.¹³ Among these, protectin (CD59) is synthesized from DHA.⁵ Furthermore, in a study conducted on atherosclerotic mice, increased CD59 expression levels were shown to be related to a decrease in blood lipids, increase in anti-apoptotic Bcl-2 protein and a decrease in pro-apoptotic Fas protein, which lead to decreased endothelial cell apoptosis, decreased MMP-2 expression, which normally increases smooth muscle proliferation, and plaque vulnerability, and the anti-atherosclerotic effects were shown to be increased with an increase in CD59 levels.¹⁴ In our study, although CD59 levels were determined to be lower in the MI and USAP groups than in the control group, the difference was not statistically significant. When the MI group was evaluated in 2 groups of <60 and >60 years of age, the CD59 levels were observed to be significantly lower in the younger group. With this finding, we considered that increasing the blood level of CD59 may be important in resolving the inflammation and avoiding the development of MI, especially in the younger group.

The importance of inflammation at the onset, destabilization, and progression of atherosclerosis has been emphasized in many studies as mentioned above.^{15,16} The levels of CRP, an acute phase reactant, have been widely used as a marker of infection, systemic inflammation, and tissue damage.¹⁵ In our study, CRP levels were found to be significantly higher in the MI group than in the control group and higher than in the USAP group, although not significantly. However, the levels of CRP being higher in the MI group than in the USAP group was evaluated as an indicator of wider inflammation and tissue damage in the MI group. The higher hs-troponin T levels in the MI group than in the USAP group may be explained by the extent of tissue damage, which was at the level of myocardial necrosis in the MI group and myocardial ischemia in the USAP group.

As mentioned above, the CD59 levels were lowest in the MI group and not statistically significant. When the levels of CD59 per CRP value within the study groups were investigated, the CD59/CRP ratio was observed to be significantly lower in the MI group than the control group. Additionally, a negative correlation was detected between the levels of CD59 and triglyceride in our study, which was compatible with the findings in the study of Li et al.¹⁴

Lipoxins have been reported to be synthesized from AA and EPA and facilitate the resolution of inflammation.¹⁷ In a study on mice, increased levels of 12/15-lipoxygenase, which is responsible for the biosynthesis of lipoxin, resolvin, and protectin, was demonstrated to block the development of atherosclerosis.⁴ In our study, it was found that lipoxin A4 levels were highest in the control group and lowest in the MI group (control > USAP > MI). However, this difference was not statistically significant. When lipoxin A4 levels per CRP within the study groups were investigated, the lipoxin A4/CRP ratio was observed to be significantly lower in the MI group than in the control group, whereas it was lower in the MI group than in the USAP group, although not statistically significant.

Increased lipid peroxidation is one of the important mechanisms of arteriosclerosis development.¹⁸ 8-Isoprostane is formed from AA with the effect of radicals.¹⁹ Because AA exists in all cell types, measurement of the 8-isoprostane level reflects the general situation of oxidative stress.²⁰ 8-Isoprostane also stimulates thromboxane receptors and contributes to platelet activation. Szułdrzyński et al²¹ demonstrated that 8-isoprostane levels were higher in patients with ACS than in those with stable angina pectoris and this increase was correlated to platelet activation. In our study, the 8-isoprostane levels were observed to be higher in the MI group than in the USAP and control groups. This finding indicates that despite various antioxidant systems present in the body, significant lipid peroxidation is present in unsaturated fatty acids in patients with ACS, and that lipid peroxidation and oxidative stress levels are significantly higher in the MI group than in the USAP group.

In the present study, HDL cholesterol levels followed each other, as the control group was greater than the USAP was greater than the MI group. However, only the levels in the control group were significantly higher than those in the MI group. Furthermore, as expected,²² HDL cholesterol levels were significantly higher in women than in men in all 3 groups. The total cholesterol and LDL cholesterol levels were found to be higher in the MI group than in the USAP group, whereas the LDL cholesterol levels were similar between the MI and control groups.

The balance in omega-3 and omega-6 fatty acids has been demonstrated in various studies to be important and reflects the risk of cardiovascular disease. Different studies have reported that AA leads to plaque destabilization, and to the contrary, EPA provides plaque

stabilization, and that AA/EPA ratios are related to the prevalence of cardiac events following acute myocardial infarction.⁷ As mentioned above, the omega-3 group of molecules in particular is necessary for the synthesis of lipid mediators (lipoxin, resolvin, protectin) that are important in the resolution of inflammation.¹³ In our study, no significant difference was observed between the groups with regard to percent EPA, DHA, AA, fatty acids, SFA, MUFA, PUFA groups and omega-3 fatty acids (EPA + DHA + ALA). Sakamoto et al²³ demonstrated that EPA, DHA, and EPA/AA ratios had relatively decreased in patients with stable CAD, previous ACS and stable CAD, and early phase ACS. In their study, they demonstrated that in the early phase ACS group where acute inflammatory events are dominant, omega-3 fatty acids were lower than in other groups. In this study, the AA/EPA and AA/DHA ratios were evaluated and no significant difference was observed between the groups. However, the AA/DHA ratio was found to be highest in the MI group, where inflammatory events are expected to be much more frequent, and lowest in the control group (MI > USAP > control). The increased AA/DHA ratio indicated increased inflammation in the group evaluated. Also, in a multi-center observational study investigating the relationship between the DHA/AA ratio, which reflects the omega-3/omega-6 ratio and ACS, it was observed that clinical characteristics of the patients changed according to DHA/AA ratio: those with lower DHA/AA ratio had a higher risk of ACS than those with a high DHA/AA ratio, which was even significant in male patients.²⁴

Studies have demonstrated that dietary intake of PUFA instead of SFA reduces the risk of cardiovascular disease, and that an increased serum ratio of PUFA/SFA reduces the level of serum cholesterol.²⁵ Likewise, in our study, the PUFA/SFA ratio in the MI group was found to be negatively correlated to the total cholesterol/HDL ratio and triglyceride levels. The increasing effect of SFA on the levels of cholesterol and triglyceride and related increased OS in the body indicate SFA's possible role in the development and progression of atherosclerosis.

MUFAs have been reported to have cardioprotective effects in epidemiological studies.²⁶ In our study, MUFA levels in women were significantly higher than those in men in the MI group, suggesting that higher MUFA levels might contribute to the less frequent occurrence of ACS in women, which is consistent with the literature.²⁷

Albumin is the most important antioxidant protein within blood serum and forms the vast majority of the proteins extracted from atherosclerotic plaques.²⁸ Our study demonstrated that albumin, a negative acute phase reactant, decreased significantly in MI and USAP groups compared with the control group. This reduction was considered to be due to albumin transmission from serum to atherosclerotic plaques to reduce the OS in these plaques with inflammatory and pro-oxidant properties, to easy removal of albumin with impaired structure altered during oxidative stress and inflammation from the bloodstream, or to reduced synthesis of albumin during oxidative stress and inflammation. Because the fatty acids within plasma are carried bound to albumin, an evaluation was made by rating fatty acid groups (SFA, MUFA, and PUFA) to albumin to reduce albumin-related causes, and it was observed that the SFA/albumin and MUFA/albumin ratios in the MI group were significantly higher than those of the control group. However, no difference was observed between the groups with regard to the PUFA/albumin ratios. The intergroup differences observed in SFA/albumin and MUFA/albumin ratios were assessed as albumin's capability of changing the levels of fatty acids and their effects. Furthermore, we found that albumin levels were significantly lower in women than in

men in the MI group. Lower albumin levels in women in the MI group may be a result of nutrition or inflammation. Previously epidemiological studies have reported an inverse relationship between serum albumin and ACS.^{29,30} Because low albumin levels are associated with a poor prognosis,³¹ it may be appropriate to evaluate women who have had MI in this regard. On the other hand, SFA/albumin and MUFA/albumin ratios were found to be significantly higher in women than in men in the MI group, which may be explained by low albumin levels and high MUFA levels in women.

Desaturases in the PUFA metabolism increase the number of double bonds in the fatty acid chain and provide the formation of unsaturated fatty acids. It has been demonstrated that in the presence of diabetes mellitus, cardiovascular events, and cancer, D6D activity is increased, and in the presence of inflammation, all desaturase activities are increased correlated to hs-CRP.³² Likewise, in our study, the D6D index in the MI group was observed to be higher than in the control group. Furthermore, the D9D index was assessed, and no significant difference was observed between the groups.

In our study, although no significant difference was observed between the groups with regard to the D9D index, the D9D-(18) index demonstrated a positive correlation with serum lipid levels in the MI group, and the increase in desaturase index was correlated to a significant increase in the levels of cholesterol, triglyceride, and non-HDL cholesterol. In another study conducted on patients presenting to the hospital due to general health control, D9D activity was found to be positively correlated to serum triglyceride and apolipoprotein B levels.¹⁰ In the present study, D9D-(16) index was higher in women than men in the MI group. It has been reported that increased D9D activity is associated with obesity and insulin resistance and therefore may contribute to the development of type 2 diabetes and cardiovascular disease.³³ Therefore, it was thought that the higher D9D-(16) index in women than in men in the MI group in our study might be due to higher body mass index in women.

In our study, a negative correlation was observed between omega-3 fatty acids with AA and MUFA in the MI group. Furthermore, the presence of a positive correlation observed between AA and total cholesterol and D9D-(18) was considered to contribute to the development of atherosclerosis.

There are many established cardiovascular disease biomarkers with a role progressing from the simple retrospective confirmation of an already diagnosed condition to a central position in screening, diagnostic, and prognostic clinical algorithms.³⁴ However, they have limited value for cardiovascular disease assessment.³⁵ For instance, although troponin I and troponin T are highly specific troponins in the early diagnosis of MI associated with coronary vessel and ventricular remodeling,^{36,37} increases in their levels are neither specific to cardiovascular disease, as they may also increase in several noncardiac conditions, nor do they indicate a specific differential cardiovascular disease etiology.^{34,38,39} Similarly, although natriuretic peptides are used as biomarkers to evaluate pathogenesis, diagnosis, prognosis, and therapy of cardiovascular diseases, their diagnostic value for cardiovascular disease is often complicated by increased levels due to noncardiac conditions with resultant decreases in accuracy or specificity.^{34,40} Therefore, there is obvious need for improved cardiovascular biomarkers with greater specificity.³⁴ On the other hand, it has been reported that the measurement of a combination of biomarkers mutually adjusted may offer additive predictive information and improve cardiovascular risk stratification,⁴¹ because multibiomarker approaches using a pathobiologically diverse

set of biomarkers could have a significant impact on the diagnosis and management of cardiovascular diseases.³⁴ In this study, we investigated the biomarkers of inflammation, oxidation, and lipid metabolism, which are different but complementary pathways involved in the atherosclerotic process in CAD. The finding of significant differences, particularly in the levels of CD59/CRP and lipoxin A4/CRP between MI, USAP, and control patients, suggests that these levels may be used in management of CAD by providing additive predictive information for temporal changes in the atherosclerotic process during the course of the disease.

Although cases of ACS appear in different clinical manifestations and severities, inflammation, oxidative stress, fatty acids, non-fatty acid lipids, and lipid mediators, risk factors are the most important components of the atherosclerosis-ACS puzzle that we are aware of now. However, not all parts of the puzzle have been found yet. Our study contributes by providing evidence that lipid mediators may offer an important advantage over well-established and widely used biomarkers of ACS by providing additive predictive insights for the evaluation of the temporal changes during the entire course of the atherosclerotic process that may contribute to the timely assessment and management of CAD. Therefore, with new and comprehensive research in the future, lipid mediators may be found to be useful in the treatment of atherosclerosis by contributing to the resolution of inflammation, which is necessary for the formation and development of atherosclerosis.

Conflict of Interest Disclosure

The authors have nothing to disclose.

REFERENCES

1. Akilli A. Association for Fighting Hypertension. X. Ege Hypertension Week, Hypertension Training Course, May 29-31, 2008.
2. Mizuno YJ, Jacob RF, Mason RRP. Inflammation and the development of atherosclerosis. *J Atheroscler Thromb*. 2011;18(5):351–358.
3. Chen Y, Zhang F, Dong L, Shu X. Long-term prognostic value of myeloperoxidase on acute coronary syndrome: a meta-analysis. *Arch Med Res*. 2011;42(5):368–374. doi:10.1016/j.arcmed.2011.07.004
4. Merched AJ, Ko K, Gotlinger KH, Serhan CN, Chan L. Atherosclerosis: evidence for impairment of resolution of vascular inflammation governed by specific lipid mediators. *FASEB J*. 2008;22(10):3595–3606. doi:10.1096/fj.08-112201
5. Serhan CN, Krishnamoorthy S, Recchiuti A, Chiang N. Novel anti-inflammatory-pro-resolving mediators and their receptors. *Curr Top Med Chem*. 2011;11(6):629–647. doi:10.2174/1568026611109060629
6. Konukoglu D. Properties, effects and relationships of omega-3 and omega-6 fatty acids with cardiovascular diseases. *Turk Aile Hek Derg*. 2008;12(3):121–129.
7. Ueeda M, Doumei T, Takaya Y, et al. Association of serum levels of arachidonic acid and eicosapentaenoic acid with prevalence of major adverse cardiac events after acute myocardial infarction. *Heart Vessels*. 2011;26(2):145–152. doi:10.1007/s00380-010-0038-8
8. Russo GL. Dietary n-6 and n-3 polyunsaturated fatty acids: from biochemistry to clinical implications in cardiovascular prevention. *Biochem Pharmacol*. 2009;77(6):937–946. doi:10.1016/j.bcp.2008.10.020
9. Das UN. Essential fatty acids and their metabolites could function as endogenous HMG-CoA reductase and ACE enzyme inhibitors, anti-arrhythmic, anti-hypertensive, anti-atherosclerotic, anti-inflammatory, cytoprotective, and cardioprotective molecules. *Lipids Health Dis*. 2008;7:37. doi:10.1186/1476-511X-7-37
10. Kim SR, Jeon SY, Lee SM. The association of cardiovascular risk factors with saturated fatty acids and fatty acid desaturase indices in erythrocyte in middle-aged Korean adults. *Lipids Health Dis*. 2015;14:133. doi:10.1186/s12944-015-0135-x
11. Ahlin F, Arvidsson J, Vargas KG, Stojkovic S, Huber K, Wojta J. MicroRNAs as circulating biomarkers in acute coronary syndromes: a review. *Vascul Pharmacol*. 2016;81:15–21. doi:10.1016/j.vph.2016.04.001
12. Levy BD. Resolvins and protectins: natural pharmacophores for resolution biology. *Prostaglandins Leukot Essent Fatty Acids*. 2010;82(4-6):327–332. doi:10.1016/j.plefa.2010.02.003
13. Serhan CN. Systems approach with inflammatory exudates uncovers novel anti-inflammatory and pro-resolving mediators. *Prostaglandins Leukot Essent Fatty Acids*. 2008;79(3-5):157–163. doi:10.1016/j.plefa.2008.09.012
14. Li B, Xu YJ, Chu XM, et al. Molecular mechanism of inhibitory effects of CD59 gene on atherosclerosis in ApoE (-/-) mice. *Immunol Lett*. 2013;156(1-2):68–81.
15. Swastini DA, Wiryanthini IA, Ariastuti NL, et al. Atherosclerosis prediction with high sensitivity c-reactive protein (hs-CRP) and related risk factor in patient with dyslipidemia. *Open Access Maced J Med Sci*. 2019;7(22):3887–3890.
16. Alexander RW. Inflammation and coronary heart disease. *N Engl J Med*. 1994;331(7):468–469. doi:10.1056/NEJM199408183310709
17. Das UN. Lipoxins as biomarkers of lupus and other inflammatory conditions. *Lipids Health Dis*. 2011;10:76. doi:10.1186/1476-511X-10-76
18. Minuz P, Fava C, Lechi A. Lipid peroxidation, isoprostanes and vascular damage. *Pharmacol Rep*. 2006;58:57–68.
19. Song WL, Paschos G, Fries S, et al. Novel eicosapentaenoic acid-derived F3-isoprostanes as biomarkers of lipid peroxidation. *J Biol Chem*. 2009;284(35):23636–23643. doi:10.1074/jbc.M109.024075
20. Milatovic D, Aschner M. Measurement of isoprostanes as markers of oxidative stress in neuronal tissue. *Curr Protoc Toxicol*. 2009;39:12–14.
21. Szuldrzynski K, Zalewski J, Machnik A, Zmudka K. Elevated levels of 8-iso-prostaglandin F2alpha in acute coronary syndromes are associated with systemic and local platelet activation. *Pol Arch Med Wewn*. 2010;120(1-2):19–24.
22. Williams CM. Lipid metabolism in women. *Proc Nutr Soc*. 2004;63(1):153–160. doi:10.1079/PNS2003314
23. Sakamoto A, Saotome M, Hosoya N, et al. Aberrant serum polyunsaturated fatty acids profile is relevant with acute coronary syndrome. *Heart Vessels*. 2016;31(8):1209–1217. doi:10.1007/s00380-015-0721-x
24. Nishizaki Y, Shimada K, Tani S, et al. Association between the docosahexaenoic acid to arachidonic acid ratio and acute coronary syndrome: a multicenter observational study. *BMC Cardiovasc Disord*. 2016;16(1):143. doi:10.1186/s12872-016-0299-y
25. Kaikkonen JE, Kresanov P, Ahotupa M, et al. High serum n6 fatty acid proportion is associated with lowered LDL oxidation and inflammation: the cardiovascular risk in young Finns study. *Free Radic Res*. 2014;48(4):420–426. doi:10.3109/10715762.2014.883071
26. Hu FB, Stampfer MJ, Manson JE, et al. Dietary fat intake and the risk of coronary heart disease in women. *N Engl J Med*. 1997;337:1491–1499. doi:10.1056/NEJM199711203372102
27. Townsend N, Wilson L, Bhatnagar P, Wickramasinghe K, Rayner M, Nichols M. Cardiovascular disease in Europe: epidemiological update 2016. *Eur Heart J*. 2016;37:3232–3245. doi:10.1093/eurheartj/ehw334
28. Lepedda AJ, Zinellu A, Nieddu G, et al. Human serum albumin Cys34 oxidative modifications following infiltration in the carotid atherosclerotic plaque. *Oxid Med Cell Longev*. 2014;2014:690953. doi:10.1155/2014/690953
29. Kuller LH, Eichner JE, Orchard TJ, Grandits GA, McCallum L, Tracy RP. The relation between serum albumin levels and risk of coronary heart disease in the Multiple Risk Factor Intervention Trial. *Am J Epidemiol*. 1991;134:1266–1277. doi:10.1093/oxfordjournals.aje.a116030

30. Danesh J, Collins R, Appleby P, Peto R. Association of fibrinogen, C-reactive protein, albumin, or leukocyte count with coronary heart disease: meta-analyses of prospective studies. *JAMA*. 1998;279:1477–1482. doi:10.1001/jama.279.18.1477
31. Yoshioka G, Tanaka A, Nishihira K, et al. Prognostic impact of follow-up serum albumin after acute myocardial infarction. *ESC Heart Fail*. 2021;8(6):5456–5465. doi:10.1002/ehf2.13640
32. Camps J, García-Heredia A. Oxidative stress and inflammation in non-communicable diseases-molecular mechanisms and perspectives in therapeutics. *Adv Exp Med Biol*. 2014;824:1–4. doi:10.1007/978-3-319-07320-0_1
33. Cho JS, Baek SH, Kim JY, Lee JH, Kim OY. Serum phospholipid monounsaturated fatty acid composition and delta-9-desaturase activity are associated with early alteration of fasting glycemic status. *Nutr Res*. 2014;34(9):733–741. doi:10.1016/j.nutres.2014.08.005
34. Omran F, Kyrou I, Osman F, Lim VG, Randeva HS, Chatha K. Cardiovascular biomarkers: lessons of the past and prospects for the future. *Int J Mol Sci*. 2022;23:5680. doi:10.3390/ijms23105680
35. Piepoli MF, Hoes AW, Agewall S, et al; ESC Scientific Document Group. 2016 European guidelines on cardiovascular disease prevention in clinical practice: the Sixth Joint Task Force of the European Society of Cardiology and Other Societies on Cardiovascular Disease Prevention in Clinical Practice (constituted by representatives of 10 societies and by invited experts): developed with the special contribution of the European Association for Cardiovascular Prevention & Rehabilitation (EACPR). *Eur Heart J*. 2016;37:2315–2381. doi:10.1093/eurheartj/ehw106
36. The Joint European Society of Cardiology/American College of Cardiology Committee. Myocardial infarction redefined—a consensus document of the Joint European Society of Cardiology/American College of Cardiology Committee for the Redefinition of Myocardial Infarction. *J Am Coll Cardiol*. 2000;36:959–969.
37. Thygesen K, Alpert JS, Jaffe AS, et al; Joint ESC/ACCF/AHA/WHF Task Force for Universal Definition of Myocardial Infarction. Third universal definition of myocardial infarction. *J Am Coll Cardiol*. 2012;60:1581–1598. doi:10.1016/j.jacc.2012.08.001
38. Thygesen K, Mair J, Katus H, et al. Recommendations for the use of cardiac troponin measurement in acute cardiac care. *Eur Heart J*. 2010;31:2197–2204.
39. Giannitsis E, Katus HA, Agewall S, Giannitsis E, Jernberg T, Katus H. Cardiac troponin level elevations not related to acute coronary syndromes. Troponin elevation in coronary vs. non-coronary disease. *Nat Rev Cardiol Eur Heart J*. 2013;2011;1032:623404–634411.
40. Pemberton CJ, Charles CJ, Richards AM. Cardiac natriuretic peptides. In: Schisler JC, Lang CH, Willis MS, eds. *Endocrinology of the Heart in Health and Disease: Integrated, Cellular, and Molecular Endocrinology of the Heart*. Academic Press; 2016:1–354.
41. Blankenberg S, Zeller T, Saarela O, et al; MORGAM Project. Contribution of 30 biomarkers to 10-year cardiovascular risk estimation in 2 population cohorts: the MONICA, Risk, Genetics, Archiving, and Monograph (MORGAM) Biomarker Project. *Circulation*. 2010;121(22):2388–2397. doi:10.1161/CIRCULATIONAHA.109.901413

The value of metagenomic next-generation sequencing for the diagnosis of pulmonary tuberculosis using bronchoalveolar lavage fluid

Jiali Gao, MD^{1,2}, Lu Zhao, MD^{1,2}, Gongqi Chen, MD^{1,2}, Chunli Huang, MM^{1,2}, Weiqiang Kong, MD^{1,2}, Yuchen Feng, MD^{1,2}, Guohua Zhen, MD^{1,2}

¹Division of Respiratory and Critical Care Medicine, Department of Internal Medicine, Tongji Hospital, Tongji Medical College, Huazhong University of Science and Technology, Wuhan, China, ²Key Laboratory of Respiratory Diseases, National Health Commission of the People's Republic of China, and National Clinical Research Center for Respiratory Diseases, Wuhan, China. Corresponding author: Guohua Zhen; ghzhen@tjh.tjmu.edu.cn

Key words: pulmonary tuberculosis; metagenomic next-generation sequencing; bronchoalveolar lavage fluid; diagnostic performance

Abbreviations: mNGS, metagenomic next-generation sequencing; MTBC, *Mycobacterium tuberculosis* complex; PTB, pulmonary tuberculosis; BALF, bronchoalveolar lavage fluid; AFB, acid-fast bacillus; ROC curve, receiver operating characteristic curve; AUC, area under the curve

Laboratory Medicine 2024;55:96-102; <https://doi.org/10.1093/labmed/lmad041>

ABSTRACT

Objective: The aim of this study was to compare metagenomic next-generation sequencing (mNGS) with other methods, including Xpert MTB/RIF, *Mycobacterium tuberculosis* (MTB) culture, and acid-fast bacillus (AFB) staining in the diagnosis of pulmonary tuberculosis (PTB) using bronchoalveolar lavage fluid (BALF).

Methods: The data of 186 patients with suspected PTB were retrospectively collected from January 2020 to May 2021 at Tongji Hospital. BALF samples were collected from all patients and analyzed using AFB staining, MTB culture, Xpert MTB/RIF, and mNGS.

Results: Of the 186 patients, 38 patients were ultimately diagnosed as PTB. Metagenomic next-generation sequencing exhibited a sensitivity of 78.95%, which was higher than AFB staining (27.59%) and MTB culture (44.12%) but similar to Xpert MTB/RIF (72.73%). Utilization of combined methods demonstrates improvement for PTB diagnosis. In support of this, the area under the receiver operating characteristic curve for the combination of mNGS and MTB culture (0.933, 95% CI: 0.871, 0.995) was larger than those of mNGS, Xpert MTB/RIF, MTB culture, and the combination of Xpert MTB/RIF and MTB culture.

Conclusion: The sensitivity of mNGS in the diagnosis of PTB using BALF specimen is similar to Xpert MTB/RIF. Metagenomic next-generation sequencing in combination with MTB culture may further improve the diagnosis of pulmonary tuberculosis.

Tuberculosis is a communicable disease caused by *Mycobacterium tuberculosis* complex (MTBC) infection, and it was one of the leading causes of ill health and death before the COVID-19 epidemic. The MTBC consists of *Mycobacterium tuberculosis*, *Mycobacterium bovis*, *Mycobacterium africanum*, *Mycobacterium microti*, *Mycobacterium pinnipedii*, *Mycobacterium caprae*, and *Mycobacterium canettii*. The disease can affect different systems but mainly affects the lungs, which is known as pulmonary tuberculosis (PTB). According to the global report of the World Health Organization in 2021, about a quarter of the world's population is infected with MTB.^{1,2}

The diagnosis of PTB relies on isolation of MTBC from the sputum or bronchoalveolar lavage fluid (BALF). The MTB culture is generally considered as the gold standard for tuberculosis diagnosis but requires a relatively long time. Solid media culture can take 4 to 8 weeks. Although liquid media culture is more sensitive and rapid than solid media culture, it requires several weeks and is more likely to be contaminated.³ Acid-fast bacillus (AFB) staining and microscopy is rapid, convenient, and inexpensive; therefore, it is widely used in the detection of MTBC in clinical practice. However, the positive rate of AFB staining is relatively low and it cannot distinguish nontuberculosis mycobacteria from MTBC.⁴ In view of the time-consuming and low positive rates of traditional methods, faster molecular and microbial diagnosis techniques are needed to facilitate early diagnosis.⁵ In 2010, the World Health Organization recommended the use of Xpert MTB/RIF, a novel nucleic acid amplification test that can simultaneously detect MTBC and rifampicin resistance.⁶ A simple and rapid method, Xpert MTB/RIF has been proven to be sensitive and highly specific in the early diagnosis of pulmonary tuberculosis.⁷

Metagenomic next-generation genome sequencing (mNGS) is a new method based on sequence identification of pathogenic microorganisms, which has been used to diagnose pathogens causing various infectious syndromes, including respiratory tract infections,^{8,9} bloodstream infection,^{10,11} meningitis, and encephalitis.^{12,13} However, the detection efficiency in the BALF specimens of patients suspected of PTB still lacks clinical application examples. Here, we compared the diagnostic

performance of mNGS for detection of MTBC in BALF with Xpert MTB/RIF, MTB culture, and AFB staining.

Methods

Study Subjects and Design

We retrospectively reviewed patients suspected of having PTB at the Tongji Hospital of Huazhong University of Science and Technology between January 2020 and May 2021. Inclusion criteria were (1) clinically suspected PTB patients with symptoms of tuberculosis infection such as subacute cough, fever, night sweat, and loss of weight; (2) chest computed tomography or X-ray with miliary pulmonary nodules or patchy shadows; and (3) BALF were submitted to mNGS test and MTB culture, Xpert MTB/RIF, or AFB staining. Exclusion criteria were (1) no paired MTB culture or Xpert MTB/RIF for the mNGS test and (2) incomplete medical history.

The criteria for the diagnosis of PTB were (1) MTB culture was positive, (2) Xpert MTB/RIF was positive, (3) mNGS was positive, or (4) the pathological features of lung biopsy were consistent with those of tuberculosis. Otherwise, patients were classified as non-PTB cases, including infectious diseases caused by pathogens other than MTB or noninfectious diseases such as tumors and autoimmune diseases.

This study was conducted in accordance with the Declaration of Helsinki (as revised in 2013). This study was approved by the Ethics Committee of Tongji Hospital, Huazhong University of Science and Technology (No. TJ-IRB20220167), and individual consent for this retrospective analysis was waived.

BALF Specimens

Bronchoalveolar lavage fluid was collected by bronchoscopy at the sites of lung lesions. All patients signed an informed consent form before undergoing bronchoscopy. Saline (60 mL–100 mL) was injected into the bronchial lumen of the segment and withdrawn after washing briefly. The qualified BALF (at least 20 mL) was divided into 4 parts, 3 of which were tested by AFB staining, MTB culture, and Xpert MTB/RIF, and the rest were stored in a sterile container at -20°C , and sent to BGI for mNGS testing.

mNGS and Analysis

The process of mNGS consisted of sample processing, nucleic acid extraction, library generation, and bioinformatic pipeline analysis as described previously.¹⁴ A RefSeq analysis at the time of testing included 6350 bacterial genomes sequence (including 133 mycobacteria and 122 *Mycoplasma/Chlamydia/Rickettsia*), 1798 genomes of DNA viruses, 1064 genomes of fungi, and 234 genomes of parasites associated with human diseases. *Mycobacterium tuberculosis* was considered positive when at least 1 read is mapped to MTBC (strictly mapped to the number of sequences at the genus level).

Statistical Analysis

The sensitivity, specificity, positive predictive value, and negative predictive value of mNGS, Xpert MTB/RIF, MTB culture, and AFB staining were calculated. McNemar's test for a paired 4-fold table were conducted for comparing the results of mNGS and Xpert MTB/RIF, MTB culture, and AFB staining. Data analysis was performed with SPSS 22.0. Receiver operating characteristic (ROC) curve was plotted with MedCalc software (MedCalc Software) among different groups, and the area under the

curve (AUC) was calculated. *P* values $<.05$ were considered significant, and all tests were two tailed.

Results

Characteristics of Participants

A total of 274 patients presenting with suspected PTB between January 2020 and May 2021 were initially included in our study. Eighty-eight patients were excluded from the study according to the exclusion criteria. Of these, 78 patients did not have a paired MTB culture test or Xpert MTB/RIF test, and 10 of them had an incomplete medical history. Finally, 186 patients with suspected PTB were eventually included in the study, of which 38 were diagnosed with PTB and 148 were diagnosed as non-PTB. Among the 38 PTB patients, 37 patients met the microbiological or molecular diagnostic criteria, and 1 patient was diagnosed based on pathological findings. Thirty-one patients were diagnosed with PTB for the first time and 7 were diagnosed with PTB and had received antituberculosis treatment before. Among the 148 non-PTB patients, 118 cases were diagnosed as lung infections caused by other pathogens, 5 cases were diagnosed as nontuberculosis mycobacteria lung disease, 9 cases were diagnosed as lung cancer, and 16 cases were diagnosed as other diseases (FIGURE 1).

The average age of PTB patients was 49.00 years (range, 30.25–57.00), and 65.8% were male. For non-PTB patients, the average age was 55.00 years (range, 42.25–62.75), and 62.2% were male (TABLE 1). There was no significant difference in underlying lung diseases (chronic obstructive pulmonary disease, bronchiectasis, connective tissue disease-related lung disease, or idiopathic pulmonary fibrosis) between the 2 groups. Patients with PTB had a higher proportion of previous history of tuberculosis ($P = .036$, TABLE 1). Therefore, it was necessary to routinely screen for active tuberculosis for patients with a history of tuberculosis. There was no significant difference in extrapulmonary diseases including diabetes, hypertension, chronic liver disease, and hematological malignancy between the 2 groups.

Detection Results and Concordance of mNGS, Xpert, and MTB Culture Using BALF

The results of mNGS, Xpert MTB/RIF, MTB culture, and AFB staining for MTBC detection in BALF were summarized and are shown in FIGURE 2A. Of the 186 enrolled patients, mNGS and Xpert showed similar overall MTBC detection efficiency (26/166, 15.66% vs 24/166, 14.46%, $P > .05$). However, mNGS and Xpert were more effective than MTB culture (27/161, 16.77% vs 15/161 9.32%, $P < .01$) and AFB staining (22/171, 12.87% vs 9/171, 5.26%, $P < .001$) (FIGURE 2B, Supplementary Table 1). There were 142 patients whose BALF specimens were tested by mNGS, Xpert MTB/RIF, and culture at the same time. Among these 142 patients, the results of mNGS, Xpert MTB/RIF, and MTB culture matched completely in 121 (85.2%) patients, including 9 PTB patients with positive findings and 112 non-PTB patients with negative findings in all 3 methods. The detection results of the remaining 21 samples were conflicting, including 7 samples being positive by mNGS only (4.9%), 4 samples being positive by Xpert MTB/RIF only (2.8%), 6 samples being positive for mNGS and Xpert MTB/RIF (4.2%), 2 samples being positive for mNGS and MTB culture (1.4%), and 2 samples being positive for Xpert MTB/RIF and MTB culture (1.4%). There were no samples that were positive by MTB culture only (FIGURE 2C).

FIGURE 1. Flow chart of patient enrollment and test results. A total of 186 patients were ultimately included for further analysis. Bronchoalveolar lavage fluid samples were tested using metagenomic next-generation sequencing (mNGS), Xpert MTB/RIF, *Mycobacterium tuberculosis* (MTB) culture, and acid-fast bacillus (AFB) staining. Patients were diagnosed with pulmonary tuberculosis (PTB) and nonpulmonary tuberculosis (non-PTB) as described in the Methods. NTM, nontuberculosis mycobacteria lung disease.

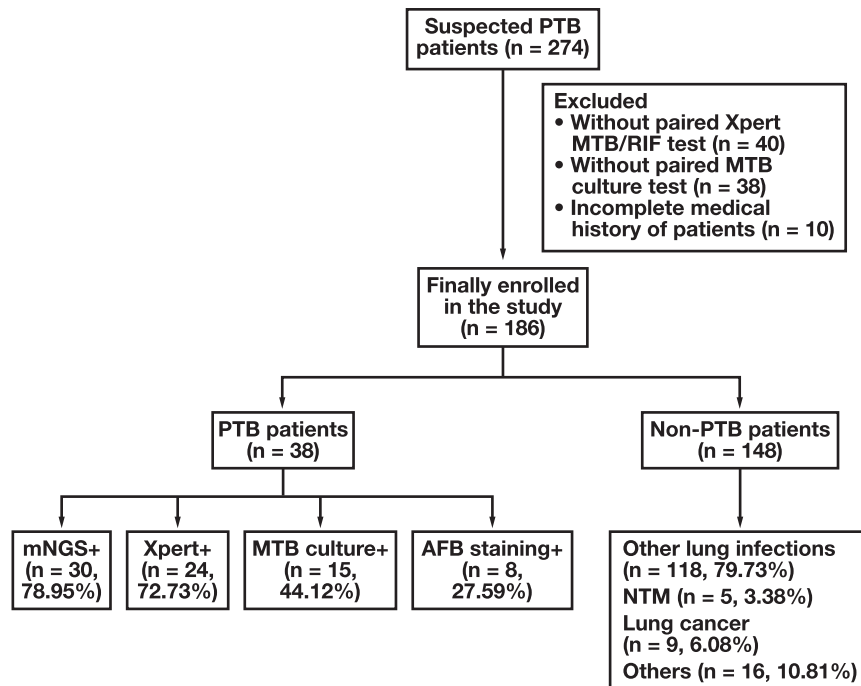


TABLE 1. Characteristics of patients with PTB and non-PTB^a

	PTB (n = 38)	Non-PTB (n = 148)	P value
Demographic data			
Average age (range), y	49.00 (30.25–57.00)	55.00 (42.25–62.75)	.057
Male	25 (65.8)	92 (62.2)	.680
Female	13 (34.2)	56 (37.8)	.680
Underlying pulmonary disease			
COPD	0	4 (2.7)	—
Bronchiectasis	0	11 (7.4)	—
Idiopathic pulmonary fibrosis	0	5 (3.4)	—
Connective tissue disease-associated pulmonary disease	0	18 (12.2)	—
Previous history of tuberculosis	7 (18.4)	9 (6.1)	.036
Underlying extrapulmonary diseases			
Diabetes	3 (7.9)	0	—
Hypertension	1 (2.6)	0	—
Chronic liver disease	3 (7.9)	0	—
Hematological malignancy	3 (7.9)	2 (1.4)	.096

COPD, chronic obstructive pulmonary disease; PTB, pulmonary tuberculosis.

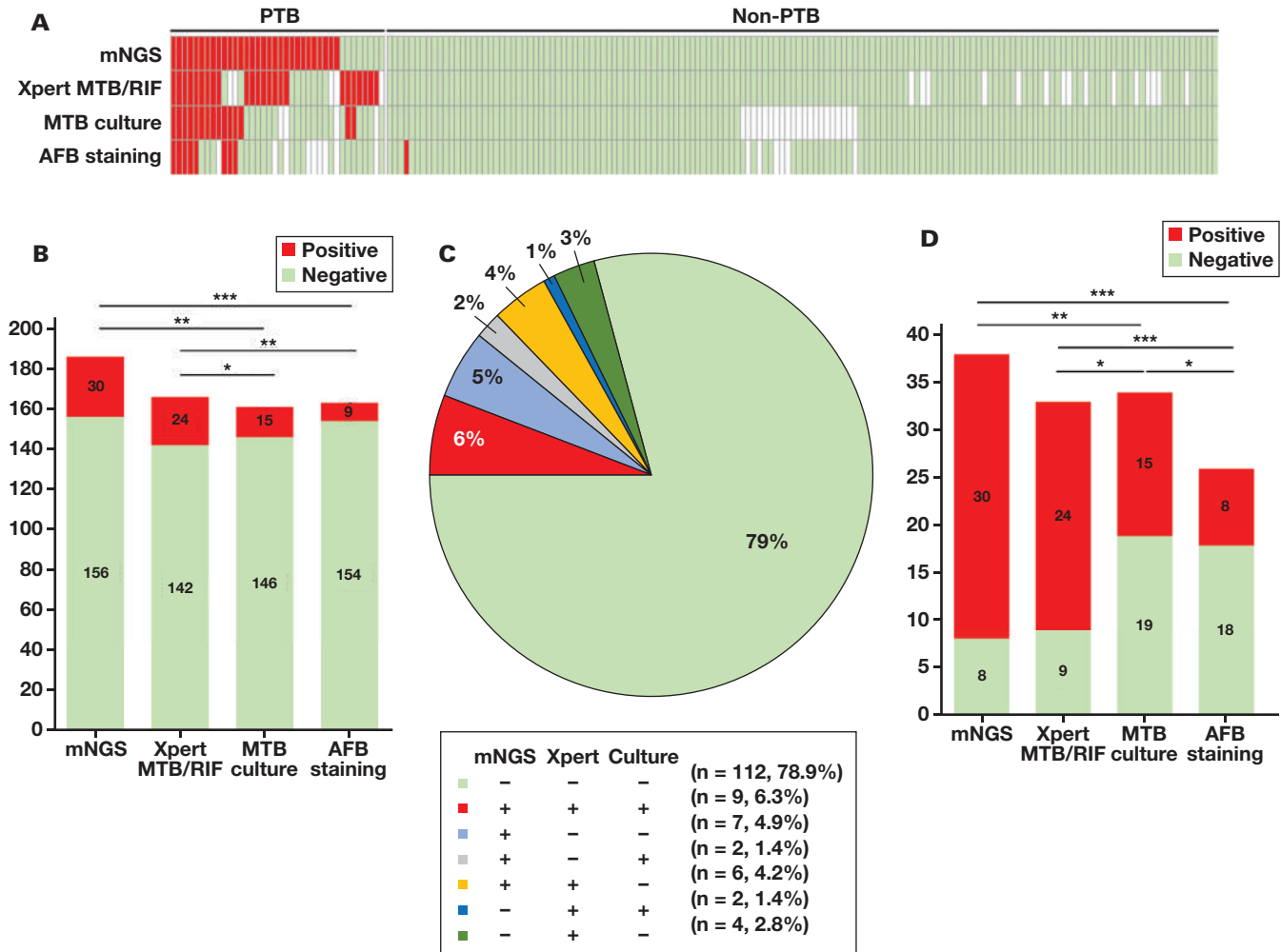
^aData are given as number (%) except where noted.

We also analyzed the detection efficiency of the 4 methods in the 38 PTB patients (FIGURE 2D, Supplementary Table 2). Of the 38 PTB patients, 30 were tested using mNGS, Xpert MTB/RIF, and MTB. Among these 30 BALF samples, 9 (9/30, 30.0%) were all positive by mNGS, Xpert MTB/RIF, and MTB culture, 6 (6/30, 20.0%) were positive by mNGS and Xpert MTB/RIF, 2 (2/30, 6.7%) were positive by mNGS and MTB culture, and 7 (7/30, 23.3%) were only positive by mNGS (FIGURE 2E and 2F).

Diagnostic Performance of mNGS, Xpert, Culture, and AFB Staining Using BALF

The diagnostic performance of mNGS, Xpert MTB/RIF, MTB culture, and AFB staining using BALF specimens was evaluated. For the 38 PTB patients, the sensitivity of mNGS (78.95%, 30/38) was similar to that of Xpert MTB/RIF (72.73%, 24/33) but significantly higher than the sensitivity of MTB culture (44.12%, 15/34) and AFB staining (27.59%,

FIGURE 2. Comparison of metagenomic next-generation sequencing (mNGS), Xpert MTB/RIF, *Mycobacterium tuberculosis* (MTB) culture, and acid-fast bacillus (AFB) staining for the detection of MTB complex (MTBC). **A**, Heatmap depicting the identification of MTBC by the 4 methods in bronchoalveolar lavage fluid samples. Each column represents a patient. **B**, The number of positive and negative findings by each of the 4 methods in all 186 enrolled patients. **C**, For mNGS, Xpert MTB/RIF, and MTB culture, the number and percentage of patients with positive or negative findings by 1, 2, or 3 methods in 142 patients are shown in the pie chart. **D**, The number of positive and negative findings by each of the 4 methods in 38 pulmonary tuberculosis (PTB) patients. * $P < .05$; ** $P < .01$; *** $P < .001$.



8/29) (TABLE 2). The negative predictive values of mNGS, Xpert MTB/RIF, MTB culture, and AFB staining were 94.87%, 93.66%, 86.99%, and 87.04%, respectively (TABLE 2).

To better understand the diagnostic performance of mNGS, Xpert MTB/RIF, MTB culture, and the combination of the 3 methods, we plotted the ROC curve and calculated the AUC. The AUC for mNGS (0.900, 95% CI: 0.827, 0.973) was larger than that of the other tests (0.850, 95% CI: 0.767, 0.933 for Xpert MTB/RIF; 0.717, 95% CI: 0.626, 0.807 for MTB culture). The AUC for MTB culture in combination with mNGS (0.933, 95% CI: 0.871, 0.995) was larger than that of the MTB culture in combination with Xpert MTB/RIF (0.883, 95% CI: 0.806, 0.960). These results suggested that mNGS has a better diagnostic performance than other methods (FIGURE 3).

Burden of MTBC Affects the Results of mNGS

The cell wall of MTBC is difficult to destroy, and this leads to the difficulty of DNA extraction for mNGS. Therefore, the sensitivity

of mNGS in detecting MTBC could be affected by the burden of MTBC. We compared reads numbers of MTBC between the patients with smear AFB staining positive and negative results. Of the 30 mNGS-positive samples, we found that the reads number of MTBC was significantly higher in AFB staining-positive groups (FIGURE 4A). Because positive findings in AFB staining indicate high burden of MTBC, our result suggests that the MTBC burden affects the reads number of mNGS.

In our study, there were 8 mNGS-positive samples with 1 read mapped to either the species or genus of MTBC. Of these 8 samples, 4 cases were also positive by Xpert or MTB culture and the other 4 cases (50%) were only positive by mNGS (FIGURE 4B). Based on the low possibility of MTBC contamination during mNGS testing^{14,15} and the previous report that samples with only 1 read of MTBC were all confirmed to be PTB,¹⁶ the other 4 cases were also diagnosed as PTB.

FIGURE 2. (cont) E, For mNGS, Xpert MTB/RIF, and MTB culture, the number and percentage of patients with positive or negative findings by 1, 2, or 3 methods in 30 PTB patients are shown. F, The number of positive findings by 1, 2, and all 3 methods including mNGS, Xpert MTB/RIF, and MTB culture in 30 PTB patients are shown in the Venn diagram.

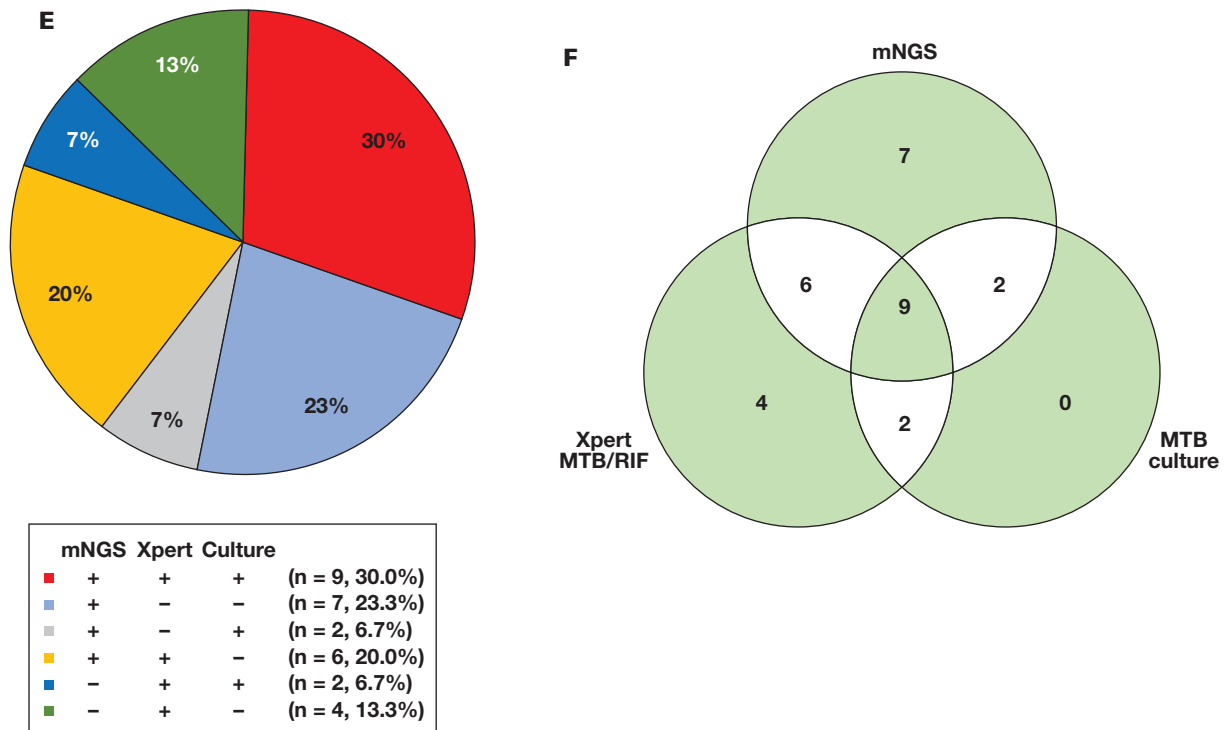


TABLE 2. Diagnostic performance of mNGS, Xpert MTB/RIF, MTB culture and AFB staining for PTB using BALF^a

	PTB	non-PTB	Sensitivity (95% CI)	Specificity (95% CI)	PPV (95% CI)	NPV (95%CI)
mNGS			78.95% (0.622-0.899)	100% (0.968-1.000)	100% (0.859-1.000)	94.87% (0.898-0.976)
Positive	30	0				
Negative	8	148				
Xpert MTB/RIF			72.73% (0.542-0.861)	100% (0.965-1.000)	100% (0.828-1.000)	93.66% (0.880-0.969)
Positive	24	0				
Negative	9	133				
MTB culture			44.12% (0.276-0.619)	100% (0.963-1.000)	100% (0.747-1.000)	86.99% (0.802-0.918)
Positive	15	0				
Negative	19	127				
AFB staining			27.59% (0.134-0.475)	99.30% (0.956-0.999)	88.89% (0.507-0.994)	87.04% (0.806-0.916)
Positive	8	1				
Negative	21	141				

AFB, acid-fast bacillus; mNGS, metagenomic next-generation sequencing; MTB, Mycobacterium tuberculosis; NPV, negative predictive value (the number of true negative cases detected by this method/the number of all negative cases detected by this method × 100%); PPV, positive predictive value (the number of true positive cases detected by this method/the number of all positive cases detected by this method × 100%); PTB, pulmonary tuberculosis. ^aSensitivity is the number of positive cases detected by this method/the number of PTB cases by clinical diagnosis × 100%. Specificity is the number of negative cases detected by this method/excluded PTB cases × 100%.

Discussion

Recently, the sensitivity of mNGS to detect mycobacteria tuberculosis in clinical specimens has received great attention due to its short turnaround time and unbiased pathogen detection.¹⁷ In the present study, we demonstrated that the sensitivity of mNGS in the diagnosis of PTB using BALF specimen is similar to Xpert MTB/RIF but significantly higher than AFB staining and MTB culture. The combination of mNGS and MTB culture may further improve the diagnosis of PTB.

A cohort of 186 patients suspected of having PTB infection were enrolled in this study, of which 38 patients were finally diagnosed with PTB. In terms of diagnostic performance in BALF samples, mNGS exhibited a sensitivity of 78.95%, which was similar to Xpert MTB/RIF (72.73%) but much higher than the sensitivity of MTB culture (44.12%) and AFB staining (27.59%). The AUC for MTB culture in combination with mNGS (0.933, 95% CI: 0.871, 0.995) was larger than that of MTB culture combined with Xpert MTB/

of Xpert or MTB culture. Although the other 4 cases were not confirmed by other tests or anti-TB therapy, based on the rationale and the study mentioned, these 4 cases were diagnosed as PTB.

The limitations of our study are that this was a retrospective study and the sample size was relatively small. This might have introduced bias in our interpretation of the data. Therefore, prospective studies with large sample sizes are required to evaluate the diagnostic efficiency of mNGS in the diagnosis of PTB using BALF specimens.

Conclusions

The sensitivity of mNGS in the diagnosis of PTB using BALF specimen is similar to Xpert MTB/RIF but much higher than MTB culture and AFB staining. The use of mNGS in combination with MTB culture may further improve the diagnosis of PTB.

Supplementary Material

Supplementary material is available at *Laboratory Medicine* online.

Funding

This work was supported by National Natural Science Foundation of China (grant No. 82170036).

Conflict of Interest Disclosure

The authors have nothing to disclose.

REFERENCES

1. Harding E. WHO global progress report on tuberculosis elimination. *Lancet Respir Med*. 2020;8:19. doi:10.1016/s2213-2600(19)30418-7
2. Zumla A, George A, Sharma V, et al. The WHO 2014 Global Tuberculosis Report—further to go. *Lancet Global Health*. 2015;3:e10–e12. doi:10.1016/S2214-109X(14)70361-4
3. World Health Organization. *Implementing Tuberculosis Diagnostics: A Policy Framework*. WHO/HTM/TB/201511. World Health Organization; 2015.
4. Philip N, William T, John DV. Diagnosis of tuberculous meningitis: challenges and promises. *Malays J Pathol*. 2015;37:1–9.
5. Rock RB, Olin M, Baker CA, et al. Central nervous system tuberculosis: pathogenesis and clinical aspects. *Clin Microbiol Rev*. 2008;21:243–261, table of contents. doi:10.1128/CMR.00042-07
6. WHO Guidelines Approved by the Guidelines Review Committee. *Policy Statement: Automated Real-Time Nucleic Acid Amplification Technology for Rapid and Simultaneous Detection of Tuberculosis and Rifampicin Resistance: Xpert MTB/RIF System*. World Health Organization; 2011.
7. Horne DJ, Kohli M, Zifodya JS, et al. Xpert MTB/RIF and Xpert MTB/RIF Ultra for pulmonary tuberculosis and rifampicin resistance in adults. *Cochrane Database Syst Rev*. 2019;6:CD009593. doi:10.1002/14651858.CD009593.pub4
8. Langelier C, Zinter MS, Kalantar K, et al. Metagenomic sequencing detects respiratory pathogens in hematopoietic cellular transplant patients. *Am J Respir Crit Care Med*. 2018;197:524–528. doi:10.1164/rccm.201706-1097le
9. Robert S, Krista Q, Keith S, et al. Viral pathogen detection by metagenomics and pan-viral group polymerase chain reaction in children with pneumonia lacking identifiable etiology. *J Infect Dis*. 2017;1407.
10. Blauwkamp TA, Thair S, Rosen MJ, et al. Analytical and clinical validation of a microbial cell-free DNA sequencing test for infectious disease. *Nat Microbiol*. 2019;4:663–674. doi:10.1038/s41564-018-0349-6
11. Goggin KP, Gonzalez-Pena V, Inaba Y, et al. Evaluation of plasma microbial cell-free DNA sequencing to predict bloodstream infection in pediatric patients with relapsed or refractory cancer. *JAMA Oncol*. 2019;6:552–556.
12. Wilson MR, Sample HA, Zorn KC, et al. Clinical metagenomic sequencing for diagnosis of meningitis and encephalitis. *N Engl J Med*. 2019;380:2327–2340.
13. Zhang JZ, Zheng P, Sun HM, et al. Next-generation sequencing combined with routine methods to detect the pathogens of encephalitis/meningitis from a Chinese tertiary pediatric neurology center. *J Infect*. 2019;78:409–421.
14. Miao Q, Ma Y, Wang Q, et al. Microbiological diagnostic performance of metagenomic next-generation sequencing when applied to clinical practice. *Clin Infect Dis*. 2018;67:S231–S240. doi:10.1093/cid/ciy693
15. Shi CL, Han P, Tang PJ, et al. Clinical metagenomic sequencing for diagnosis of pulmonary tuberculosis. *J Infect*. 2020;81:567–574. doi:10.1016/j.jinf.2020.08.004
16. Liu X, Chen Y, Ouyang H, et al. Tuberculosis diagnosis by metagenomic next-generation sequencing on bronchoalveolar lavage fluid: a cross-sectional analysis. *Int J Infect Dis*. 2021;104:50–57. doi:10.1016/j.ijid.2020.12.063
17. Gu W, Miller S, Chiu CY. Clinical metagenomic next-generation sequencing for pathogen detection. *Annu Rev Pathol*. 2019;14:319–338. doi:10.1146/annurev-pathmechdis-012418-012751
18. Zhou X, Wu H, Ruan Q, et al. Clinical evaluation of diagnosis efficacy of active mycobacterium tuberculosis complex infection via metagenomic next-generation sequencing of direct clinical samples. *Front Cell Infect Microbiol*. 2019;9:351. doi:10.3389/fcimb.2019.00351
19. Doughty EL, Sergeant MJ, Adetifa I, et al. Culture-independent detection and characterisation of *Mycobacterium tuberculosis* and *M. africanum* in sputum samples using shotgun metagenomics on a benchtop sequencer. *PeerJ*. 2014;2:e585. doi:10.7717/peerj.585a

Digynic monoandric triploidy in the setting of recurrent pregnancy loss: a case report and literature review

Caitlin Raymond, MD, PhD¹*, Song Han, PhD¹, Gengming Huang, PhD¹, Cecilia Clement, MD¹, Harshwardhan Thaker, MD, PhD¹, Jianli Dong MD, PhD¹*

¹Department of Pathology, University of Texas Medical Branch, Galveston, TX, US. Corresponding author: Jianli Dong; jjdong@UTMB.EDU

Key words: product of conception; triploid gestation; digynic triploid; chromosome microarray; microsatellite DNA; genetics

Abbreviations: CMA, chromosomal microarray analysis; CNVs, copy number variants; SNV, single nucleotide variant; POC, product of conception; PCR, polymerase chain reaction; STR, short tandem repeat; IVF, in vitro fertilization

Laboratory Medicine 2024;55:103-105; <https://doi.org/10.1093/labmed/lmad036>

ABSTRACT

Triploidy is a genetic occurrence in which the chromosome count is $3n = 69$ with a double ($2n$) chromosomal contribution to the conceptus from one parent. Such pregnancies are usually nonviable and are estimated to account for approximately 1% of recognized conceptions and 10% of recognized miscarriages. Majority opinion is that fetal losses due to triploidies are caused by the presence of 2 copies of paternal chromosomes. In this study, we present a digynic monoandric triploid miscarriage from a 32-year-old G7P1051 at approximately 13 weeks gestation, in which 2 copies of the maternal chromosomes are present in the fetus. This unusual phenomenon is supported by nonmolar placental histology, chromosomal microarray, and short tandem repeat assays, with the latter 2 being discussed in detail. Furthermore, this study includes discussion of recurrent miscarriage, recurrent triploidy, and long-term clinical follow-up of the patient.

Clinical History

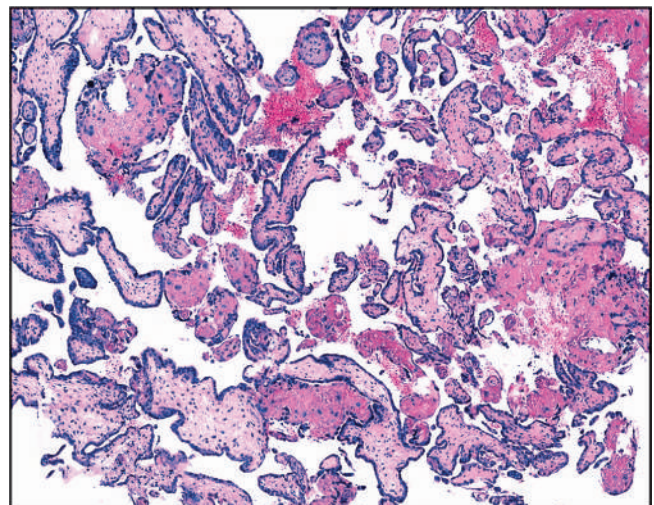
A 32-year-old female G7P1051, at approximately 13 weeks gestation by last menstrual period, presented to our clinic for routine prenatal care. Chart review established the patient as a “habitual aborter” with 5 abortions (1 therapeutic and 4 spontaneous). Clinical staff were unable to identify fetal heart tones via Doppler and referred the patient to the maternal-fetal medicine department for a viability ultrasound. The viability ultrasound was negative (gestational age was corrected to 12 weeks and 3 days) and patient was diagnosed with a missed abortion. One week later, the patient presented

for inpatient management with misoprostol but experienced heavy vaginal bleeding unresponsive to uterotonics and underwent an emergent dilation and curettage. Pathologic evaluation revealed the placental tissue to be grossly normal in appearance (not cystic), and microscopic examination of the placental tissue demonstrated nonmolar chorionic villi with mildly accelerated maturation (**FIGURE 1**). The fetus was small for gestation (weight 15 g vs expected 30 g and crown-rump length 6.5 cm vs expected 8.7 cm) and there was discordance between head versus abdominal circumferences (asymmetric intrauterine growth restriction) (data not shown). There were no other gross anomalies on external examination of the fetus, with normal facies, intact lips and palate, patent nares and choanae, normally placed ears, a normally placed patent anus and normally formed immature genitalia. These pathologic features are consistent with a triploid gestation.^{1,2} Tissue was subsequently sent to the molecular laboratory for genetic testing.

Laboratory Role in Diagnosis

Chromosomal microarray analysis (CMA) is used to determine whether there are aberrations in DNA copy number (or copy number variants, CNVs) in a sample. The CMA has become a first-tier assay for prenatal chromosomal analysis.^{3,4} There are 2 ways to generate CMA signals.^{5,6} The first is

FIGURE 1. Histologic examination of products of conception. H&E stain of placental tissue demonstrating nonmolar chorionic villi, an important feature of digynic monoandric gestations.



comparative genomic hybridization, in which genomic DNA from both the patient sample and a reference control is enzymatically cut, fluorescently labeled with different fluorophores, mixed in a 50:50 ratio, and then allowed to competitively hybridize to oligonucleotide DNA probes on a microarray. The presence of a relative fluorescence signal in a sample versus reference is compared to check for DNA gains and losses in patient sample. A second way to generate CMA results is by labeling only DNA from patient sample competitive hybridization to control DNA. Instead, the intensity of labeled patient DNA is compared with an *in silico* reference set.^{5,6} Both oligonucleotide and single nucleotide variant (SNV) probes are used for CMA assays. Oligo probes are used to measure gains and losses of DNA copy numbers, and SNV probes are located at specific SNV loci allowing CMAs to genotype nucleotide variations at single base pair sites, a feature that is used to examine long regions of homozygosity. Chromosomal microarray analyses for clinical use contain several hundred thousand to a couple million oligo and SNV probes to have whole genome coverage.^{5,6}

Chromosomal microarray in this case was performed using a formalin-fixed umbilical cord sample, which avoids maternal cell contamination, and examined with Affymetrix OncoScan microarray (Thermo Fisher Scientific). This array consists of over 220,000 oligonucleotide and SNV probes. It uses molecular inversion probes and has been validated for genomic profiling of constitutional cytogenomic abnormalities in formalin-fixed product of conception (POC) samples.⁷ Genomic DNA was extracted and purified using QIAamp DNA FFPE Tissue Kit (Qiagen). Procedures for DNA anneal, gap fill, polymerase chain reaction (PCR), amplicon DNA fragmentation, restriction digestion, and hybridization of arrays were performed according to manufacturer's instructions (Affymetrix). Results were investigated using the Chromosome Analysis Suite made by Affymetrix (Thermo Fisher Scientific). The settings for the smallest CNV regions in the Chromosome Analysis Suite were 25 Kb and 25 markers for losses and 50 Kb and 50 markers for gains. Interpretation of the results was done by using publicly available CNV databases and published literature following practice guidelines.⁸ The CMA result in the POC sample was triploidy: arr(X)x2,(Y)x1,(1-22)x3, consistent with 69, XXY karyotype (FIGURE 2).

To identify the parental origin of the extra set of chromosomes, short tandem repeat (STR) testing was performed using Applied Biosystem

AmpFLSTR Identifier PCR Amplification Kit (Thermo Fisher Scientific). The STR loci are definable microsatellite repeats of genomic DNA. A maternal blood sample was available for the analysis. Conceptually, each chromosome in the mother should have uniquely identifiable STR loci, which can then be compared with the STR loci present in the conceptus to determine the origin of the additional chromosome complement.⁹ The maternal blood sample was extracted and purified using Qiagen Blood Mini Kit (Qiagen). The STR loci were PCR amplified from both the conceptus and maternal DNA and microsatellite patterns compared according to the manufacturer's instructions. The results of this testing were consistent with digynic monoandric triploid gestation, in which 2 copies of the chromosomes were inherited from the mother and 1 copy from the father (TABLE 1).

The patient in this case had a history of recurrent miscarriage. Although the conceptus here was identified to have triploidy, no samples from prior pregnancy losses were available for comparison or investigation into potential causes of recurrent miscarriage. Using the samples available to us, we performed CMA of the maternal sample and exome sequencing of both conceptus and maternal samples to identify genetic causes of recurrent miscarriage. However, no pathogenic or likely pathogenic variants known to cause miscarriage were identified (data not shown).

Discussion

In this study, we present a case of digynic monoandric triploidy leading to miscarriage in a G7P1051 female at 12 weeks and 3 days gestation. Although the exact percentage of digynic triploidy in the pregnancies varies by study, there is a general consensus that it accounts for a small number of triploid fetal losses where the majority arise from paternal origin.¹⁰ Notably, the genotype in this case, 69, XXY, could arise from either maternal or paternal origin with different clinical implications. Diandric triploidy is commonly the consequence of dispermy, in which 2 sperms fertilize 1 egg. Rarely, it can result from a diploid sperm fertilizing a normal haploid egg. Digynic triploidy is usually due to fertilization of a diploid egg by a normal haploid sperm.^{10,11}

Diandric triploidy is often associated with a molar and largely nonviable pregnancy. Classically, molar pregnancies can be complete or partial. Complete moles have only 2 complements of chromosomes ($2n = 46$), both of which are of paternal origin and arise from fertilization of an "empty" egg. Complete moles can be homozygous from a single sperm, in which the haploid genome of the sperm duplicates after fertilization, or heterozygous from 2 sperm fertilizing the same egg. Complete moles have a substantially higher risk of converting to choriocarcinoma.¹² Histologically, they are classically associated with clusters of cystic structures in the placental tissue and typically do not give rise to fetal tissue. In contrast, partial moles have 1 complement of chromosomes of maternal origin and 2 from paternal origin, leading to 3 complements of chromosomes ($3n = 69$). The distinction between partial moles and digynic monoandric gestations is important because of the risk of choriocarcinoma in a partial molar but not digynic triploid pregnancy, although at less risk than a complete molar gestation.^{11,12} Thus, the distinction between a partial mole and digynic monoandric gestation made through STR testing becomes important. In this case, STR testing was most consistent with the inheritance of 2 maternal chromosome complements or digynic monoandric gestation (TABLE 1). Importantly, many patients with triploid miscarriage are lost to follow-up and never complete the work-up with STR testing.

FIGURE 2. Results of chromosome microarray. The result is arr(X)x2,(Y)x1,(1-22)x3, consistent with a karyotype of 69, XXY. Top: karyoview. Blue bars indicate gains of signal on every autosome. Bottom: whole genome view.

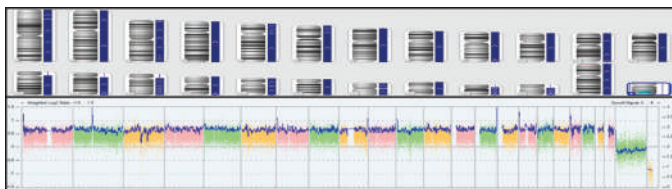


TABLE 1. Short tandem repeat analysis^a

Marker	vWA	TPOX	D16S539
Fetal alleles	17, 18, 14	8, 9, 10	11, 13, 9
Maternal alleles	17, 18	8, 9	11, 13

^aRepresentative informative short tandem repeat alleles found in fetal and maternal genomic DNA, consistent with the presence of 2 complements of maternal chromosomes, therefore a digynic monoandric gestation.

Recurrent pregnancy loss is defined as 2 or more failed pregnancies. Given the patient's history of multiple spontaneous abortions, she was evaluated for antiphospholipid syndrome with both anti-B2 glycoprotein I and anticardiolipin antibody panels. Both were negative. Her blood type was noted to be O+, with negative antibody screen, making RhD isoimmunization unlikely. No uterine or structural abnormalities were noted on ultrasound performed on presentation. Other potential causative factors in the parents include large and small DNA variations, sperm anomalies, hormonal imbalances, and advanced age.¹¹ The patient was seen for genetic counseling 2 months after her dilation and curettage, at which time she and her partner reported having normal G-banded karyotypes on a prior work-up at another institution. The CMA of the maternal sample and exome sequencing of the POC and maternal specimens were negative for pathogenic and likely pathogenic variants known to cause miscarriages (data not shown).

Given the sporadic nature of triploidy, the couple's recurrence risk for triploidy is similar to the general population, or 1% to 2%. However, there have been reported cases of recurrent triploid pregnancies,^{13,14} indicating that there are genetic factors that may increase their risk. Suspicion for recurrent triploidy is higher in this couple, given their history of 5 previous miscarriages, but cannot be assessed without samples from prior pregnancy losses.

Clinical Follow-up

After genetic counseling, the patient and her partner indicated a desire to try in vitro fertilization (IVF) with preconception genetic screening. The patient successfully became pregnant after multiple rounds of IVF but her pregnancy was complicated by symptoms of a threatened miscarriage. However, with treatment she was able to carry to term and successfully gave birth to a normal baby via repeat cesarean section at an outside hospital. A year later, she again became pregnant through IVF with preconception genetic screening and was able to carry to term another normal baby.

Conflict of Interest Disclosure

The authors have nothing to disclose.

REFERENCES

1. Archie JG, Collins JS, Lebel RR. Quantitative standards for fetal and neonatal autopsy. *Am J Clin Pathol*. 2006;126(2):256–265. doi:10.1309/FK9D-5WBA-1UEP-T5BB
2. McFadden DE, Robinson WP. Phenotype of triploid embryos. *J Med Genet*. 2006;43(7):609–612. doi:10.1136/jmg.2005.037747
3. Vora NL, Romero ST, Ralston SJ, Dugoff L, Kuller JA. Committee opinion no.682: microarrays and next-generation sequencing technology: the use of advanced genetic diagnostic tools in obstetrics and gynecology. *Obstetrics & Gynecology*. 2016;128(6):e262–e268.
4. South ST, Lee C, Lamb AN, Higgins AW, Kearney HM, Committee WGftACoMGaGLQA. ACMG standards and guidelines for constitutional cytogenomic microarray analysis, including postnatal and prenatal applications: revision 2013. *Genet Med*. 2013;15(11):901–909.
5. Schaaf CP, Wiszniewska J, Beaud AL. Copy number and SNP arrays in clinical diagnostics. *Annu Rev Genomics Hum Genet*. 2011;12:25–51.
6. Shao L, Akkari Y, Cooley LD, et al. Chromosomal microarray analysis, including constitutional and neoplastic disease applications, 2021 revision: a technical standard of the American College of Medical Genetics and Genomics (ACMG). *Genet Med*. 2021;23(10):1818–1829. doi:10.1038/s41436-021-01214-w
7. Gliem TJ, Aypar U. Development of a chromosomal microarray test for the detection of abnormalities in formalin-fixed, paraffin-embedded products of conception specimens. *J Mol Diagn*. 2017;19(6):843–847. doi:10.1016/j.jmoldx.2017.07.001
8. Riggs ER, Andersen EF, Cherry AM, et al. Technical standards for the interpretation and reporting of constitutional copy-number variants: a joint consensus recommendation of the American College of Medical Genetics and Genomics (ACMG) and the Clinical Genome Resource (ClinGen). *Genet Med*. 2020;22(2):245–257. doi:10.1038/s41436-019-0686-8
9. Butler JM. Short tandem repeat typing technologies used in human identity testing. *Biotechniques*. 2007;43(4):ii–iv. doi:10.2144/000112582
10. Massalska D, Ozdarska K, Roszkowski T, et al. Distribution of diandric and digynic triploidy depending on gestational age. *J Assist Reprod Genet*. 2021;38(9):2391–2395. doi:10.1007/s10815-021-02202-4
11. Pinar MH, Gibbins K, He M, Kostadinov S, Silver R. Early pregnancy losses: review of nomenclature, histopathology, and possible etiologies. *Fetal Pediatr Pathol*. 2018;37(3):191–209. doi:10.1080/15513815.2018.1455775
12. Zheng XZ, Qin XY, Chen SW, et al. Heterozygous/dispermic complete mole confers a significantly higher risk for post-molar gestational trophoblastic disease. *Mod Pathol*. 2020;33(10):1979–1988. doi:10.1038/s41379-020-0566-4
13. Robinson B, Brock JA, Midgen C, Coolen J. Molar and nonmolar triploidy: recurrence or bad luck. *Clin Case Rep*. 2020;8(5):785–789. doi:10.1002/ccr3.2703
14. Fontoura Oliveira A, Torrão MM, Nogueira R, Ferreira M. Recurrent fetal triploidy: is there a genetic cause? *BMJ Case Rep*. 2021;14(3):e239843. doi:10.1136/bcr-2020-239843

Defect in Automated Antigen Excess Detection Discovered after Reviewing Serum Free Light Chain Results in Context with Clinical Findings

Kriselle Maris Lao, MD, Ashbita Pokharel, MBBS, Mai Mohamed Mohamed Ibrahim Elzieny, MBBCh, Elizabeth Sykes, MD, Steven M. Truscott, PhD^o

Corewell Health William Beaumont University Hospital, Royal Oak, MI, US.
Corresponding author: Steven M. Truscott; steven.truscott@beaumont.edu

Key words: monoclonal gammopathy, serum free light chains, serum protein electrophoresis, urine protein electrophoresis, antigen excess, turbidimetric and nephelometric immunoassays

Abbreviations: MM, multiple myeloma; sFLC, serum free light chain; SPE, serum protein electrophoresis

Laboratory Medicine 2024;55:106-108; <https://doi.org/10.1093/labmed/lmad043>

ABSTRACT

Serum κ and λ free light chains can be markedly elevated in monoclonal gammopathies; consequently, serum free light chain (sFLC) immunoassays are susceptible to inaccuracies caused by antigen excess. As a result, diagnostics manufacturers have attempted to automate antigen excess detection. A 75-year-old African-American woman had laboratory findings consistent with severe anemia, acute kidney injury, and moderate hypercalcemia. Serum and urine protein electrophoresis and sFLC testing were ordered. The sFLC results initially showed mildly elevated free λ light chains and normal free κ . The pathologist noted that sFLC results were discrepant with the bone marrow biopsy, electrophoresis, and immunofixation results. After manual dilution of the serum, repeat sFLC testing revealed significantly higher λ sFLC results. Antigen excess causing falsely low sFLC quantitation may not be detected by immunoassay instruments as intended. Correlation with clinical history, serum and urine protein electrophoresis results, and other laboratory findings is essential when interpreting sFLC results.

Clinical History

A 75-year-old African-American woman with a medical history of long-standing hypertension presented to the emergency department with intermittent confusion, left leg swelling, fatigue, and shortness of breath. Physical examination findings included bilateral pitting edema of the lower

extremities extending to the mid-calves. Laboratory findings included severe anemia (hemoglobin, 4.6 g/dL [normal range, 12.1–15.0 g/dL]), acute kidney injury with markedly elevated creatinine (6.83 mg/dL [0.5–1.1 mg/dL]), and moderate hypercalcemia (12.2 mg/dL [8.5–10.5 mg/dL]). Radiological investigations revealed moderate degenerative changes at the lumbosacral junction and no acute intracranial process. The main concerns on admission were acute kidney injury and severe anemia. There was no evidence of gastrointestinal bleeding. The patient had received an initial transfusion of 3 units of packed red blood cells. Hemodialysis was started 2 days after admission.

Multiple myeloma (MM) was considered in the differential diagnosis; therefore, serum and urine protein electrophoresis and serum free light chain (sFLC) testing were ordered shortly after admission. The sFLC report indicated mildly elevated free λ light chains (10.96 mg/dL [normal range, 0.57–2.63 mg/dL]) and normal free kappa light chains with a decrease in the sFLC κ/λ ratio (0.15 [0.26–1.65]). sFLC testing was performed on the SPA Plus instrument using the Freelite turbidimetric immunoassay (both manufactured by The Binding Site). Based on the sFLC results and the nephrotic-range proteinuria (5860 mg/24 hours [<150 mg/24 hours]), a renal biopsy was performed, revealing λ monoclonal cast nephropathy. The results of a bone marrow biopsy showed involvement of plasma cell myeloma (80%–90% λ -restricted plasma cells).

The serum protein electrophoresis (SPE) and immunofixation results indicated the presence of free λ monoclonal protein with a concentration of 800 mg/dL. Urine protein immunofixation electrophoresis clearly revealed abundant λ monoclonal protein and an elevated urine total protein concentration of 1160 mg/dL. The results of subsequent SPE testing and immunofixation revealed a similar monoclonal concentration, again with only a slightly elevated serum free λ light chain concentration of 10.07 mg/dL. We questioned these sFLC results because they were inconsistent with serum electrophoresis, urine electrophoresis, and urine immunofixation results. Based on manufacturer claims, as well as our previous experience with the capabilities of this immunoturbidimetry test system, the analyzer should have detected the specimens with sFLC antigen excess.

Discussion

Quantification of sFLCs plays an increasingly important role in the diagnosis, prognostication, and classification of serum monoclonal gammopathies. This is particularly true of light chain only myelomas,

which are involved in 15% of cases of MM. A stringent complete response to therapy, as defined by the International Myeloma Working Group, requires a normal sFLC ratio, along with the absence of measurable M-proteins and clonal plasma cells.¹ Recently published guidelines from the College of American Pathologists² strongly recommend that clinical care providers order SPE and sFLC testing for the initial detection of monoclonal gammopathies.

The Freelite assay is a widely used latex-enhanced assay that uses polyclonal antibodies to detect epitopes on free light chains that are hidden when light chains are incorporated into intact immunoglobulin.³ Nephelometric and turbidimetric automated platforms are available for use with this assay. Given the wide concentration range in which monoclonal free light chains may be found, sFLC assays are vulnerable to antigen excess, resulting in falsely low immunoassay results due to saturation of reagent antibody-binding sites.

A purported advantage of the SPA Plus and Optilite (The Binding Site) analyzers, compared with other platforms, is their ability to immediately detect a falsely low result caused by antigen excess. These analyzers detect antigen excess in the first specimen collection by monitoring the immunoassay reaction kinetics of each specimen.^{4,5}

When free light chains are highly elevated, an initial burst of reaction progress is detected, but this progress then slows significantly during the time course of the assay because reagent antibody sites are saturated. The initial sFLC result in such specimens is falsely low, yet it is not reported because the instrument flags the specimen for further automated or manual dilution. According to the manufacturer, this approach is based on the kinetic analysis of a library of specimens from normal and abnormal (myeloma) cases. Free light chains produced by individual clones may react uniquely with the polyclonal reagents, with distinct reaction rate patterns. In practice, the vast majority of patients with sFLC elevation have clones that match patterns in this library^{6,7}; thus, antigen excess is detected by the analyzer and flagged appropriately for further dilution. The question arises as to what can be done in rare cases in which this automated antigen excess detection might fail.

For our patient, the discrepancy between the amount of monoclonal protein quantified by SPE and the measured amount of sFLC was not always apparent during the course of clinical care. The patient underwent months-long treatment for light chain myeloma and had several SPE and sFLC studies performed (TABLE 1).

At time points 1 and 2, the SPE monoclonal protein was associated with a slightly elevated λ sFLC (approximately 10 mg/dL). However, these λ sFLC results were lower than expected, given the amount of monoclonal protein detected by SPE (equivalent to 800-1200 mg/dL) and in the urine. The total urine protein of 1160 mg/dL was primarily λ monoclonal protein, as determined by immunofixation electrophoresis.

At time point 3, this discrepancy was recognized, and manual dilution and repeat sFLC testing of the specimen was performed. This process yielded a greatly increased final λ sFLC result, indicating that the analyzer had initially failed to detect antigen excess in the specimen. The concentration of free λ light chains in the serum of the patient decreased with her treatment, and the failure to detect antigen excess did not occur (specimen 4 and specimen 5). These 2 specimens were flagged appropriately by the analyzer as having values higher than the analytical measuring range, and hence were diluted appropriately. Free light chains continued to be monitored over time, but free λ light chains eventually began to increase again (specimen 7). The analyzer detected antigen excess and performed automated dilutions as intended for specimens 6-8 with elevated sFLC.

TABLE 1. Patient SPE and λ sFLC Results During the 15-Month Treatment Course

Time Point	SPE Monoclonal Quantitation (g/dL)	Free λ Initial Instrument Result (mg/dL)	Free λ Final Reported Result (mg/dL)
1	0.8	10.96	10.96 ^a
2	1.2	10.07	10.07 ^a
3	0.8	12.45	2864.00
4	0.2	>17.6	254.80
5	NP	>17.6 ^b	283.00
6	0.1	>15.78 ^b	177.86
7	0.2	>15.78	548.47
8	NP	>15.78	606.64
9	0.6	12.79	1957.00
10	0.8	12.85	3350.68
11	0.4	>15.78	2013.00
12	0.3	>15.78	971.00
13	0.2	>15.78	946.18

NP, not performed; sFLC, serum free light chain; SPE, serum protein electrophoresis.

^a λ sFLC results reported before the pathologist (E.S.) noted the discrepancy. Manual dilutions were performed for all subsequent specimens for this patient.

^bNote that the SPA Plus (The Binding Site Group) analytical measuring ranges (eg, > upper limits) differ with each reagent lot.

By this time, the unusual λ sFLC results and clinical situation of the patient were well known to us in the laboratory. It appeared that above a certain concentration of this specific free λ clone, the antigen excess detection consistently failed on the SPA Plus analyzer. Indeed, the discrepancy due to failure to detect antigen excess was noted again (in specimen 9) in an initial run of λ sFLC testing, and manual dilution was performed to determine the accurate sFLC concentration before reporting.

With the remnants of a subsequent specimen (specimen 10) for which antigen excess detection had also failed, we performed serial dilutions to determine a concentration threshold at which the instrument reaction rate analysis would again function properly for this rare clone (TABLE 2). Once diluted 1:3, or at approximately 1100 mg/dL, the instrument started detecting a high concentration of free λ light chains. It seems reasonable to suggest that manual dilution of the affected clone sufficiently changed the reaction rate profile detected by the analyzer; so, the specimen was flagged by the analyzer for further dilution. With these observations, it was decided that subsequent specimens from this patient would undergo the manufacturer-approved manual dilution (1:100) before sFLC testing, regardless of whether an accompanying SPE quantitation was ordered for the specimen.

At the time of λ monoclonal cast nephropathy diagnosis, the λ sFLC value for the patient was reported as being 10.96 mg/dL. Monoclonal cast nephropathy is extremely unlikely to occur if the involved sFLC is <50 mg/dL.⁸ However, in this case, the anemia and acute kidney injury, along with elevated urine protein, prompted a diagnostic biopsy. The case clearly demonstrated the need to correlate sFLC findings with other laboratory results and the clinical presentation.

Rare instances of low sFLC results due to the presence of a unique clone have been described, and the manufacturer recommends including, on all reports, a comment to alert physicians that rare undetected antigen excess may occur. Also, turbidimetric and nephelometric assays

TABLE 2. Serial Dilution of Specimen 10 with Excess λ sFLC and Initial λ sFLC Results from the SPA Plus Immunoturbidimeter

Dilution	Expected Concentration (mg/dL)	Initial Instrument Result (mg/dL)
Undiluted	3350.68	12.85
2:3	2233.79	13.80
1:2	1675.34	14.72
1:3	1116.89	>157.8
1:5	670.14	>157.8
1:10	335.07	>157.8

sFLC, serum free light chain; SPE, serum protein electrophoresis.

may also be subject to positive interferences that cause sFLC results much higher than SPE quantitation in the same specimen. This finding has been attributed to the ability of some monoclonal sFLCs to aggregate and form polymers.⁹ However, these potential problems do not detract from the importance of detecting and monitoring sFLC.

In many cases, changes in sFLCs precede changes in SPE quantitation or serum immunofixation detection and are a sensitive early indicator of relapses or remissions. Therefore, we believe it is prudent to take note early in the course of disease whether a patient has an unusual clone that eludes automated antigen excess detection, so that specimens can be diluted appropriately. Our case demonstrates that serum and urine protein electrophoresis and immunofixation continue to have a crucial role in the evaluation of monoclonal gammopathies; in this case, these assays brought to our attention the failure of automated antigen-excess detection. The use of other sFLC methods that employ distinct reagent antibodies would be another valid approach to addressing this analytical limitation of the commonly used Freelite assays for sFLC.

We conclude that the plasma cell clone in our patient was producing high concentrations of a free λ monoclonal protein, a rare clone for which antigen excess was not adequately detected by manufacturer algorithms. Since encountering this case, we have added an alert to all sFLC reports indicating the possibility of undetected antigen excess. This alert continues to be recommended for use with Freelite reagents on the Optilite analyzer, which is the latest model of immunoturbidimeter available from this manufacturer.

After we received the final specimen for testing, the patient transferred to another health system. She died a few weeks later due to complications of COVID-19, metabolic encephalopathy, and kidney disease.

Takeaways

- If not detected, antigen excess will result in falsely low sFLC quantitation. Detection of antigen excess kinetics is a feature of some au-

tomated instruments; however, rare clones may not be flagged. An sFLC result that is suspiciously low should prompt the laboratory to dilute the specimen to obtain an accurate result.

- In light chain only MM, consider the possibility of undetected antigen excess when the involved sFLC quantitation is considerably lower than the quantitation by SPE or when monoclonal light chains are detected by urine immunofixation electrophoresis. When monoclonal cast nephropathy is observed, the involved sFLC is generally >50 mg/dL.
- When interpreting sFLC results, correlation with clinical history and other laboratory findings is essential.

Acknowledgments

We thank Shannon O'Malley, MLS (ASCP)^{CM}, for assistance with additional testing of the patient specimens using the SPA Plus instrument.

Conflict of Interest Disclosure

The authors have nothing to disclose.

REFERENCES

1. Kumar S, Paiva B, Anderson KC, et al. International Myeloma Working Group consensus criteria for response and minimal residual disease assessment in multiple myeloma. *Lancet Oncol*. 2016;17(8):e328–e346. doi:10.1016/S1470-2045(16)30206-6
2. Kerren DF, Bosci G, Billman BL, et al. Laboratory detection and initial diagnosis of monoclonal gammopathies: guideline from the College of American Pathologists in collaboration with the American Association for Clinical Chemistry and the American Society for Clinical Pathology. *Arch Pathol Lab Med*. 2022;146(5):575–590.
3. Bhole MV, Sadler R, Ramasamy K. Serum-free light-chain assay: clinical utility and limitations. *Ann Clin Biochem*. 2014;51(5):528–542.
4. The Binding Site. *SPA Plus Instructions for Use*. 2014.
5. Price CP, Spencer K, Whicher J. Light-scattering immunoassay of specific proteins: a review. *Ann Clin Biochem*. 1983;20(1):1–14. doi:10.1177/000456328302000101
6. Cha K-H, Sim YB, Chae H, et al. The analytical performance evaluation of FreeliteTM human kappa free and human lambda free on the SPAPLUSTM immunoturbidimetric analyzer. *J Clin Lab Anal*. 2014;28(3):229–236.
7. Messiaen A-S, De Sloovere MMW, Claus P-E, et al. Performance evaluation of serum free light chain analysis: nephelometry vs turbidimetry, monoclonal vs polyclonal reagents. *Am J Clin Pathol*. 2017;147(6):611–622.
8. Yadav P, Sathick IJ, Leung N, et al. Serum free light chain level at diagnosis in myeloma cast nephropathy—a multicentre study. *Blood Cancer J*. 2020;10:28. doi:10.1038/s41408-020-0295-4
9. Pekar J-D, Schraen S, Grzych G, Manier S, Onraed B. Antigen excess pitfall for free light chains measurements solved by ELISA assay. *Am J Hematology*. 2019;94(5):1–2.